Nd^{3+}-SENSITIZED UCNPS WITH SUPERIOR LUMINESCENT PROPERTIES, ANISOTROPIC GROWTH AND LUMINESCENT JANUS SYSTEM

GUO SHUAI

Ph.D

The Hong Kong Polytechnic University

2018

The Hong Kong Polytechnic University

Department of Applied Biology and Chemical Technology

Nd^{3+}-Sensitized UCNPs with Superior Luminescent Properties, Anisotropic Growth and Luminescent Janus System

Guo Shuai

A thesis submitted in partial fulfilment of the requirements for the degree of Doctor of Philosophy

June, 2017

Certificate of Originality

I hereby declare that this thesis is my own work and that, to the best of my knowledge and belief, it reproduces no material previously published or written, nor material that has been accepted for the award of any other degree or diploma, except where due acknowledgement has been made in the text.

________________________________(Signed)

GUO Shuai (Name of student)

Abstract

In this thesis, we have generalized the research work that focus on construction, synthesis and characterization, luminescent properties study of Nd^{3+}-sensitized upconversion nanoparticles:

Firstly, we have developed the Nd^{3+}-harvest-transfer-sensitization trinity system (Nd^{3+}-Trinity system), which is used to coating on the $NaGdF_4$:Yb, X(Er/Tm/Ho) or the EMU [$NaGdF_4$:Yb,Tm@$NaGdF_4$:Yb,X(Eu/Tb) or $NaGdF_4$:Yb,X(Eu/Tb)@$NaGdF_4$:Yb,Tm] cores, to develop the Nd^{3+}-sensitized UCNPs with excitation of 808 nm laser to avoid the over-heating effect caused by the traditionally used 980 nm laser as well as shielding all the quenching factors in the Nd^{3+}-sensitized UCNPs with well design of the Nd^{3+}-Trinity system. And the UCNPs with Nd^{3+}-Trinity system coating have shown superior luminescent properties, including the enhanced luminescence intensity, prolonged lifetime, deeper luminescence penetration, larger partition of red emission. Furthermore, we have generalized that the enhanced luminescence intensity comes from the higher absorption of Nd^{3+} ions to 808 nm laser; the prolonged lifetime is proposed to be result in the 1056 nm photon selectively participation in the ETU process; deeper luminescence penetration is in consequence of the avoidance of the over-heating effect by the utilization of the 808 nm laser as the photo-luminescence source, larger partition of red emission is proposed to be influenced by the cross-relaxation of the Nd^{3+}-X(Er/Tm/Ho)$^{3+}$.

Secondly, when Nd^{3+}-harvest-transfer-sensitization trinity system is coated on the $NaYF_4$:Yb, X(Er/Tm/Ho), the phenomenon of the anisotropic growth is observed, which could be generalized as a longitudianl growth of the $NaYF_4$:Yb, X(Er/Tm/Ho) by the preference of the oleate binding to the (001) facets, as well as the etching of the $NaYF_4$ cores which result in the $NaYF_4$ cores dissolving. Furthermore, the layer-by-layer coating of the multiple shells of the Nd^{3+}-Trinity system, intensifies the anisotropic growth, which has influence on the luminescent properties.

Lastly, we have put forward the concept of the “Luminescent Janus” nanoparticles, which could be illustrated as the same UCNPs, that displays various luminescent properties, which is mainly the emission band, by the particular excitation source (808 nm c.w. or pulsed laser, 980 nm c.w. or pulsed laser). Also, we have developed three types of “Luminescent Janus” nanoparticles, which are driven by the energy migration upconversion (EMU) system with excitation of 808 nm/980 nm pulsed laser, to realize the RGB (red-green-blue)/full-color tenability.

Variations of the Nd^{3+}-harvest-transfer-sensitization system

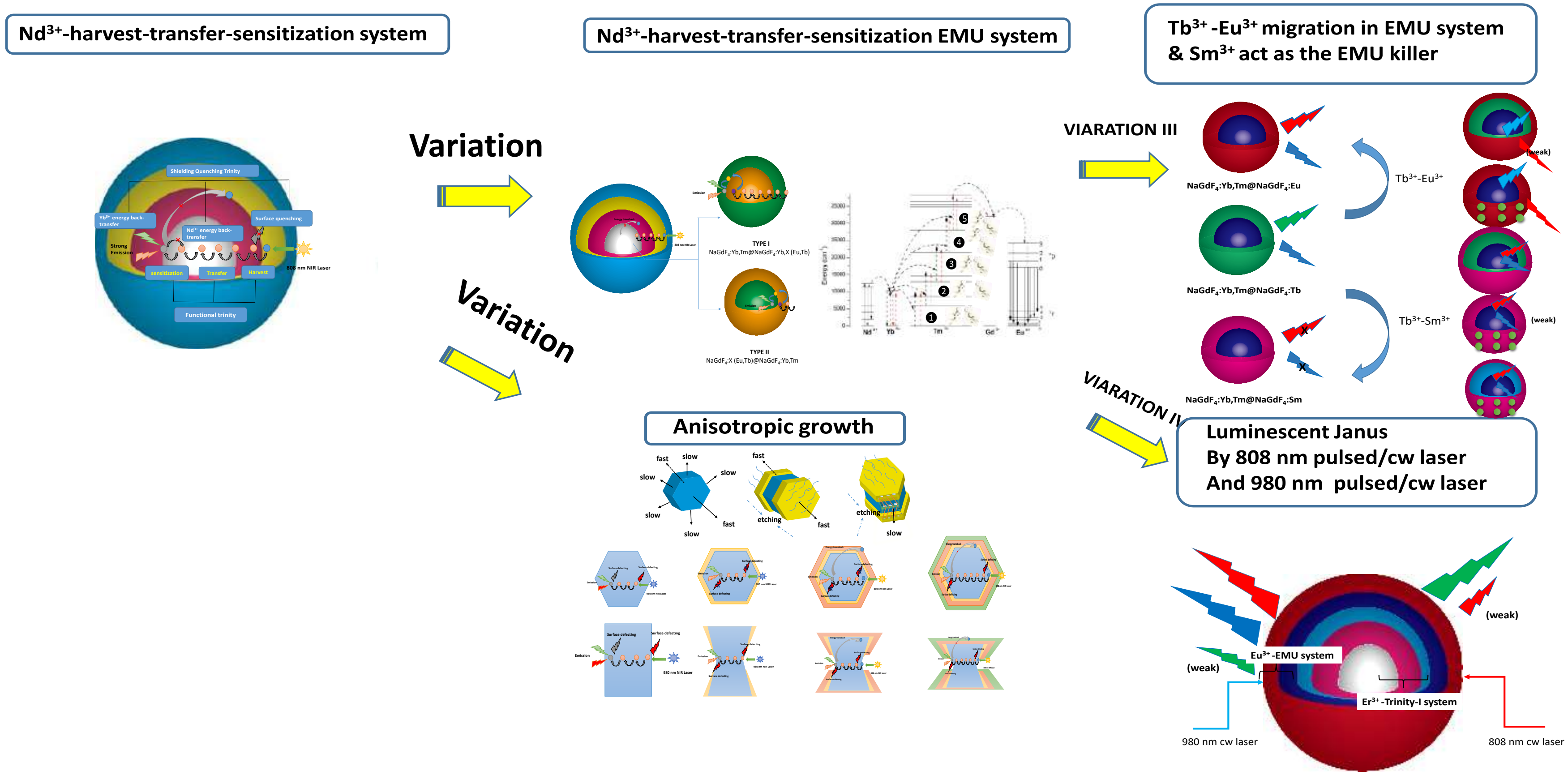

Scheme 1. Nd^{3+}-Trinity system and the variation.

Acknowledgement

My initial thanks must go to Prof. Wing-Tak Wong who is my supervisor, for his unlimited support and plentiful encouragements in my research work.

And I would like to give thanks to all the group numbers.

Also, I would like appreciate the support by Department of Applied Physics, HK polytechnic University, Lehn Institute of Functional Materials (Sun Yat-sen University), Dr. Yumei Lin (Xiamen University) and Prof. Jianhua Hao (AP, Hong Kong Polytechnic University) for the assistance and advice on measurement of the lifetime and fluorescent quantum yield.

Lastly, I would like to express my appreciate my family for their full support.

Contents

Abbreviations and Symbols

Abbreviations

^{1}H-NMR	**proton nuclear magnetic resonance**
c.w. or CW	**continuous wavelength**
DLS	**dynamic laser scattering**
EDX/EDS/EDXS	**Energy-dispersive X-ray spectroscopy**
EXP-ETU	**expletive energy transfer upconversion**
ESA	**excited state absorption**
ETU	**energy transfer upconversion**
EMU	**energy migration upconversion**
HAADF-STEM	**high angle annular dark field-scanning transmission electron microscopy**
HR-TEM	**high-resolution transmission electron microscopy**
MRI	**magnetic resonance imaging**
NPs	**nanoparticles**
OA	**oleic acid**
ODE	**octadecene**
PA	**photon avalanche**

PAA	**polyacrylic acid**
PEG	**poly-(ethylene glycol)**
PEI	**polyethylenimine**
PMT	**photomultiplier tube**
PVP	**polyvinylpyrrolidone**
QDs	**quantum dots**
SAED	**selected area electron diffraction**
TEM	**transmission electron microscopy**
UCNPs	**upconversion nanoparticles**
UV	**ultraviolet**
XRD	**X-Ray power diffraction**

Symbols

ζ :Zeta Potential

r_1: longitudinal relaxivity

T_1: relaxation times

$1/T_1$: inverse longitudinal relaxation times

Chapter 1. Introduction

- **Generalization on the Rare-earth (RE), Upconversion nanoparticles (UCNPs) and recent progress**

- **Generalization of our view minds of design of the Nd^{3+}-sensitized UCNPs and basic method in the research work**

- **Generalization of the methods in research work**

1.1. Generalization of the Rare earth (RE)

Rare-earth (RE) is defined as the is one of a set of 17 chemical elements in the periodic table, specifically the 15 lanthanides, including cerium (Ce), dysprosium (Dy), erbium (Er), europium (Eu), gadolinium (Gd), holmium (Ho), lanthanum (La), lutetium (Lu), neodymium (Nd), praseodymium (Pr), promethium (Pm), samarium (Sm), terbium (Tb), thulium (Tm), ytterbium (Yb) and yttrium (Y), as well as scandium (Sc) and yttrium (Y). Since the luminescent properties of the rare earth elements has been reported, they have been utilized in many fields such bio-imaging, bio-sensor, phosphor powder, etc.

RE elements essentially exist as trivalent ions (Re^{3+}), which is considered to be the most stable state in oxidation. The Re^{3+} ions feature an electron configuration of $4f^n$ ($0< n <14$) and the arrangements of electrons within this configuration are substantially diverse, thus resulting in the multiple energy levels. Most of the luminescent properties could be attribute to the transitions among the energy levels.

The energy levels of free lanthanide ions in 4f-orbitals are determined by **Coulombic interaction** and the **spin–orbit coupling between f-electrons**, which represents the mutual repulsion of the electrons, generates the total orbital angular momentum (L) and total spin angular momentum (S). Furthermore, the spin–orbit coupling makes the total angular momentum (J) of the f-electrons. Each set of L, S, and J corresponds to a specific distribution of electrons within the 4f-shell and defines a particular energy level. According to the Russell–Saunders notation, the energy levels are characterized by "$^{2S+1}L_J$", where *2S+1* represents the total spin multiplicity.

As shown in Figure 1, the energy levels of the rare earth/lanthanide are calculated and measured; the main ground state and excited state are shown in Table 1; the emission peaks the Re^{3+} are shown in Figure 2. [1]

Ref:

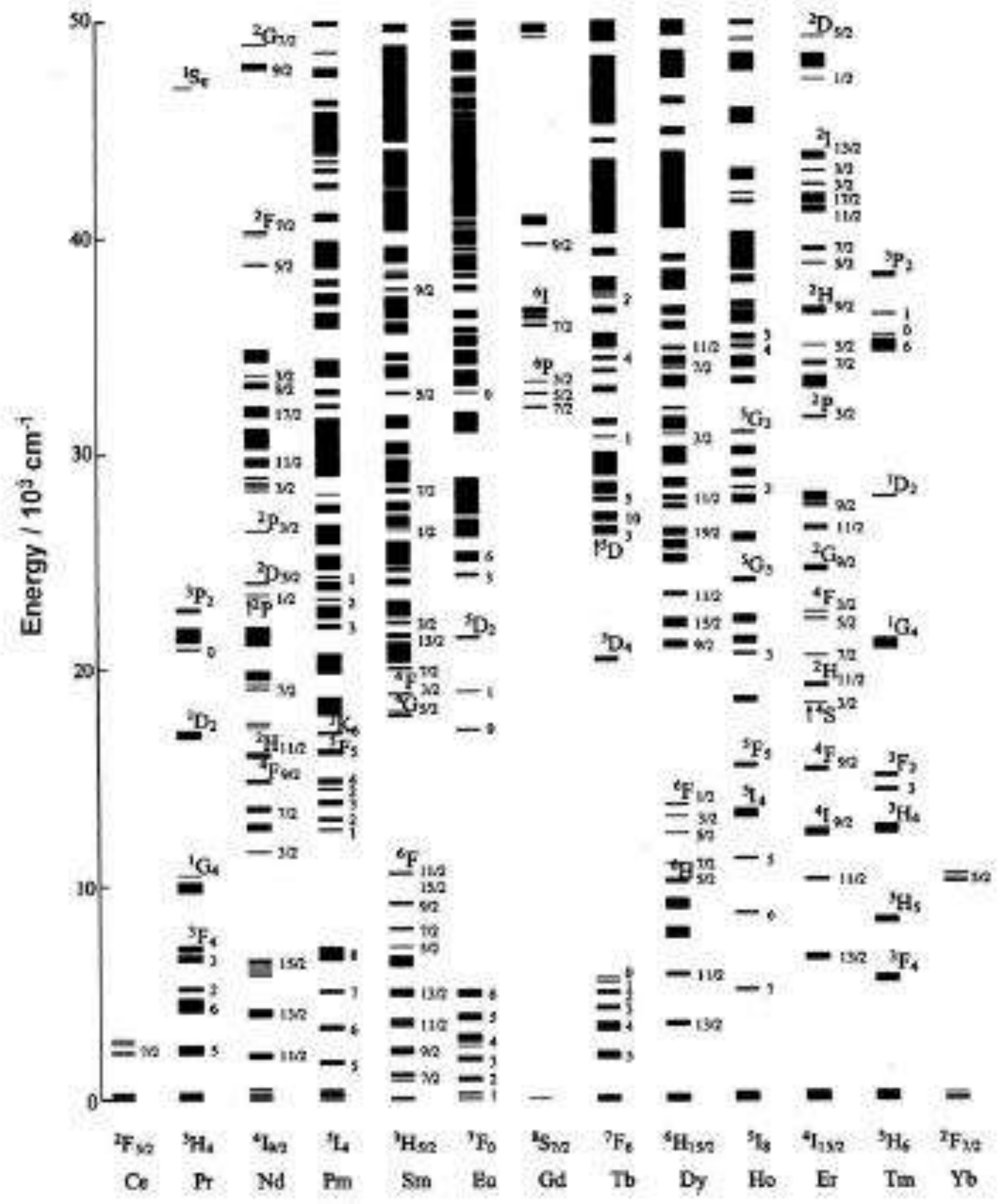

Figure 1. Energy levels diagram of the lanthanides doped in a low-symmetry crystal (LaF_3).

[1]

Ref:

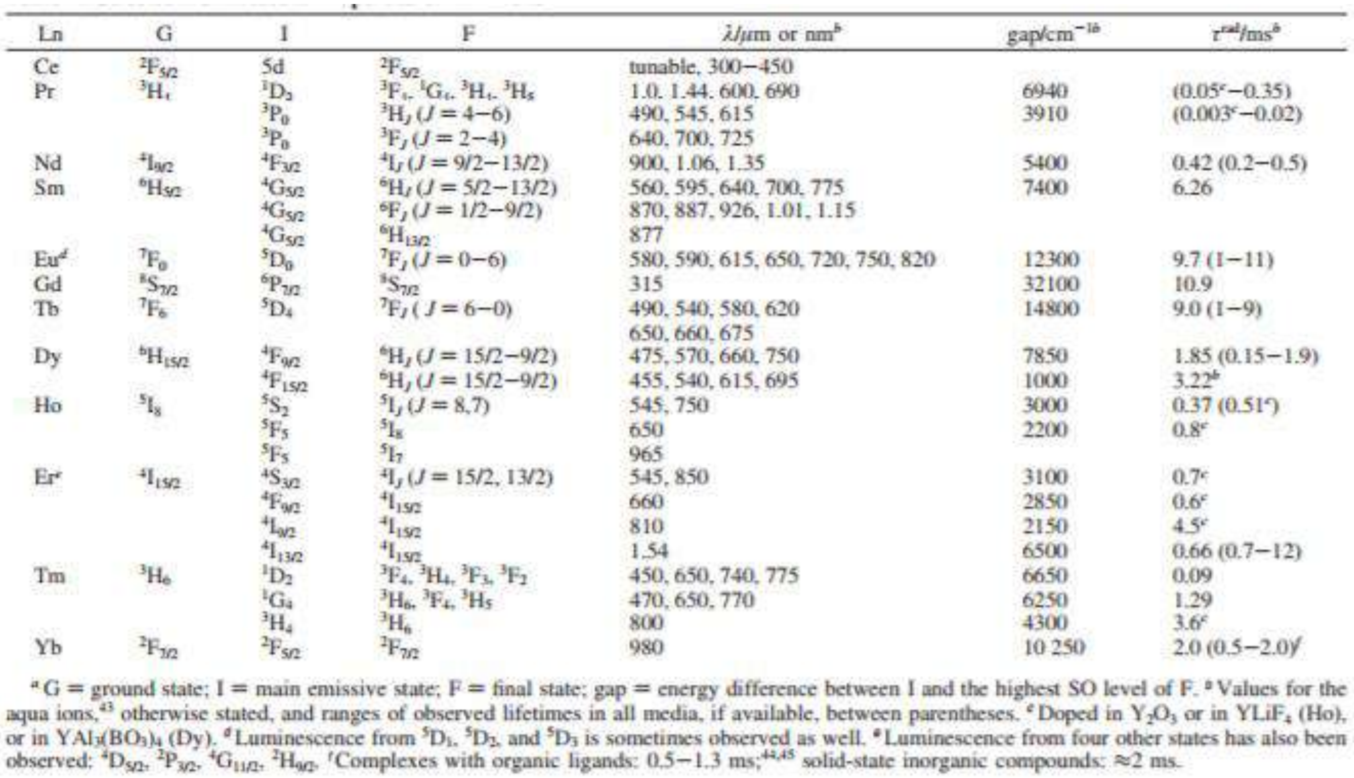

Ln	G	I	F	$\lambda/\mu m$ or nm^b	gap/cm^{-1b}	τ^{rad}/ms^b
Ce	$^2F_{5/2}$	5d	$^2F_{5/2}$	tunable, 300−450		
Pr	$^3H_4$	$^1D_2$	$^3F_4$, $^1G_4$, $^3H_4$, $^3H_5$	1.0, 1.44, 600, 690	6940	(0.05^c−0.35)
		$^3P_0$	^3H_J ($J = 4-6$)	490, 545, 615	3910	(0.003^c−0.02)
		$^3P_0$	^3F_J ($J = 2-4$)	640, 700, 725		
Nd	$^4I_{9/2}$	$^4F_{3/2}$	^4I_J ($J = 9/2-13/2$)	900, 1.06, 1.35	5400	0.42 (0.2−0.5)
Sm	$^6H_{5/2}$	$^4G_{5/2}$	^6H_J ($J = 5/2-13/2$)	560, 595, 640, 700, 775	7400	6.26
		$^4G_{5/2}$	^6F_J ($J = 1/2-9/2$)	870, 887, 926, 1.01, 1.15		
		$^4G_{5/2}$	$^6H_{13/2}$	877		
Eu^d	$^7F_0$	$^5D_0$	^7F_J ($J = 0-6$)	580, 590, 615, 650, 720, 750, 820	12300	9.7 (1−11)
Gd	$^8S_{7/2}$	$^6P_{7/2}$	$^8S_{7/2}$	315	32100	10.9
Tb	$^7F_6$	$^5D_4$	^7F_J ($J = 6-0$)	490, 540, 580, 620 650, 660, 675	14800	9.0 (1−9)
Dy	$^6H_{15/2}$	$^4F_{9/2}$	^6H_J ($J = 15/2-9/2$)	475, 570, 660, 750	7850	1.85 (0.15−1.9)
		$^4F_{15/2}$	^6H_J ($J = 15/2-9/2$)	455, 540, 615, 695	1000	3.22^b
Ho	$^5I_8$	$^5S_2$	^5I_J ($J = 8,7$)	545, 750	3000	0.37 (0.51^c)
		$^5F_5$	$^5I_8$	650	2200	0.8^c
		$^5F_5$	$^5I_7$	965		
Er^e	$^4I_{15/2}$	$^4S_{3/2}$	^4I_J ($J = 15/2, 13/2$)	545, 850	3100	0.7^c
		$^4F_{9/2}$	$^4I_{15/2}$	660	2850	0.6^c
		$^4I_{9/2}$	$^4I_{15/2}$	810	2150	4.5^c
		$^4I_{13/2}$	$^4I_{15/2}$	1.54	6500	0.66 (0.7−12)
Tm	$^3H_6$	$^1D_2$	$^3F_4$, $^3H_4$, $^3F_3$, $^3F_2$	450, 650, 740, 775	6650	0.09
		$^1G_4$	$^3H_6$, $^3F_4$, $^3H_5$	470, 650, 770	6250	1.29
		$^3H_4$	$^3H_6$	800	4300	3.6^c
Yb	$^2F_{7/2}$	$^2F_{5/2}$	$^2F_{7/2}$	980	10 250	2.0 (0.5−2.0)^f

[a] G = ground state; I = main emissive state; F = final state; gap = energy difference between I and the highest SO level of F. [b] Values for the aqua ions,[43] otherwise stated, and ranges of observed lifetimes in all media, if available, between parentheses. [c] Doped in Y_2O_3 or in $YLiF_4$ (Ho), or in $YAl_3(BO_3)_4$ (Dy). [d] Luminescence from $^5D_1$, $^5D_2$, and $^5D_3$ is sometimes observed as well. [e] Luminescence from four other states has also been observed: $^4D_{5/2}$, $^2P_{3/2}$, $^4G_{11/2}$, $^2H_{9/2}$. [f] Complexes with organic ligands: 0.5−1.3 ms;[44,45] solid-state inorganic compounds: ≈2 ms.

Table 1. Ground and excited states and the main transitions of the Re^{3+} ions [1]

Ref:

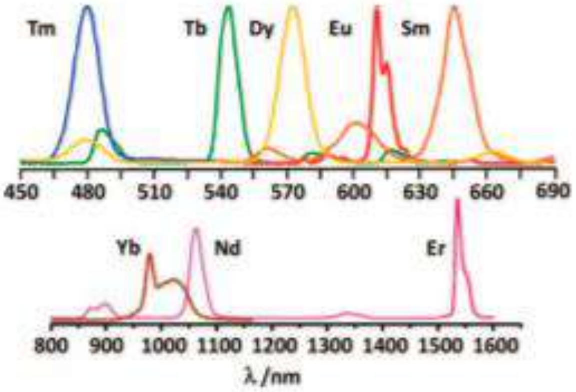

Figure 2. Emission of lanthanides. [1]

For the situation that the rare-earth elements that utilized in our research work, which is upconversion materials, could be generalized as:

Host matrices: yttrium and gadolinium are used as the host matrices in the $NaReF_4$ nanocrystals. The differences is that the $NaYF_4$ nanocrystals are always in larger size but not so easy to cut off the phonons in the energy transfer by the vibration of the nanocrystals lattice while the $NaGdF_4$ nanocrystals are in smaller size but with more phonons cut-off.

Sensitizer Type I: that is Yb^{3+}, which is a traditionally used sensitizer in upconversion materials that is used to absorb the 980 nm photons and sensitize the activators.

Sensitizer Type II: that is Nd^{3+}, which is used to absorb the 795/800/808 nm photons, and transfer to Yb^{3+} with Nd^{3+}-Yb^{3+} energy transfer.

Activator Type I: that is Er^{3+}, Tm^{3+} and Ho^{3+}, which is sensitized by Yb^{3+} with 980 nm excitation or $Nd^{3+}\rightarrow Yb^{3+}$ energy transfer with 795/800/808 nm excitation.

Activator Type II: that is Eu^{3+} and Tb^{3+}, which are excited by Gd^{3+} $^6P_{7/2}$ (~31000 cm^{-1}) by accumulation of Tm^{3+} for 5-phonon accumulation in the energy migration upconversion (EMU) system. For Dy^{3+}, it shows very low efficiency in the EMU system. For Sm^{3+}, we found it just act as the EMU killer.

Accumulator: that is Tm^{3+}, that used to accumulate 5 phonon in the EMU system, which is sensitized by Yb^{3+} with 980 nm excitation or $Nd^{3+}\rightarrow Yb^{3+}$ energy transfer with 795/800/808 nm excitation (Chapter 3) .

Ref:

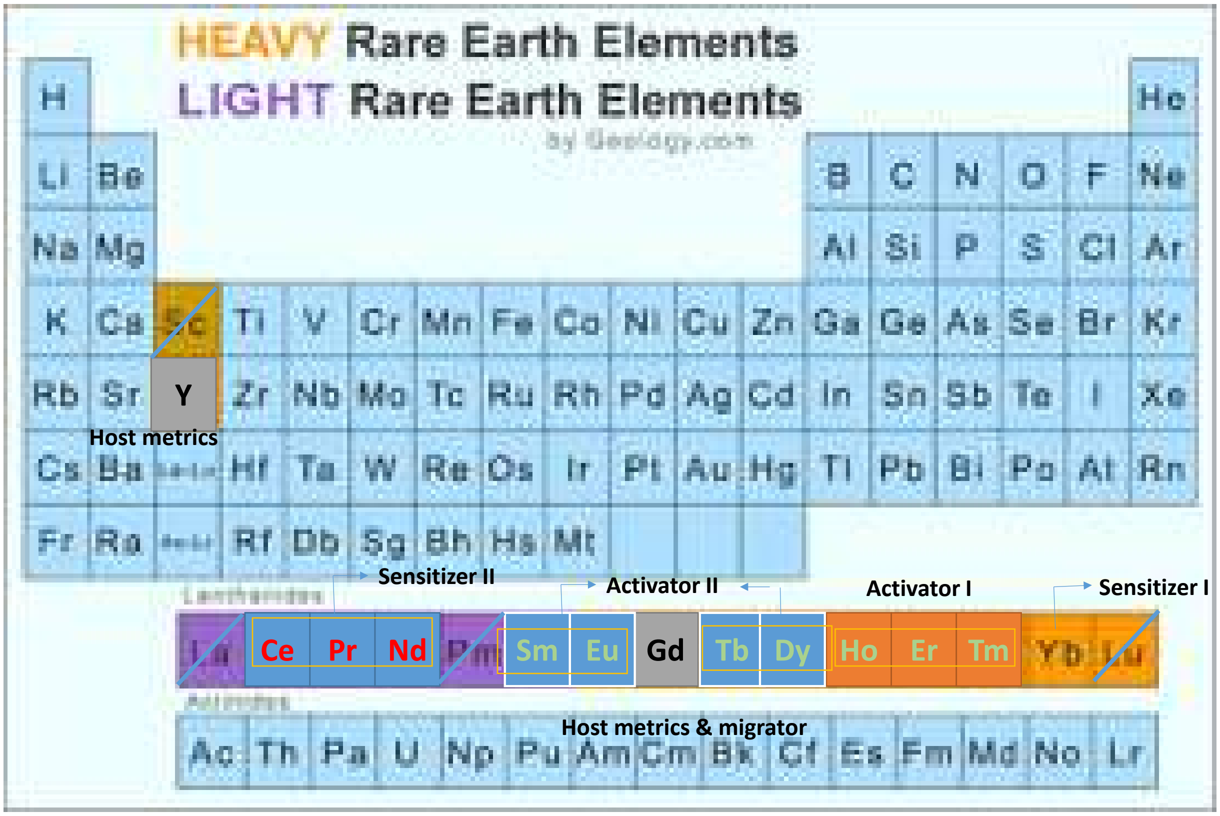

Figure 3. Generalization of the utilization of Re^{3+} elements in our research work, which illustrating the roles of Re^{3+} elements in upconversion process.

1.2 Generalization of the Upconversion Nanoparticles (UCNPs)

1.2.1. General Background of Upconversion Nanoparticles (UCNPs)

"Upconversion" is defined as the process that absorbing the low energy photons with emitting of the high energy photons, which always shows remarkable ability in the utilization in upconversion nanoparticles (UCNPs), that is the 2 or multiple 980 nm photons are absorbed by Yb^{3+}, or 795/800/808 nm photons are absorbed by Nd^{3+} ions and transfer to Yb^{3+} by $Nd^{3+} \rightarrow Yb^{3+}$ energy transfer, then sensitizing the activator, with ultra-violet and visible emission, which is the anti-Stokes shift process. The lanthanides ions, including the host matrices, sensitizer and activators exist in the $NaReF_4$ nanocrystals as the trivalent ions.

What should be noticed in recent process of the UCNPs would be generalized as: a. the low upconversion efficiency as reported; b. the luminescence performance should be further developed; c. the over-heating effect that causes the hazards in cells and tissues. [2-8]

1.2.1.1. Principle and energy transfer of Upconversion Nanoparticles (UCNPs)

Here, we would like to summarize the basic mechanism and the major energy transfer in the upconversion process, as shown in Scheme. 1.

Firstly, is the traditionally used mechanism, which we would like to address it as **“Yb^{3+}-X(Er/Tm/Ho)$^{3+}$”** could be generalized as: by Yb^{3+} sensitizing and the excited state absorption (ESA) process of the activators, the activators are excited by the energy transfer upconversion process; with process of photons avalanche (PA), by non-radiative and radiative transition with emissions.

Secondly, the **CET process**, which is the co-operate energy transfer, could be used to depict the energy transfer between $Yb^{3+}$and Tb^{3+} , that are the two-photons upconversion process that with Yb^{3+} sensitization of Tb^{3+} or the lowest excited states of Tb^{3+} are quenched by two nearby Yb^{3+} ions.

Thirdly, the **energy migration upconversion (EMU)** system, that is the Yb^{3+} absorbs the 980 nm photons, and then transfer to Tm^{3+}; Tm^{3+} exciting Gd^{3+} lowest excited state with accumulating 5 phonons that transferred by Yb^{3+}; Gd^{3+} exciting the activators that is Tb^{3+} , Eu^{3+} , Sm^{3+} and Dy^{3+} [2-8]

Ref:

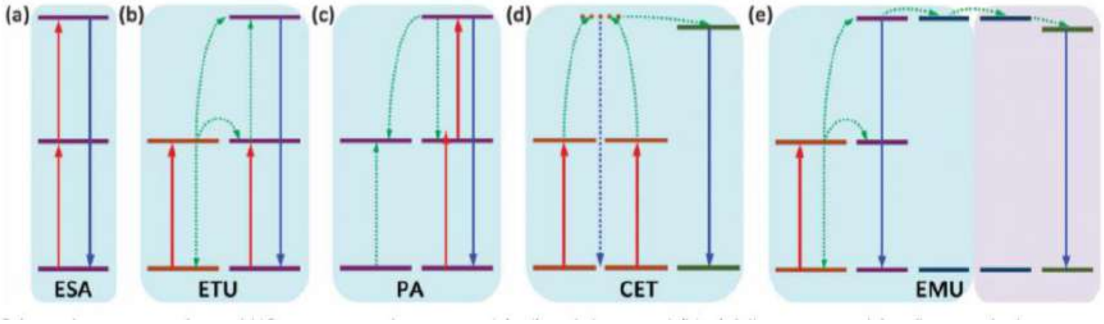

Scheme 1. Summarization of energy transfer progress in upconversion process: (a) ESA, (b) ETU, (c) PA, (d) CET, (e) EMU.[4]

1.2.2.2. Photons and Phonons

"Photons" are defined as: the elementary particle, the quantum of the electromagnetic field including electromagnetic radiation such as light, and the force carrier for the electromagnetic force (even when static via virtual photons). The photon has zero rest mass and is always moving at the speed of light.[9]

"Phonons" is defined as: the collective excitation in a periodic, elastic arrangement of atoms or molecules in condensed matter, like solids and some liquids. Often designated a quasiparticle, it represents an excited state in the quantum mechanical quantization of the modes of vibrations of elastic structures of interacting particles.[10]

And in our research, the Yb^{3+} ions absorbed and the activator emitted are considered to be the photons which is the ***particle*** of the light; while the so called "energy" that transferred in the lattice of the nanocrystals should be called as the "phonons" which is the ***quasiparticle***.

1.2.3. Synthesis and Characterization of Upconversion Nanoparticles (UCNPs)

1.2.3.1. Synthesis Methods

The commonly used methods of syntheses of the UCNPs, are thermal decomposition and hydrothermal [3-8, 11, 12].

For the hydrothermal, the experimental in details are concluded as:.[11-14]

EG (80 mL) was poured in the solution of the $RECl_3$ (0.8 mmol) solution, which is composed of YCl_3, $YbCl_3$ and $ErCl_3$ with the ratio of 78:2:2, along with the PEI (branched, ~ 100000 KDa, 1.2g), and $NaNO_3$ (0.408g, 4.8 mmol). The reaction mixture was heated to 80 ℃ for10 min to form a homogeneous solution with vigorous stirring, and then an EG (10 mL) solution of NH_4F (0.71 g, 19.2 mmol) was added drop-wisely. After aging at 80 ℃ for another 10 min, the reaction mixture was transferred to a 100 mL teflon-lined stainless steel autoclave and was allowed to be treated hydrothermally at180 ℃ for 3 h. After cooling to room temperature, the products were collected by centrifugation (10min at 10000rpm), purified with distilled water and 95 % ethanol three times, and dried in a vacuum oven at 80 ℃. [11-14]

Advantages: the UCNPs that synthesized by the method of hydrothermal, has shown in Figure 4, advantages in the utilization for they are simple and easily to be obtained, fitting for the application of bio-imaging and they are convenient for the surface modification.

Ref:

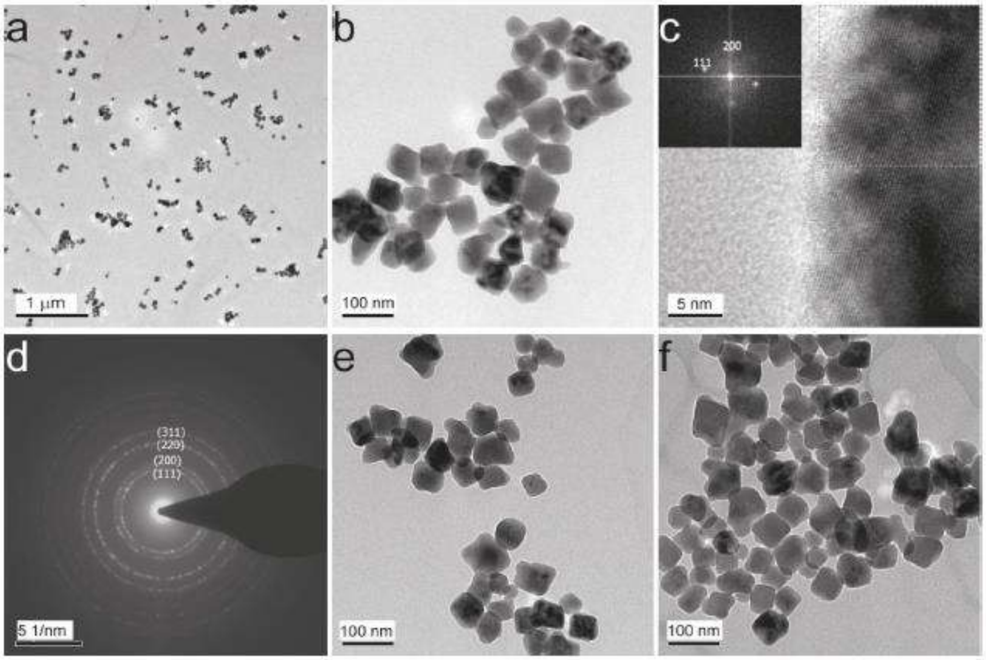

Figure 4. The obtained $NaYF_4$ reported by J.F. Jin *et al.* by the method of hydrothermal. [11, 12]

Ligand exchange: the synthesis of the PEI coated $NaYF_4$ UCNPs is convenient for ligand exchange of PAA, PVP etc., which shows advantageous on surface modification. Briefly, for the synthesis of PEI-coated UCNPs, 50 mg of UCNP-PVP was dispersed in a 20 mL DMF solution containing 40 mg of branched PEI by sonication, and the reaction mixture was stirred at 80 ℃ for 2 h. After cooling, the products were isolated by centrifugation (20 min at 14000 rpm), purified with distilled water and 95 % ethanol three times.

Water-solubility: the obtained PEI-UCNPs that are coated with polymers such as the PEI, PVP and PAA, has good water-solubility, which has advantages in bio-imaging.

Disadvantage: however, as shown in Figure 4, by characterization on the morphology and the phase, on the $NaYF_4$ nanocrystals, we found that it is not suitable for further development of the UPCNs for the reason that:

Phase: the phase is cubic phased, and it is not a good host matrix for the UCNPs which are used as bio-image probes for the reason that cubic phase UCNPs has weaker luminescence performance than the hexagonal ones.

Size distribution: as shown in Figure 4, the size of the PEI-$NaYF_4$:Yb, Er with diameter of ~60 nm and the size distribution of the UCNPs is broad, which should be treated as the disadvantages in the further utilization.

Core-shell synthesis invalid: as the development of the UCNPs, it is imperative to construct the core-shell structures for further enhancement and studying the luminescence; moreover, since the Nd^{3+}-sensitized UCNPs are invented, the core-shell structured UCNPs should be treated as a must in the research work, for the Nd^{3+} ions has strong quenching effect on the activators including the Er^{3+}, Tm^{3+}, Ho, Tb^{3+}, Eu^{3+}.[15-18]

For the **thermal decomposition**, the experimental in details are:

For $NaGdF_4$:Yb (20 %), Er (2 %)/ Yb (49 %), Tm(1 %)/ Yb (20 %), Ho (2 %) cores: 8 mL oleic acid and $Ln(CH_3CO_2)_3$•xH_2O DI water solution (0.8 mmol Ln^{3+} in total) were placed in a 100 mL three-neck flask, and degassed by nitrogen for 15 min. The mixture was heated to 150 ℃ and the temperature was kept for 0.5 h to remove water. 12 mL 1-ODE was then added and the mixture was kept at 150 ℃ for 0.5 h to form a uniform solution. Cooling down the solution to 50 ℃, 5 mL MeOH that containing 80 mg NaOH and 240 mg NH_4F was added drop wise. Then solution was stirred for 0.5 h at 50 ℃. The solution was then heated to 120 ℃ to remove water and methanol, and keeping under vacuum for 10 min to prevent bumping at high temperature. And then heated to 290 ℃ and kept for 1.5 h. The product was achieved by predication by adding exceeded ethanol and collection by centrifugation at 12, 000 rpm for 10 min and washed by ethanol for 3 times.

Core-shell structures by "seeded growth": 4 mL oleic acid and $Ln(CH_3CO_2)_3 \cdot xH_2O$ DI water solution (0.4 mmol Ln^{3+} in total) were placed in a 100 mL three-neck flask, and degassed by nitrogen for 15 min. The mixture was heated to 150 ℃ and the temperature was kept for 0.5 h to remove water. 6 mL 1-ODE was then added and the mixture was kept at 150 ℃ for 0.5 h to form a uniform solution. Cooling down the solution to 50 ℃, the "seed" UCNPs (0.8 mmol) that dispersed in cyclohexane were added, along with 5 mL MeOH that containing 80 mg NaOH and 240 mg NH_4F was added drop wise. Then solution was stirred for 0.5 h at 50 ℃. The solution was then heated to 120 °C to remove water and methanol, and keeping under vacuum for 10 min to prevent bumping at high temperature. And then heated to 290 ℃ and kept for 1.5 h. The product was achieved by predicated by adding exceeded ethanol and collection by centrifugation at 12, 000 rpm for 10 min and washed by ethanol for 3 times. [15, 17-21]

Core-multishells by "layer-by-layer" epitaxial growth: the same with the "seeded growth", which is coating layer on the core/shell or the core-multishells nanoparticles. As shown in Figure 5, all the obtained UCNPs are in well self-assembly and in uniform size.

Ref:

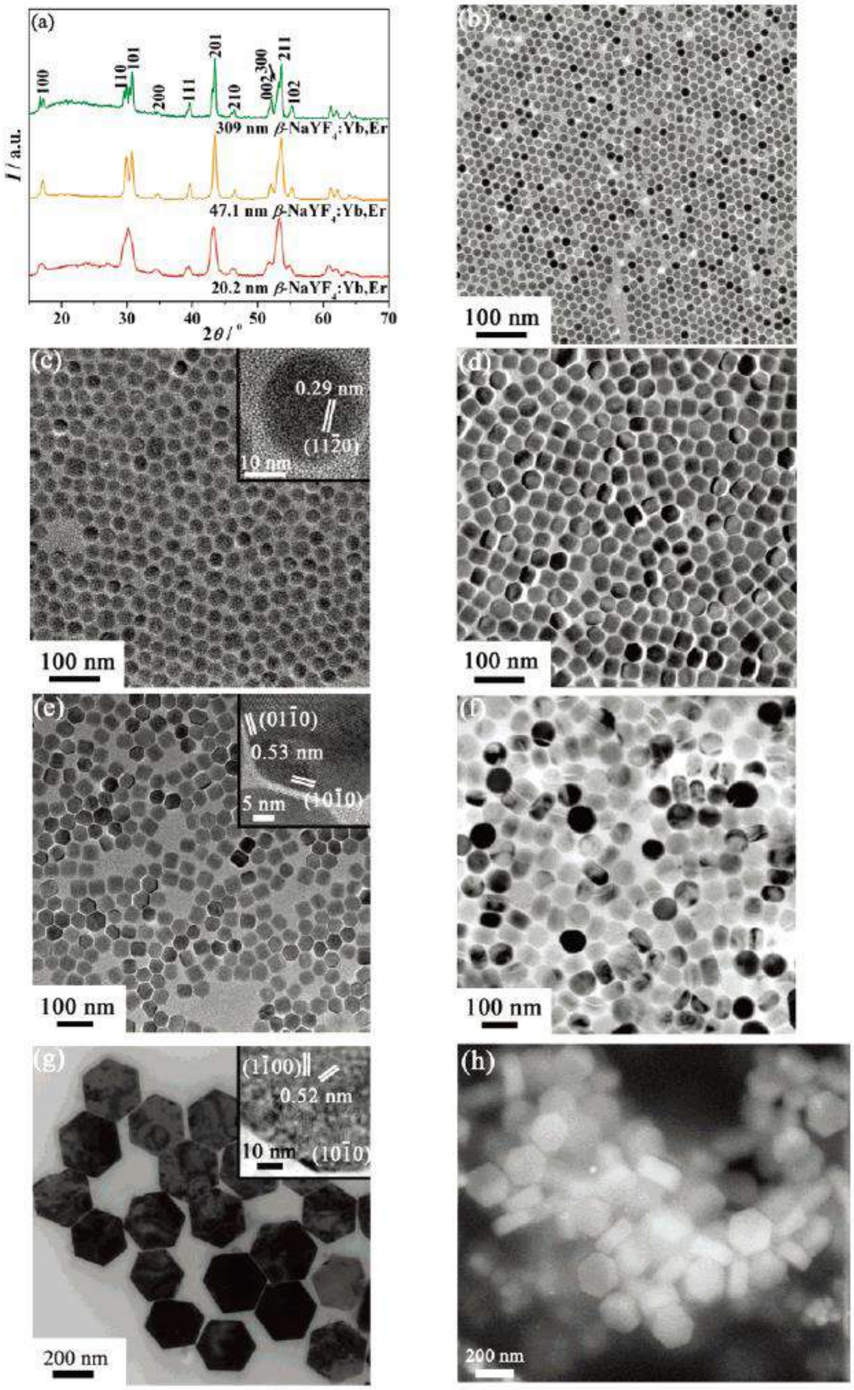

Figure 5. the as obtained $NaYF_4$ UCNPs reported by Mai, H.X. *et al.* [19]

Advantages: the method of thermal decomposition shows significances in the research of the UCNPs for the higher demand on the luminescence properties, minimizing the size and preference on the hexagonal phased UCNPs.

Minimized size and narrow size distribution: in our research work, the $NaGdF_4$ UCNPs are with the diameter of ~8 nm and the $NaYF_4$ UCNPs are with the diameter of ~ 40 nm. Among the previous work, the $NaYF_4$ UCNPs have been reported as the below ~ 50 nm; and the $NaGdF_4$ UCNPs have been reported as the below ~ 30 nm. And the uniform size make the UCNPs with narrow size distribution, as discussed below in the part of characterization of the UCNPs.

Preferred luminescence properties: the heating temperature of thermal decomposition, which is always 290-300 ℃, which result in hexagonal phase UCNPs that are preferred in luminescence, for the hexagonal phased UCNPs has 2.4 folds on luminescence than the cubic phased ones. [19]

Disadvantages:

Exchange from the lipophilic UCNPs to hydrophilic UCNPs: for the UCNPs that obtained by the thermal decomposition, are coated with oleate, which is lipophilic and it should be transferred to hydrophilic in the further utilization.

Difficulties in the operation of the thermal decomposition: in the process of the thermal decomposition, the oleic acid is very easy to be oxidized under the high temperature, more attention should be paid on.

1.3. Characterization of the UCNPs

1.3.1. Methods

The methods in characterization of the morphology in our researches of the UCNPs could be generalized as TEM, SEM, HAAD-STEM, and ELS-line or mapping. The TEM and SEM are used to characterize the morphology and size of the nanoparticles; the HAADF-STEM and ELLS mapping or line are used to characterize the elements distribution in the nanoparticles; XRD patterns and the SAED are used to characterize the phase of the nanocrystals; EDX is used to analyze the elements composition of the UCNPs.

Transmission Electron Microscope (TEM): is a microcopy that using a electron beam to transmit the specimen, with interacting the specimen. The images of TEM reflect the interaction between the electrons transmitted through the specimen. TEM has significantly high resolution than the optical microscopes. And the high-resolution Transmission Electron Microscopy (HR-TEM) are used as a direct map of atomic arrangements that can be obtained in the high resolution mode. [22]

Scanning Electron Microscopy (SEM) is a type of electron microscopy method for the high-resolution image of the surface by scanning the samples with a focused electron beam. SEM obtained advantages such as higher magnification (>100,000X) and greater depth of field than Optical Microscopy. Also it could be used as qualitative and quantitative analysis of the samples. [23]

High Angle Annular Dark Field Scanning Transmission Electron Microscope (HAADF-TEM): is a specific form of STEM, in which the images are formed by collecting scattered electrons with an annular dark-field detector. The basic principle could be concluded that the detectors collects the electron from annulus around the beam, sampling far more scattered electron than can pass through an objective aperture, which result in high efficiency in signal collection.

The method utilize the "Z" contrast to form the bright field and the dark field, which could be generalized as the atoms with larger atomic number contribute to the brightness while the atoms with smaller atomic number contribute to the darkness. Usually, the difference between the atomic numbers should be at least 12 that could be utilized in the characterization of difference layers of the core-shell nanoparticles. [24-26]

Ref:

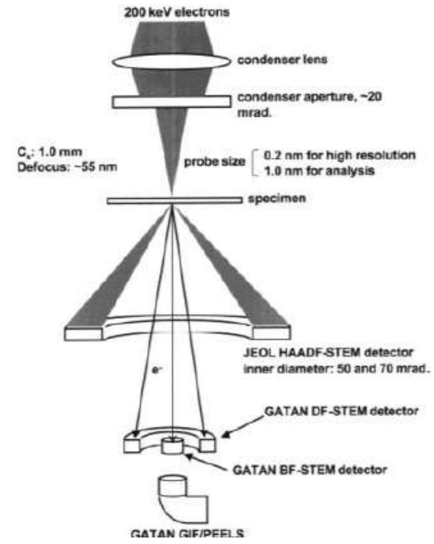

Figure 6. Schematic illustration of the electron microscope configuration used in the HAADF-STEM mode (JEOL JEM 2010 F).[25]

Electron Energy Loss Spectroscopy (EELS), measures changes in the electron distribution when the electron beam is transmitted through the specimen. It acts as the complementary to energy-dispersive x-ray spectroscopy. The difference between them is that EDX always focus on the characterization of the composition of the nanoparticles while the EELS has more complex functions, including measuring atomic composition, chemical bonding, valence and conduction band electronic properties, surface properties, and element-specific pair distance distribution. And EELS is always utilized as EELS-mapping, or EELS line in characterization of the element distribution. [27]

Also, the surfactants of the UCNPs should be characterized: the oleate that coating on the UCNPs, that act as the plasticizer by FTIR and the co-polymer, that is the PEI-PEG copolymer conjugated on the UCNPs by ligand exchange, by ^{1}H-NMR and ^{13}C-NMR spectroscopy.

The characterization of the nanoparticles in our research work of synthesis are shown below:

For the **$NaYF_4$:Yb, Er nanocrystals** (as shown in Figure 7-8):

Under the temperature of 290 ℃, the nanoparticles size are in sub-40 nm on the (001) facets and sub-50 nm on the (100) facets; the XRD patterns shows the nanocrystals are in hexagonal phase; by analyzing the composition of the $NaYF_4$:Yb, Er nanocrystals, it shows the lanthanide ions ratio is that Y:Yb:Er is 90: 8.9: 1.1, which could be concluded with coincidence with the previous reports[15, 18, 20, 28] and could be further utilized in the studying of the principle of the epitaxial growth of the UCNPs and luminescence properties,

At the temperature of 320 ℃, the nanoparticles size are in sub-100 nm on the (001) facets, which is considered to be caused by the aggregation of the nanoparticles in the process of thermal decomposition. And it should be avoided in our study for its size is not considered to be practical in bio-imaging, which should be considered to be the final aims.

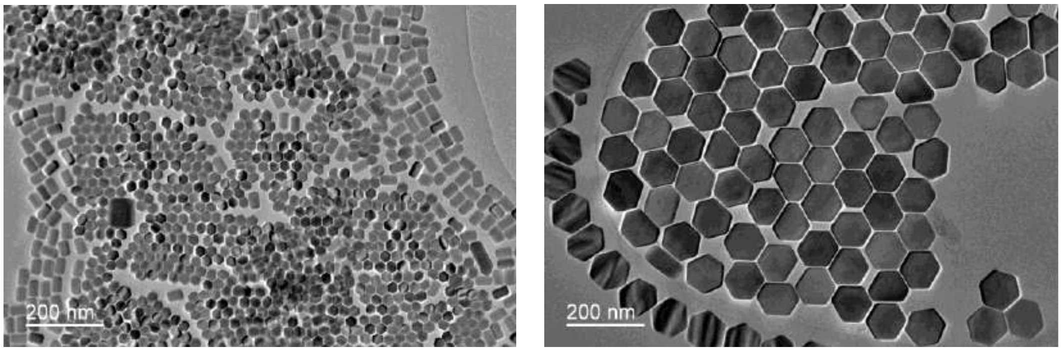

290 °C

320 °C

Figure 7. TEM images of the $NaYF_4$:Yb, Er synthesized by the method of thermal decomposition with the temperature of 290 ℃ and 320 ℃.

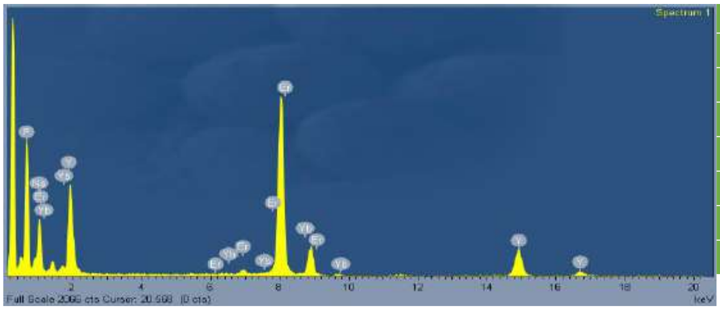

Element	Weight%	Atomic%
F K	37.04	67.68
Na K	8.49	12.82
Y L	45.17	17.63
Er M	1.10	0.23
Yb L	8.20	1.64
Totals	100.00	

Figure 8. EDX of the $NaYF_4$:Yb, Er, synthesized by the method of thermal decomposition.

1.3.2. Characterization of the morphology, size and phase of the (core) UCNPs

For the **$NaGdF_4$:Yb, Er nanocrystals**, the characterization on morphology, size, phase, elemental composition and the surfactant of the $NaGdF_4$:Yb, Er nanocrystals are shown in Figure 9-12.

As shown in Figure 9, when the $NaGdF_4$:Yb, Er nanocrystals are synthesized under the temperature of 310 ℃, the nanocrystals are in hexagonal phased, which with the size is sub ~ 25 nm; when the $NaGdF_4$:Yb, Er nanocrystals are synthesized under the temperature of 290 ℃, the TEM images show the nanocrystals are in smaller sized that is the ~7 nm with sphere shape, the element composition could be seen in Figure 11(a), that is the EDX spectra. By the characterization of XRD patterns (Figure 12) and SAED (Figure 11-b), it could be confirmed that the nanocrystals are in hexagonal phase.

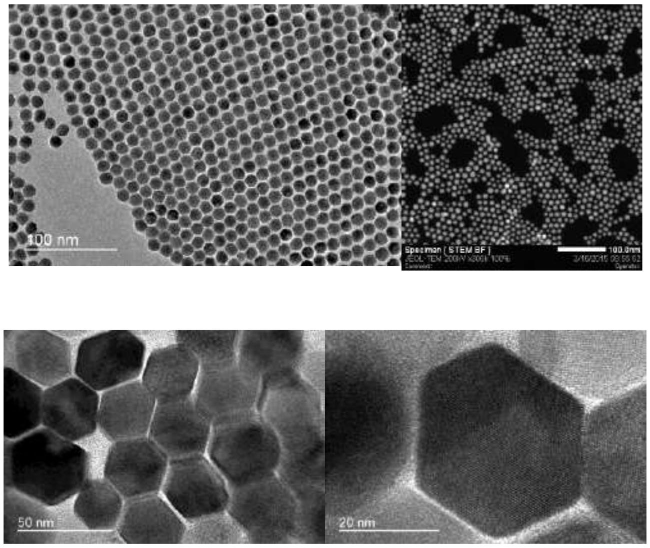

Figure 9. TEM images of the NaGdF$_4$:Yb, Er synthesized by the method of thermal decomposition with the temperature of 310 ℃

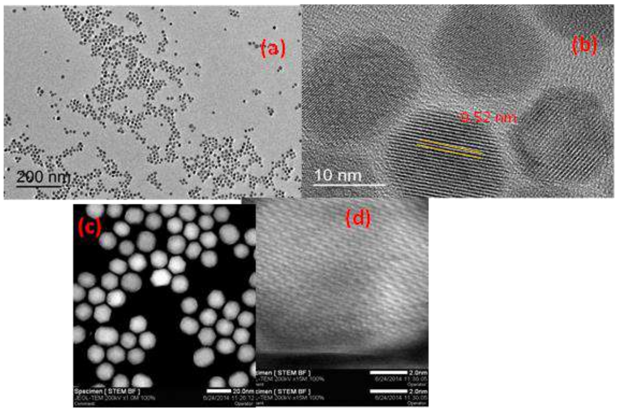

Figure 10. TEM and HAADF-STEM images of the NaGdF$_4$:Yb, Er synthesized by the method of thermal decomposition with the temperature of 290 ℃.

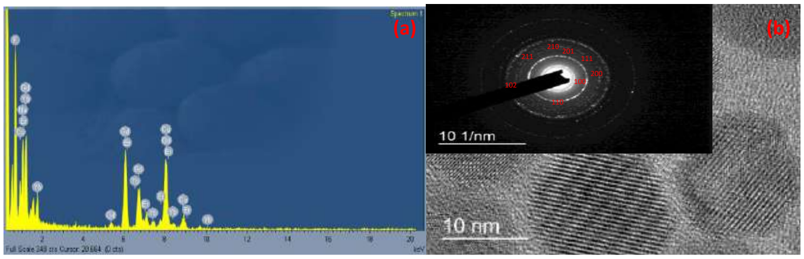

Figure 11. EDX of the $NaGdF_4$:Yb, Er, synthesized under the temperature of 290 ℃ in the method of thermal decomposition and the high-resolution TEM images and SAED patterns.

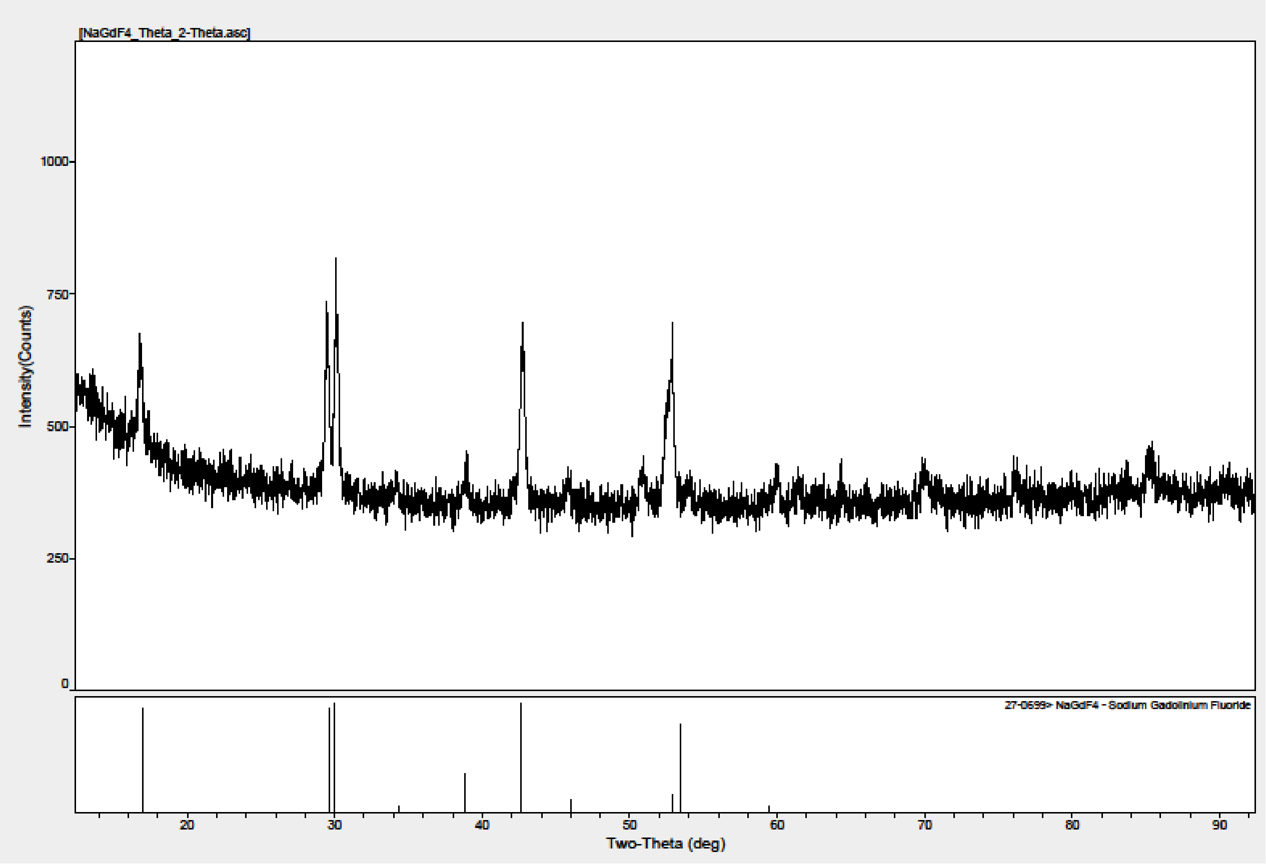

Figure 12. XRD patterns of the β-$NaGdF_4$:Yb, Er

For the characterization of the stabilization of the oleic acid, that is $CH_3(CH_2)_7CH=CH(CH_2)_7COOH$, the functional group could be characterized by FTIR [29]:

O-H stretching on 3450 cm $^{-1}$, C-H stretching on 2924,2854 cm $^{-1}$, O-H bending on 1640 cm $^{-1}$, C=O stretching on 1554 and 1458 cm $^{-1}$, as shown in Figure 13. And the oleate-capping on the UCNPs could be removed by HCl washing to avoid the quenching on the luminescent on the UCNPs.

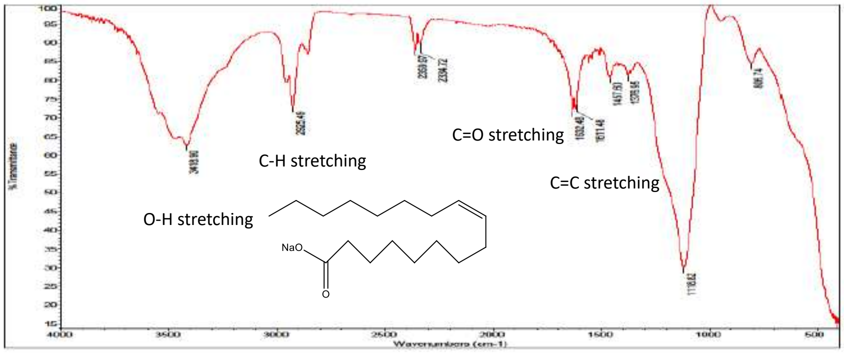

Figure 13. FTIR spectrum of the OA-$NaGdF_4$:Yb, Er

1.3.3. Characterization of the morphology, size and phase of the core-shell UCNPs

For the core-shell or the core-multishells UCNPs [29-36] have been developed rapidly in these years, to make definitive characterization on the core-shell or the core-multishells UCNPs is becoming increasingly vital. And here we would like to summarize the methods in the characterization on the size, phase, elements composition of the core-shell or core-multishells UCNPs with heterogeneous host matrices, such as $NaGdF_4$@$NaGdF_4$, $NaYF_4$@$NaYF_4$; and homogeneous host matrices, such as $NaGdF_4$@$NaYF_4$, $NaYF_4$@$NaGdF_4$, $NaGdF_4$@$NaYbF_4$.

For the core-multishells UCNPs with **homogeneous host matrices**, which is also called as **identical-UNCNPs**, that is the core and shell of the UCNPs are in exactly the same nanocrystals for the composition and phase. The characterization method could be concluded as: by the size growth, or the diverse of the morphology of the UCNPs when the phase of the core-shell layer is the same, that are all β- or α-; when the phase of the two layers are different, for example, with the α-core @ β-shell, the distance of the lattice is usually 0.32 nm for the α-phased nanocrystals and 0.52 nm for the α-phased nanocrystals, as summarized in Figure 14.

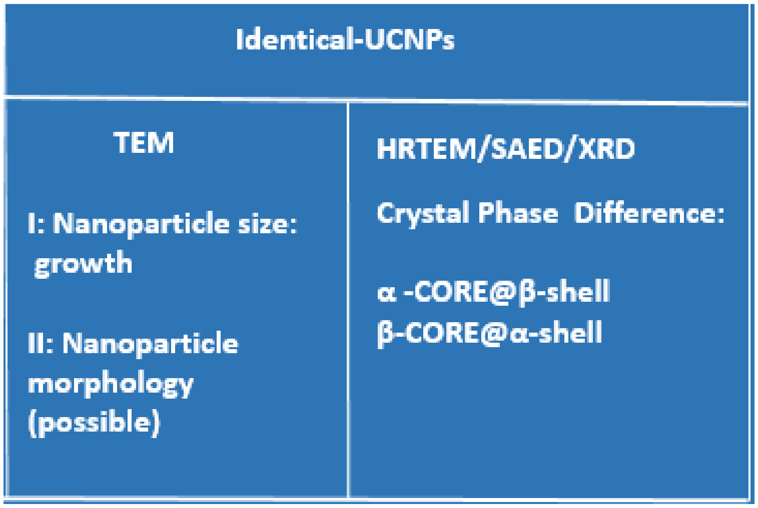

Identical-UCNPs	
TEM	HRTEM/SAED/XRD
I: Nanoparticle size: growth II: Nanoparticle morphology (possible)	Crystal Phase Difference: α -CORE@β-shell β-CORE@α-shell

Figure 14. Methods in characterization on the homogeneous UCNPs.

For example, as shown in Figure 15, in the synthesis of the core-multishells UCNPs, that we have discussed in Chapter 1 and Chapter 2, which is the gadolinium based-UCNPs core are coated with multiple shells with well design on the Yb^{3+} and Nd^{3+} doping to obtain the optimized luminescence performance. By the size growth, we would interpret the “layer by layer” epitaxial growth [29, 32, 35, 36] by the size growth:

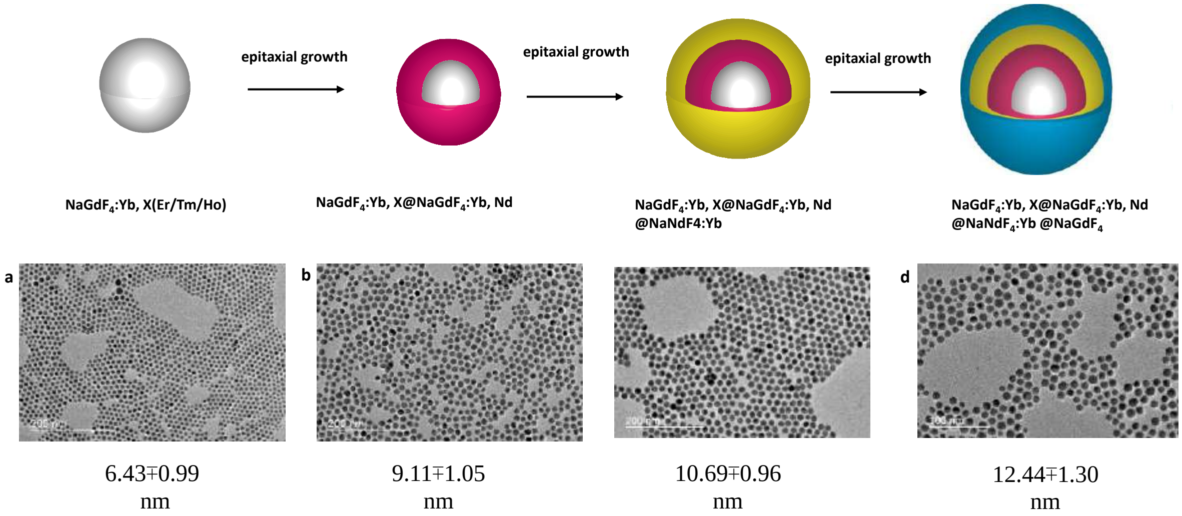

Figure 15. Epitaxial growth of the Nd^{3+}-Trinity system that coating on the $NaGdF_4$:Yb, Er cores.

For the core-multishells UCNPs with **heterogeneous host matrices**, which could also be called as **un-identical UCNPs**, the characterization of the core-shell structures could be generalized as: firstly, the observing the size growth and diverse of the morphology by TEM images; secondly, by HRTEM, XRD patterns to make sure the crystal phase and composition; thirdly, the HAADF-STEM, in the contrast of the bright field and the dark field, which is determined by the atomic number, could make sure the growth of the shell layer; lastly, the EELS-mapping or EELS line could further make sure of the element distribution.

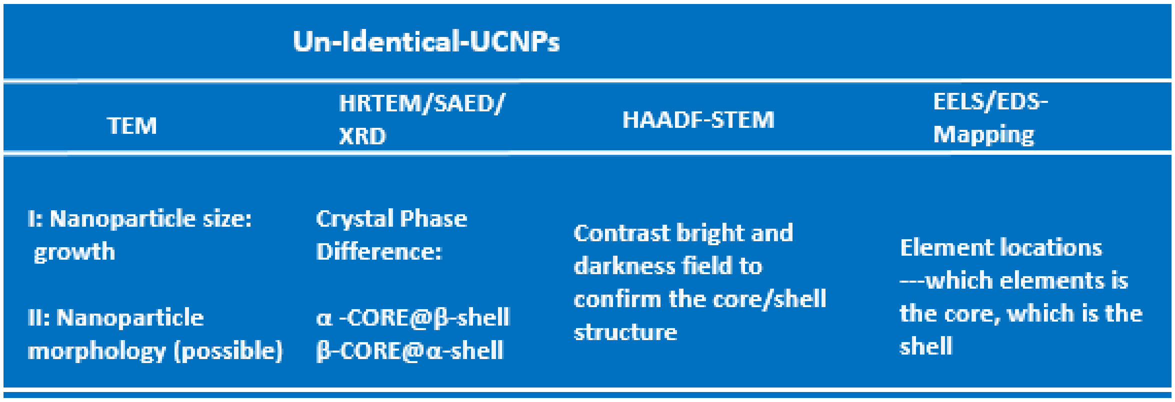

Un-Identical-UCNPs

TEM	HRTEM/SAED/ XRD	HAADF-STEM	EELS/EDS-Mapping
I: Nanoparticle size: growth II: Nanoparticle morphology (possible)	Crystal Phase Difference: α -CORE@β-shell β-CORE@α-shell	Contrast bright and darkness field to confirm the core/shell structure	Element locations ---which elements is the core, which is the shell

Figure 16. Methods in characterization of the homogeneous UCNPs.

Here, we would like to take example on characterization of the heterogeneous core-shell UCNPs, as shown in Figure 17.

a. in the characterization on the α-$NaGdF_4$:Yb,Er@β-$NaGdF_4$, for the core and the shell are composed of the α-/β- phased $NaGdF_4$ UCNPs, the distance of the lattice could be used to distinguish the α-phased $NaGdF_4$ and β-phased $NaGdF_4$ nanocrystals: 0.32 nm for the α-phase $NaGdF_4$ nanocrystals and 0.52 nm for the β-phased $NaGdF_4$ nanocrystals.

b. in the characterization of the $NaYF_4$@$NaGdF_4$ UCNPs, the technique that is HAADF-STEM plays an important role for by the contrast of the brightness and darkness, for the atomic numbers of yttrium is 39 which shows darkness field while for gadolinium is 64 which shows brighteness field.

c. another technique that could be used in $NaYF_4$@$NaGdF_4$ is the EELS mapping (or EELS line), as shown in Figure c. In our consideration, the EELS mapping or EELS lines illustrating on the element distribution, could further be utilized in the heterogeneous UCNPs that cannot be characterized by the HAADF-STEM, such as the $NaYbF_4$@$NaGdF_4$, for the atomic number of ytterbium is 72 while the atomic number of gadolinium is 64, with the difference is smaller than 12 that makes the contrast not obvious that cannot be used in the characterization.

d. similarly, in the characterization of $NaGdF_4@NaYF_4$, as shown in Figure 17, the brightness in the inner layer could characterized as $NaGdF_4$ while the darkness in the outer layer could be characterized as the coated $NaYF_4$.

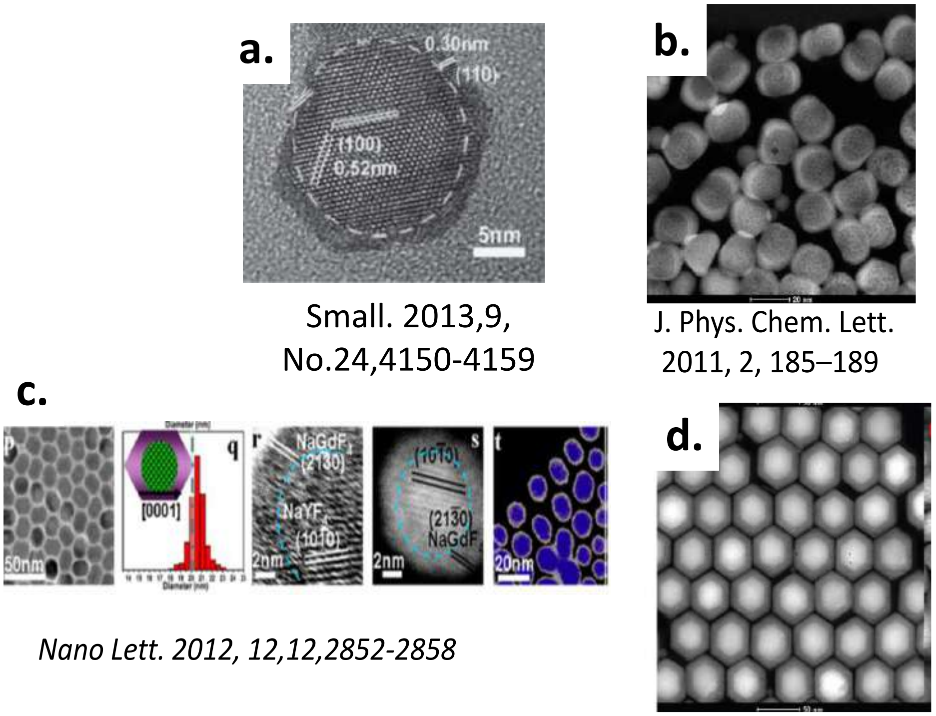

Small. 2013,9, No.24,4150-4159

J. Phys. Chem. Lett. 2011, 2, 185–189

Nano Lett. 2012, 12,12,2852-2858

Dalton Trans, 2014,43, 11299-11304

Figure 17. Literature: examples in characterization on the heterogeneous UCNPs**.**

Learnt from the previous work, we have utilized the characterization methods in our research work that is the synthesis of the core-shell or the core-multishells UCNPs, which is used to construct the newly designed UCNPs to obtain optimized luminescent performance:

For the synthesis of **$NaGdF_4$:Yb,Er@$NaYF_4$** UCNPs, which is the $NaGdF_4$ is used as the core, coating a layer which is $NaYF_4$ that synthesized by epitaxial growth, the images of HAADF-STEM EELS-mapping illustrating the success in synthesis. As shown in Figure 18, the TEM images (a-1, a-2) shown the size growth form sub-7 nm $NaGdF_4$:Yb, Er UCNPs by coating of the $NaYF_4$ layer to sub 10 nm. The images of HAADF-STEM (b-1, b-2), shows contrast on the brightness and darkness, which in details is the bright fields in the inner layer while the darkness field in the outer layer for the larger atomic number of gadolinium. Additionally, the EELS-lines (c-1,2,3,4) illustrating the element distribution that is the yttrium is in the broader range than the gadolinium.

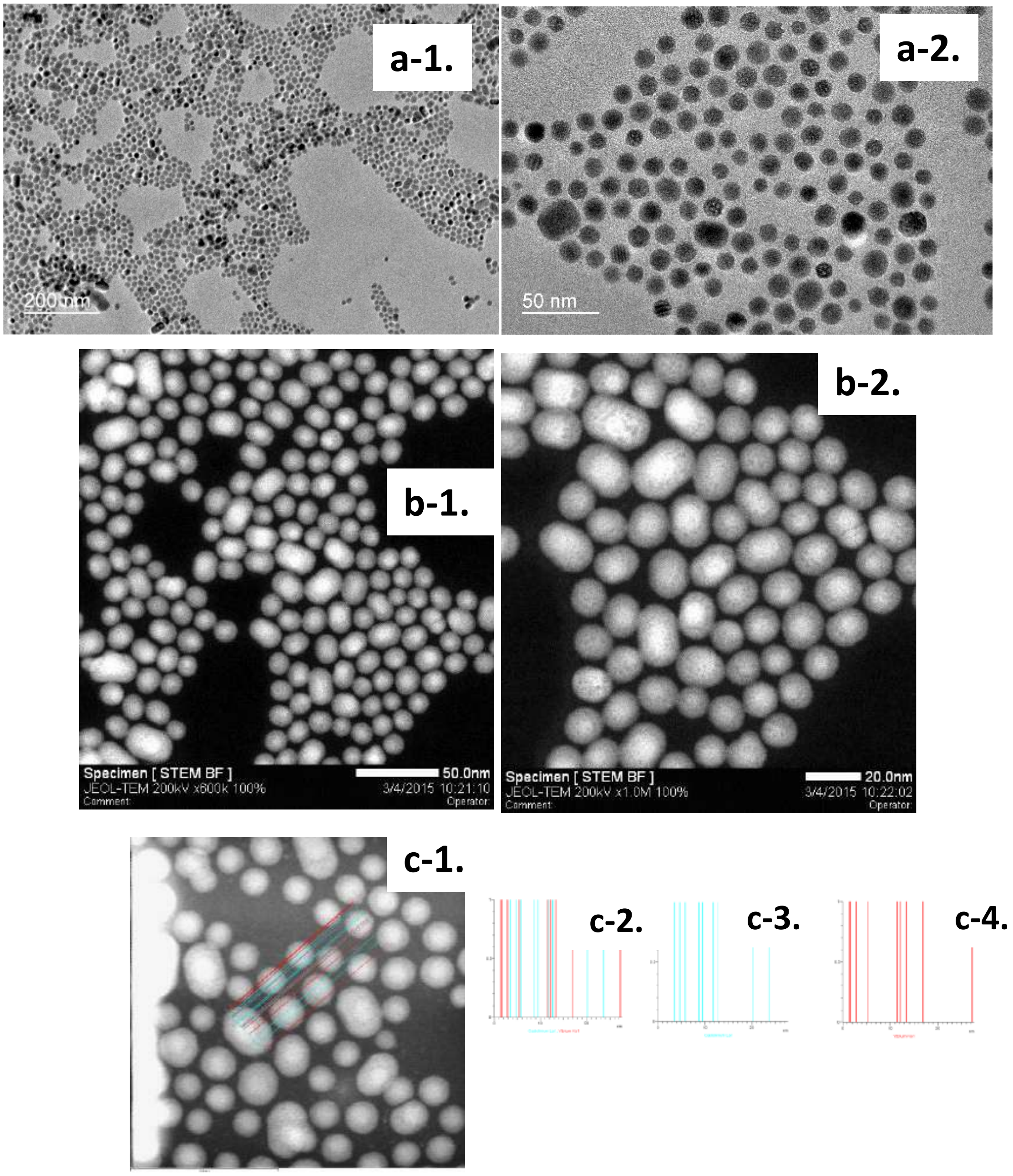

Figure 18. TEM images (a-1,2), HAADF-STEM (b-1,2) images and EDS-lines (c-1,2,3,4) of NaGdF$_4$:Yb,Er@NaYF$_4$ UCNPs. (c-1). Measuring scope; (c-2). Yttrium and Gadolinium lines; (c-3). Gadolinium lines; (c-4). Yttrium and Gadolinium lines

For the synthesis of **$NaYF_4$:Yb,Er@$NaGdF_4$** UCNPs, as shown in Figure 19, the TEM images (a) displays the sub-30 nm $NaYF_4$:Yb, Er nanocrystals coated with a thin layer of $NaGdF_4$, which could be depicted as the $NaYF_4$:Yb, Er that is the darkness that in the inner layer and the $NaGdF_4$:Yb, Er that is the brightness field in the outer layer in the HAADF-STEM images (b). And the EELS-lines (c-1,2,3,4) further illustrates the nano-structure which is the lines representing the Gd^{3+} ions wraps the lines represent the Y^{3+} ions. Also, the $NaYF_4$:Yb, Er coating with $NaGdF_4$, $NaNdF_4$ or $NaYbF_4$ coating on the $NaYF_4$:Yb, Er nanocrystals results in the anisotropic growth as we discuss in Chapter 4.

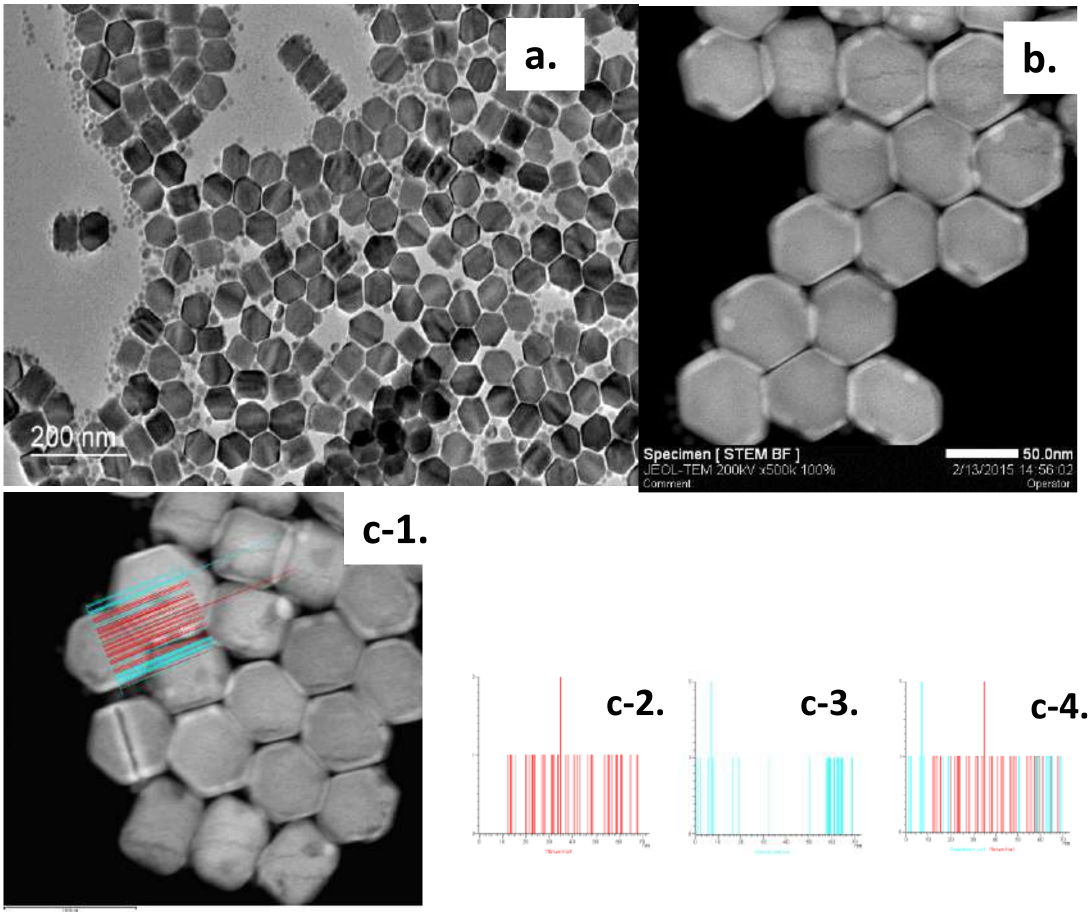

Figure 19. TEM images (a), HAADF-STEM (b) images and EDS-lines (c-1,2,3,4) of $NaGdF_4$:Yb,Er@$NaYF_4$ UCNPs. (c-1). Measuring scope; (c-2). Yttrium lines; (c-3). Gadolinium lines; (c-4). Yttrium and Gadolinium lines

For the synthesis of core-multishells UCNPs, which could be utilized in Nd^{3+}-sensitized UCNPs, as shown in Figure 20, when the $NaGdF_4$:$Yb_{20\,\%}$, $Er_{2\,\%}$ cores are coated with the transition layer, which is the $NaYF_4$:$Yb_{10\%}$,$Nd_{20\,\%}$, the $NaGdF_4$:$Yb_{20\,\%}$, $Er_{2\,\%}$ @ $NaYF_4$: $NaYF_4$:$Yb_{10\%}$,$Nd_{20\,\%}$ shows the size growth by the outer layer in darkness filed in the Figure of HAADF-STEM; $NaGdF_4$:$Yb_{20\,\%}$, $Er_{2\,\%}$@ $NaYF_4$: $NaYF_4$:$Yb_{10\%}$,$Nd_{20\,\%}$ @NaYF4, and the $NaGdF_4$:$Yb_{20\,\%}$, $Er_{2\,\%}$@ $NaYF_4$: $NaYF_4$:$Yb_{10\%}$,$Nd_{20\,\%}$@$NaGdF_4$, which is the transition layer coating with $NaGdF_4$ or $NaYF_4$, that further avoiding of the surface quenching, it could be characterized by the size growth; for the $NaYF_4$:Yb, Er nanocrystals, when coated with gadolinium-based transition layer, similar with the situation of the $NaYF_4$:Yb, Er@$NaGdF_4$ nanocrystals, shows the contrast of the darkness of the $NaYF_4$:Yb, Er cores and the brightness of the $NaGdF_4$ shells. Furthermore, when further coating a $NaGdF_4$ shells, the TEM images shows the size growth along with the more obvious overlapping the two bottom/end surfaces of the UCNPs; when further coating with $NaYF_4$ shells, the HAADF-STEM shows the cross of the contrast of the brightness and the darkness.

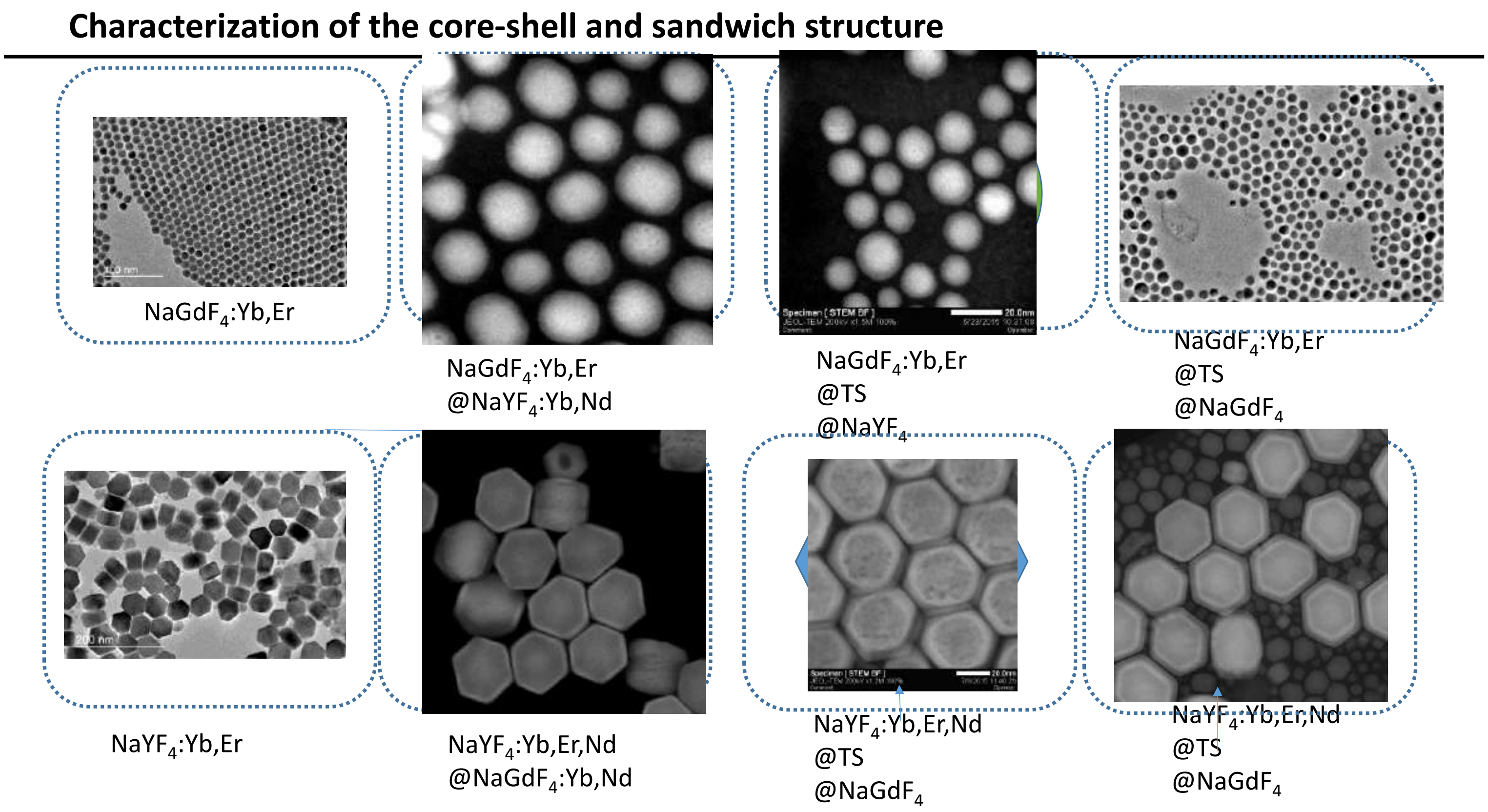

Figure 20. TEM and HAADF-STEM images of the core-mulitshells UCNPs by layer-by-layer epitaxial growth

Conclusion for the synthesis and characterization of the UCNPs

For the synthesis methods, we preferred the methods of thermal decomposition rather than hydrothermal, for the obtained UCNPs are uniform in size and in very well self-assemble. Moreover, it is beneficial in synthesis of the core-shell or the core-multishells UCNPs.

For the design of the nanostructures, we prefer the design of the core-shell or core-multishells UCNPs rather than the mono-cores for the core-shell design makes the UCNPs to shield the factors of quenching as possible. Furthermore, since the Nd^{3+}-sensitized UCNPs have been proved to be efficient in avoiding the over-heating effect, the core-multishells UCNPs shows advantages in construction of the Nd^{3+}-sensitized UCNPs to obtain preferred luminescent performance.

Compared with the previous work, we have successfully followed the methods in synthesis and characterization of the $NaGd/YF_4$ UCNPs as well as construction of the core-multishells UCNPs by the epitaxial growth, which will further contributes in the study of luminescent properties.

1.3.4. Characterization of luminescent properties

The final goal in our researches is to study and improve the luminescence properties of the UCNPs, including the luminescence performance by the emission spectra, the stability of the excited state by the lifetime decay, the upconversion efficiency by the fluorescence quantum yield, and the ratio of emission by the pulsed laser. Furthermore, we expect our UCNPs with specially design could be utilized in the application of bio-imaging.

Emission spectra: we have made modification on our Edinburgh Spectrometer (FLS 920) by conjugation of the 808 nm and 980 nm NIR laser in the optical source entrance, as shown in Figure 21.

Lifetime and pulsed laser induced emission spectra: the delay/pulsed generator that is the DG-535, is used to generalize the pulsed laser to measure the lifetime or measure the emission spectra with excitation of 980 nm or 808 nm pulsed laser.

Fluorescence quantum yield: conjugation of the 808 nm and 980 nm laser to the Edinburg Spectrometer (FLS 980), by the reflector and the focus lenses, makes the laser beam focused and entered in the integrating sphere. And the photons number of excitation and emission are measured to calculate the fluorescence quantum yield. What should be noted is that: to prevent the saturation of the PMT when the photons of excitation, an attenuator measure is used; when the fluorescence quantum yield with 808 nm excitation is measured, a correction on the NIR PMT and visible PMT is in need.

As shown in Figure 21, the as synthesized UCNPs are measured under the excitation of 808 nm or 980 c.w. laser, the luminescence performance could be interpreted by the intensity; and the location of the emission peaks depends on the energy levels of the activators; the emission photons numbers are reflected by the peak area of the emission spectra. And in Figure 21, it could be seen that the emission spectra has on one hand reflected the variation of the emission when coating with shell layers with excitation of 980 nm and 808 nm laser; on the other hand, it reveals the success of synthesis of the Nd^{3+}-sensitized UCNPs.

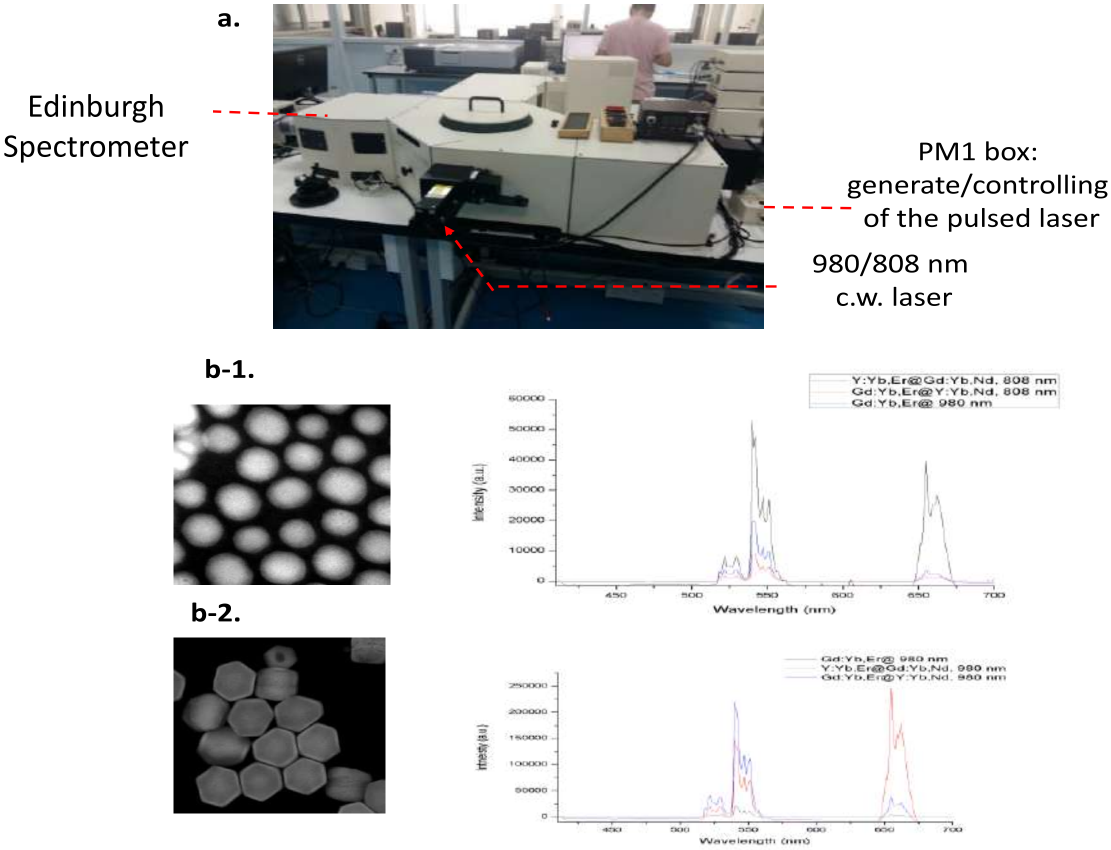

Figure 21. Modification on the Edinburgh spectrometers (a) and characterization of the luminescent properties of core-shell UCNPs with emission spectra (b-1,2).

1.4. Nd^{3+}-sensitized, 795/808/800 nm excited Upconversion Nanoparticles (UCNPs)

1.4.1. Over-heating effect

As it is known that the over-heating effect [37] of the 980 nm laser (as shown in Figure 22), which is proposed be resulted from the water abosorbing of the 980 nm photons, and leading to the violent rising of the temperature of water, which causes potential hazards to the cell and tissues when the UCNPs are utilized as the nanoprobe in bio-imaging: as reported by Prof. X.G. Liu's group, the 980 nm laser shows hazards to the cells and tissues, which is proved by the HeLa cells that irradiated by 980 nm and 808 nm laser for a certain time, with approving that the 980 nm laser killing most of the HeLa cells [28]; as reported by Prof. Chun-Hua Yan's group, when the tissues are exposed under the radiation of 980 nm and 808 nm laser, the temperature shows violent rising under 980 nm radiation which is about 10 ℃ in 50 seconds in contrast with there is almost no change under 808 nm radiation, as shown in Figure 23. [17]

Ref:

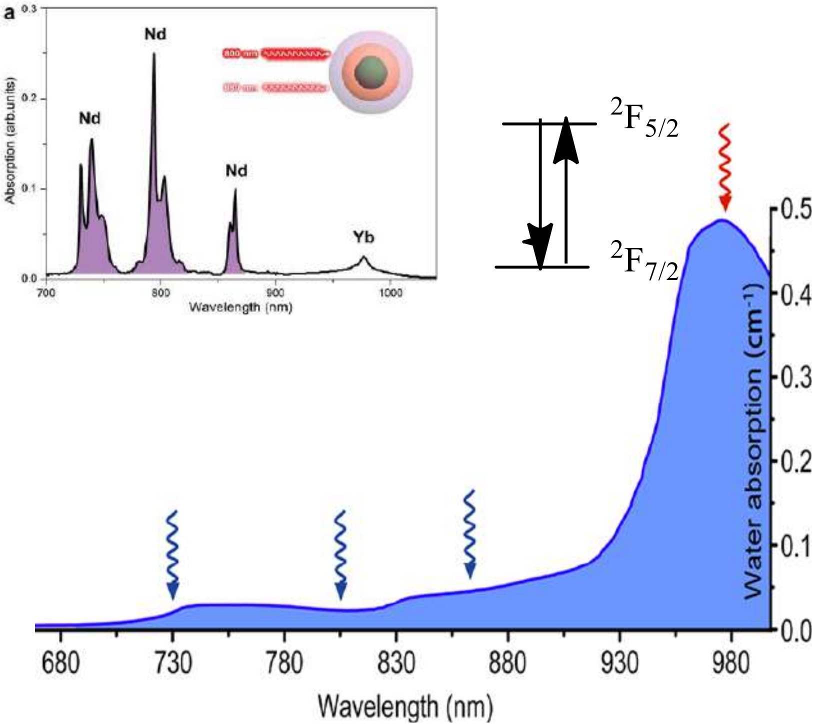

Figure 22. Water absorption of the photons, from 680 -1000 nm. [17]

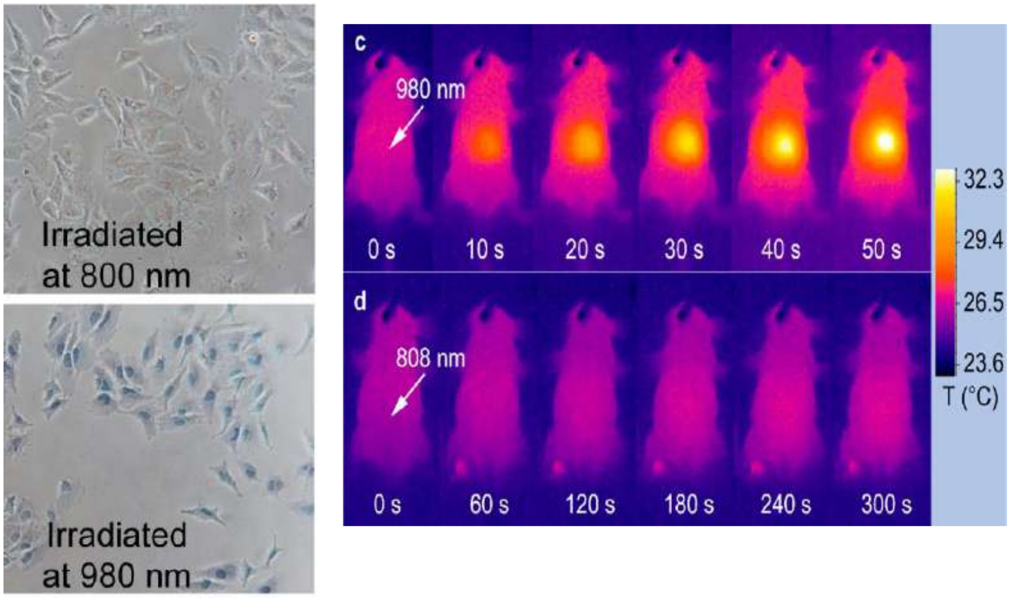

Figure 23. Over-heating effect of the 980 nm laser shows hazards on the cells (a) and (b) [28] and tissues(c) and (d) [17].

1.4.2. Attenuation of the photoluminescence source

As shown in Figure 24, water absorption not only cause the over-heating effect but also the large attenuation of the photo-luminescence source.

Ref:

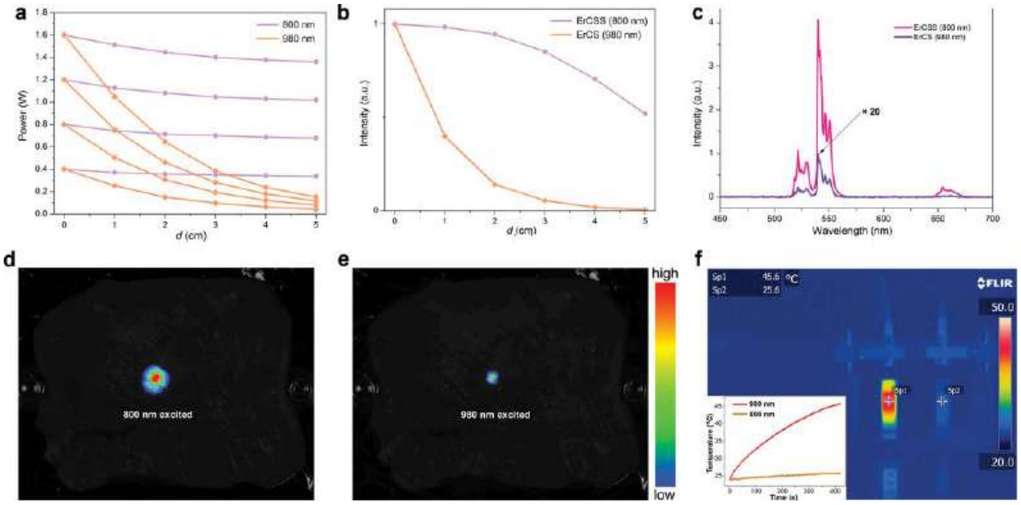

Figure 24. Photo-luminescence source attenuation of the 980 nm laser. [15]

1.4.2. Nd^{3+}-sensitized UCNPs: design, mechanism and advantages of the Nd^{3+}-sensitized UCNPs

The basic mechanism of the Nd^{3+}-sensitized UCNPs could be concluded : the Nd^{3+} ions absorbs the 808/800/795 nm photons, and then transfer to Yb^{3+} ions by $Nd^{3+}\rightarrow Yb^{3+}$ energy transfer with high efficiency that is ~ 70 % as reported [38-46]. Then the Yb^{3+} ions transfer energy to activators such as the Er^{3+}, Tm^{3+} and Ho^{3+}, that is sensitization of the activators. [15-18, 21, 28, 37, 47-54]

Also, the direct proof for the $Nd^{3+}\rightarrow Yb^{3+}$ energy transfer is shown in Figure 25, when the $NaYF_4$:Nd is excited by 795 nm laser, the Nd^{3+} ions shows long lifetime at 864 nm; with

Yb^{3+} ions doping, the Nd^{3+} shows shortened lifetime at 864 nm. The phenomenon reveals the existence of the $Nd^{3+}\rightarrow Yb^{3+}$ energy transfer. Furthermore, the $Nd^{3+}\rightarrow Yb^{3+}$ energy transfer are affected by surface quenching of Yb^{3+}, for the surface coating that is the $NaYF_4$ on the $NaYF_4$:Nd/Yb, makes the Yb^{3+} shows prolonged lifetime.[28]

Ref:

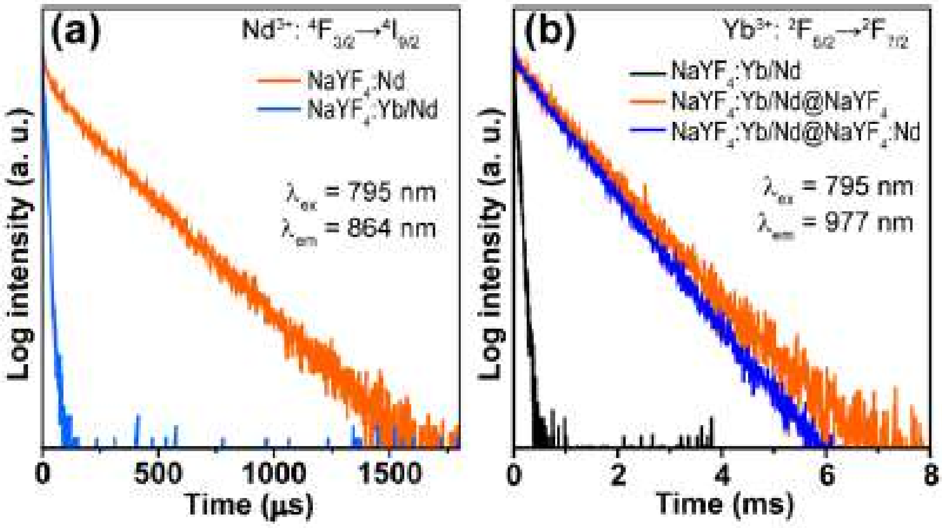

Figure 25. Decay curves of the Nd^{3+} and Yb^{3+}, which reveals the $Nd^{3+}\rightarrow Yb^{3+}$ energy transfer. [28]

The Nd^{3+}-sensitized UCNPs with 795/800/808 nm excitation have shown advantages rather than the Yb^{3+}-sensitized UCNPs with excitation of 980 nm laser, for the reasons that (as summarized in Table 2):

a. the over-heating effect avoiding when the UCNPs has are excited by 808 nm laser; with deeper penetration of the emission for the enhanced luminescence intensity and the attenuation of the photo-luminescence source avoiding;

b. higher absorption of the Nd^{3+} ions to 808 nm photons, which is $1.2*10^{-19}$ cm^{2}, than the Yb^{3+} ions to 980 nm photons, which is $1.2*10^{-20}cm^{2}$. Also, the Nd^{3+}→Yb^{3+} energy transfer are in very high efficiency. Thus, the Nd^{3+}-sensitized UCNPs shows advantages in luminescence performance.

c. with larger partition of red emission of the activators, which has been reported by Prof. X.G. Liu, is preferred in the utilization bio-imaging. And in our research, we just propose it is affected by the Nd^{3+}-Er^{3+}/Tm^{3+}/Ho^{3+} cross-relaxation, which makes PA (photon avalanche) process prone to emit the red emission;

d. by the measurement of the lifetime decay curves of emission bands, we found that the Nd^{3+}-sensitized UCNPs shows prolonged lifetime, which is preferred in the utilization, such as the FRET bio-sensor.

Items **Photo-Luminescence source**	**Absorption Band (nm)**	**Intensity (Absorption cross section)**	**Over-heating effect**	**Photo-luminescence source Attenuation by water**	**Luminescence Penetration**
980 nm NIR Laser Yb^{3+}	980	$1.2*10^{-20}cm^{2}$	Serious	Serious	Attenuated
800 nm NIR Laser Nd^{3+}-Yb^{3+}	808, (730, 870)	$1.2*10^{-19}$ cm^{2} (Nd^{3+} to Yb^{3+} ET:~75 %)	NONE	NONE	Deeper

Table 2. Comparison of the Yb^{3+}-sensitized UCNPs and Nd^{3+}-sensitized UCNPs.

1.4.3. The strategies in construction of the Nd^{3+}-sensitized UCNPs

The basic principles in the construction of the Nd^{3+}-sensitized UCNPs in our research work are the three most commonly used mechanism of upconversion [3-8, 19, 28, 29], as shown in Figure 26:

a. **Yb^{3+}-sensitized, Yb^{3+}→$X(Er/Tm/Ho)^{3+}$:** which could be illustrated as Yb^{3+} ions act as the activator that absorb the 980 nm photons, by populated the Yb^{3+}

$^2F_{5/2}$→$^2F_{7/2}$, and transfer energy to activator by Yb^{3+} $^2F_{7/2}$, which is the Yb^{3+}-sensitization. With the ESA process, the exited states of the activators are populated; with the PA process, the activators emit emission with the non-radiative transition.[19]

b. **Energy migration upconversion (EMU) system:** which is by Yb^{3+} sensitization [29] that sensitize the accumulator that is Tm^{3+} ions; by Tm^{3+} accumulation which is absorbs 5 phonons that populate the Tm^{3+}; the migrators that is Gd^{3+} ions are excited by the Tm^{3+} and migrated the energy by $^6P_{7/2}$ (~31000 cm^{-1}); the activators that are Eu^{3+}, Tb^{3+}, Sm^{3+} and Dy^{3+}, were excited with emitting of emission..

c. **Nd^{3+}-sensitized, Nd^{3+}→Yb^{3+}→$X(Er/Tm/Ho)^{3+}$:** Nd^{3+} ions absorbs the 795/800/808 nm photons and transfer energy to Yb^{3+} that is Nd^{3+}→Yb^{3+} energy transfer (as discussed in Chapter 2), which is the Nd^{3+}-sensitization. And Yb^{3+} transfer energy to activators ($Er^{3+}/Tm^{3+}/Ho^{3+}$), which is the same with Yb^{3+}-sensitized, Yb^{3+}→$X(Er/Tm/Ho)^{3+}$.[28]

The main goal of our research work is to construct the Nd^{3+}-sensitized UCNPs with optimized luminescence properties, that could be further used in bio-imaging in the tumor diagnosis. The main idea is that to combine the Nd^{3+}→Yb^{3+} system with 808 nm excitation with the Yb^{3+}-$X(Er/Tm/Ho)^{3+}$ and the EMU system with activators of Eu^{3+} and Tb^{3+} with specially design to realize the Nd^{3+}→Yb^{3+} energy transfer, Yb^{3+}→Yb^{3+}(~ 10250 cm^{-1}) and the Gd^{3+}→Gd^{3+} (~ 31000 cm^{-1}) energy bridge with high efficiency, which further result in preferred luminescence performance; the specific method to optimize the composition of the UCNPs is by adjusting the composition of the UCNPs, which is characterized by the emission spectra.

What should be paid specially attention is that the all the potentially quenching factors in the Nd^{3+}-sensitized UCNPs, which we have done numerous investigation, and concluded to be: Yb^{3+}-$X(Er/Tm/Ho)^{3+}$ cross-relaxation, and the Nd^{3+}-$X(Er/Tm/Ho)^{3+}$ cross-relaxation, which is the work of construction the Nd^{3+}-sensitized UCNPs should focus on. And the basic strategies could be concluded as “isolation”, “doping” and “remedy”.

Isolation, is commonly used to isolate the high concentration of Nd^{3+} ions with the activators including Er^{3+}, Tm^{3+}, Ho^{3+}, Eu^{3+} and Tb^{3+} by sandwich a transition layer that is $NaGdF_4$:Yb and $NaYF_4$:Yb to segregate them.

Doping, is commonly used to build the $Yb^{3+} \rightarrow Yb^{3+}$ energy bridge by doping certain amount of Yb^{3+} ions in each layer of the core-multishells of the Nd^{3+}-sensitized UCNPs.

Remedy, is commonly used to shield the surface quenching of Yb^{3+} which is caused by the F^- vacancy on the surface of the nanocrystals, which is wrapping a $NaGdF_4$ or $NaYF_4$ shell on the UCNPs.

Ref:

Upconversion Mechanism

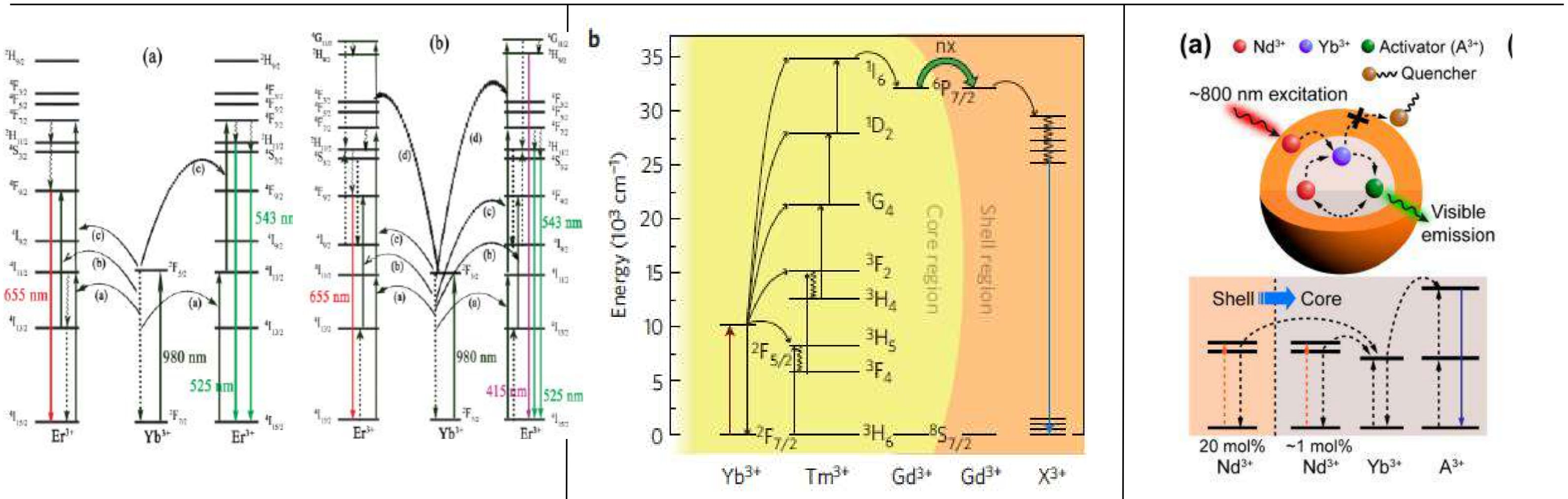

Excitation : 980 nm laser

Activator :Er^{3+} , Tm^{3+} , Ho^{3+}

Sensitizer: Yb^{3+}

J. Phys. Chem. C, Vol. 111, No. 37, 2007

Excitation : 980 nm laser

Activator :Eu^{3+} , Tb^{3+}

Sensitizer: Yb^{3+}

NATURE MATERIALS, 2011, 10, 968–973

Excitation : 808/980 nm laser

Activator :Er^{3+} , Tm^{3+} , Ho^{3+}

Sensitizer: Yb^{3+} , Nd^{3+}

J. Am. Chem. Soc. 2013, 135, 12608–12611

Figure 26. The summarization of the basic mechanism in upconversion materials [19, 28, 29]

1.4.4. Recent progress of the Nd^{3+}-sensitized UCNPs

As shown in Figure 27, since the Nd^{3+}-sensitized UCNPs are invented in the year 2013, by the group of Prof. X.G. Liu, as we have discussed above, with enhanced luminescence and larger partition of red emission by sensitization of the activator (Er^{3+}/Tm^{3+}/Ho^{3+}), there has been variations of the Nd^{3+}-sensitized UCNPs.[28] As shown in Figure 27, Professor Jun Lin's group has developed the $NaYF_4$:Yb,Er@$NaYF_4$:Nd system to utilized in the drug delivery by coating the $mSiO_2$ with DOX; Professor Chun-Hua Yan's group, has established the photo-sensitive UCNPs with ultraviolent emission by excitation of 980 nm laser while green and red emission by 808 nm laser with the special design. Also, the gadolinium-based Nd^{3+}-sensitized UCNPs has also been invented.

Ref:

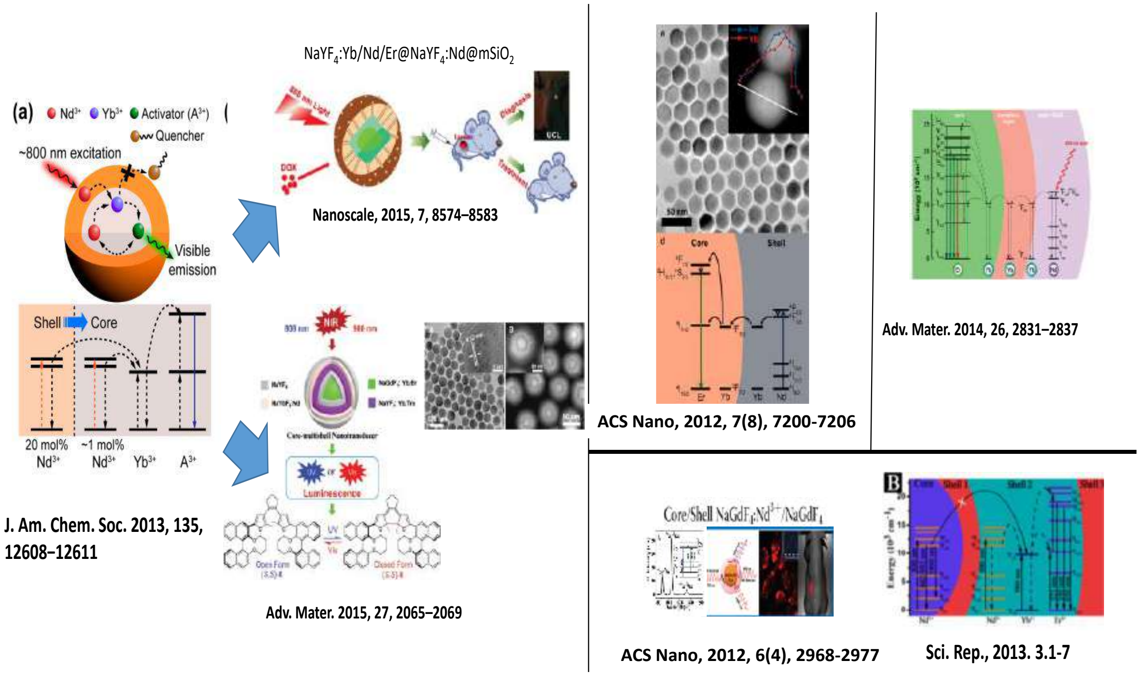

J. Am. Chem. Soc. 2013, 135, 12608–12611

Nanoscale, 2015, 7, 8574–8583

Adv. Mater. 2015, 27, 2065–2069

ACS Nano, 2012, 7(8), 7200-7206

Adv. Mater. 2014, 26, 2831–2837

ACS Nano, 2012, 6(4), 2968-2977

Sci. Rep., 2013. 3.1-7

Figure 27. Recent progress of the development of the Nd^{3+}-sensitized UCNPs

Moreover, there have been reports on the Nd^{3+}-Yb^{3+} sensitized Tb^{3+} and Eu^{3+} systems with excitation of 808 nm laser, with green and red emission, as shown in Figure 28. [55]

Ref:

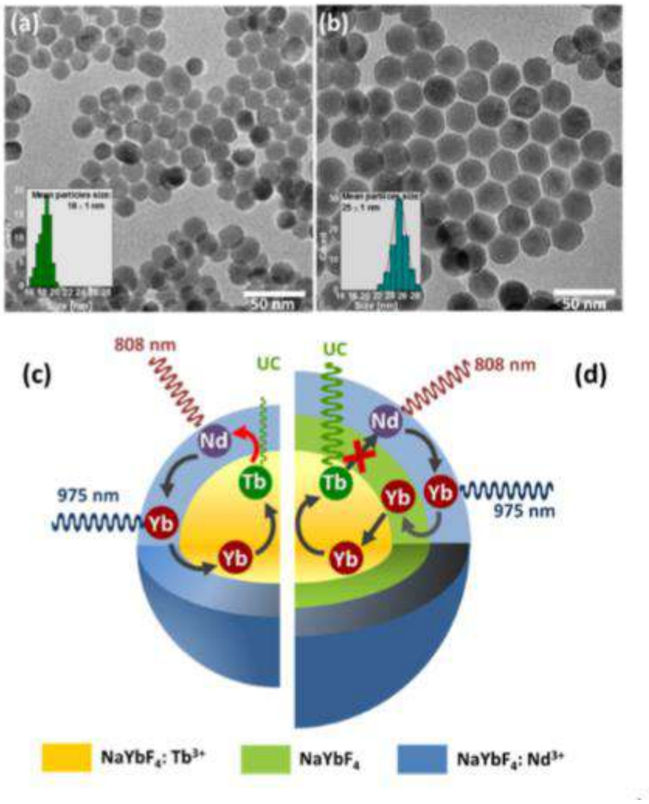

Figure 28. Nd^{3+}-Yb^{3+} sensitized Tb^{3+} and Eu^{3+} system. [55]

Furthermore, the quenching caused by Nd^{3+} ions has drawn attention, which could be illustrated as affected by the Nd^{3+}-Er^{3+}/Tm^{3+}/Ho^{3+} cross relaxation, a sandwich structure is invented to segregated the activator with the high concentration of Nd^{3+} ions. And further it shows enhanced luminescence intensity.

Additionally, the Nd^{3+} NIR emission, which are induced by the Nd^{3+} down-conversion has also been utilized in the construction of the nanoprobe. Also, the dual-model Nd^{3+}-

sensitized UCNPs has been invented which combine the upconversion and down-conversion in the same system.

The Nd^{3+}-sensitized UCNPs has shown their advantages in utilization, including being used as the nanoprobe in bio-imaging and carrier in drug delivery.

1.4.5. Limitations of the development of the UCNPs and luminescence of the previous work

Still, there are problems that limit the development of the UCNPs, which could be generalized as:

a. **The saturation effect of the UCNPs**: the saturation effect of the UCNPs are caused by the saturated luminescence center, which could be illustrated as high absorption and transferring of the 980 nm photons, that is why the luminescence intensity is not always enhanced with the increase of the power density [56, 57]. When the situation come to the 808 nm excitation, the saturation effect appears more violently for the higher absorption of the 808 nm laser , that should be attributed to the high absorption of the Nd^{3+} ions to 808 nm laser as well as the more violent cross-relaxation caused by Nd^{3+} or Yb^{3+} .

b. **The low upconversion efficiency**: there exits difficulties in meausuring the florescent quantum yield, which reveals the efficiency of upconversion . Since the difficulties have been settled with the development of the technique, there has been more and more reports on the florescent quantum yield of the UCNPs, there is growing recognition that the upconversion material is the one with very low upconversion efficiency, the highest one that reported is only 0.8 % (with 808 nm excitation)compares with others. [21, 58, 59] And the one that we have achieved is 0.42 % with 808 nm excitation and 980 nm excitation.

c. **The much more complex situation of quenching in the whole Nd^{3+}-sensitized system**: as reported by Y.T. Zhong *et al.*, the conspicuous Nd^{3+}-Er^{3+} cross-relaxation [15] along with other quenching factors including: cross-relaxation between Nd^{3+} and other activators including Tm^{3+} and Ho^{3+}, the cross-relaxation between the activators is why the concentration of the activators should be limited to be very low; the cross-relaxation between Yb^{3+} and activators (Er^{3+}/Tm^{3+}/Ho^{3+}) caused by very high concentration of Yb^{3+} and Yb^{3+} surface quenching.

In our view mind, the Nd^{3+}-$X(Er/Tm/Ho)^{3+}$ cross-relaxation could be settled with sandwich a transition layer to segregate the activators with Nd^{3+} ions; the Yb^{3+}-$X(Er/Tm/Ho)^{3+}$ cross-relaxation: for the situation that caused by high concentration of Yb^{3+}, could be settled by adjusting the Yb^{3+} concentration; for the situation of surface quenching, could be settled by the surface coating to remedy the surface defect caused by F^- vacancy.

However, the real "bottleneck" of the development of the UCNPs is the concentration of the activators, for the high concentration of the activators will cause violent cross-relaxation. To deal with the problems, there should be more research work on the modification of the nanocrystals, which transfers energy by the lattice vibration, thus trying to obtain the more preferred host matrices for UCNPs.

d. **The anisotropic epitaxial growth of the UCNPs**

The core-multishells UCNPs are synthesized by the method of layer-by-layer epitaxial growth, which could be illustrated as the outer layer should be efficiently coated on the inner layer, to realize the design of segregation, doping or remedy as the strategies we discussed above.

However, we have found that the anisotropic growth of the Nd^{3+}-trinity system in our shows anisotropy that further influence the luminescence performance as well as the upconversion efficiency.

Here comes to the conclusion that, for further utilization of UCNPs, what we should focus on in our research work is that:

a. To elevate the upconversion efficiency, the possible quenching factors should be shielded as possible;
b. The growth principles of the core-multishells of the Nd^{3+}-sensitized UCNPs
c. The investigation on the mechanism of the Nd^{3+}-sensitization are required.

1.5. Generalization of the magnetism of the gadolinium-based UCNPs

The gadolinium nanoparticles have the potential to be used as the MRI contrast agent. Here, we have summarized the factors of r_1, as shown in Figure 29, for the value of T1, is effected by the inner sphere, second sphere and outer sphere.

For the inner sphere, as shown the equation for calculation the r_1^{IS} for nanoparticles, the diameter determine factor, which could be understood as: with larger diameter of the nanoparticles, with smaller value of of r_1^{IS}; with smaller diameter of the nanoparticles, with larger value of of r_1^{IS}.

For the second sphere and the outer sphere of the nanoparticles, that are determined by the surfactant, that is the ability of binding water of the polymers such as PEG with –OH and PEI with -NH_2 group, which could bind water by hydrogen bonds. [60, 61]

Ref:

The inner–sphere longitudinal relaxivity is given by equation 1.19:

$$r_{1,inner-sphere} = \frac{Cq}{55.6}\frac{1}{T_{1m}+\tau_m} \qquad (1.19)$$

where

$r_{1,inner-sphere}$	is the longitudinal inner–sphere relaxivity of the CA.
C	is the molar concentration of the paramagnetic compound.
q	is the hydration number (water molecules that directly coordinate to the Gd(III) ion centre).
τ_m	is the residency lifetime of bound water molecules.
T_{1m}	is the longitudinal relaxation time of bound water molecules, this parameter also depends on electron relaxation time (T_e), rotational correlation time (τ_R) and τ_m.

Tumbling time of the NPs (τ_R)

$$\tau_R = 4\pi\eta a^3/3k_BT$$

$$r_1^{obs} = \overset{\text{Inner-sphere}}{r_1^{IS}} + \underset{\text{Second-sphere}}{r_1^{SS}} + \overset{\text{Outer-sphere}}{r_1^{OS}}$$

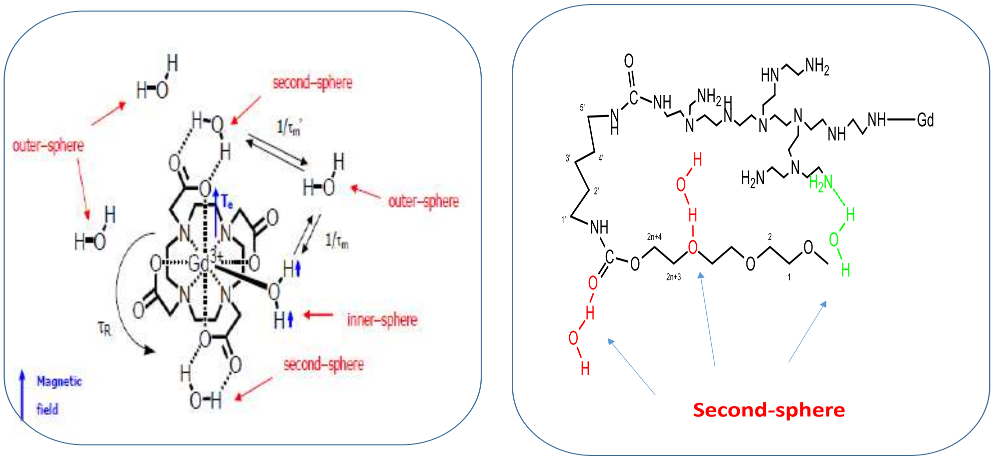

Scheme: Interaction between Gd-DOTA and coordination sphere

Scheme: Interaction between Copolymer conjugated Gd^{3+} -based nanoparticle and coordination sphere

Figure 29. Factors on the relaxivity of the gadolinium-based nanoparticles.

Thus, the factor that affect the r_1 value of the nanoparticles could be generalized as the size and the polymer's binding water. As shown in Figure 30, with larger size of the NaGdF4 nanoparticles, with smaller value of r_1, which illustrates the size effect on the relaxivity; as shown in Figure 31, the surfactant of PVP or PEG shows larger r_1 value which illustrating the effect of polymer on the relaxivity.

Ref:

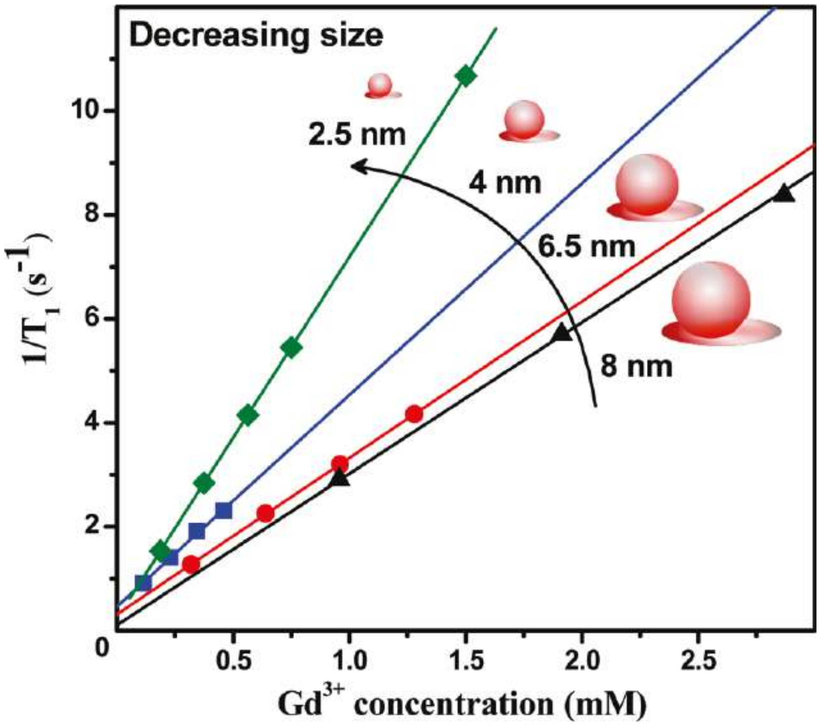

Figure 30. Effect of the size on r_1 relaxivity of the gadolinium-based nanoparticles. [62]

Ref:

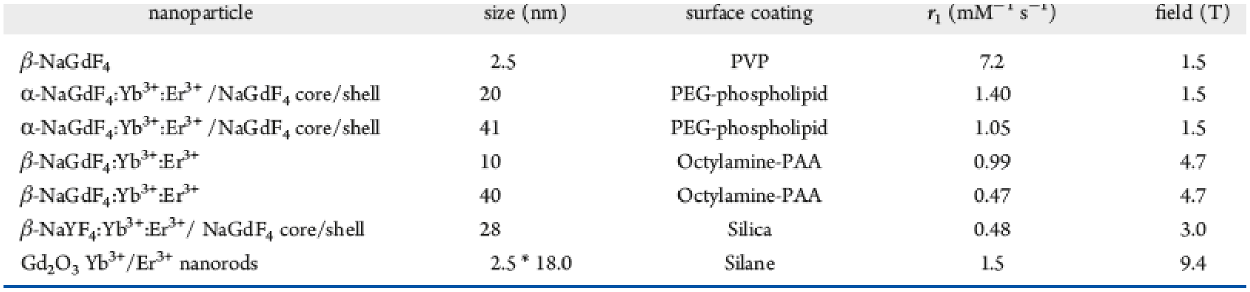

nanoparticle	size (nm)	surface coating	r_1 (mM^{-1} s^{-1})	field (T)
β-$NaGdF_4$	2.5	PVP	7.2	1.5
α-$NaGdF_4$:Yb^{3+}:Er^{3+} /$NaGdF_4$ core/shell	20	PEG-phospholipid	1.40	1.5
α-$NaGdF_4$:Yb^{3+}:Er^{3+} /$NaGdF_4$ core/shell	41	PEG-phospholipid	1.05	1.5
β-$NaGdF_4$:Yb^{3+}:Er^{3+}	10	Octylamine-PAA	0.99	4.7
β-$NaGdF_4$:Yb^{3+}:Er^{3+}	40	Octylamine-PAA	0.47	4.7
β-$NaYF_4$:Yb^{3+}:Er^{3+}/ $NaGdF_4$ core/shell	28	Silica	0.48	3.0
Gd_2O_3 Yb^{3+}/Er^{3+} nanorods	2.5 * 18.0	Silane	1.5	9.4

Figure 31. Effect of the surfactant and size on the gadolinium-based nanoparticles.[62]

1.6. Generalization of the research and structure of the thesis

We have developed the Nd^{3+}-harvest-transfer-sensitization trinity system to optimize the luminescent properties of the UCNPs, including the Yb-X(Er/Tm/Ho)$^{3+}$ system and the Energy Migration Upconversion system by layer by layer epitaxial growth , that is called core-multishells UCNPs. The Nd^{3+}-trinity system driven Yb^{3+}-X(Er/Tm/Ho)$^{3+}$ or EMU system shows superior luminescent properties, including the largely enhanced luminescence, prolonged lifetime, deeper penetration, larger partition of red emission (for Er^{3+} and Tm^{3+}) and high quantum yield. Also, we found the principle of the anisotropic growth of the Nd^{3+}-trinity system. The research could be depicted in details:

a. the Nd^{3+}-trinity system, which is composed of the transition layer, optimized harvest layer and the activation layer, are coating on the $NaGdF_4$:Yb,Er/Tm/Ho cores, result in UCNPs minimized size, largely enhanced luminescence, prolonged lifetime, deeper penetration, larger partition of red emission (for Er^{3+} and Tm^{3+}) and high quantum yield (Chapter 2).

b. Nd^{3+}-trinity system coated EMU system, which is the EMU system with excitation of 808 nm laser, with enhanced luminescence, deeper penetration and prolonged lifetime and over-heating effect. (Chapter 3).

c. the Nd^{3+}-trinity system is coating on the yttrium based UCNPs cores, that is $NaYF_4$:Yb,Er/Tm/Ho, result in incomplete coating and extrusion of the yttrium based UCNPs cores, which influence on the optical properties (Chapter 4).

d. the development of the Luminescent Janus nanoparticles with excitation of 980 nm and 808 nm, that with the tenability of emission colors. (Chapter 5).

References

1. Bünzli, J.-C.G., *Lanthanide Luminescence for Biomedical Analyses and Imaging.* Chemical Reviews, 2010. **110**(5): p. 2729-2755.
2. Han, S., R. Deng, X. Xie, and X. Liu, *Enhancing Luminescence in Lanthanide-Doped Upconversion Nanoparticles.* Angewandte Chemie International Edition, 2014. **53**(44): p. 11702-11715.
3. Chen, G., H. Qiu, P.N. Prasad, and X. Chen, *Upconversion Nanoparticles: Design, Nanochemistry, and Applications in Theranostics.* Chemical Reviews, 2014. **114**(10): p. 5161-5214.
4. Dong, H., L.-D. Sun, and C.-H. Yan, *Energy transfer in lanthanide upconversion studies for extended optical applications.* Chemical Society Reviews, 2015. **44**(6): p. 1608-1634.
5. Ramasamy, P., P. Manivasakan, and J. Kim, *Upconversion nanophosphors for solar cell applications.* RSC Advances, 2014. **4**(66): p. 34873-34895.
6. Wang, C., L. Cheng, and Z. Liu, *Drug delivery with upconversion nanoparticles for multi-functional targeted cancer cell imaging and therapy.* Biomaterials, 2011. **32**(4): p. 1110-1120.
7. Wang, F., D. Banerjee, Y. Liu, X. Chen, and X. Liu, *Upconversion nanoparticles in biological labeling, imaging, and therapy.* Analyst, 2010. **135**(8): p. 1839-1854.
8. Wang, M., C.-C. Mi, W.-X. Wang, C.-H. Liu, Y.-F. Wu, Z.-R. Xu, C.-B. Mao, and S.-K. Xu, *Immunolabeling and NIR-Excited Fluorescent Imaging of HeLa Cells by Using* $NaYF_4$*:Yb,Er Upconversion Nanoparticles.* ACS nano, 2009. **3**(6): p. 1580-1586.
9. Britannica, T.E.o.E. *photon*. 2016 [cited 2017 11,04,2017]; Available from: https://global.britannica.com/science/photon.
10. Perkowitz, S. *phonon*. 2009 [cited 2017 11 , 04 , 2017]; Available from: https://global.britannica.com/science/phonon.

11. Jin, J., Z. Xu, Y. Zhang, Y.-J. Gu, M.H.-W. Lam, and W.-T. Wong, *Upconversion Nanoparticles Conjugated with* Gd^{3+}*-DOTA and RGD for Targeted Dual-Modality Imaging of Brain Tumor Xenografts.* Advanced Healthcare Materials, 2013. **2**(11): p. 1501-1512.

12. Jin, J., Y.-J. Gu, C.W.-Y. Man, J. Cheng, Z. Xu, Y. Zhang, H. Wang, V.H.-Y. Lee, S.H. Cheng, and W.-T. Wong, *Polymer-Coated* $NaYF_4:Yb^{3+}$, Er^{3+} *Upconversion Nanoparticles for Charge-Dependent Cellular Imaging.* ACS nano, 2011. **5**(10): p. 7838-7847.

13. Li, C., Z. Quan, J. Yang, P. Yang, and J. Lin, *Highly Uniform and Monodisperse β-*$NaYF_4:Ln^{3+}$ *(Ln = Eu, Tb, Yb/Er, and Yb/Tm) Hexagonal Microprism Crystals: Hydrothermal Synthesis and Luminescent Properties.* Inorganic Chemistry, 2007. **46**(16): p. 6329-6337.

14. He, X., H. Li, Y. Liu, H. Huang, Z. Kang, and S.-T. Lee, *Water soluble carbon nanoparticles: Hydrothermal synthesis and excellent photoluminescence properties.* Colloids and Surfaces B: Biointerfaces, 2011. **87**(2): p. 326-332.

15. Zhong, Y., G. Tian, Z. Gu, Y. Yang, L. Gu, Y. Zhao, Y. Ma, and J. Yao, *Elimination of Photon Quenching by a Transition Layer to Fabricate a Quenching-Shield Sandwich Structure for 800 nm Excited Upconversion Luminescence of* Nd^{3+}*-Sensitized Nanoparticles.* Advanced Materials, 2014. **26**(18): p. 2831-2837.

16. Xu, B., X. Zhang, W. Huang, Y. Yang, Y. Ma, Z. Gu, T. Zhai, and Y. Zhao, *Nd3+ sensitized dumbbell-like upconversion nanoparticles for photodynamic therapy application.* Journal of Materials Chemistry B, 2016. **4**(16): p. 2776-2784.

17. Wang, Y.-F., G.-Y. Liu, L.-D. Sun, J.-W. Xiao, J.-C. Zhou, and C.-H. Yan, Nd^{3+}*-sensitized upconversion nanophosphors: Efficient in vivo bioimaging probes with minimized heating effect.* ACS nano, 2013. **7**(8): p. 7200-7206.

18. Li, X., R. Wang, F. Zhang, L. Zhou, D. Shen, C. Yao, and D. Zhao, *Nd3+ Sensitized Up/Down Converting Dual-Mode Nanomaterials for Efficient In-vitro and In-vivo Bioimaging Excited at 800 nm.* Scientific Reports, 2013. **3**: p. 3536.

19. Mai, H.-X., Y.-W. Zhang, L.-D. Sun, and C.-H. Yan, *Size- and Phase-Controlled Synthesis of Monodisperse* $NaYF_4$*:Yb,Er Nanocrystals from a Unique Delayed Nucleation Pathway Monitored with Upconversion Spectroscopy.* The Journal of Physical Chemistry C, 2007. **111**(37): p. 13730-13739.

20. Liu, D., X. Xu, Y. Du, X. Qin, Y. Zhang, C. Ma, S. Wen, W. Ren, E.M. Goldys, J.A. Piper, S. Dou, X. Liu, and D. Jin, *Three-dimensional controlled growth of monodisperse sub-50 nm heterogeneous nanocrystals.* Nature Communications, 2016. **7**: p. 10254.

21. Deng, R., F. Qin, R. Chen, W. Huang, M. Hong, and X. Liu, *Temporal full-colour tuning through non-steady-state upconversion.* Nat Nano, 2015. **10**(3): p. 237-242.

22. Carter, D.B.W.C.B., *TRANSMISSION ELECTRON MICROSCOPY*. 2009.

23. Reimer, L., *Scanning Electron Microscopy: Physics of Image Formation and Microanalysis*. Optical Science Springer.

24. Leary, R., Z. Saghi, M. Armbrüster, G. Wowsnick, R. Schlögl, J.M. Thomas, and P.A. Midgley, *Quantitative High-Angle Annular Dark-Field Scanning Transmission Electron Microscope (HAADF-STEM) Tomography and High-Resolution Electron Microscopy of Unsupported Intermetallic GaPd2 Catalysts.* The Journal of Physical Chemistry C, 2012. **116**(24): p. 13343-13352.

25. Utsunomiya, S. and R.C. Ewing, *Application of High-Angle Annular Dark Field Scanning Transmission Electron Microscopy, Scanning Transmission Electron Microscopy-Energy Dispersive X-ray Spectrometry, and Energy-Filtered Transmission Electron Microscopy to the Characterization of Nanoparticles in the Environment.* Environmental Science & Technology, 2003. **37**(4): p. 786-791.

26. Van Aert, S., J. Verbeeck, R. Erni, S. Bals, M. Luysberg, D.V. Dyck, and G.V. Tendeloo, *Quantitative atomic resolution mapping using high-angle annular dark field scanning transmission electron microscopy*. Ultramicroscopy, 2009. **109**(10): p. 1236-1244.

27. Egerton, R.F., *Electron Energy Loss Spectroscopy in the Electron Microscope*. 1996: New York: Plenum. .

28. Xie, X., N. Gao, R. Deng, Q. Sun, Q.-H. Xu, and X. Liu, *Mechanistic investigation of photon upconversion in* Nd^{3+}*-sensitized core–shell nanoparticles*. Journal of the American Chemical Society, 2013. **135**(34): p. 12608-12611.

29. Wang, F., R. Deng, J. Wang, Q. Wang, Y. Han, H. Zhu, X. Chen, and X. Liu, *Tuning upconversion through energy migration in core–shell nanoparticles.* Nat Mater, 2011. **10**(12): p. 968-973.

30. Hu, H., L. Xiong, J. Zhou, F. Li, T. Cao, and C. Huang, *Multimodal-Luminescence Core–Shell Nanocomposites for Targeted Imaging of Tumor Cells.* Chemistry – A European Journal, 2009. **15**(14): p. 3577-3584.

31. Lei, L., D. Chen, W. Zhu, J. Xu, and Y. Wang, *Impact of High Ytterbium (III) Concentration in the Shell on Upconversion Luminescence of Core–Shell Nanocrystals.* Chemistry–An Asian Journal, 2014. **9**(10): p. 2765-2770.

32. Li, X., D. Shen, J. Yang, C. Yao, R. Che, F. Zhang, and D. Zhao, *Successive Layer-by-Layer Strategy for Multi-Shell Epitaxial Growth: Shell Thickness and Doping Position Dependence in Upconverting Optical Properties.* Chemistry of Materials, 2013. **25**(1): p. 106-112.

33. Ren, W., G. Tian, S. Jian, Z. Gu, L. Zhou, L. Yan, S. Jin, W. Yin, and Y. Zhao, *TWEEN coated* $NaYF_4$*:Yb,Er/*$NaYF_4$ *core/shell upconversion nanoparticles for bioimaging and drug delivery*. RSC Advances, 2012. **2**(18): p. 7037-7041.

34. Shen, J., G. Chen, T.Y. Ohulchanskyy, S.J. Kesseli, S. Buchholz, Z. Li, P.N. Prasad, and G. Han, *Tunable Near Infrared to Ultraviolet Upconversion Luminescence Enhancement*

in (α-NaYF4:Yb,Tm)/CaF$_2$ Core/Shell Nanoparticles for In situ Real-time Recorded Biocompatible Photoactivation. Small, 2013. **9**(19): p. 3213-3217.

35. Vetrone, F., R. Naccache, V. Mahalingam, C.G. Morgan, and J.A. Capobianco, *The Active-Core/Active-Shell Approach: A Strategy to Enhance the Upconversion Luminescence in Lanthanide-Doped Nanoparticles.* Advanced Functional Materials, 2009. **19**(18): p. 2924-2929.

36. Wang, Y., K. Liu, X. Liu, K. Dohnalová, T. Gregorkiewicz, X. Kong, M.C.G. Aalders, W.J. Buma, and H. Zhang, *Critical Shell Thickness of Core/Shell Upconversion Luminescence Nanoplatform for FRET Application.* The Journal of Physical Chemistry Letters, 2011. **2**(17): p. 2083-2088.

37. Zhan, Q., J. Qian, H. Liang, G. Somesfalean, D. Wang, S. He, Z. Zhang, and S. Andersson-Engels, *Using 915 nm Laser Excited Tm^{3+}/Er^{3+}/Ho^{3+}-Doped NaYbF$_4$ Upconversion Nanoparticles for in Vitro and Deeper in Vivo Bioimaging without Over-heating Irradiation.* ACS nano, 2011. **5**(5): p. 3744-3757.

38. Azkargorta, J., I. Iparraguirre, R. Balda, and J. Fernández, *On the origin of bichromatic laser emission in Nd^{3+}-doped fluoride glasses.* Optics Express, 2008. **16**(16): p. 11894-11906.

39. Banerjee, S., J. Koerner, M. Siebold, Q. Yang, K. Ertel, P.D. Mason, P.J. Phillips, M. Loeser, H. Zhang, S. Lu, J. Hein, U. Schramm, M.C. Kaluza, and J.L. Collier, *Temperature dependent emission and absorption cross section of Yb^{3+} doped yttrium lanthanum oxide (YLO) ceramic and its application in diode pumped amplifier.* Optics Express, 2013. **21**(S4): p. A726-A734.

40. João, C., J. Wemans, and G. Figueira, *Numerical Simulation of High-Energy, Ytterbium-Doped Amplifier Tunability.* Applied Sciences, 2013. **3**(1): p. 288.

41. Kushida, T., H.M. Marcos, and J.E. Geusic, *Laser Transition Cross Section and Fluorescence Branching Ratio for Nd*$^{3+}$ *in Yttrium Aluminum Garnet.* Physical Review, 1968. **167**(2): p. 289-291.

42. Lupei, V., A. Lupei, C. Gheorghe, S. Hau, and A. Ikesue, *Efficient sensitization of Yb*$^{3+}$ *emission by Nd*$^{3+}$ *in* Y_2O_3 *transparent ceramics and the prospect for high-energy Yb lasers.* Optics Letters, 2009. **34**(14): p. 2141-2143.

43. Marciniak, L., A. Bednarkiewicz, M. Stefanski, R. Tomala, D. Hreniak, and W. Strek, *Near infrared absorbing near infrared emitting highly-sensitive luminescent nanothermometer based on Nd*$^{3+}$ *to Yb*$^{3+}$ *energy transfer.* Physical Chemistry Chemical Physics, 2015. **17**(37): p. 24315-24321.

44. Pukhkaya, V., P. Goldner, A. Ferrier, and N. Ollier, *Impact of rare earth element clusters on the excited state lifetime evolution under irradiation in oxide glasses.* Optics Express, 2015. **23**(3): p. 3270-3281.

45. Rivera-López, F., Babu, P., Basavapoornima, Ch., and Jayasankar, C. K. Lavín, V. *Efficient Nd*$^{3+}\rightarrow$*Yb*$^{3+}$ *energy transfer processes in high phonon energy phosphate glasses for 1.0* μ*m Yb*$^{3+}$ *laser.* Journal of Applied Physics, 2011. **109**(12): p. 123514.

46. Zhiyi Wei, B.Z., Yongdong Zhang, Yuwan Zou, Xin Zhong, Changwen Xu and Zhiguo Zhang. , *All Solid-State Passively Mode-Locked Ultrafast Lasers Based on Nd, Yb, and Cr Doped Media*, in *Laser Pulses - Theory, Technology, and Applications*, P.I.P.E. , Editor. 2012, InTech.

47. Chen, Y., B. Liu, X. Deng, S. Huang, Z. Hou, C. Li, and J. Lin, *Multifunctional Nd3+-sensitized upconversion nanomaterials for synchronous tumor diagnosis and treatment.* Nanoscale, 2015. **7**(18): p. 8574-8583.

48. He, F., C. Li, X. Zhang, Y. Chen, X. Deng, B. Liu, Z. Hou, S. Huang, D. Jin, and J. Lin, *Optimization of upconversion luminescence of Nd*$^{3+}$*-sensitized* $BaGdF_5$*-based*

nanostructures and their application in dual-modality imaging and drug delivery. Dalton Transactions, 2016. **45**(4): p. 1708-1716.

49. Hou, Z., K. Deng, C. Li, X. Deng, H. Lian, Z. Cheng, D. Jin, and J. Lin, *808 nm Light-triggered and hyaluronic acid-targeted dual-photosensitizers nanoplatform by fully utilizing* Nd^{3+}*-sensitized upconversion emission with enhanced anti-tumor efficacy.* Biomaterials, 2016. **101**: p. 32-46.
50. Lu, F., L. Yang, Y. Ding, and J.-J. Zhu, *Highly Emissive* Nd^{3+}*-Sensitized Multilayered Upconversion Nanoparticles for Efficient 795 nm Operated Photodynamic Therapy.* Advanced Functional Materials, 2016: p. n/a-n/a.
51. Wang, L., H. Dong, Y. Li, R. Liu, Y.-F. Wang, H.K. Bisoyi, L.-D. Sun, C.-H. Yan, and Q. Li, *Luminescence-Driven Reversible Handedness Inversion of Self-Organized Helical Superstructures Enabled by a Novel Near-Infrared Light Nanotransducer.* Advanced Materials, 2015. **27**(12): p. 2065-2069.
52. Wang, R., X. Li, L. Zhou, and F. Zhang, *Epitaxial Seeded Growth of Rare-Earth Nanocrystals with Efficient 800 nm Near-Infrared to 1525 nm Short-Wavelength Infrared Downconversion Photoluminescence for In Vivo Bioimaging.* Angewandte Chemie, 2014. **126**(45): p. 12282-12286.
53. Xi, Y., Z. Chang, X. Ye, H. Huang, Y. Huang, Q. Xiao, and H. Lin, *Ultra-small* Nd^{3+}*-doped nanoparticles as near-infrared luminescent biolabels of hemin in bacteria.* Nanoscale, 2016. **8**(3): p. 1288-1292.
54. Zhong, Y., I. Rostami, Z. Wang, H. Dai, and Z. Hu, *Energy Migration Engineering of Bright Rare-Earth Upconversion Nanoparticles for Excitation by Light-Emitting Diodes.* Advanced Materials, 2015. **27**(41): p. 6418-6422.
55. Prorok, K., M. Pawlyta, W. Stręk, and A. Bednarkiewicz, *Energy Migration Up-conversion of* Tb^{3+} *in* Yb^{3+} *and* Nd^{3+} *Codoped Active-Core/Active-Shell Colloidal Nanoparticles.* Chemistry of Materials, 2016. **28**(7): p. 2295-2300.

56. Lei, Y., H. Song, L. Yang, L. Yu, Z. Liu, G. Pan, X. Bai, and L. Fan, *Upconversion luminescence, intensity saturation effect, and thermal effect in* $Gd_2O_3:Er^{3+},Yb^{3+}$ *nanowires.* The Journal of Chemical Physics, 2005. **123**(17): p. 174710.

57. Wang, F., F. Song, G. Zhang, Y. Han, Q. Li, C. Ming, and J. Tian, *Upconversion and pump saturation mechanisms in* Er^{3+}/Yb^{3+} *co-doped* $Y_2Ti_2O_7$ *nanocrystals.* Journal of Applied Physics, 2014. **115**(13): p. 134310.

58. Liu, B., Y. Chen, C. Li, F. He, Z. Hou, S. Huang, H. Zhu, X. Chen, and J. Lin, *Poly(Acrylic Acid) Modification of* Nd^{3+}*-Sensitized Upconversion Nanophosphors for Highly Efficient UCL Imaging and pH-Responsive Drug Delivery.* Advanced Functional Materials, 2015. **25**(29): p. 4717-4729.

59. Liu, Y., N. Kang, J. Lv, Z. Zhou, Q. Zhao, L. Ma, Z. Chen, L. Ren, and L. Nie, *Deep Photoacoustic/Luminescence/Magnetic Resonance Multimodal Imaging in Living Subjects Using High-Efficiency Upconversion Nanocomposites.* Advanced Materials, 2016. **28**(30): p. 6411-6419.

60. Hou, Y., R. Qiao, F. Fang, X. Wang, C. Dong, K. Liu, C. Liu, Z. Liu, H. Lei, F. Wang, and M. Gao, $NaGdF_4$ *Nanoparticle-Based Molecular Probes for Magnetic Resonance Imaging of Intraperitoneal Tumor Xenografts in Vivo.* ACS nano, 2013. **7**(1): p. 330-338.

61. Li, F., W. Gu, H. Wang, Y. Qi, Y. Deng, N. Xiao, Y. Liu, Q. Xu, and L. Ye, *Effect of surface functionalities on relaxometric properties of MR contrast agents based on NaGdF4 nanoparticles.* RSC Advances, 2013. **3**(16): p. 5386-5392.

62. Johnson, N.J., W. Oakden, G.J. Stanisz, R. Scott Prosser, and F.C. van Veggel, *Size-tunable, ultrasmall* $NaGdF_4$ *nanoparticles: insights into their T1 MRI contrast enhancement.* Chemistry of Materials, 2011. **23**(16): p. 3714-3722.

Chapter 2.

Mechanism and Construction Strategies Investigation on Nd^{3+}-harvest-transfer-sensitization system developed Nd^{3+}-sensitized UCNPs with Superior Luminescent Properties

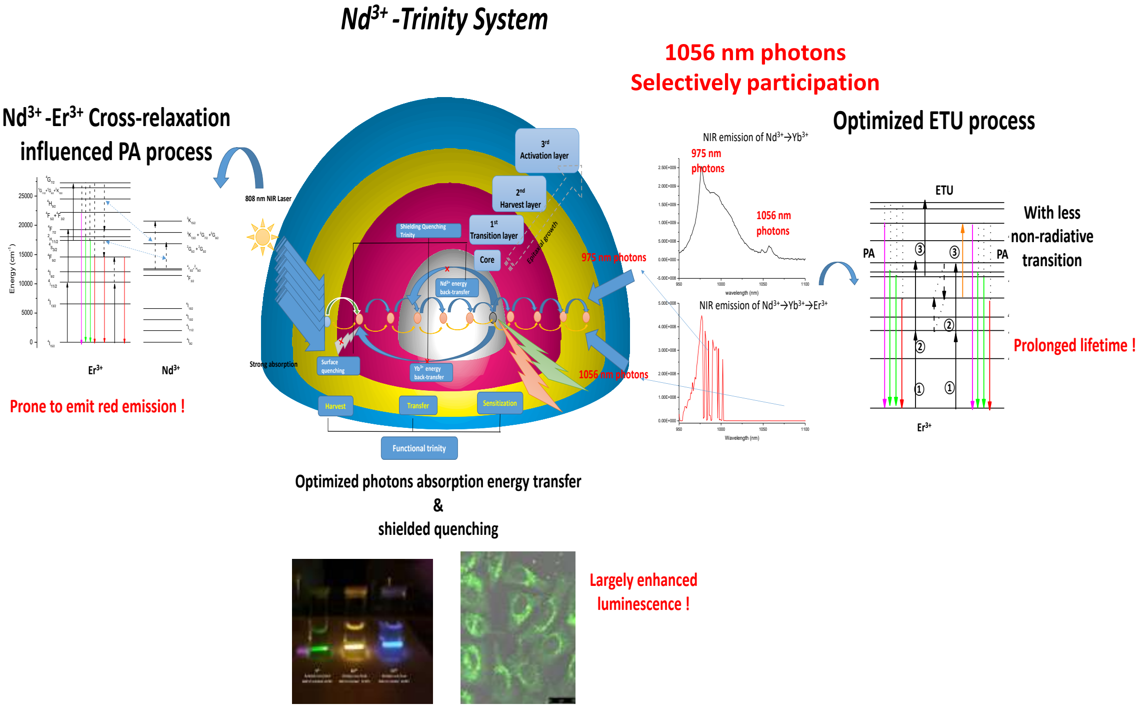

Figure 1. Nd^{3+}-harvest-transfer-sensitization system.

2.1. Background and previous work

Since the photo-luminescence source of the upconversion nanoparticles (UCNPs), that is 980 nm laser, is reported as the culprit of the increasing the temperature of the tissue in bio-imaging, which makes the cell and tissues in a high risk [37], scientists have developed the Nd^{3+}-sensitized upconversion nanoparticles to avoid the over-heating effect by utilizing the 808/800/795 nm laser as the photo-luminescence source [28]. Later on, various Nd^{3+}-sensitized UCNPs has been constructed [15-18, 21, 28, 47-51, 53]. And in our research work, we have developed the Nd^{3+}-harvest-transfer-sensitization system, as shown in Figure 1, which is coated on the $NaGdF_4$:Yb, Er/Tm/Ho cores, proving to be equipped with superior luminescent properties excited by 808 nm laser.

2.1.1. Why 808 nm laser is preferred?

The traditionally developed, 980 nm excited, Yb^{3+}-sensitized UCNPs have shown their drawbacks in utilization of bio-imaging, for the absorption of 980 nm photons by water, which result in dramatically rising of the temperature of water as well as the attenuation of the photo-luminescence source. The rising of the temperature result in damage of the tissue and cells as well as the attenuation the photo-luminescence source leading to shallow penetration of the emission.

To conquer the sticky issue, an alternative photo-luminescence source is in need urgently. There has been reports on the $Nd^{3+} \rightarrow Yb^{3+}$ energy transfer, which could be explained as the Nd^{3+} $^4F_{5/2}$+$^2H_{11/2}$ absorbs 795(800/808) nm photons and transfer to Nd^{3+} $^4F_{3/2}$, and then exciting Yb^{3+} $^2F_{7/2}$, with 940-1030 and 1056 nm emission [17, 28, 47, 50]. the $Nd^{3+} \rightarrow Yb^{3+}$ energy transfer could be explained by "phonons assisted energy transfer", which is "$Nd^{3+} \rightarrow Yb^{3+}$ phonons assistant transfer" which could be illustrated as: by generation of the “k” phonons by Yb^{3+} ions and “n-k” phonons by Nd^{3+} ions, one hand, makes the overlapped Nd^{3+} $^4F_{3/2}$ emission and Yb^{3+} $^2F_{5/2}$ absorption to the equal virtual intermediate level, thus makes the Nd^{3+} $^4F_{3/2}$+ Yb^{3+} $^2F_{7/2}$ →Yb^{3+} $^2F_{5/2}$+ Nd^{3+} $^4I_{9/2}$ in high efficiency; on the other hand, realized Nd^{3+} $^4F_{3/2}$+ Yb^{3+} $^2F_{7/2}$ →Yb^{3+} $^2F_{5/2}$+ Nd^{3+} $^4I_{11/2}$ [43, 45]. And we have fabricated the core-multishells NaRe(Gd,Nd,Yb)F_4 nanoparticles to make sure the Nd^{3+}→Yb^{3+} energy transfer is tenable in the NaRe(Gd,Nd,Yb)F_4 nanocrystals. As shown in Figure 2, the $NaGdF_4$:Yb@$NaGdF_4$:Yb@$NaNdF_4$:Yb@$NaGdF_4$ is excited by 808 nm laser, by measuring the NIR emission spectra, we would confirm the Nd^{3+}→Yb^{3+} energy transfer could be utilized in our nanoparticles.

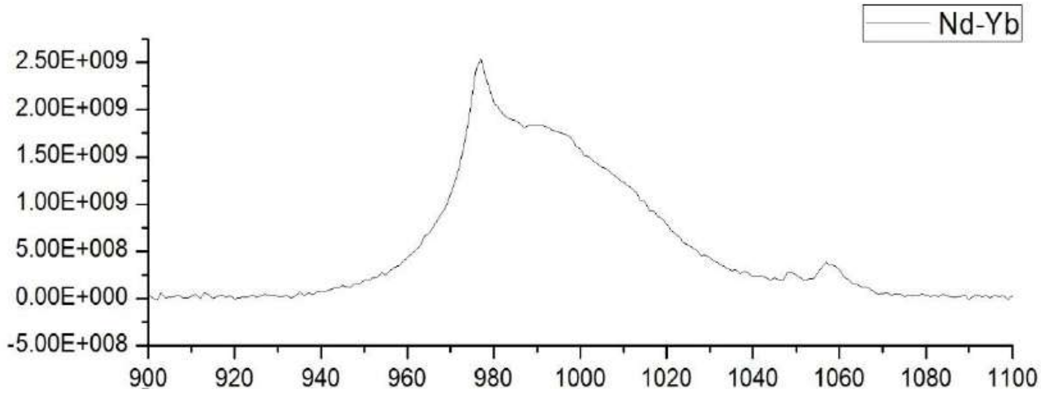

Figure 2. NIR emission spectra of $NaGdF_4$:Yb@$NaGdF_4$:Yb@$NaNdF_4$:Yb@$NaGdF_4$ with 808 nm excitation.

Professor X.G. Liu’s group has invented the Nd^{3+}-sensitized UCNPs in 2013, which should be treated as the great advance in the development of UCNPs, that is Nd^{3+}→Yb^{3+}→$X(Er/Tm/Ho)^{3+}$ system with excitation of 795 nm and emission in UV and visible band, which is similar with the 980 nm excited traditionally developed

Yb^{3+}→X(Er/Tm/Ho)$^{3+}$ system. Furthermore, the luminescent properties has been optimized for the enhancement of the luminescence intensity and larger partition of red emission. Previous work reports on the Nd^{3+}-sensitized UCNPs has been summarized in Chapter 1.

2.2. Investigations on the construction of the Nd^{3+}-sensitized UCNPs

The situation of energy transfer in the Nd^{3+}-sensitized UCNPs, has been generalized in Scheme 1(a), that is: Nd^{3+} ions absorbs 808 nm photons and transfer energy to Yb^{3+}, that is the ET-I. Furthermore, both Yb^{3+}→Er^{3+} energy transfer, with the coefficient of 2.4×10^{-16} $cm^3\bullet s^{-1}$ **[63]** which promotes the ETU process, and Er^{3+}→Yb^{3+} energy transfer, with the coefficient of 1.6×10^{-16} $cm^3\bullet s^{-1}$ **[63]** which is defined as "energy back-transfer" **[64]** shown as ET-II. Besides, the Nd^{3+} ions has been reported to quench the luminescence of the activators by the Nd^{3+} manifolds of the ^4I_J energy levels [15], that is the Nd^{3+} energy back-transfer, also defined as the ET-III in Scheme. 1(a).

Additionally, besides the Yb^{3+} and Nd^{3+} energy back-transfer, we have put forward that the surface quenching that caused by the absence of F^- ions on the surface of nanocrystals will quench the luminescence, including the surface quenching of Yb^{3+} and activators (Er/Tm/Ho), as shown in Scheme 1(a-1). However, the surface quenching of Nd^{3+} is reported displays no significance effect on the luminescent performance [15]. Moreover, to shield the surface quenching of activators, the remedy of the surface defect that is the surface coating of the $NaGd/YF_4$ is required, which is called as the "activation layer".

Thus, the main conflicts in construction of the Nd^{3+}-sensitized UCNPs could be generalized as: on one hand, the Nd^{3+} ions and Yb^{3+} ions are dispensable in Nd^{3+}-

sensitization for the 808 nm harvesting, energy transfer and sensitization of the activators; on the other hand, both Nd^{3+} ions and Yb^{3+} ions cause conspicuous quenching on the activators with the three main quenching factors could be generalized as: Nd^{3+} energy back-transfer, Yb3^{3+}energy back-transfer and Yb^{3+} surface quenching, as shown in Scheme.1 (a-2).

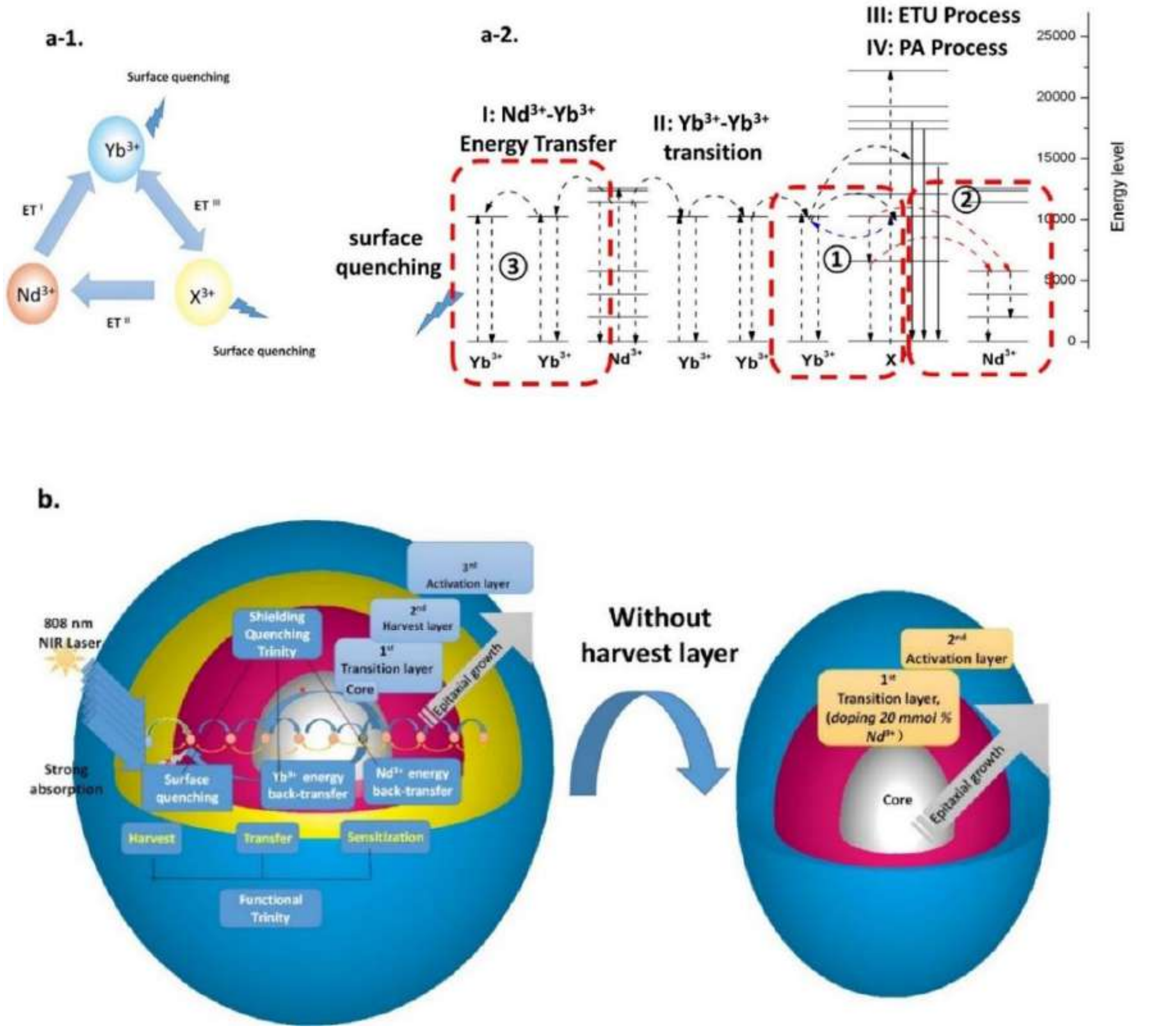

Scheme 1. (a-1). Generalization of the energy transfer in Nd^{3+}-sensitized UCNPs (ET-I: Nd^{3+}→Yb^{3+}energy transfer; ET-II: Nd^{3+} energy back-transfer; ET-III: Yb^{3+}→X^{3+} energy transfer and Yb^{3+} energy back-transfer); (a-2). Energy transfer in Nd^{3+}-sensitized UCNPs

and quenching factors in Nd^{3+}-sensitized UCNPs.(① energy back-transfer of Yb^{3+}; ② energy back-transfer of Nd^{3+}; ③ Yb^{3+} surface quenching; (b). Design of the type I and type II Nd^{3+}-Trinity system.

2.2.1. Investigation on the quenching factors

We have done investigation on the quenching factors: for Nd^{3+} ions, the manifolds of Nd^{3+} energy levels is proposed to energy back transfer from the excited state of the activators (Er^{3+}, Tm^{3+} and Ho^{3+}); for Yb^{3+} ions, very high concentration Yb^{3+} ions and Yb^{3+} surface quenching will cause serious Yb^{3+}- $X(Er/Tm/Ho)^{3+}$ energy back transfer, as shown in Scheme 1(b-2).

2.2.1.1. Nd^{3+} energy back-transfer:

As shown in Figure 3(a), we found only 1 mmol % Nd^{3+} ions doping in the $NaGdF_4$:Yb, Er/Tm/Ho, resulting in large quenching of the luminescence, which reminds us that the Nd^{3+} ions should be segregated with that activators by the core-shell structure. As shown in Figure 4 (a): Nd^{3+} ions is proposed to quench the first photons that transfer form Yb^{3+} to the activator by Nd^{3+} ^4I_J manifolds, that is Nd^{3+}-X^{3+} (Er^{3+}/Tm^{3+} /Ho^{3+}) cross-relaxation, which could be explained in details, Nd^{3+}-Er^{3+} cross-relaxation is: Er^{3+}-Nd^{3+} cross-relaxation: $Er^{3+}\ ^4I_{11/2} + Nd^{3+}\ ^4I_{9/2} \rightarrow Er^{3+}\ ^4I_{9/2} + Nd^{3+}\ ^4I_{11/2}$; $Er^{3+}\ ^4I_{13/2} + Nd^{3+}\ ^4I_{9/2} \rightarrow Er^{3+}\ ^4I_{15/2} + Nd^{3+}\ ^4I_{13/2}$, as reported. [15]

However, in our further investigation, we found that the high concentration of Nd^{3+} still cause manifest quenching. As shown in Figure 5, when the $NaNdF_4$, $NaGdF_4$, and $NaGdF_4$:Yb(10 %), Nd(20 %) shells are coated on the $NaGdF_4$:Yb, Er cores, the emission spectra (with excitation of 980 nm and 808 nm laser) indicates that: in contrast with the "active" effect of $NaGdF_4$ and $NaGdF_4$:$Yb_{10\ \%}$, $Nd_{20\ \%}$ shells that enhanced the luminescence, the $NaNdF_4$ shell displays "in-active" effect rather than "active" effect, for the luminescence is depressed with both 980 nm and 808 nm excitation, which is proposed to be caused by Nd^{3+} energy back-transfer; and lifetime measurement displays "shorten" lifetime, as shown in Table 1. Also, the Nd^{3+} ions is proposed to directly quench the green and red luminescence of the activators, which could be directly confirmed by the Nd^{3+}-sensitized energy migration upconversion system with the activator of Eu^{3+} and Tb^{3+}. As shown in the Figure 5 (d), very high concentration of Nd^{3+} in the nearby layer of the Eu^{3+} or Tb^{3+}, result in large quenching of the Eu^{3+}/Tb^{3+} emission. Conclusively, the energy back-transfer of Nd^{3+} is widely and conspicuously effective on all the activators of the UCNPs with quenching the emission and excited state.

Lifetime (μs) / Nanoparticle Structures	Photo-luminescence source (nm)	Wavelength (nm)		
		522	541	655
$NaGdF_4$:Yb, Er	980	57.69	62.58	80.47
$NaGdF_4$:Yb, Er@$NaNdF_4$	980	76.99	78.03	45.47
	808	58.06	51.50	44.02
$NaGdF_4$:Yb, Er@$NaGdF_4$: Yb, Nd	980	74.53	79.77	88.59
	808	14.49	84.63	18.66

Table 1. Lifetime of $NaGdF_4$:Yb, Er and $NaGdF_4$: Yb, Er coated with $NaNdF_4$, $NaGdF_4$: Yb, Nd layer with excitation of 808/980 nm laser.

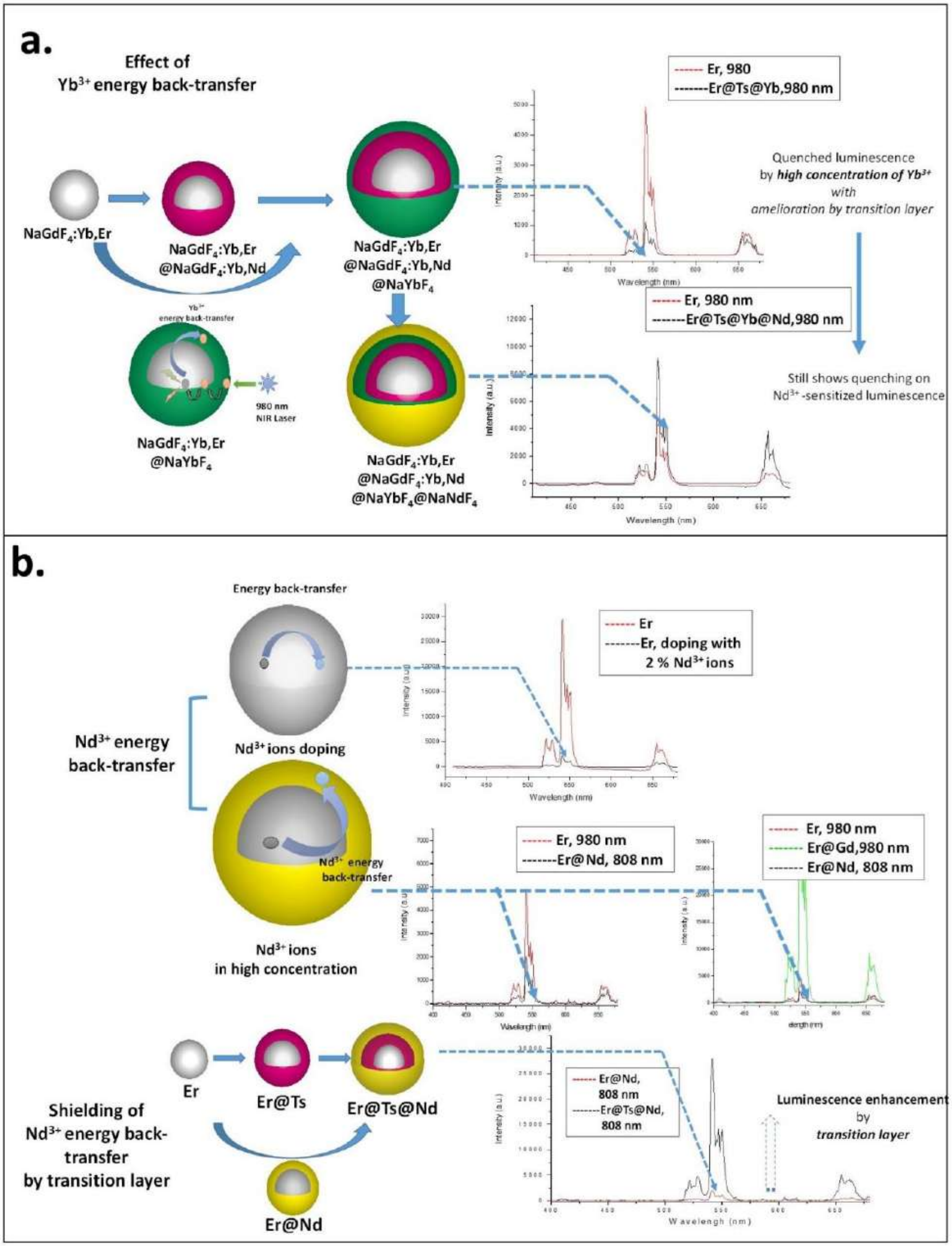
a.
Effect of
Yb^{3+} energy back-transfer
NaGdF$_4$:Yb,Er
NaGdF$_4$:Yb,Er
@NaGdF$_4$:Yb,Nd
NaGdF$_4$:Yb,Er
@NaGdF$_4$:Yb,Nd
@NaYbF$_4$
Yb^{3+}
energy back-transfer
980 nm
NIR Laser
NaGdF$_4$:Yb,Er
@NaYbF$_4$
NaGdF$_4$:Yb,Er
@NaGdF$_4$:Yb,Nd
@NaYbF$_4$@NaNdF$_4$
Er, 980
Er@Ts@Yb,980 nm
Intensity (a.u.)
Wavelength (nm)
Quenched luminescence
by high concentration of Yb^{3+}
with
amelioration by transition layer
Er, 980 nm
Er@Ts@Yb@Nd,980 nm
Intensity (a.u.)
Wavelength (nm)
Still shows quenching on
Nd^{3+}-sensitized luminescence
b.
Energy back-transfer
Nd^{3+} energy
back-transfer
Nd^{3+} ions doping
Nd^{3+} energy
back-transfer
Nd^{3+} ions
in high concentration
Er
Er, doping with
2 % Nd^{3+} ions
Intensity (a.u.)
Wavelength (nm)
Er, 980 nm
Er@Nd, 808 nm
Intensity (a.u.)
Wavelength (nm)
Er, 980 nm
Er@Gd,980 nm
Er@Nd, 808 nm
Intensity (a.u.)
Wavelength (nm)
Er
Er@Ts
Er@Ts@Nd
Er@Nd
Shielding of
Nd^{3+} energy back-
transfer
by transition layer
Er@Nd,
808 nm
Er@Ts@Nd,
808 nm
Intensity (a.u.)
Wavelength (nm)
Luminescence enhancement
by
transition layer

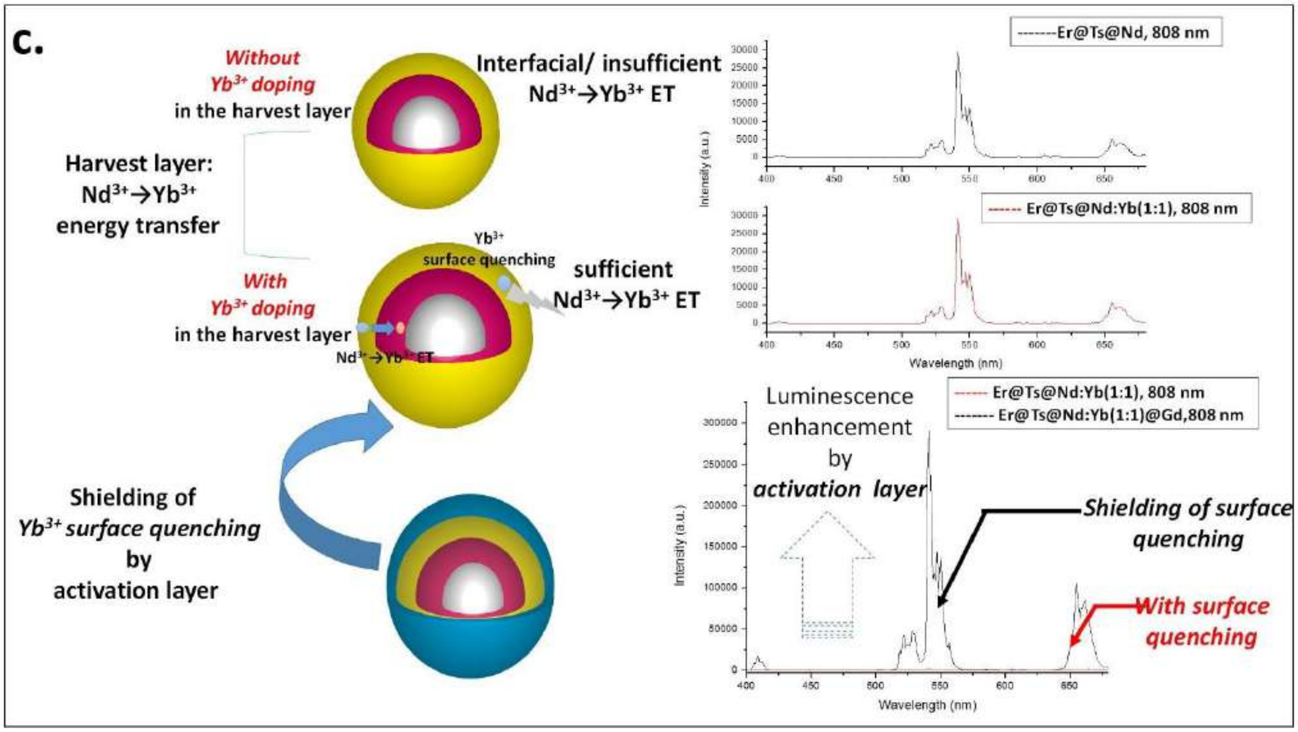

Figure 3. Investigations on Yb^{3+} energy back-transfer (a), Nd^{3+} energy back-transfer (b), Nd^{3+}→Yb^{3+} energy transfer and Yb^{3+} surface quenching (c). (Er: $NaGdF_4$:$Yb_{20\%}$,$Er_{2\%}$; Ts: $NaGdF_4$:$Yb_{10\%}$,$Nd_{20\%}$; ***Yb:*** $NaYbF_4$; ***Nd:*** $NaNdF_4$; ***Gd:*** $NaGdF_4$; Nd:Yb: doping certain amount of Yb^{3+} ions in $NaNdF_4$ layer)

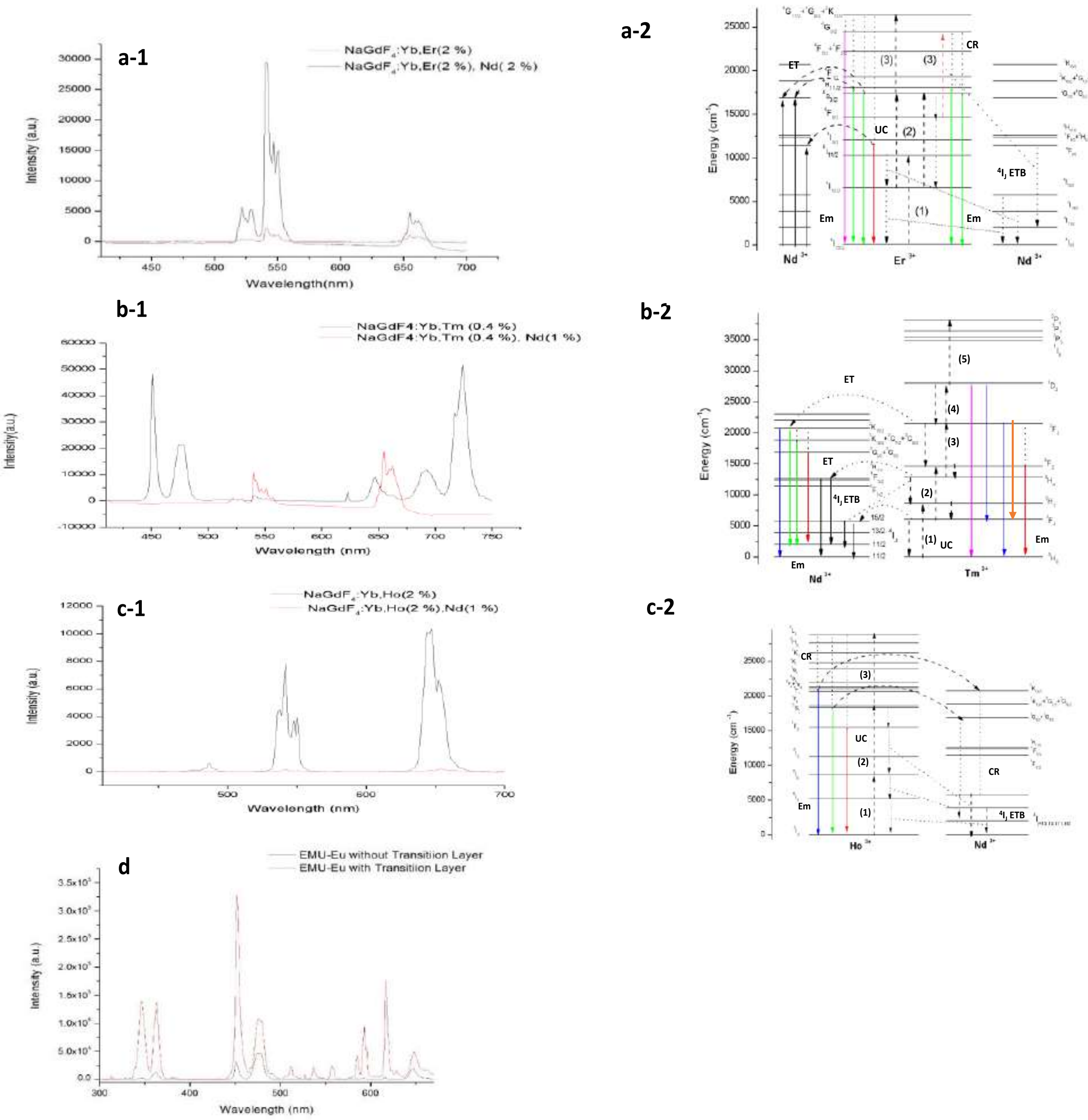

Figure 4. Nd^{3+} energy back-transfer. Emission spectra of NaGdF$_4$: Yb, Er/Ho/Tm compared with 1-2 mmol % Nd^{3+} ions doping NaGdF$_4$: Yb, Er/Ho/Tm (a-1, b-1 and c-1) and energy levels illustrating Nd^{3+} energy back-transfer effect of activators (a-2, b-2 and c-2). And the proof that Nd^{3+} ions is proposed to quench the red/green emission of the activators in the Nd^{3+}-sensitized Eu^{3+} system (d). Measurement conditions: power density:

80 mW/ 1 mm^2 for 808/ 980 nm diode laser; emission bandwidth: 2 nm, concentration: 1.0 wt %. (UC: upconversion; Em: emission; ET: energy transfer; EBT: energy back-transfer).

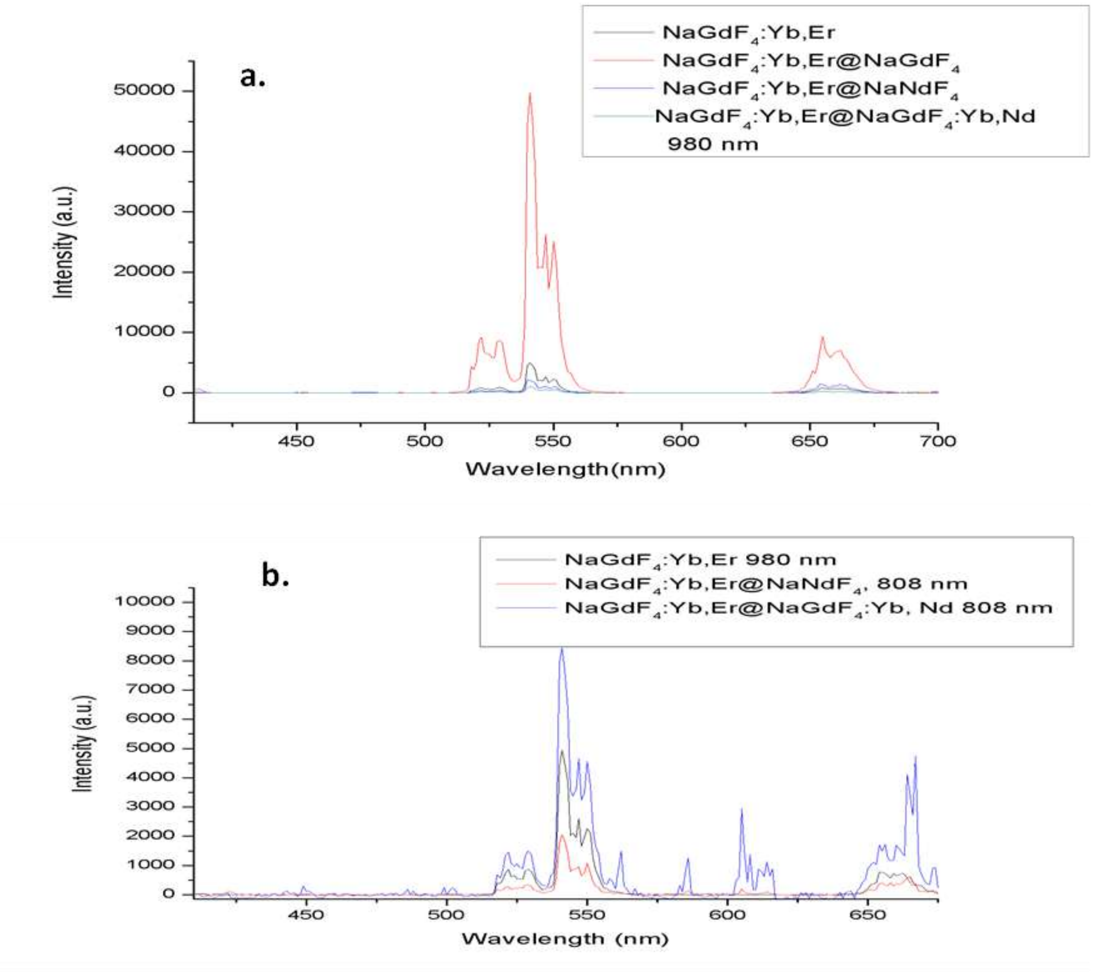

Figure 5. Emission spectra of $NaGdF_4$:Yb, Er and $NaGdF_4$: Yb, Er coated with $NaNdF_4$, $NaGdF_4$:Yb, Nd and $NaGdF_4$ layer with excitation of 808 nm (a) and 980 nm (b) laser . Measurement conditions: power density: 80 mW/ 1 mm^2 for 808/ 980 nm diode laser; emission bandwidth: 2 nm, concentration: 1.0 wt %.

2.2.1.2. Yb^{3+} energy back-transfer by high concentration

According to L. Lei, *et al.*, very high concentration of Yb^{3+} result in large quenching of the luminescence of the activators in the Yb^{3+}-sensitized UCNPs with 980 nm excitation, for the strong Yb^{3+} energy back-transfer .[31] Similarly, in our investigations, we found that the very high concentration also results in deleterious Yb$^{3+}\rightarrow$X^{3+} (Er^{3+}/Tm^{3+}/Ho^{3+}) energy transfer.

As stated by Lei L. *et al.* , the very high concentration of Yb^{3+} in the nearby layer of the NaYF4:Yb,Er cores, leads to large quenching of the activators; in contrast, while a transition layer is sandwiched in the NaYF$_4$:Yb$_{20\ \%}$,Er$_{2\ \%}$@NaYbF$_4$, that is NaYF$_4$:Yb$_{20\ \%}$,Er$_{2\ \%}$@NaYbF$_4$, shows great amelioration [31] . However, in our investigations which is constructed by the gadolinium based UCNPs, the transition layer still cannot do any salvation on the quenching caused by high concentration Yb^{3+}, and even involves Nd^{3+}-sensitization into inefficiency. As shown in Figure 3(b) and Figure 6, the 980 nm excited NaGdF$_4$: Yb$_{20\ \%}$,Er$_{2\ \%}$@NaGdF$_4$:Yb$_{10\ \%}$@NaYbF$_4$ shows even lower upconversion efficiency than the NaGdF$_4$:Yb,Er; when coating with NaNdF$_4$, which is NaGdF$_4$: Yb$_{20\ \%}$,Er$_{2\ \%}$@NaGdF$_4$:Yb$_{10\ \%}$@NaYbF$_4$@NaNdF$_4$, it still shows unsatisfactory luminescent performance as inefficient as NaGdF$_4$: Yb$_{20\ \%}$,Er$_{2\ \%}$, only under the excitation of 808 nm but also 980 nm. And our invesigation highlighted the delecterious corss-relaxation of Yb^{3+}-X^{3+}(Er^{3+}/Tm^{3+}/Ho^{3+}) cuased by high concentration of Yb^{3+} in the Nd^{3+}-sensitized UCNPs.

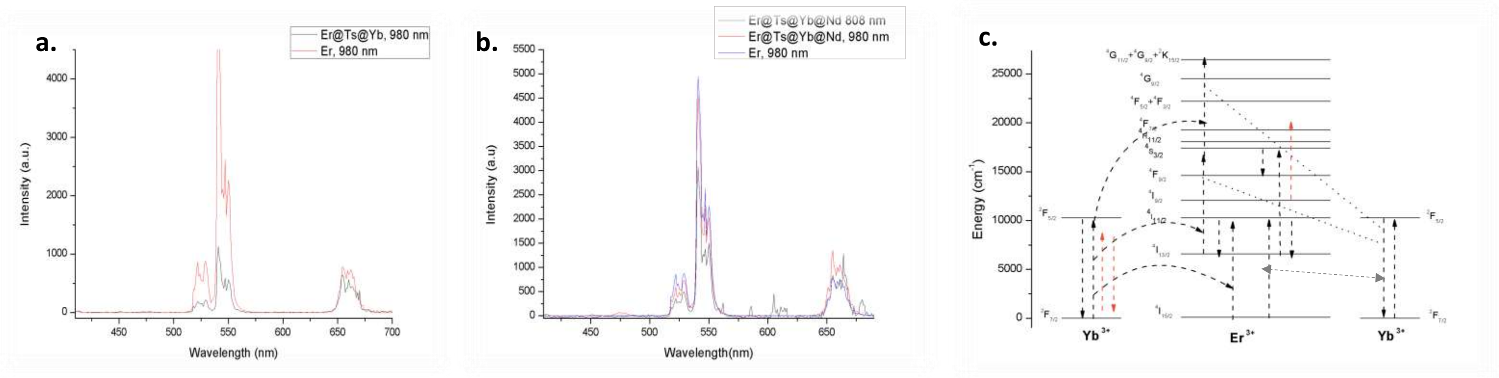

Figure 6. Yb^{3+} energy back-transfer. (a) Emission spectra of NaGdF$_4$:Yb, Er and NaGdF$_4$:Yb, Er coated with NaGdF$_4$:Yb, Nd and NaYbF$_4$ when excited by 980 nm laser,

illustrating quenching effect of $NaYbF_4$. (b) Emission spectra of $NaGdF_4$: $Yb_{20\,\%}$,$Er_{2\,\%}$@$NaGdF_4$:$Yb_{10\,\%}$@$NaYbF_4$@$NaNdF_4$ excited by 980 nm laser and 808 nm laser compared with $NaGdF_4$: $Yb_{20\,\%}$,$Er_{2\,\%}$ excited by 980 nm laser, illustrating quenching effect of $NaYbF_4$. (c) Energy levels illustrating the quenching effect of Yb^{3+} back-transfer. Measurement conditions: power density: 80 mW/ 1 mm^2 for 808/ 980 nm diode laser; emission bandwidth: 2 nm, concentration: 1.0 wt %.

2.2.1.3. Importance and amelioration of the harvest layer:

As reported by Y.T., Zhong *et al.*, a harvest layer ($NaNdF_4$) is in need to develop the luminescence performance of the Nd^{3+}-sensitized UCNPs.[15] In our research work, we found that: firstly, certain amount of Yb^{3+} ions should be doped in the harvest layer to build efficient Nd^{3+}→Yb^{3+} energy transfer; secondly, the surface quenching caused by the Yb^{3+} ions that doped in the harvest layer should be remedied by a surface coating; lastly, the composition of the harvest layer should be optimized to gain the optimum of the luminescence performance.

As we have stated that the harvest layer is indispensable in the construction of the Nd^{3+}-sensitized UCNPs, for the one of the basic original intension of Nd^{3+}-sensitized construction is that enhancement of the luminescence intensity (the other one is over-heating effect avoiding). As utilization a $NaNdF_4$ layer as a harvest layer and sandwiching a $NaGdF_4$:Yb layer as a transition layer has been proposed [15], we tried to ameliorate and optimize the whole Nd^{3+}-trinity system by adjusting the composition of the harvest layer.

Firstly, we have confirmed that without efficient Nd^{3+}→Yb^{3+} energy transfer, the $NaNdF_4$ harvest layer is proved to be photons dissipation. As shown in Figure 7, compares with the Nd^{3+}-sensitized UCNPs with the structures that is $NaGdF_4$:Yb

$_{20\ \%}$,$Er_{2\ \%}$@$NaGdF_4$:$Yb_{10\ \%}$, $Nd_{20\ \%}$@$NaGdF_4$ and $NaGdF_4$:Yb $_{20\ \%}$,$Er_{2\ \%}$@$NaGdF_4$:$Yb_{10\ \%}$, $Nd_{20\ \%}$@$NaNdF_4$, we surprisingly found that the only 50 % percentage Nd^{3+} ions doping in the UCNPs appears to obtained with better luminescent performance than the UCNPs that equipped with sandwiching a transition layer into the harvest layer and the cores, although both of them have avoided the quenching caused by Yb^{3+} surface defect. And what remind us is that Yb^{3+} ions should be doped into the $NaNdF_4$ layers to guarantee the efficient Nd^{3+} -Yb^{3+} energy transfer, along with avoiding the Yb^{3+} surface quenching by coating a activation layer ($NaGdF_4$), as shown in Figure 3 (c).

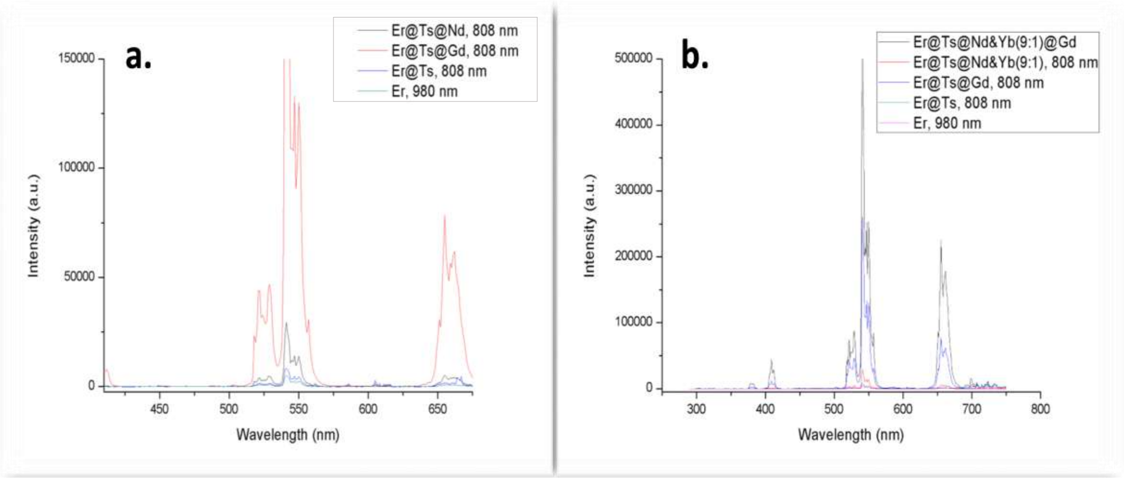

Figure 7. Harvest layer. (a). $NaGdF_4$:Yb $_{20\ \%}$,$Er_{2\ \%}$@$NaGdF_4$:$Yb_{10\ \%}$, $Nd_{20\ \%}$, $NaGdF_4$:Yb $_{20\ \%}$,$Er_{2\ \%}$@$NaGdF_4$: $NaGdF_4$:$Yb_{10\ \%}$, $Nd_{20\ \%}$@$NaGdF_4$ and $NaGdF_4$:Yb $_{20\ \%}$,$Er_{2\ \%}$@$NaGdF_4$:$Yb_{10\ \%}$, $Nd_{20\ \%}$@$NaGdF_4$ excited by 808 nm laser compared with $NaGdF_4$:Yb, Er excited by 980 nm laser. (b). $NaGdF_4$:Yb, Er @$NaGdF_4$: $Yb_{10\ \%}$, $Nd_{20\ \%}$@$NaNdF_4$:Yb (9:1), $NaGdF_4$:Yb $_{20\ \%}$,$Er_{2\ \%}$@$NaGdF_4$:$Yb_{10\ \%}$, $Nd_{20\ \%}$@$NaNdF_4$:Yb $_{10\ \%}$@$NaGdF_4$, $NaGdF_4$:Yb $_{20\ \%}$,$Er_{2\ \%}$@$NaGdF_4$:$Yb_{10\ \%}$, $Nd_{20\ \%}$@$NaGdF_4$, $NaGdF_4$:Yb $_{20\ \%}$,$Er_{2\ \%}$@$NaGdF_4$:$Yb_{10\ \%}$, $Nd_{20\ \%}$ excited by 808 nm compared with $NaGdF_4$:Yb $_{20\ \%}$,$Er_{2\ \%}$ excited by 980 nm laser. It reveals more 808 nm photons could be harvested by utilizing

$NaNdF_4$ layer. However, the luminescence performance of $NaGdF_4$:Yb, Er @$NaGdF_4$: $Yb_{10\ \%}$, $Nd_{20\ \%}$@$NaNdF_4$ was much lower than $NaGdF_4$:Yb, Er @$NaGdF_4$: $Yb_{10\ \%}$, $Nd_{20\ \%}$@$NaGdF_4$. This situation could be developed by doping 10 mmol % Yb^{3+} , for the luminescence performance was improved by coating with a $NaGdF_4$ layer. (Measurement conditions: power density: 80 mW/ 1 mm ^{2} for 808/ 980 nm diode laser; emission bandwidth: 2 nm, concentration: 1.0 wt %.)

Secondly, in our investigations, we found that doping certain amount of Yb^{3+} in the $NaNdF_4$ layer, will largely improve the luminescent performance, which could be attribute to the ameliorated Nd^{3+}-Yb^{3+} energy transfer. As shown in Figure 3 (c)., doping 10 % percentage of Yb^{3+} ion in the $NaNdF_4$ layer, and then coating a $NaGdF_4$ layer to shield the surface defect, leading to large enhancement of the emission.

Lastly, the harvest layer should be optimized by adjusting the composition of the harvest layer. As shown in Figure 8, in the Nd^{3+}-trinity system coated $NaGdF_4$:Yb,Er UCNPs, we found by adjusting the composition of the harvest layer, which is $NaNdF_4$:Yb_x (x = 10, 20, 30 ……90), the amount of Yb^{3+} doping is form 10 % to 90 % percentage. The emission spectra of UCNPs with various composition of harvest layer are shown in table 2 and Figure10.The optimized luminescent performance could be achieved when the concentration of Yb^{3+} doping is 20 %.

Also, the Nd^{3+}-trinity system coated $NaGdF_4$:Yb, Tm UCNPs and Nd^{3+}-trinity system coated $NaGdF_4$:Yb,Ho UCNPs has also been optimized by adjusting the composition of the harvest layer. As shown in Figure, by adjusting the harvest layer, which is $NaGd_{90\ \%-x}$ F_4:$Yb_{10\ \%}$, Nd_x , the emission spectra shows that when doping concentration of Nd^{3+} is 50 %, the Nd^{3+}-trinity system showed the optimized harvest, transfer and sensitization effect on the NaGdF$_4$:Yb,Tm and NaGdF$_4$:Yb,Ho cores.

Conclusively, the Nd^{3+}→Yb^{3+} energy transfer could be treated as the double-edged sword which on one hand enables the 808 nm laser to drive the UCNPs; on the other hand, the Nd^{3+}-Yb^{3+} energy transfer is surely to cause the manifest quenching as we have demonstrated above. The significant of construction of the Nd^{3+}-trinity system is to develop the over-heating effect avoiding and attenuation of photo-luminescence source preventing UCNPs with excitation of 808 nm laser, as well as to gain sufficient 808 nm photon harvest and Nd^{3+}-Yb^{3+} energy transfer along with shielding all the quenching factors.

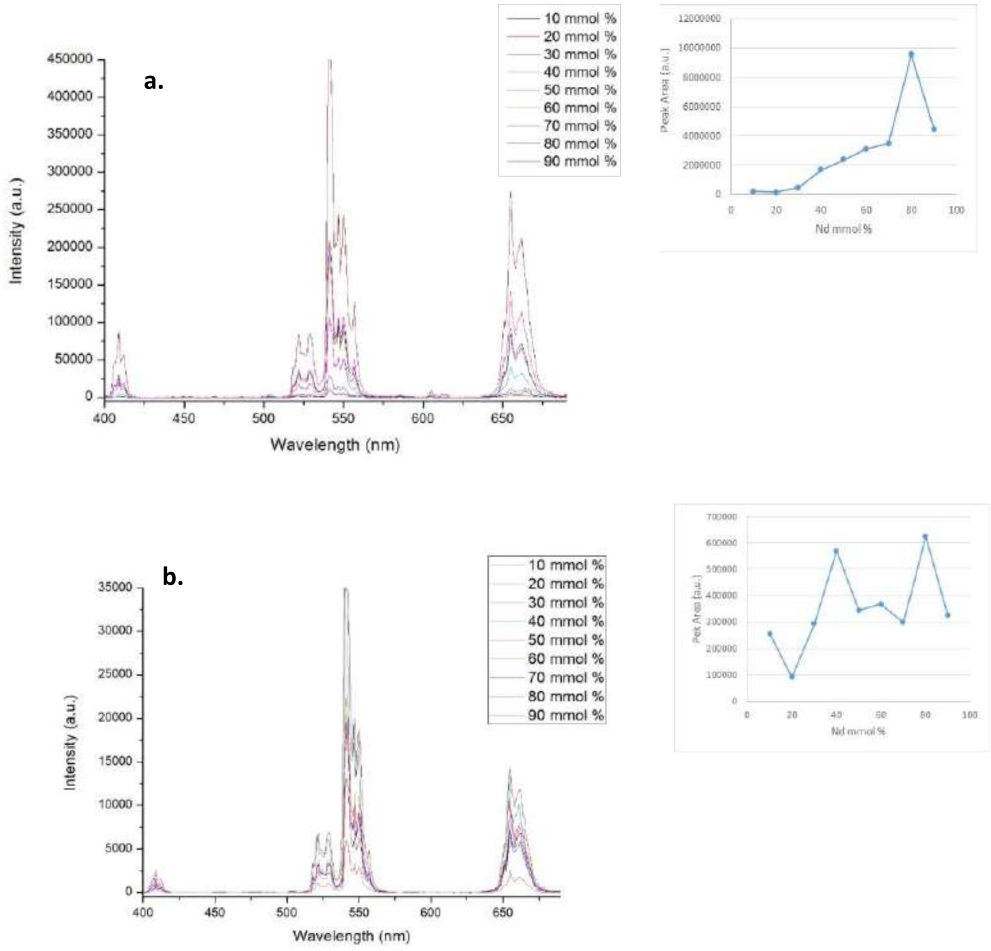

Figure 8. Optimization of Harvest layer of the $NaGdF_4$: Yb $_{20\,\%}$, $Er_{2\,\%}$ @$NaGdF_4$:$Yb_{10\,\%}$, $Nd_{20\,\%}$@$NaNdF_4$:Yb@$NaGdF_4$ by adjusting Yb^{3+} concentration in $NaNdF_4$:Yb layer from 10-90 mmol %. Emission spectra was measured under 808 nm (a) and 980 nm (b) exciation. (Measurement conditions: power density: 80 mW/ 1 mm^2 for 808/ 980 nm diode laser; emission bandwidth: 0.5 nm, concentration: 1.0 wt %.)

Lifetime (μs) / Nanoparticle Structures	808 nm excited				980 nm excited			
	Wavelength (nm)				Wavelength (nm)			
	414	522	541	655	414	522	541	655
NaGdF$_4$:Yb,Er @NaGdF$_4$:Yb,Nd @NaNd&Yb(1:9)F$_4$@NaGdF$_4$	8.10	5.96	21.65	5.43	60.03	100.02	96.65	137.35
NaGdF$_4$:Yb,Er @NaGdF$_4$:Yb,Nd @NaNd&Yb(2:8)F$_4$@NaGdF$_4$	5.49	65.00	81.49	39.05	59.29	68.24	81.10	81.10
NaGdF$_4$:Yb,Er @NaGdF$_4$:Yb,Nd @NaNd&Yb(3:7)F$_4$@NaGdF$_4$	-	-	-	-	63.83	100.59	99.90	145.56
NaGdF$_4$:Yb,Er @NaGdF$_4$:Yb,Nd @NaNd&Yb(4:6)F$_4$@NaGdF$_4$	6.04	106.64	115.97	90.28	82.70	117.69	118.98	173.58
NaGdF$_4$:Yb,Er @NaGdF$_4$:Yb,Nd @NaNd&Yb(5:5)F$_4$@NaGdF$_4$	6.51	-	128.76	166.30	-	86.68	87.61	129.47
NaGdF$_4$:Yb,Er @NaGdF$_4$:Yb,Nd @NaNd&Yb(6:4)F$_4$@NaGdF$_4$	-	98.94	91.12	123.79	72.46	81.44	89.99	119.48
NaGdF$_4$:Yb,Er @NaGdF$_4$:Yb,Nd @NaNd&Yb(7:3)F$_4$@NaGdF$_4$	71.10	86.98	-	103.05	89.86	115.22	108.86	150.26
NaGdF$_4$:Yb,Er @NaGdF$_4$:Yb,Nd @NaNd&Yb(8:2)F$_4$@NaGdF$_4$	104.9	133.01	127.48	149.79	85.30	120.76	122.24	170.19
NaGdF$_4$:Yb,Er @NaGdF$_4$:Yb,Nd @NaNd&Yb(9:1)F$_4$@NaGdF$_4$	97.56	130.10	131.49	162.63	60.03	100.02	96.65	137.35

Table 4. Lifetime of NaGdF$_4$:Yb, Er @NaGdF$_4$:Yb,Nd @NaNdF$_4$:Yb(10-90 mmol %)@NaGdF$_4$ excited by 980/808 nm laser.

2.2.1.4. Yb^{3+} surface quenching

As shown in Figure 9, the Yb^{3+} surface quenching that caused by the Yb^{3+} ions doped in the harvest layer should be shielded by a surface coating, which further largely enhance the luminescence. For the requirement of developing a MRI contrast agent as discussed below, a $NaGdF_4$ layer has been chosen.

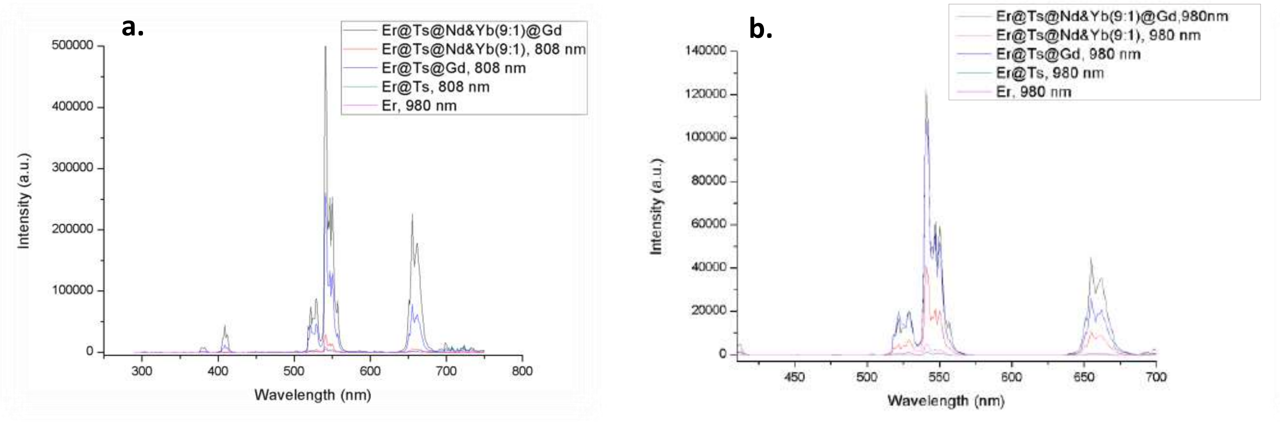

Figure 9. Effect of activation layer. (a). $NaGdF_4$:$Yb_{20\ \%}$, $Er_{2\ \%}$ @$NaGdF_4$:$Yb_{10\ \%}$, $Nd_{20\ \%}$, $NaGdF_4$:$Yb_{20\ \%}$, $Er_{2\ \%}$ @$NaGdF_4$:$Yb_{10\ \%}$, $Nd_{20\ \%}$@ $NaGdF_4$, $NaGdF_4$:$Yb_{20\ \%}$, $Er_{2\ \%}$ @$NaGdF_4$:$Yb_{10\ \%}$, $Nd_{20\ \%}$@$NaNdF_4$:$Yb_{50\ \%}$ and $NaGdF_4$:$Yb_{20\ \%}$, $Er_{2\ \%}$ @$NaGdF_4$:$Yb_{10\ \%}$, $Nd_{20\ \%}$@$NaNdF_4$:$Yb_{50\ \%}$@$NaGdF_4$ excited by 808 nm laser compares with $NaGdF_4$:Yb, Er excited by 980 nm laser. (b).Comparison of $NaGdF_4$:$Yb_{20\ \%}$, $Er_{2\ \%}$ @$NaGdF_4$:$Yb_{10\ \%}$, $Nd_{20\ \%}$, $NaGdF_4$:$Yb_{20\ \%}$, $Er_{2\ \%}$ @$NaGdF_4$:$Yb_{10\ \%}$, $Nd_{20\ \%}$@ $NaGdF_4$, $NaGdF_4$:$Yb_{20\ \%}$, $Er_{2\ \%}$ @$NaGdF_4$:$Yb_{10\ \%}$, $Nd_{20\ \%}$@$NaNdF_4$: $Yb_{50\ \%}$, $NaGdF_4$:$Yb_{20\ \%}$, $Er_{2\ \%}$ @$NaGdF_4$:$Yb_{10\ \%}$, $Nd_{20\ \%}$@$NaNdF_4$: $Yb_{50\ \%}$@$NaGdF_4$ and $NaGdF_4$:$Yb_{20\ \%}$, $Er_{2\ \%}$ excited by 980 nm laser. (c). Comparison between the emission spectra of $NaGdF_4$:$Yb_{20\ \%}$, $Er_{2\ \%}$ @$NaGdF_4$:$Yb_{10\ \%}$, $Nd_{20\ \%}$@$NaNdF_4$: $Yb_{50\ \%}$@$NaGdF_4$ with excitation of 808 nm and 980 nm laser. As shown in Figures S5 (a) and S5 (b), compared with coating $NaGdF_4$ layer, the luminescence of

$NaGdF_4$:$Yb_{20\ \%}$, $Er_{2\ \%}$ @$NaGdF_4$:$Yb_{10\ \%}$, $Nd_{20\ \%}$@$NaNdF_4$: $Yb_{50\ \%}$ was largely enhanced when excited by 980 nm and 808 nm. (Measurement conditions: power density: 80 mW/ 1 mm ^{2} for 808/ 980 nm diode laser; emission bandwidth: 2 nm, concentration: 1.0 wt %.)

2.2.2. Design

By drawing lessons from previous work and the investigations on the quenching factors, we have designed the core-multishells UCNPs that is the $NaGdF_4$:Yb, X(Er/Tm/Ho) coating with **Nd^{3+}-harvest-transfer-sensitization trinity (Nd^{3+}-Trinity) system**, which is compose of the transition layer, harvest layer and activation layer, to guarantee the best harvesting and energy transfer as well as shielding all the quenching factors in the system. It could be illustrated as function trinity that realizes three functions that are harvesting the 808 nm photons, $Nd^{3+}\rightarrow Yb^{3+}$ energy transfer and sensitize the activator in one system and quenching shielding trinity that is shielding three quenching including Yb^{3+} energy back transfer, Nd^{3+} energy back transfer and Yb^{3+} surface quenching.

The Nd^{3+}-Trinity system, in specifically is that: $NaGdF_4$:Yb, X(Er/Tm/Ho) cores coating with transition layer ($NaGdF_4$:Yb), harvest layer ($NaNdF_4$:Yb or $NaGdF_4$:$Yb_{10\ \%}$,$Nd_{\ 50\ \%}$) and activation layer ($NaGdF_4$), as show in Scheme 1(b). As the design has gained with superior luminescent properties, which is proposed to be contributed by the harvest layer, to make clear more phenomenon and mechanism of Nd^{3+}-sensitization, we have developed another system that is the $NaGdF_4$:Yb,X(Er/Tm/Ho)$^{3+}$ cores coated with $NaGdF_4$:$Yb_{10\ \%}$,$Nd_{20\ \%}$, and $NaGdF_4$ (activation layer) (type II Nd^{3+}-trinity), with difference that is the just doped with 20 % mmol Nd^{3+} ions in the transition layer instead of use the harvest layer compares with the former design (type Nd^{3+}-trinity), as shown in Scheme 1(b). (**Type I Nd^{3+}-Trinity System**)

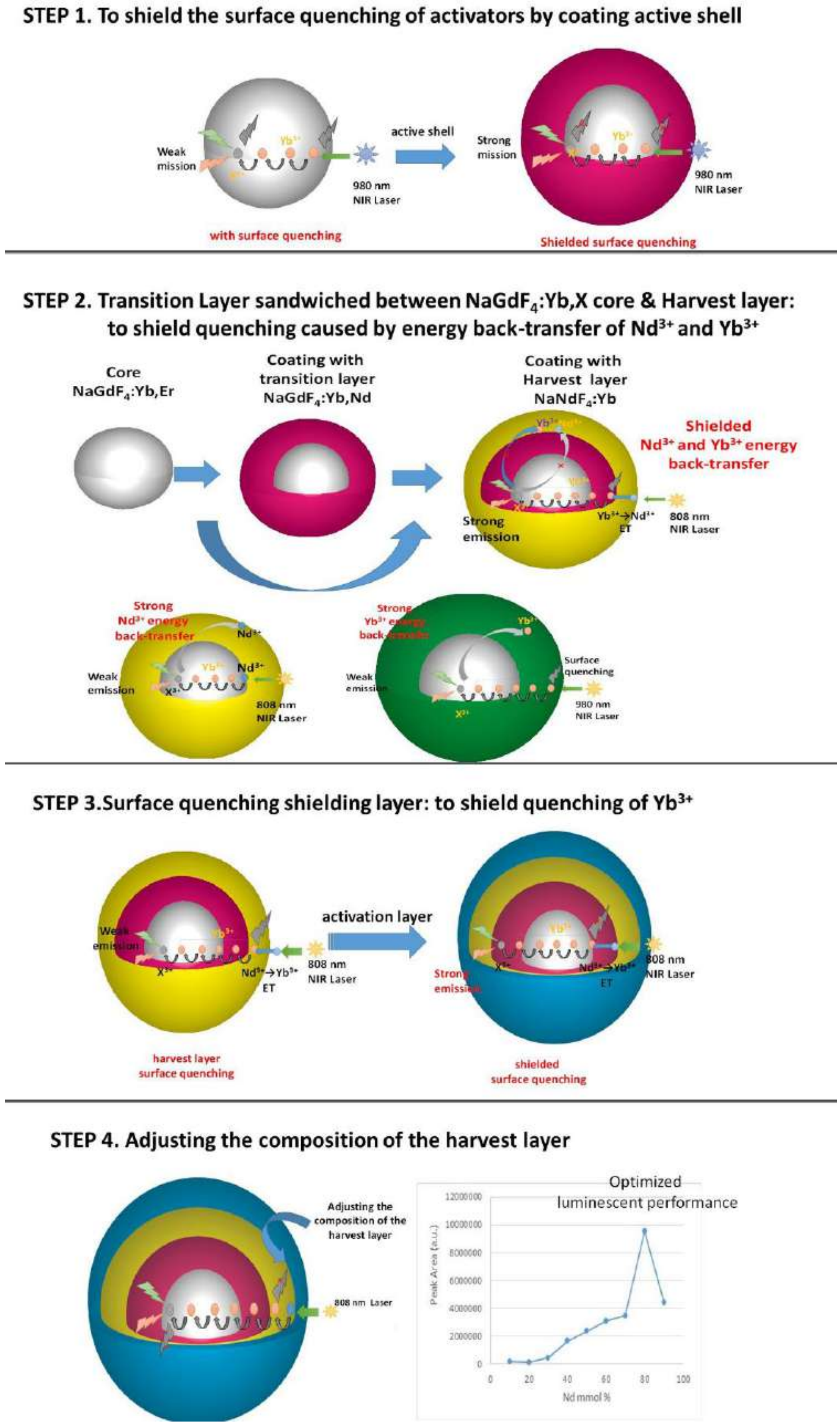

Scheme 2. The strategies in construction of the Nd^{3+}-Trinity system

The strategies of construction of the Nd^{3+} -sensitized UCNPs could be generalized as i. to avoid energy back-transfer of Yb^{3+} and Nd^{3+} by sandwiching the transition layer with the $NaGdF_4$:Yb, X(Er/Tm/Ho) core and the harvest layer; ii. to harvest sufficient 808 nm photons and guarantee efficient $Nd^{3+}\rightarrow Yb^{3+}$ energy transfer by appropriately doping Yb^{3+} in the $NaNdF_4$ layer, which could be concluded as optimized harvest layer; iii. to shield the surface quenching of Yb^{3+} by coating a $NaGdF_4$ activation layer; iv. the harvest layer should be optimized by adjusting the ratio of Yb^{3+}/Nd^{3+} or concentration of Nd^{3+}, as shown in Scheme 2.

For further investigation on the effect of the harvest layer and Nd^{3+} -sensitization, we have developed the Type II Nd^{3+} -Trinity System, which is which is $NaGdF_4$: Yb, Er/Tm/Ho@$NaGdF_4$:$Yb_{10\ \%}$, Nd $_{20\ \%}$@$NaGdF_4$ (Core@Ts@Gd in short). The difference with Type I Nd^{3+}-Trinity system is that, as shown in Scheme 1(b), instead of inducing the harvest layer, just doping 20 mmol% Nd^{3+} ions in the transition layer, that is $NaGdF_4$:$Yb_{10\%}$,$Nd_{20\%}$, which also realize the harvest, transfer and sensitization function as well shielding the quenching factors by activation layer by doping small amount of Yb^{3+} and Nd^{3+}, however, with limitation on the 808 nm photons absorption. The comparison of the luminescent properties between Type I and Type II Nd^{3+}-Trinity system UCNPs, act as an efficient tool to illustrate the effect of the harvest layer, the specific mechanism and phenomenon of the Nd^{3+}-sensitization, as discussed below.

2.3. Synthesis and Characterization

Synthesis the core-shell structured UCNPs by "seeded" growth: all the nanoparticles were synthesized by thermal decomposition [29]. The basic mechanism of the synthesis of the core-shell is epitaxial growth that is the replacement of the oleate by the F^- and further in "seeded growth" process [33, 35, 36]; and the core-multishells structures are synthesized by "layer-by-layer " [32] epitaxial growth, as shown in Scheme 3.

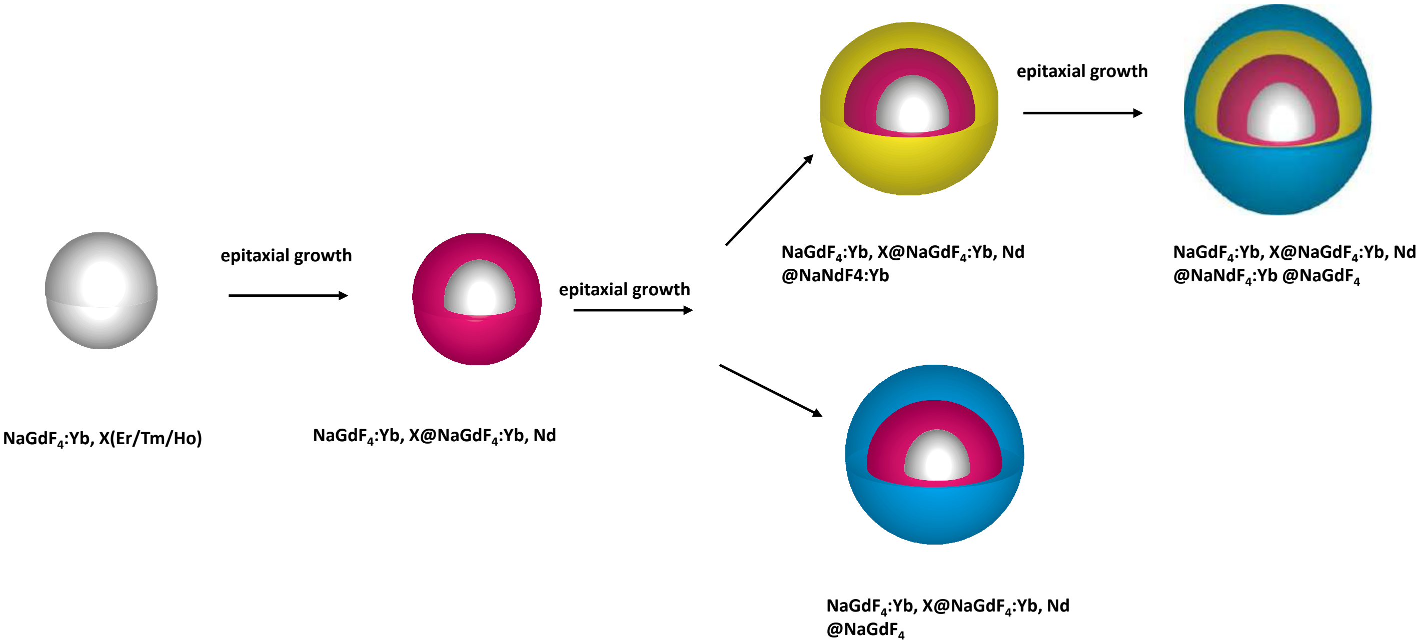

Scheme 3. Synthesis of the core-multishells by layer-by-layer epitaxial growth.

2.4. Characterization of the Morphologic, Luminescent and Magnetic Properties

By the characterization of the Nd^{3+}-Trinity system coated UCNPs, it is proven that they are in minimized size and show superior upconversion luminescent properties including largely enhanced luminescence intensity, prolonged lifetime, deeper penetration in water, larger partition of red emission and higher quantum yield, along with the satisfactory magnetic properties. Additionally, we have proposed that the largely enhanced intensity of luminescence is contributed by the high absorption of Nd^{3+} ions and the well design of the Nd^{3+}-trinity system; the prolonged lifetime is contributed by the selectively participation of the 1056 nm phonons in the ETU process which is result in the Nd^{3+}-Yb^{3+} phonon-assistant energy transfer; the deeper penetration is contributed by the substitution of 980 nm laser excitation of 808 nm excitation, which result in enhanced luminescence and shielding attenuation of photoluminescence source, along with the over-heating effect.

2.4.1. Minimized Size

As demonstrated in previous part (Chapter 1 and 2.3 Synthesis and Characterization), the UCNPs are synthesized by the method of thermal decomposition, result in minimized size and well self-assembly by the stabilization of oleic acid. As shown in Figure 10, by "layer by layer" epitaxial growth of the core-shell UCNPs, could we obtain the core-multishells that are Nd^{3+}-trinity system coating on the $NaGdF_4$:Yb,Er/Tm/Ho core, for the type I Nd^{3+}-trinity system sensitized UCNPs, which could be explained in details as $NaGdF_4$:Yb, Er cores coating with the $NaGdF_4:Yb_{10\,\%}$, $Nd_{20\,\%}$ layer (transition layer), and then coating with $NaNdF_4:Yb_{20\,\%}$ layer (harvest layer), and then coating with $NaGdF_4$ layer (activation layer); or $NaGdF_4$:Yb, Tm/Ho cores coating with the $NaGdF_4:Yb_{10\,\%}$, layer (transition layer), and then coating with $NaGdF_4:Nd_{50\,\%},Yb_{10\,\%}$ layer (harvest layer), and then coating with $NaGdF_4$ layer (activation layer). For the type II Nd^{3+}-trinity system sensitized UCNPs, could be explained in details as $NaGdF_4$:Yb, Er/Tm/Ho cores coating with the $NaGdF_4$:Yb(10 %), Nd(20 %) layer (transition layer), and then coating with $NaGdF_4$ layer (activation layer).

By the size growth, we would characterize the successfully synthesized Nd^{3+}-Trinity system coated UCNPs, as shown in Figure 10, the diameter of the β-$NaGdF_4:Yb_{20\%},Er_{2\%}$ cores result in diameter of 6.43±0.99 nm; by epitaxial "layer-by-layer" growth [32] of the transition layer ($NaGdF_4:Yb_{20\%},Nd_{10\%}$), harvest layer ($NaNdF_4:Yb_{20\%}$) and activation layer($NaGdF_4$), the diameter of the β-phased UCNPs result in 9.11±1.05 nm,10.69±0.96 nm and 12.44±1.30 nm . For the characterization on the individual UCNPs could be seen in Figure 11 and Figure 12. The thickness is about 0.9 ~ 1.3 nm for each layer. And the very thin layers make the gadolinium-based, core-multishells structure in minimized size, which is advantageous in bio-imaging and beneficial to the development of multiple functional bio-imaging probes, such as MRI contrast agent for the minimized size and gadolinium coating as discussed below.

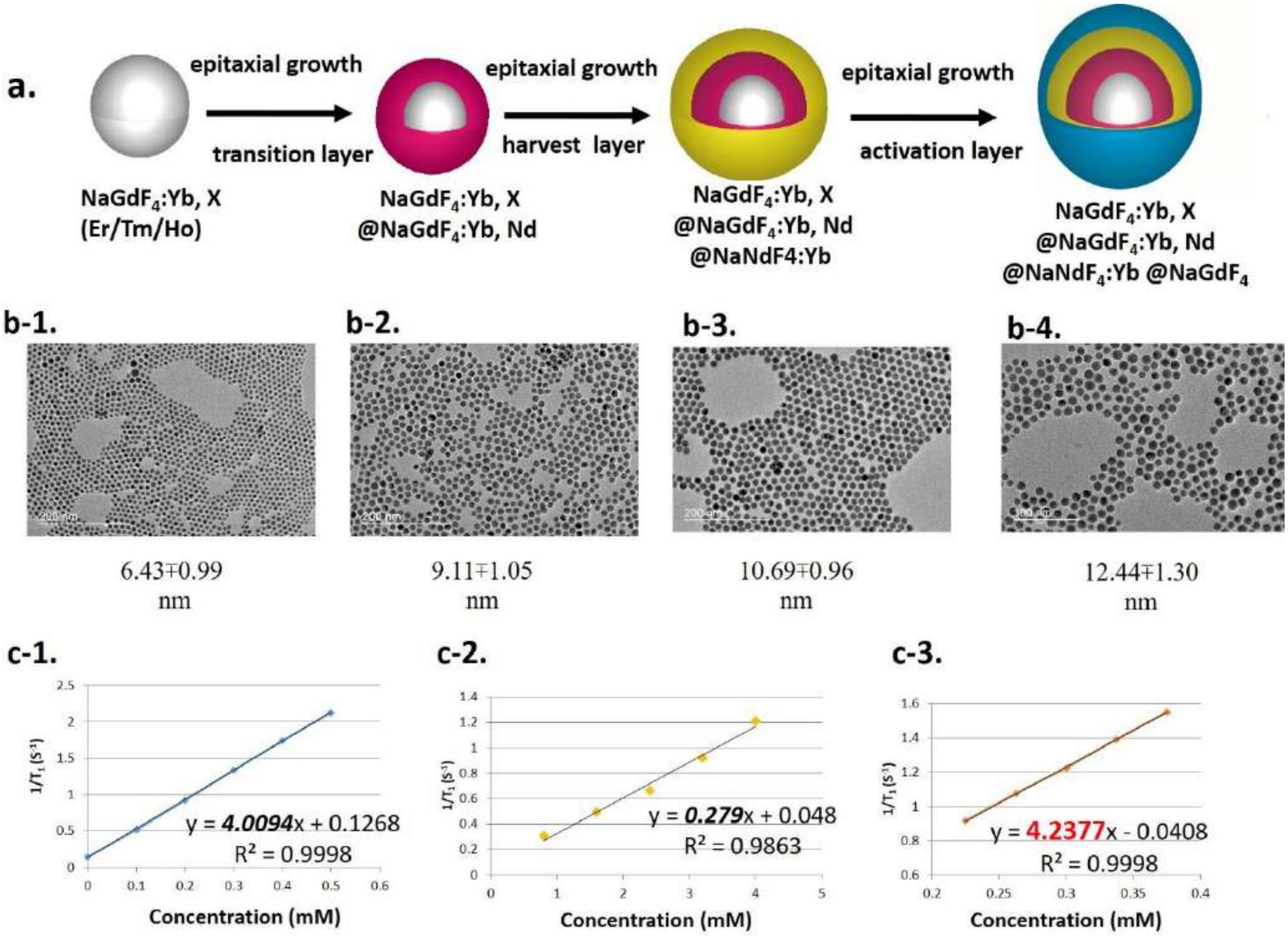

Figure 10. (a). Scheme and (b).TEM images of size growth of the Type II Nd^{3+}-Trinity system by "layer-by-layer" epitaxial growth. (c) r_1 relaxivity measurement of the Gd-DOTA(c-1), UCNPs as shown in (b-4) with washing by HCl that removed oleate (c-2) and the branched PEI exchanged UCNPs (c-3).

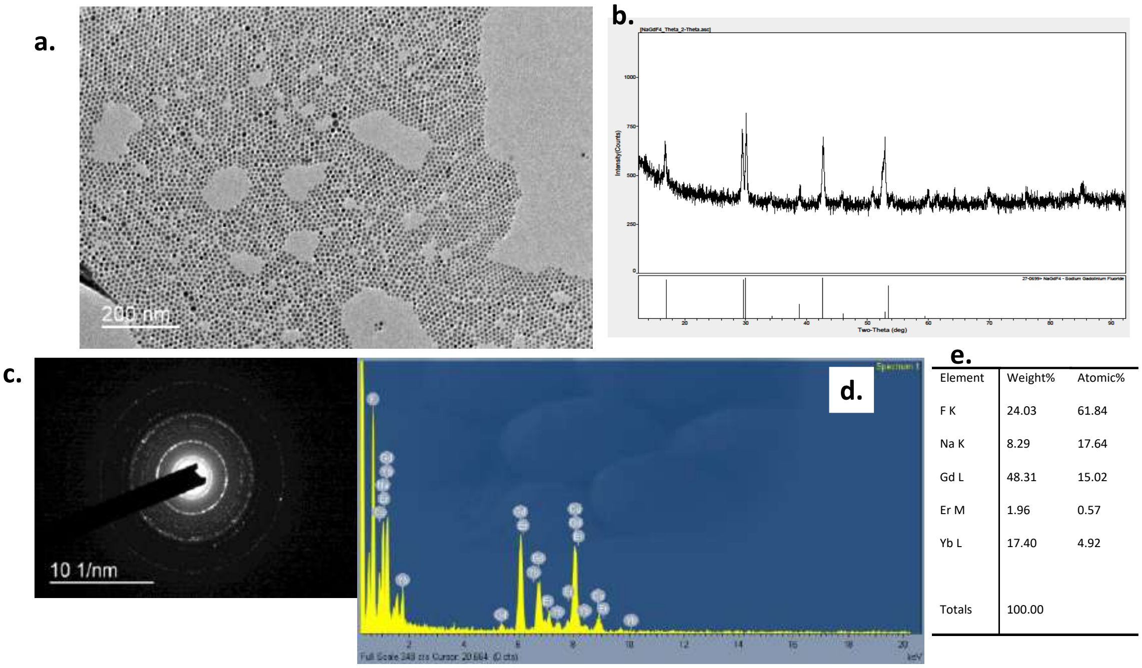

Element	Weight%	Atomic%
F K	24.03	61.84
Na K	8.29	17.64
Gd L	48.31	15.02
Er M	1.96	0.57
Yb L	17.40	4.92
Totals	100.00	

Figure 11. TEM (a), XRD pattern (b), SEAD (c) and EDX (d, e) of the $NaGdF_4$:$Yb_{20\ \%}$,$Er_{2\ \%}$ nanoparticles.

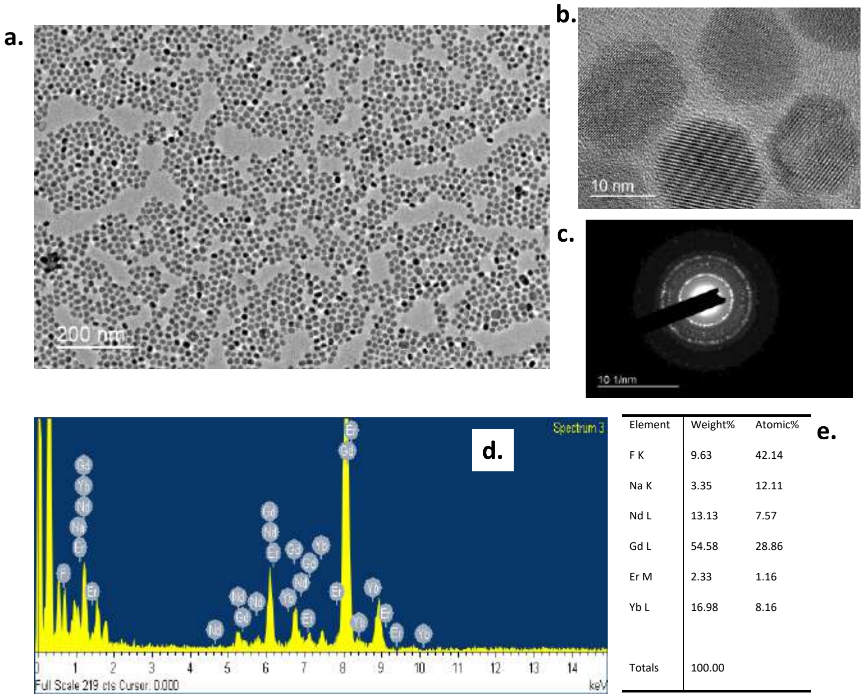

Element	Weight%	Atomic%
F K	9.63	42.14
Na K	3.35	12.11
Nd L	13.13	7.57
Gd L	54.58	28.86
Er M	2.33	1.16
Yb L	16.98	8.16
Totals	100.00	

Figure 12. TEM (a), HR-TEM (b), SEAD (c) and EDX (d, e) of the $NaGdF_4{:}Yb_{20\,\%},Er_{2\,\%}@NaGdF_4{:}Yb_{10\,\%},Nd_{20\,\%}@NaNdF_4{:}Yb_{20\,\%}@NaGdF_4$ nanoparticles

2.4.2. Largely enhanced luminescence intensity

Both of the two types of the Nd^{3+}-trinity system could largely enhance the luminescence of the UCNPs with excitation of 808 nm when compared with the UCNPs cores with excitation of 980 nm laser. As shown in Table 5, under the same measurement conditions (which must strictly requires on the power density of 980 nm and 808 nm c.w. laser), the type II structures were measured under 808 nm excitation to give the following folds of the peak area to $NaGdF_4$: Yb, Er/Tm/Ho cores with 980 nm excitation as: 44.66 (Er^{3+}), 31.13 (Tm^{3+}) and 45.10 (Ho^{3+}) folds; while the folds for the type II structures were 231.97(Er^{3+}), 449.78 (Tm^{3+}) and 195.08 (Ho^{3+}) folds, which illustrates the effect of the harvest layer. The emission spectra, luminescence performance photography could be seen in Figure 13.

Nd^{3+}-trinity system Activators in the UCNP core	**Type I**	Type II
Er^{3+}	*231.98*	44.66
Tm^{3+}	*499.79*	48.18
Ho $^{3+}$	*195.08*	45.10

Table 5. The effect of Nd^{3+}-trinity system: scale of the enhancement for the type I and type II Nd^{3+}-Trinity System coated $NaGdF_4$:Yb, Er/Tm/Ho UCNPs (ratio of peak area of the emission spectra).

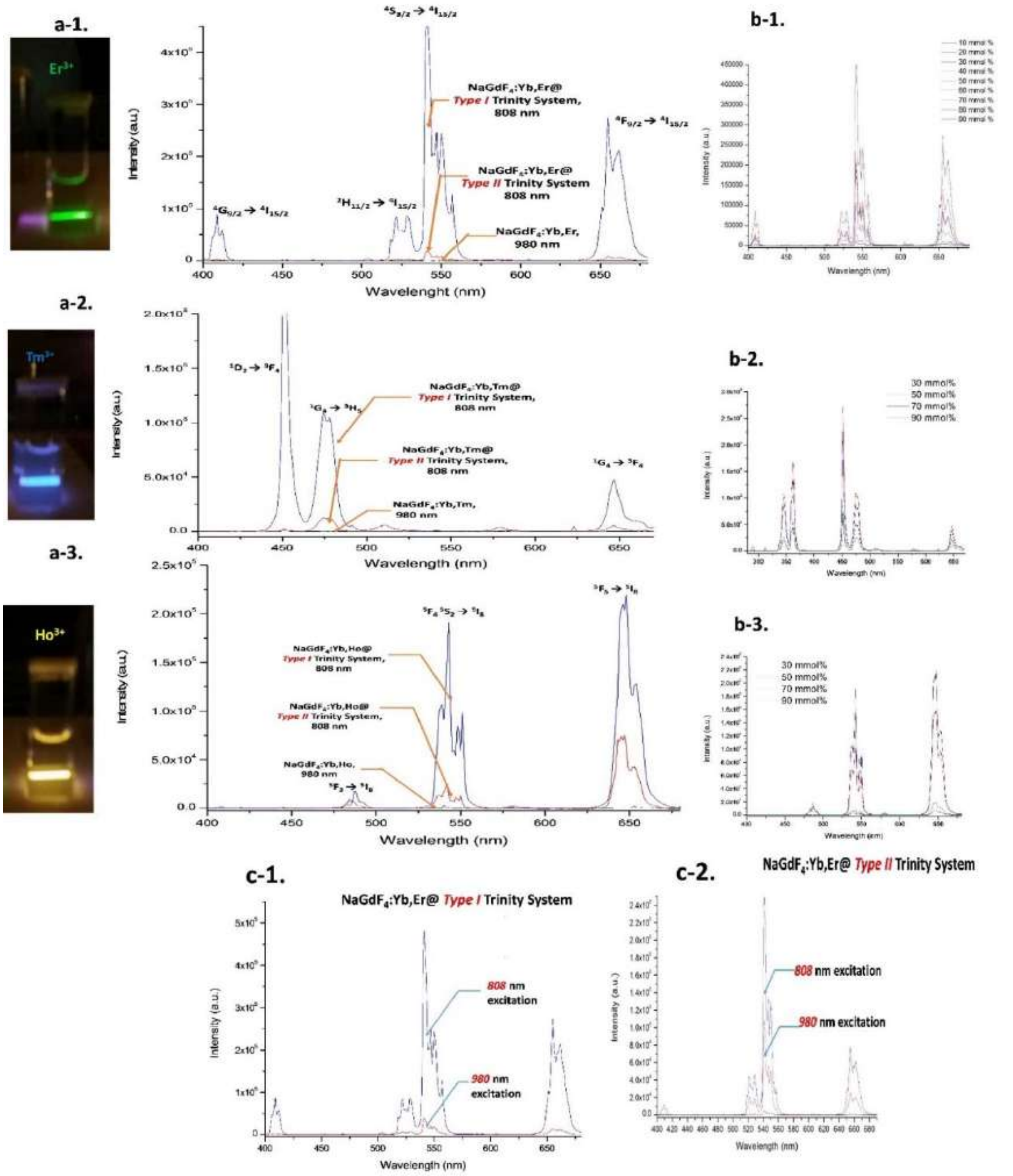

Figure 13. Photographs of luminescent performance and emission spectra of the Nd^{3+}-Trinity system(type I)coating coated NaGdF$_4$:Yb$_{20\%}$,Er$^{3+}{}_{2\%}$ (a-1), NaGdF$_4$:Yb$_{49\%}$,Tm$^{3+}{}_{1\%}$ (a-2) and NaGdF$_4$:Yb$_{20\%}$,Ho$^{3+}{}_{2\%}$ (a-3). The optimization of the harvest layer of the type I Nd^{3+}-Trinity system coated NaGdF$_4$:Yb$_{20\%}$,Er$^{3+}{}_{2\%}$ (b-1), NaGdF$_4$:Yb$_{49\%}$,Tm$^{3+}{}_{1\%}$ (b-2) and NaGdF$_4$:Yb$_{20\%}$,Ho$^{3+}{}_{2\%}$ (b-3). Comparison of emission spectra of NaGdF$_4$:Yb,Er@type I

Nd^{3+}-Trinity system (c-1) and II (c-2) with 980 nm and 808 nm excitation. (Measurement conditions: power density: 80 mW/1 mm^2 for 808/980 nm diode laser; emission bandwidth: 0.2 nm (2.0 nm for c-2), concentration: 1.0 wt %.)

Also the UCNPs coating with Nd^{3+}-trinity system shows better luminescence performance under the excitation of 980 nm, as shown in Figure 13, which could be attributed to the remedy of the surface defect of the activators (Er^{3+}/Tm^{3+}/Ho^{3+}) and the sensitizer as we have stated above. For the same Nd^{3+}-trinity system coated UCNPs, it shows almost 10 times luminescence under 808 nm excitation than the 980 nm excitation, as shown in Figure 13 (c), which could be attributed to the high absorption of Nd^{3+} ions to 808 nm photons.

2.4.3. Bio-imaging of the Type II Nd^{3+}-Trinity system coated $NaGdF_4$:Yb, Er

When the Nd^{3+}-Trinity system coated UCNPs are utilized in vitro bio-imaging, it also shows satisfied luminescence performance as well as the deeper luminescence penetration under 808 nm excitation.

Surface modification have been made on the UCNPs that is Nd^{3+}-Trinity system coated $NaGdF_4$:$Yb_{20\,\%}$, $Er_{2\,\%}$ with coating the silica shells to make the hydrophobic UCNPs to be the lipophilic ones along with preventing the potential toxically of the Gd^{3+} ions.

As shown in Figure 14, in the research work of the in vitro fluorescence bio-imaging, when the Type I Nd^{3+}-Trinity system UCNPs with the activator of Er^{3+} are coated with silica shells and incubate with the HeLa cells for 20 h, it display satisfied luminescence performance under 808 nm excitation; furthermore, the in vitro bio-imaging fluorescence under 808 nm excitation, although with lower power density, shows better luminescence performance than the situation that with 980 nm excitation, although in higher power density. Similarly, the deeper in vitro fluorescence should be consider to be contributed by the enhanced luminescence of Nd^{3+}-sensitization as well as the avoiding of the attenuation of the photo-luminescence source.

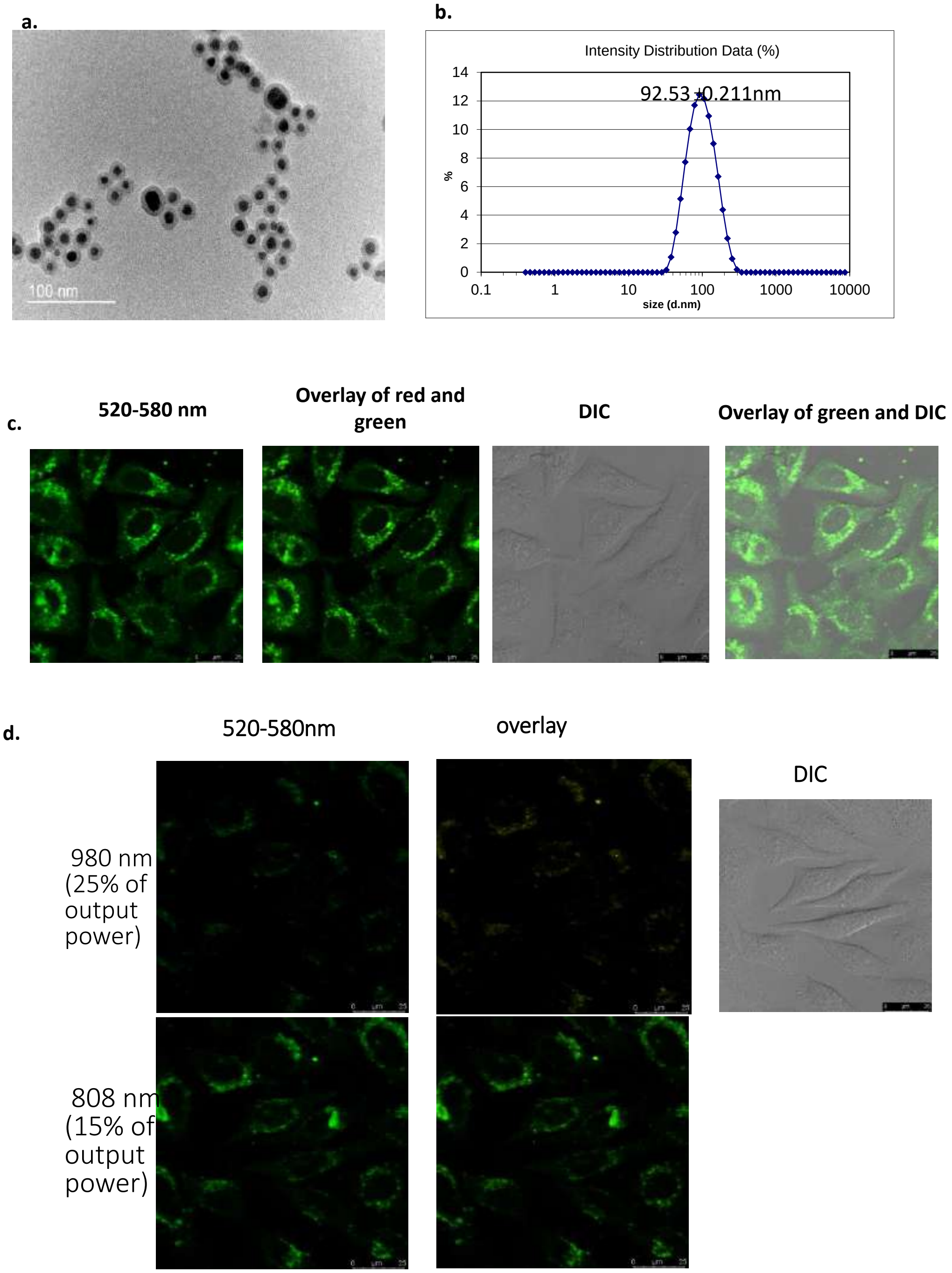

Figure 14. In vitro fluorescence imaging of type I Nd^{3+}-Trinity System UCNPs with activators of Er^{3+}. (a,b) type I Nd^{3+}-Trinity System UCNPs coating with silica shell and the DLS measurement. (c). In vitro fluorescence imaging of type I Nd^{3+}-Trinity System UCNPs with activators of Er^{3+} under excitation of 808 nm laser. (d).comparison of the 808 nm and 980 nm excitation in in vitro fluorescence imaging.

2.4.4. Prolonged lifetime

What worth to be mentioned is that when the UCNPs cores, that is NaGdF$_{4.}$:Yb,X(Er/Tm/Ho), are driven by the Nd^{3+}-trinity system, including type I and type II Nd^{3+}-trinity system, display prolonged lifetime under excitation of 808 nm and 980 nm laser, which means more stable excited state of the emissions. Moreover, the type II Nd^{3+}-trinity system coated UCNPs shows even more prolonged lifetime than the type I Nd^{3+}-trinity system coated UCNPs. Furthermore, for the same Nd^{3+}-trinity system driven UCNPs, in most of the situations, the lifetime under 808 nm excitation is longer than the 980 nm excited lifetime, as shown in Table 6- 8, which reveals that for the same Nd^{3+}-trinity system driven UCNPs, 808 nm excitation makes the excited state of the activators more stable. And we have just proposed it is cause by the Nd^{3+}→Yb^{3+} energy transfer under excitation of 808 nm, which has been reported as phonon-assistant energy transfer that makes not only 980 nm photons but also 1056 nm phonons are transferred to Yb^{3+}form Nd^{3+} $^{4}F_{3/2}$, thus makes the 1056 nm phonons participate in the energy transfer upconversion (ETU) process and leadi less non-radiative transition in the process of phonon avalanche (PA), that is prolonged lifetime, as we discuss below.

Lifetime (μs)	Wavelength

UCNPs	**Photo-luminescence source (nm)**	**(nm)**			
		414	**522**	**541**	**655**
Er	980	58.68	57.69	62.58	80.47
Er@GdTs@Gd	980	88.51	94.53	96.14	125.64
	808	68.63	109.15	106.2	115.16
Er@GdTs@Nd:Yb@Gd	980	89.86	115.22	108.86	150.26
	808	104.9	133.01	127.48	149.79

Table 6. Lifetime of UCNPs Nd^{3+}-harvest-transfer-sensitization trinity system, with Er^{3+} ions as activator.(**Er**: NaGdF$_4$:Yb, Er; **GdTs**: gadolinium-based transition layer; **Nd:Yb**: harvest layer; **Gd**: activation layer)

Lifetime (μs) **Nanoparticle Structures**	**Photo-luminescence source**	**Wavelength(nm)**		
		487	**542**	**647**
Ho	*980 nm*	-	55.00	55.14
Ho@GdTs@Gd	980 nm	221.50	237.54	460.28
	808 nm	235.23	251.36	495.36
Ho@GdTs@Harvest Gd	980 nm	66.09	355.97	626.17
	808 nm	434.43	381.25	615.69

(**Ho**: NaGdF$_4$:Yb, Ho; **GdTs**: Gadolinium based transition layer; **YTs**: Yttrium based transition layer; **Nd:Yb**: Harvest layer; **Gd**: Activation layer)

Table 7. Lifetime of Nd^{3+}- sensitized Upconversion Nanoparticles with activator of Ho $^{3+}$ ions.

Lifetime (μs) **UCNPs**	**Photo-luminescence source**	**Wavelength(nm)**		
		450	**475**	**647**
Tm	*980 nm*	226.80	480.59	448.69
Tm@GdTs@Gd	980 nm	455.36	926.00	1098.46
	808 nm	501.48	866.56	895.69
	980 nm	342.47	586.24	511.14

Tm@GdTs@Harvest @Gd	808 nm	332.31	562.36	489.85

(**Tm**: NaGdF$_4$:Yb, Tm; **GdTs**: gadolinium-based transition layer; **YTs**: yttrium-based transition layer; **Nd:Yb**: harvest layer; **Gd**: activation layer)

Table 8. Lifetime of Nd^{3+}-sensitized upconversion nanoparticles with activator of Tm^{3+} ions.

2.4.5. Larger partition of red emission

Beside the largely enhanced luminescence and the prolonged lifetime, we found that the other characteristics that makes the Nd^{3+}-trinity system advantageous in the utilization of bio-imaging is that the larger partition of red emission in the NaGdF$_4$:Yb, Er and NaGdF$_4$:Yb, Ho driven by Nd^{3+}-trinity system. By analyzing the ratio of peak area, as shown in Table 9, we found that the NaGdF$_4$:Yb, Er driven by Nd^{3+}-trinity system (including type I and type II), shows smaller values of the $f_{g/r}$ [which is the ratio of peak area, that is green emission (525,545 nm) to red emission (655nm)] whatever excited by 980 nm or 808 nm laser. And what should be noticed is that when compares type II Nd^{3+}-trinity system driven NaGdF$_4$:Yb, Er with type I ones, it shows even smaller $f_{g/r}$ values, which illustrated that the harvest layer, which is high concentration of Nd^{3+} ions that makes the whole system tend to emit red emission; also, the it is obvious that the activation layer makes the red emission with larger partition for the $f_{g/r}$ values is smaller, which means that the Yb^{3+} surface quenching also have influence on the process of the PA. Thus, it could be concluded that the Nd^{3+}-Er^{3+} or Yb^{3+}-Er^{3+} cross-relaxation affect process of PA, and further adjust the ratio of the peak area of the emission bands.

However, the situation is quite different in the Nd^{3+}-trinity system (including type I and type II) driven NaGdF$_4$:Yb, Tm/Ho, as shown in Table 10, 11, which could be attributed to the specific situation of the Nd^{3+}-Tm^{3+}/Ho^{3+} or Yb^{3+}-Tm^{3+}/Ho^{3+} cross-relaxation. As shown in Table 10, for the $NaGdF_4$:Yb, Tm^{3+} driven by Nd^{3+}-trinity system, which is just on the contrary, shows smaller red emission partition, and it is obvious that the harvest layer or the high concentration of Nd^{3+} makes the red emission with smaller partition, that is with larger value of $f_{b/r}$ (ratio of peak area of blue emission to red emission). It could be concluded that the Nd^{3+}-Tm^{3+}or Yb^{3+}-Tm^{3+} cross-relaxation makes the PA process in the ETU process of the are prone to emit red emission. And in the situation of the $NaGdF_4$:Yb, Ho driven by Nd^{3+}-trinity system, the harvest layer or the high concentration of Nd^{3+} makes the red emission with larger partition well the activation layer make the system with smaller partition with 980 nm excitation and larger partition with 808 nm excitation. It could be concluded that Nd^{3+}-Ho^{3+} cross-relaxation makes the PA process are prone to emit red emission; Yb^{3+}-Ho^{3+} cross-relaxation makes the 808 nm excited PA process in the ETU process are prone to emit green emission well in the 808 nm excited PA process in the ETU process are prone to emit red emission, which could be further explained by the 1560 nm selectively participated ETU process with the excitation of 808 nm laser as demonstrated in below in the part of 2.5.Mechanism.

Photo-luminescence source	**UCNP structures**	**value of $f_{g/r}$**
980 nm	Er	4.14
	Er@Ts	3.38
	Er@Ts@Gd	3.36
	Er@Ts@Nd:Yb(9:1)	2.09
	Er@Ts@Nd:Yb(9:1)@Gd	1.50
808 nm	Er@Ts	2.35
	Er@Ts@Gd	2.73
	Er@Ts@Nd:Yb(9:1)	3.38
	Er@Ts@Nd:Yb(9:1)@Gd	1.30

Table 9. Luminescence enhancement and $f_{g/r}$ values of core-multishells UCNPs Nd^{3+}-harvest-transfer-sensitization trinity system with activator of Er^{3+}.

(**Er**: $NaGdF_4$:Yb, Er; **GdTs**: gadolinium-based transition layer; **Nd:Yb**: harvest layer; **Gd**: surface defecting shielding layer)

	Structure of Nd^{3+}-sensitized upconversion nanoparticle	Ib/Ir	Peak Area ratio to $NaGdF_4$:Yb,Tm excited by 980 nm
980 nm laser excited	Tm	0.62	-
	Tm@Ts	3.60	0.42
	Tm@Ts@Gd	3.70	60.6
808 nm laser excited	Tm@Ts	- (the luminescence is too weak to be calculated)	0.22
	Tm@Ts@Gd	3.54	48.18

Table 10. Luminescence enhancement and Ib/Ir values of core/multiple shells Nd^{3+}-sensitized upconversion nanoparticles with activator of Tm^{3+}.

Photo-luminescence source	**UCNP structures**	**Ig/Ir**
980 nm laser excited	Ho	0.46
	Ho@Ts	0.36
	Ho@Ts@Gd	0.32
	Ho@Ts@Harvest@Gd	
808 nm laser excited	Ho@Ts	0.29
	Ho@Ts@Gd	0.33
	Ho@Ts@Harvest@Gd	

Table 11. Luminescence enhancement and Ig/Ir values of core/multiple shells Nd^{3+}-sensitized upconversion nanoparticles with activator of Ho^{3+}.

2.4.6. Deeper luminescence penetration in water

Furthermore, the 808 nm excited UCNPs has been reported to be with deeper luminescence penetration as well as over-heating effect avoiding in water. As reported by Y.T. Zhong *et al*., water is proved to attenuate the photo-luminescence source that 980 nm laser by the vigorous decreasing of the laser power when the laser beam pass through water [15]. The attenuation of the photo-luminescence source could be explained as the absorption of 980 nm photons by water. And in our research, we have proved the conclusion by our Nd^{3+}-trinity system coated UCNPs (structure: $NaGdF_4$:$Yb_{20\ \%}$,$Er_{2\ \%}$ @$NaGdF_4$:$Yb_{10\ \%}$,$Nd_{20\ \%}$@$NaNdF_4$:Yb@$NaGdF_4$). As shown in Figure 15, that in our specially fabricated cuvette, with inner shell that used to carry samples that dissolved in cyclohexane and outer shell that used to carry water, we found that the peak area that with 808 nm excitation are almost 20 times than it with 980 nm excitation under the same measurement condition, as shown in Figure 16 and Table 12 and 13.

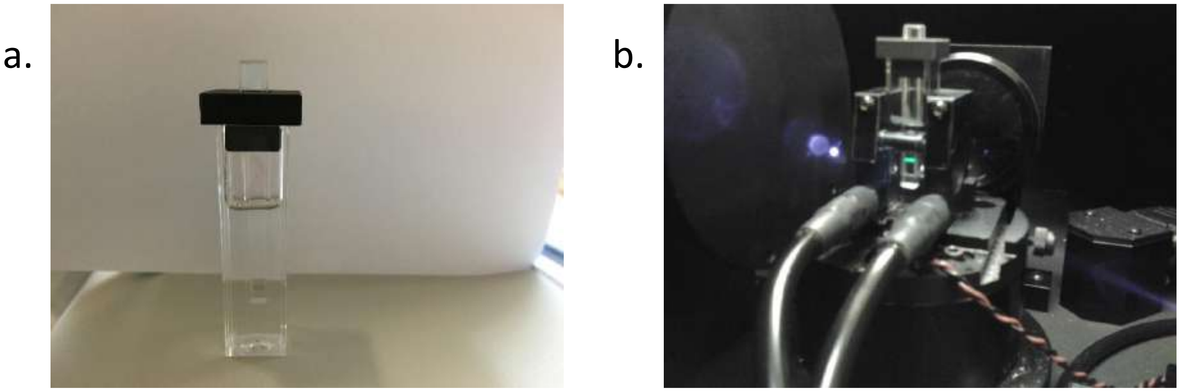

Figure 15. Measurement of penetration of $NaGdF_4$:Yb, Er@$NaGdF_4$:Yb, Nd @$NaNdF_4$:Yb@$NaGdF_4$ in water and cyclohexane in the outer cuvette.

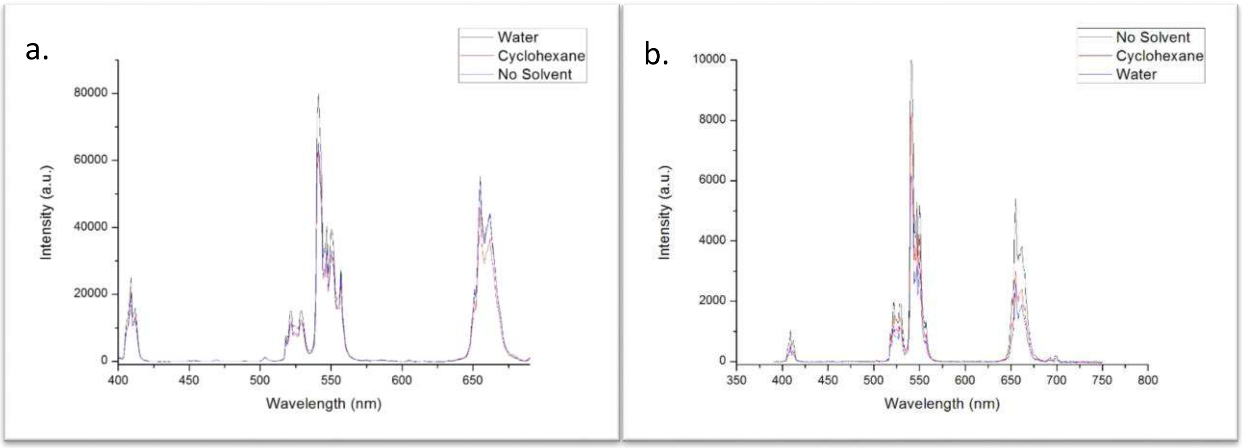

Figure 16. Emission spectra of $NaGdF_4$:Yb, Er@$NaGdF_4$:Yb, Nd @$NaNdF_4$:Yb@ $NaGdF_4$ in water and cyclohexane in the outer cuvette excited by 808/980 nm diode laser . (Measurement conditions: power density: 80 mW/ 1 mm ^{2} for 808/ 980 nm diode laser; emission bandwidth: 0.5 nm; concentration: 1.0 wt %.)

Wavelength (nm)	**Peak area Ratio to no solvent in outer cuvette**	
	Cyclohexane in outer cuvette	Water in outer cuvette
414	1.04	1.26
522	0.94	1.22
541	0.93	1.17
655	0.83	1.01
In total	0.9	1.03

Table 12. Peak area of emission spectra of $NaGdF_4$:Yb, Er@$NaGdF_4$:Yb, Nd @$NaNdF_4$:Yb@ $NaGdF_4$ in water and cyclohexane in the outer cuvette excited by 808 nm diode laser.

Wavelength (nm)	**Peak area Ratio to no solvent in outer cuvette**	
	Cyclohexane in outer cuvette	Water in outer cuvette
414	0.55	0.43
522	0.78	0.61
541	0.79	0.62
655	0.6	0.46
In total	0.71	0.55

Table 13. Peak area of emission spectra of $NaGdF_4$:$Yb_{20\ \%}$,$Er_{2\ \%}$@$NaGdF_4$:$Yb_{10\ \%}$,$Nd_{20\ \%}$@$NaNdF_4$:Yb@$NaGdF_4$ in water and cyclohexane in the outer cuvette excited by 980 nm diode .

2.4.7. Higher florescent quantum yield

Furthermore, we found that the optimized $NaGdF_4$:$Yb_{20\ \%}$,$Er_{2\ \%}$ driven by Type I Nd^{3+}-trinity system(structure: $NaGdF_4$:$Yb_{20\ \%}$,$Er_{2\ \%}$@$NaGdF_4$:$Yb_{10\ \%}$, $Nd_{20\ \%}$@$NaNdF_4$:Yb@$NaGdF_4$) shows higher florescent quantum yield, as shown in Figure 17, the value of QY with 808 nm excitation is 0.42 % and 0.84 % under 980 nm excitation, with is comparatively higher than the previous report. As reported by R.R. Deng *et al.*, the florescent quantum yield core-multishells of the 980 nm or 808 nm excited UCNPs which is used as 3D printer by non-steady state upconversion utilized in full color-tuning which is less than 0.1 %.[21]

What we would like to state is that the florescent quantum yield of upconversion should be very low which is depend on the upconversion efficiency: as reported by, the rate of $Yb^{3+}\rightarrow Er^{3+}$ energy transfer is fast compares with the radiative and non-radiative emission; also the energy back-transfer of $Er^{3+}\rightarrow Yb^{3+}$ is faster than $Yb^{3+}\rightarrow Er^{3+}$ energy transfer; in our investigation, as stated in previous part, the cross-relaxation of $Er^{3+}\rightarrow Yb^{3+}$ and $Er^{3+}\rightarrow Nd^{3+}$ will further exacerbate the situation; the low concentration of the activators, makes the upconversion process tend to be saturated.

The high quantum yield of the UCNPs by the well-designed core-multishells structures to guarantee the optimized 808 nm harvesting and $Nd^{3+}\rightarrow Yb^{3+}$ energy transfer as well as shielding all the quenching factors.

Moreover, for the same UCNPs structures, we found that the florescent quantum yield with 808 nm is lower than 980 nm ones, which could be concluded as: firstly, although, Nd^{3+}-Yb^{3+} energy transfer has been reported with high efficiency that is 75 %, there is still energy loss in the process; secondly, in the mechanism Nd^{3+}-sensitized upconversion process, there has been more pathways for self-quenching as discussed in the part; thirdly, the high absorption of Nd^{3+} ions to 808 nm laser make the upconversion saturation effect more seriously.

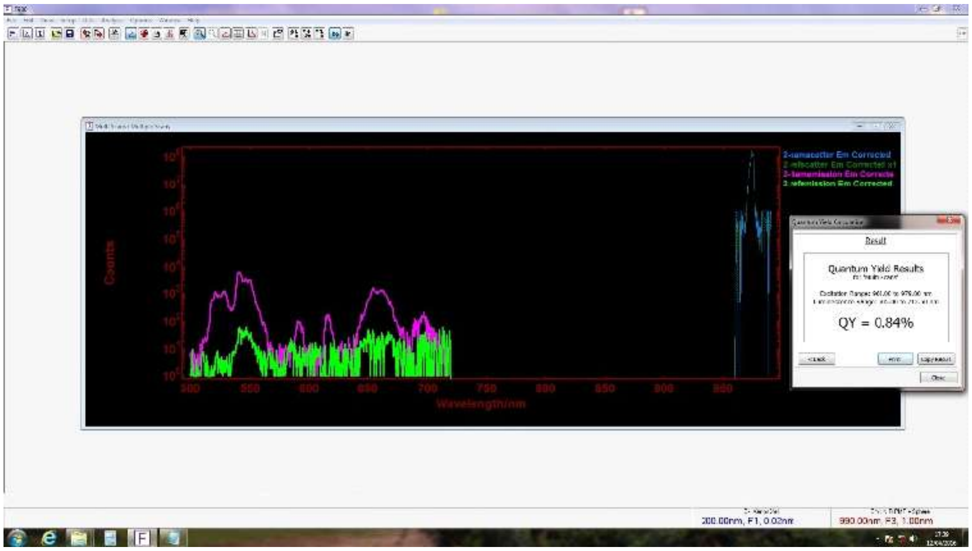

Result

Quantum Yield Results

QY = 0.84%

Result

Quantum Yield Results

QY = 0.42%

Figure 17. Measurement of absolute quantum yield of NaGdF$_4$:Yb, Er@NaGdF$_4$:Yb, Nd@NaNdF$_4$:Yb@NaGdF$_4$ with excitation of 808 nm (a) and 980 nm (b) diode laser.

2.4.8. Relaxivity (r_1)

As shown in Figure 10, the type I Nd^{3+}-trinity system coated UCNPs with the diameter of sub ~12 nm, showed the potential to be utilized as a MRI contrast agent with a high value of the r_1 relaxivity, which is 4.23 mM^{-1}s^{-1}. The obtained oleate capped UCNPs were transferred to hydrophilic ones by ligand exchange with branched PEI (~25, 000 KDa), is higher than the r_1 value of Gd-DOTA that is 4.00 mM^{-1}•s^{-1}. The high r_1 relaxivity value could be illustrated that is attributed to the surfactant that is PEI (with comparison of the ligand free UCNPs) and the minimized size as reported. [13, 14]

2.5. Mechanism investigation

Since we have found that for the same UCNPs that coated with Nd^{3+}-Trinity system, when excited by 980 nm and 808 nm, besides the enhanced luminescence which is proposed to be contributed by the high absorption of Nd^{3+} ions, the UCNPs still shows difference in lifteime, ratio of the peak area under the 808 nm and 980 nm photoluminescence source We have proposed that the mechanism of the Nd^{3+}-senisitization and Yb^{3+}-senisitization upconversion process, besides the Nd^{3+}→Yb^{3+} enenrgy transfer, do exsit other difference: i. Nd^{3+}-Trinity system coated UCNPs shows prolonged lifetime than the naked UCNPs; ii. for the same Nd^{3+}-Trinity system coated UCNPs, it shows prolonged lifetime under 808 nm excitation rather than 980 nm excitation, which indicates that the Nd^{3+}-sensitization induce the prolonged lifetime; iii. the emission specra of Nd^{3+}-Trinity system coated UCNPs show larger partition under excitation of 808 nm and 980 nm rather than the naked

UCNPs, which indicates that the Nd^{3+}-sensatizaion make the whole system prone to emit red emission.

By conveying more investigations of the mechanism of Nd^{3+}-trinity system coated UCNPs and analysing the energy levels of the lanthanides, we just propose that: a. the 1056 nm phonons selectively participate in the ETU process, and further makes the PA process with less non-raditive transition; b. the Nd^{3+}-Er^{3+}/Tm^{3+}/Ho^{3+} cross-relaxation and Yb^{3+}-Er^{3+}/Tm^{3+}/Ho^{3+} cross-relaxation have effect on the peak ratio of the emission.

2.5.1. 1056 nm phonons have been proven to participated in the ETU process

The 1056 nm phonons are proposed to participate in the upconversion process along with the 940-1030 nm phonons which could be reflected in NIR emission spectra. Comparing NIR emission spectra of nanoparticles that are Nd^{3+}-Trinity system with $NaGdF_4$: Yb and $NaGdF_4$:Yb, Er cores ($NaGdF_4$:$Yb_{20\,\%}$$NaGdF_4$:$Yb_{10\,\%}$, $Nd_{20\,\%}$@$NaNdF_4$:Yb@$NaGdF_4$ and $NaGdF_4$:$Yb_{20\,\%}$,$Er_{2\,\%}$@$NaGdF_4$:$Yb_{10\,\%}$, $Nd_{20\,\%}$@$NaNdF_4$:Yb@$NaGdF_4$), the energy difference between $Nd^{3+}\rightarrow Yb^{3+}$ and $Nd^{3+}\rightarrow Yb^{3+}\rightarrow Er^{3+}$ energy transfer system is revealed, which indicates the NIR phonons that participate in the ETU process. In the NIR emission spectra of $Nd^{3+}\rightarrow Yb^{3+}$ energy transfer system with 808 nm excitation, as shown in Figure 18(a-2), shows a broad emission band (940-1030 nm) with maximum at 975 nm, which could be interpreted as the Yb^{3+} emission with excitation of Nd^{3+} $^4F_{3/2}$ [38]; the peak located in 1048 nm could be explained as in consequence of transitions between sublevels of Yb^{3+}(sublevels :10327 cm^{-1} and 785 cm^{-1} [40], as shown in Figure 19, which is caused by crystal field splitting [65], as shown in Figure 18 (b); compared with Yb^{3+} emission as reported previously, which shows maxima at 975 nm and 1029 nm [44], the peak around 1056 nm could be concluded as induced by Nd^{3+}. Associated with "$Nd^{3+}\rightarrow Yb^{3+}$ phonon-assisted energy transfer” as reported [43, 45], as shown in Figure 20, 1056 nm emission is proposed to be : generated by $Nd^{3+} \rightarrow Yb^{3+}$ energy transfer, which is Nd^{3+} $^4F_{3/2}$ + Yb^{3+} $^2F_{7/2} \rightarrow Nd^{3+}$ $^4I_{11/2}$ + Yb^{3+} $^2F_{5/2}$; migrated in the $Yb^{3+} \rightarrow Yb^{3+}$ transition by Yb^{3+} sublevels 10248 cm^{-1} and 785 cm^{-1}; emitted by Yb^{3+} $^2F_{5/2}$ (10248 cm^{-1})$\rightarrow$$^2F_{7/2}$ (785 cm^{-1}) transition, as shown in Figure 4 (a-1). Accordingly, there are two kinds of photons in $Nd^{3+} \rightarrow Yb^{3+}$ energy transfer and $Yb^{3+} \rightarrow Yb^{3+}$ transition: (i) photons located at 940-1030 nm with maximum at 975 nm; (ii) 1056 nm phonons. In the $Nd^{3+} \rightarrow Yb^{3+} \rightarrow Er^{3+}$ energy transfer system, the region of the board peak (940-1030 nm) appears discontinuous with sharp peaks, along with disappearance of 1056 nm. The partial disappearance is proposed to be the photons that are transferred to Er^{3+} and participating in the ETU process, which are not only the 940-1030 nm (with maximum at 975 nm) photons but also the 1056 nm phonons. Moreover, sharp peaks (Figure 18 b-1) could be explained as result in the recurring cycles of energy transfer and energy back-transfer between Er^{3+} and Yb^{3+}, as shown in Figure 21, which could be depicted as photons back-transfer from Er^{3+} to Yb^{3+} and then only part of them is transfer to Er^{3+} to participate in ETU process once again and the remaining phonons are emitted.

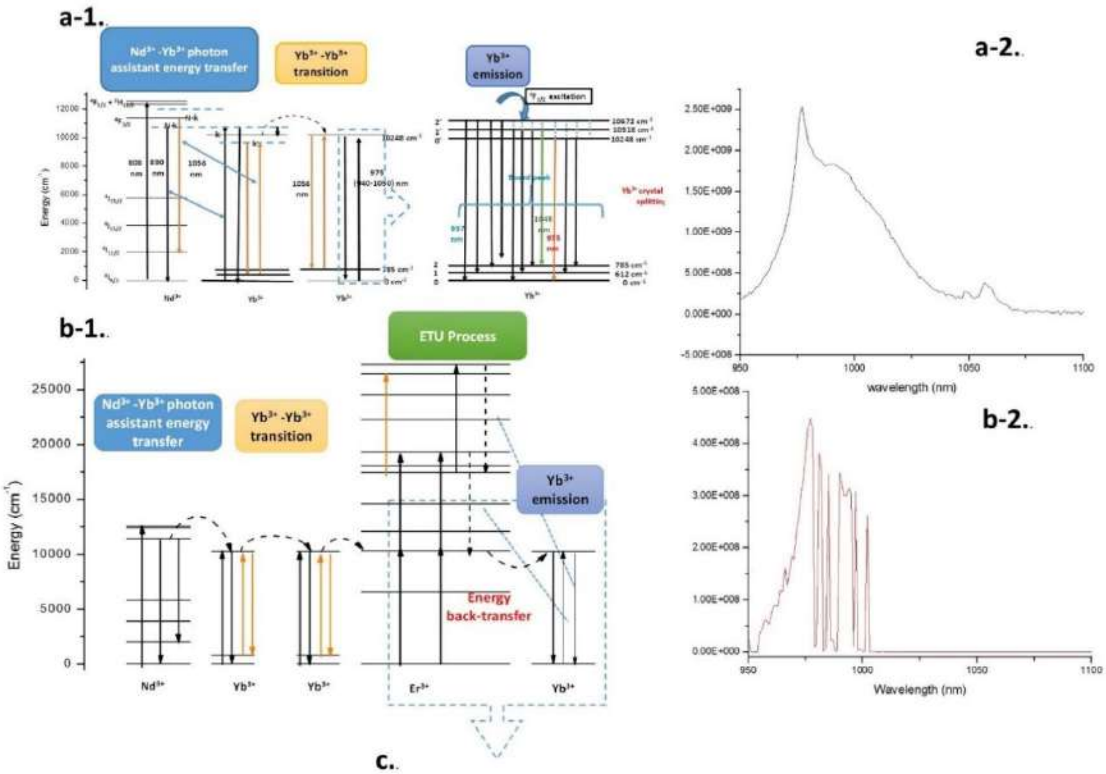

Figure 18. NIR emission spectra and proposed mechanism of the Type I Nd^{3+}-Trinity system sensitized $NaGdF_4$:$Yb_{20\%}$ and $NaGdF_4$:$Yb_{20\%}$, $Er_{2\%}$, which reveals the difference between $Nd^{3+}\rightarrow Yb^{3+}$ energy transfer (a) and $Nd^{3+}\rightarrow Yb^{3+}\rightarrow Er^{3+}$ energy transfer (b). Proposed energy transfer process involved Yb^{3+} ions, including: $Yb^{3+}\rightarrow Er^{3+}$ energy transfer and $Er^{3+}\rightarrow Yb^{3+}$ energy back-transfer, with Yb^{3+} sharp emission peaks (c).

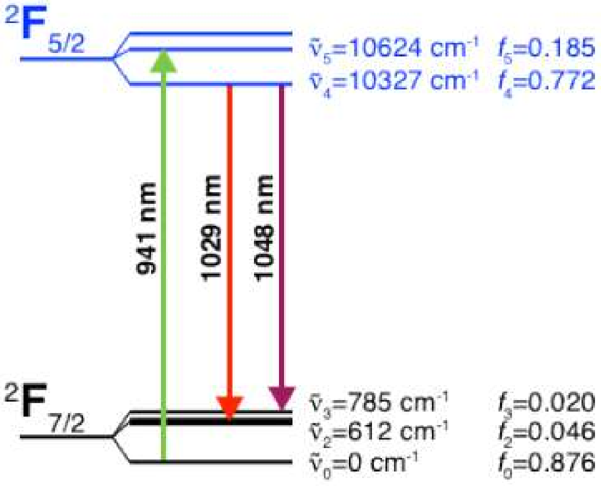

Figure 19. Yb^{3+} upper and ground energy level. [40]

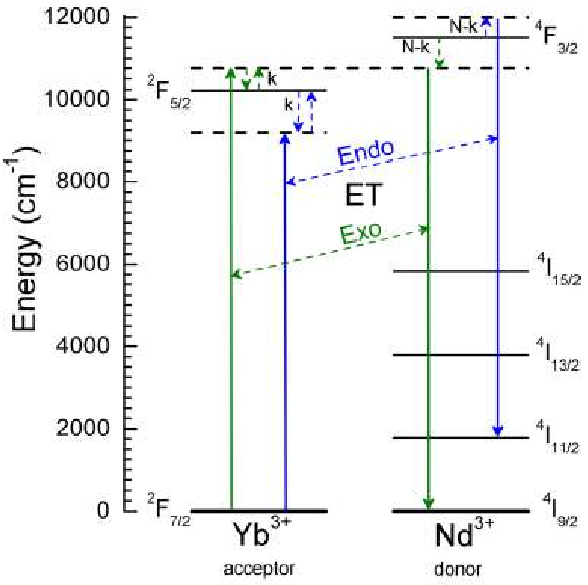

Figure 20. Photon-assisted Nd^{3+}→Yb^{3+} energy transfer [43, 45].

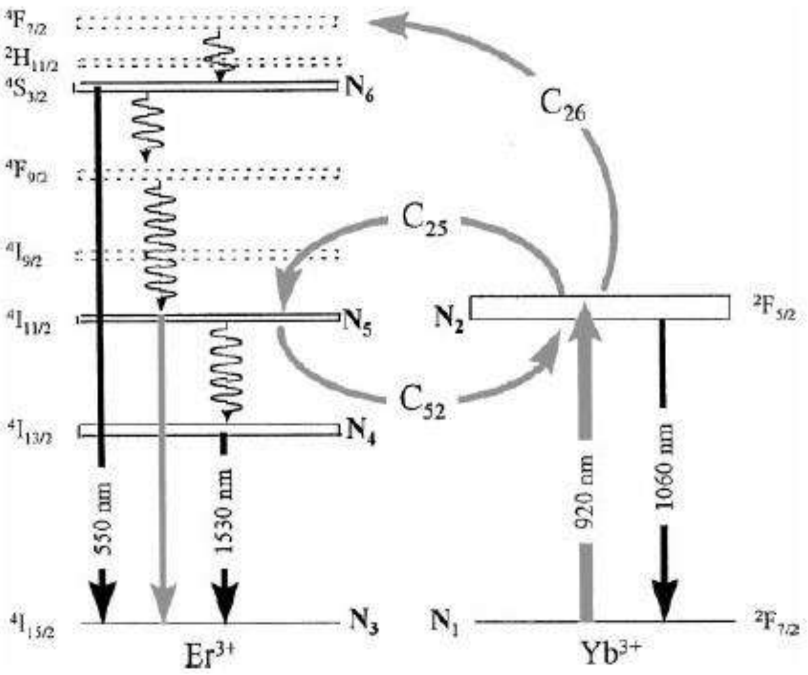

Figure 21. Energy transfer and energy back-transfer of Er^{3+}→Yb^{3+}.[63]

Here comes to the question that why the 1056 nm phonons could participate in the ETU process along with 940-1030 nm (with maximum at 975 nm) phonons? The answer is given by analyzing the energy gaps of transitions of in the ETU process of the activators (Er^{3+}/Tm^{3+}/Ho^{3+}). As shown in Table 14 and Figure 22, in the ETU process of Er^{3+}, the energy gap of the transitions Er^{3+}:$^4I_{15/2} \rightarrow ^4I_{11/2}$, $^4I_{11/2} \rightarrow ^4F_{7/2}$, $^4S_{3/2} \rightarrow ^4G_{7/2}$ match 940-1030 nm phonons while the energy gap of the transition Er^{3+}: $^4F_{9/2} \rightarrow ^4G_{9/2}$ is close to the 1056 nm phonons. In the ETU process of Ho^{3+}, the transition of Ho^{3+}: $^5I_6 \rightarrow ^5S_2 + ^5F_4$ matches with 940-1030 nm phonons while Ho^{3+}: $^5F_5 \rightarrow ^5G_4$ matches the 1056 nm phonons; it is easier for the transition of Ho^{3+}: $^5I_6 \rightarrow ^5I_8$ (with the energy gap~ 9309 cm^{-1}) that is lower than 940-1030 nm phonons and 1056 nm phonons, to be filled by 1056 nm phonons, for the non-radiative transition during the down-conversion in the Yb^{3+}→Ho^{3+} energy transfer is less.

In the ETU process of Tm^{3+}, very similar with the situation of transition of Ho^{3+} $^5I_6 \rightarrow ^5I_8$, the transition of Tm^{3+}: $^3H_6 \rightarrow ^3H_5$, $^3F_4 \rightarrow ^3F_2$, $^3H_4 \rightarrow ^1G_4$, $^1G_4 \rightarrow ^1D_2$ are easier to utilize 1056 nm phonons rather than 940-1030 nm phonons. The participation of the 1056 nm phonons along with the 940-1030 (with maximum at 975 nm) photons result in selectivity in the ETU process, due to the matching of the energy gaps of transitions and energy of the phonons.

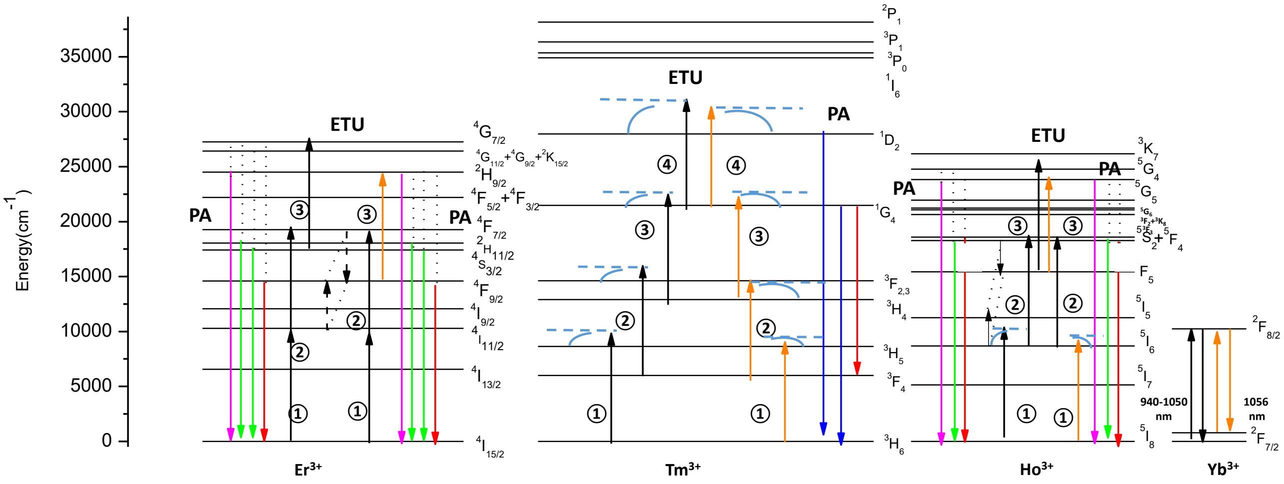

Figure 22. Selectively 1056 nm phonons participation in ETU (energy transfer upconversion) process in Er^{3+}, Tm^{3+} and Ho^{3+}. (i) 940-1030 nm (with maximum at 975 nm) photons; (ii) 1056 nm phonons .

Transitions & Energy gaps / Activa-tors	phonons in 940-1030 nm with maximum at 975 nm (with energy gap: 10638~9523 cm^{-1}) preferred transitions		phonons in 1056 nm (with energy gap: ~ 9469 cm^{-1}) preferred transitions	
	Transitions	Energy gaps (cm^{-1})	Transitions	Energy gaps

				(cm^{-1})
Er^{3+} [66]	$^4I_{15/2}$ → $^4I_{11/2}$	9767~10395	$^4F_{9/2} \rightarrow {}^4G_{9/2}$	9960 ~ 9039
	$^4I_{11/2}$ → $^4F_{7/2}$	10267~10354		
	‘$^4S_{3/2}$ → $^4G_{7/2}$	9733~9849		
Ho^{3+} [67]	$^5I_6 \rightarrow {}^5S_2 + {}^5F_4$	~ 9916	$^5F_5 \rightarrow {}^5G_4$	~ 9309
			$^5I_6 \rightarrow {}^5I_8$	~ 8679
Tm^{3+} [68]	-		$^3H_6 \rightarrow {}^3H_5$	7752~8577
			$^3F_4 \rightarrow {}^3F_2$	9071~9453
			$^3H_4 \rightarrow {}^1G_4$	8159~8900
			$^1G_4 \rightarrow {}^1D_2$	6448~6944

Table 14. Transitions and energy gaps (cm^{-1}) in ETU process with activator of Er^{3+}, Tm^{3+} and Ho^{3+}.

The 1056 nm phonons selective participation in the ETU process is proposed to optimize the ETU process, which could be generalized as: with less non-radiative transition in ETU and PA process, consequence in more stable excited state which is revealed by prolonged lifetime. As shown in Figure 23 (a), 1056 nm and 940-1030 nm phonons selectively participated Er^{3+}-ETU and PA process could be generalized as: for ETU and PA process I (with 1056 nm participation), a. the first photon: 940-1030 nm, populate $^4I_{11/2}$ level from the ground-state $^4I_{15/2}$; b. the second photon: 940-1030 nm populate the $^4F_{7/2}$; c. the third photon: 1056 nm populate the $^4H_{9/2}$ from $^4F_{9/2}$ (the $^4F_{9/2}$ is result in the cross-relaxation between two Er^{3+} ions, which is Er^{3+}: $^4F_{7/2}+{}^4I_{11/2} \rightarrow {}^4F_{9/2}+{}^4F_{9/2}$). The PA process is proposed to be: emitting violet emission (415 nm, $^4H_{9/2} \rightarrow {}^4I_{15/2}$); form $^4H_{9/2}$ relaxing non-raditively to $^2H_{11/2}$, $^4S_{3/2}$ and $^4I_{9/2}$, followed by emitting green emission (525 nm, $^4H_{9/2} \rightarrow {}^4I_{15/2}$; 545 nm, $^4S_{3/2} \rightarrow {}^4I_{15/2}$) and red emission (655 nm, $^4I_{9/2} \rightarrow {}^4I_{15/2}$); for ETU and PA process II (without 1056 nm participation): the first and second 940-1030 nm phonons being absorbed and populating the $^4F_{7/2}$ is the same with ETU process I; by relaxing non-radiatively to $^4S_{3/2}$, the third 940-1030 nm photon populate $^4F_{7/2}$. The PA process is proposed to be: by relaxing non-radiatively from $^4G_{7/2}$ to $^4H_{9/2}$, $^2H_{11/2}$, $^4S_{3/2}$ and $^4I_{9/2}$ followed by emitting violet emission (415 nm, $^4H_{9/2}$→$^4I_{15/2}$), green emission (525 nm, $^4H_{9/2}$→$^4I_{15/2}$; 545 nm, $^4S_{3/2}$ →$^4I_{15/2}$) and red emission (655 nm, $^4I_{9/2}$→$^4I_{15/2}$). Both ETU process I and II exist in 808 nm excitation; only ETU process II exists in 980 nm excitation. Additionally, the red emission (655 nm, $^4I_{9/2}$→$^4I_{15/2}$) is also occurred and affected by cross-relaxation between two Er^{3+} ions (which is Er^{3+}: $^4F_{7/2}+^4I_{11/2}\rightarrow^4F_{9/2}+^4F_{9/2}$). And we would like to call the ETU process as “expletive ETU for red emission” (EXP ETU in short), which is proposed to exist in both ETU process I and II, as shown in Figure 23 (a). It could be explained as: in one Er^{3+} ions, $^4F_{7/2}$ is populated by absorption of the first and second 940-1056 nm phonons, and quenched to $^4I_{11/2}$ by two Er^{3+} ions cross-relaxation. And this process makes the 1056 nm phonons to be absorbed with more possibilities; in the other Er^{3+} ions, the transition $^4I_{11/2}$→$^4F_{9/2}$ that caused by the two Er^{3+} cross-relaxation and another 940-1030 nm photon is absorbed and populate the $^4I_{11/2}$, leading to the population of $^4F_{9/2}$, and emitting the red emission (655 nm, Er^{3+}: $^4I_{9/2}$→$^4I_{15/2}$). Comparing PA process in ETU process I with II, it could be concluded that for each individual emission band, the participation of the 1056 nm phonons reduce the non-radiative transition, which is revealed by the prolonged lifetime of UCNPs with Nd^{3+}-harvest-transfer-sensitization trinity system with activator of Er^{3+}. The situation of 1056 nm selective participation ETU process in Ho^{3+} is very similar with Er^{3+}; meanwhile, in the situation of Tm^{3+}, the 1056 nm phonons selectively participate in the 3-photon or 4-photon ETU process resulting in less non-radiative transition in the energy transfer of Yb^{3+}-

Tm^{3+} rather than 940-1056 nm phonons, thus leading to more stable excited state ($^1D_2$, result in 4-photons ETU and $^3F_3$, result in 3-photons ETU) of transitions of $^1D_2\rightarrow^3H_6$ (450 nm), $^3F_3\rightarrow^3H_6$ (475 nm) and $^3F_3\rightarrow^3F_4$ (647 nm), as shown in Figure 24. Compared with the 980 nm excited, Yb^{3+}-sensitized ETU process, as shown in Figure 25, the 808 nm excited, Nd^{3+}-sensitized ETU process results in less non-radiative transition in the upconversion process, thus leading to prolonged lifetime.

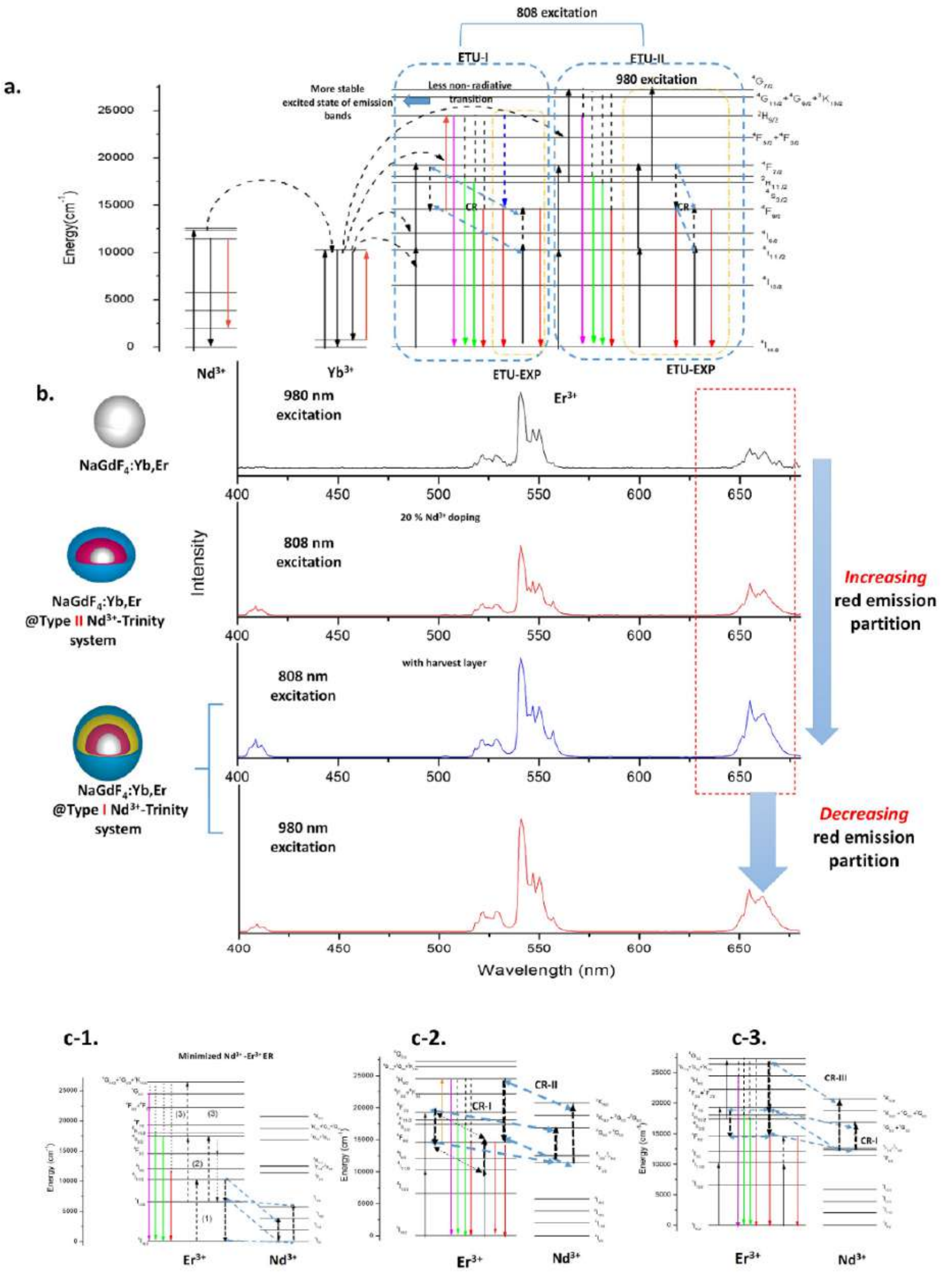
a.
808 excitation
ETU-I
ETU-II
980 excitation
More stable excited state of emission bands
Less non- radiative transition
CR
ETU-EXP
Energy(cm⁻¹)
0
5000
10000
15000
20000
25000
Nd³⁺
Yb³⁺
⁴G7/2
⁴G11/2+⁴G9/2+²K15/2
²H9/2
⁴F5/2+⁴F3/2
⁴F7/2
²H11/2
⁴S3/2
⁴F9/2
⁴I9/2
⁴I11/2
⁴I13/2
⁴I15/2
b.
NaGdF4:Yb,Er
NaGdF4:Yb,Er @Type II Nd³⁺-Trinity system
NaGdF4:Yb,Er @Type I Nd³⁺-Trinity system
980 nm excitation
Er³⁺
808 nm excitation
20 % Nd³⁺ doping
808 nm excitation
with harvest layer
980 nm excitation
Intensity
Wavelength (nm)
400
450
500
550
600
650
Increasing red emission partition
Decreasing red emission partition
c-1.
Minimized Nd³⁺-Er³⁺ ER
(1)
(2)
(3)
Energy (cm⁻¹)
Er³⁺
Nd³⁺
c-2.
CR-I
CR-II
Energy (cm⁻¹)
Er³⁺
Nd³⁺
c-3.
CR-III
CR-I
Energy (cm⁻¹)
Er³⁺
Nd³⁺

Figure 23. The proposed ETU and PA process sensitized by Nd^{3+}-Trinity system with activator of Er^{3+}, including ETU-1, ETU-II and EXP-ETU (expletive ETU for red emission)(a); the increasing partition of red emission observed from the emission spectra of the UCNPs: $NaGdF_4$:Yb,Er (980 nm excitation), $NaGdF_4$:Yb,Er@Type II Nd^{3+}-Trinity system (808 nm excitation), and $NaGdF_4$:Yb,Er@Type I Nd^{3+}-Trinity system (808 nm excitation) and the comparison of the $NaGdF_4$:Yb,Er@Type I Nd^{3+}-Trinity system with 980 nm and 808 nm excitation (b). The proposed Nd^{3+}-Er^{3+} cross-relaxation (c-1,2,3) influenced the ETU and PA process.

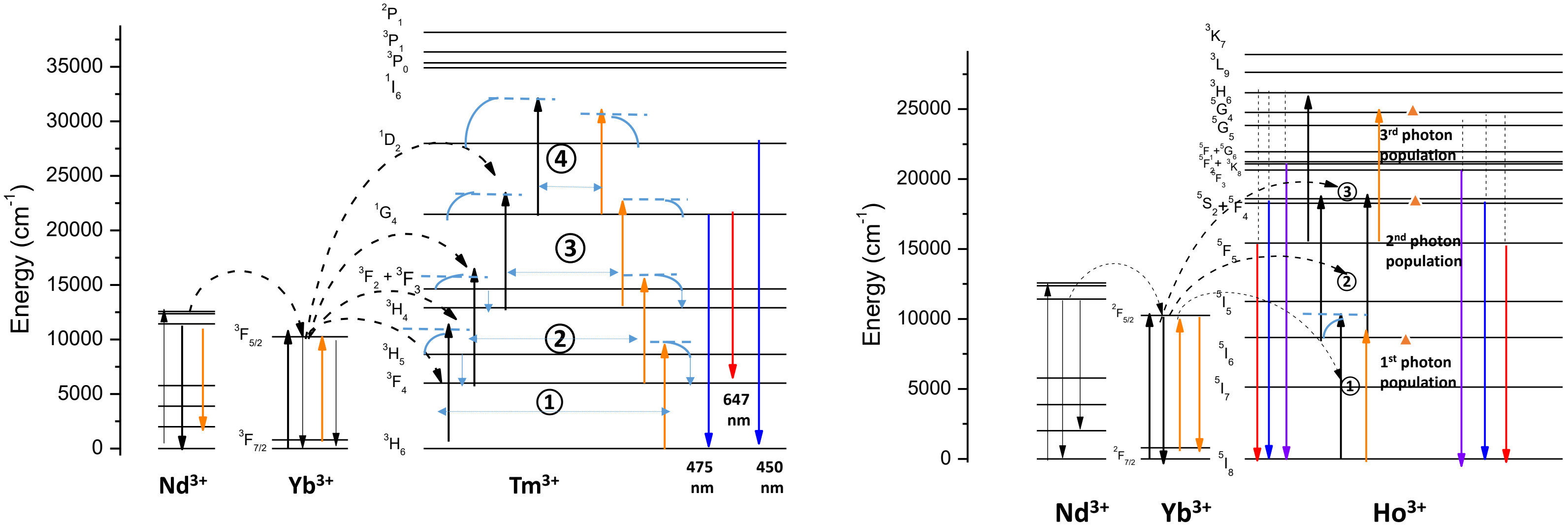

Figure 24. Proposed mechanism of Nd^{3+}-Yb^{3+}-X(Tm^{3+}/Ho^{3+}) upconversion process excited by 808 nm laser.

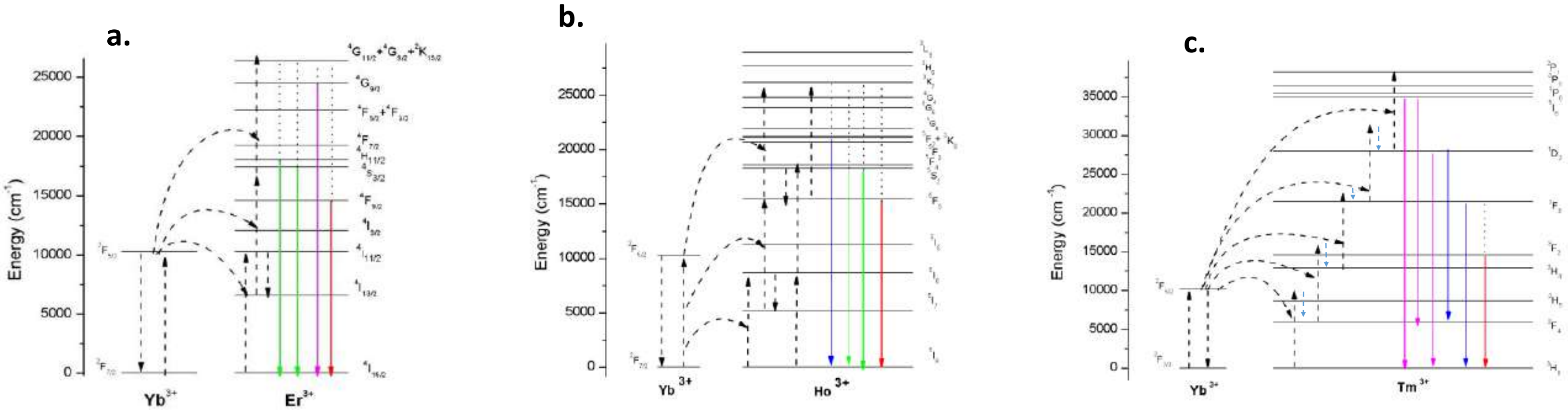

Figure 25. Simplified energy diagram of Yb^{3+}-X(Er^{3+}/Tm^{3+}/Ho^{3+}) three-photons upconversion process. [4]

2.5.2. Red emission partition influenced by the Nd^{3+}-X^{3+}(Er^{3+}/Tm^{3+}/Ho^{3+}) cross-relaxation and Yb^{3+}-X^{3+}(Er^{3+}/Tm^{3+}/Ho^{3+}) cross-relaxation

Accordingly, the partition of red emission, as shown in Figure 23 (b), shows dramatically decreasing by coataing of the Nd^{3+}-Trinity system, that could be concluded as influenced by Nd^{3+}-X^{3+}(Er^{3+}/Tm^{3+}/Ho^{3+}) cross-relaxation and Yb^{3+} surface quenching shielding. In the UCNPs of Nd^{3+}-harvest-transfer-sensitization trinity system with activator of Er^{3+}, the Nd^{3+}-Er^{3+} cross-relaxation: Nd^{3+} $^4I_{9/2}$ + Er^{3+} $^4I_{13/2}$→ Nd^{3+} $^4I_{15}$ + Er^{3+} $^4I_{15/2}$ and Nd^{3+} $^4I_{9/2}$ + Er^{3+} $^4I_{11/2}$→ Nd^{3+} $^4I_{13}$ + Er^{3+} $^4I_{13/2}$ has been minimized by the design that sandwiches transition layer between $NaGdF_4$: Yb, Er core and harvest layer; however it is proposed that there still exists Nd^{3+}-Er^{3+} cross-relaxation (shown in Figure 23 c-1, as Nd^{3+}-Er^{3+} CR-I, II, III). In ETU and PA process I, as shown in Figure 23 (c-2), the Nd^{3+}-Er^{3+} CR-II: Nd^{3+} $^4F_{3/2}$ + Er^{3+} $^4F_{3/2+5/2}$→ Nd^{3+} $^2K_{15/2}$ + Er^{3+} $^4F_{9/2}$, results in Er^{3+} $^2H_{9/2}$ tending to relax non-raditively to Er^{3+} $^4F_{9/2}$, followed by emitting red emission (655 nm, $^4F_{9/2}$→$^4I_{15/2}$); in ETU and PA process II, as shown in Figure 23(c-3), the Nd^{3+}-Er^{3+} CR-III: Nd^{3+} $^4F_{5/2}$, $^2H_{9/2}$ + Er^{3+} $^4F_{7/2}$→ Nd^{3+} $^2K_{15/2}$ + Er^{3+} $^4F_{7/2}$ result in easier non-raditively from Er^{3+} $^4G_{7/2}$ to Er^{3+} $^4F_{7/2}$; still the Nd^{3+}-Er^{3+} CR-I: Nd^{3+} $^4F_{5/2}$ + Er^{3+} $^4F_{7/2}$→ Nd^{3+} $^2G_{3/2+5/2}$ + Er^{3+} $^4F_{9/2}$ makes Er^{3+} $^4F_{7/2}$ to be prone to relax non-raditively to $^4F_{9/2}$, followed by emitting red emission (655 nm, $^4F_{9/2}$→$^4I_{15/2}$). It could be concluded that the larger partition of red emission in the Nd^{3+}-harvest-transfer-sensitization trinity system with activators of Er^{3+} as mentioned above, could be attributed to Nd^{3+}-Er^{3+} cross-relaxation which makes the red emission occurs with more possibilities in ETU process I and II, and further explain the why the harvest layer makes the $f_{g/r}$ values smaller. The phenomenon that surface quenching of Yb^{3+} has more influence on red emission in Er^{3+}-UCNPs as mentioned above, could be explained as: red emissions is generated by ETU process I, II and expletive ETU for red emission, thus has more chance to be quenched by the strong Yb^{3+}-Er^{3+} cross-relaxation that is caused by Yb^{3+}-surface quenching.

The influence of Nd^{3+}-X^{3+}(Tm^{3+}/Ho^{3+}) cross-relaxation and Yb^{3+} surface quenching on the partition of red emission in UCNPs with Nd^{3+}-harvest-transfer-sensitization trinity system with activators of Ho^{3+} or Tm^{3+}, however, display diversities as discussed in the Figure 26-29.

For the situation of Nd^{3+}-Trinity system coated UCNPs with activators of Tm^{3+}: the Nd^{3+}-Tm^{3+} cross-relaxation: Tm^{3+} $^1D_2$ + Nd^{3+} $^4J_{15/2} \rightarrow$ Tm^{3+} $^2F_{2,3}$ + Nd^{3+} $^2K_{13/2}$ makes the 4-photon ETU process prone to emit non-radiatively and result in larger partition of red emission (683 nm, Tm^{3+}: $^2F_{2,3} \rightarrow {}^2H_6$), as shown in Figure 26; when Yb^{3+} surface quenching is shielded, the partition of red emission result in 3-photons ETU process is smaller, that are blue emission (475 nm, Tm^{3+} $^1G_4 \rightarrow {}^3H_6$) and red emission (651 nm, Tm^{3+} $^1G_4 \rightarrow {}^3F_4$), which could be explained as the 4-photons ETU process occurs with more possibilities, as shown in Figure 27.

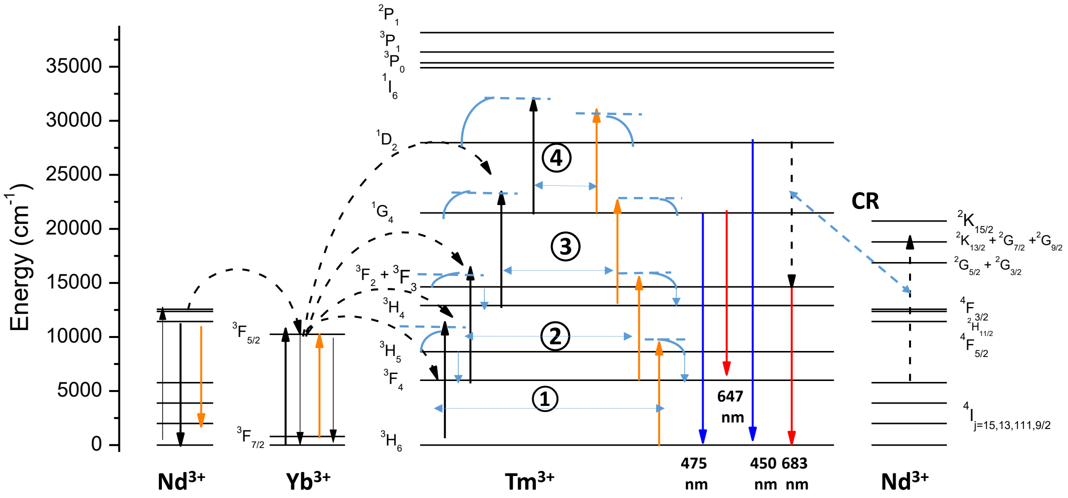

Figure 26. Effect of Tm^{3+}-Nd^{3+} cross-relaxation on red emission of Tm^{3+}.

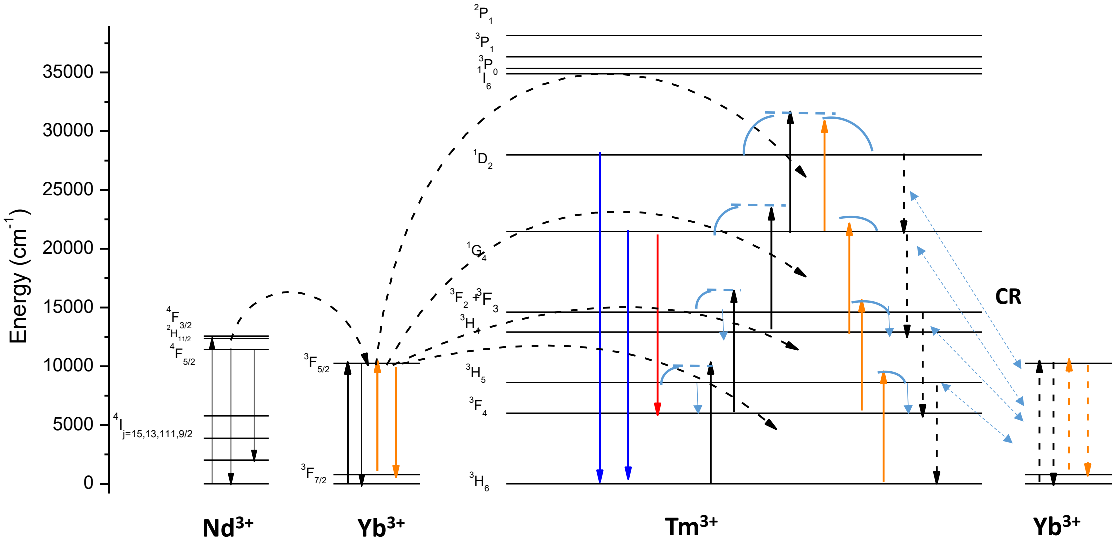

Figure 27. Effect of Yb^{3+} surface quenching on Tm^{3+} emission.

For the situation of Nd^{3+}-Trinity system coated UCNPs with activators of Ho^{3+}: the Nd^{3+}-Ho^{3+} cross-relaxation makes Ho^{3+} prone to emit red emission, as shown in Figure 28; the shielding of surface quenching of Yb^{3+} make to red emission with smaller partition, which could be concluded Yb^{3+}-Ho^{3+} cross-relaxation quenches the excited states of the green emission (550 nm, Ho^{3+} $^5S_2$+$^5F_4$→$^5I_8$) and blue emission (470 nm, Ho^{3+} $^3H_6$→$^5I_8$), that is : Ho^{3+}: $^5S_2$,$^5F_4$ + Yb^{3+} $^2F_{7/2}$→ Ho^{3+} $^5I_6$ +Yb^{3+} $^2F_{5/2}$ (with the energy gap of 9919 cm^{-1}), which resulting in quenching the excited state of the green emission (550 nm, Ho^{3+} $^5S_2$+$^5F_4$→$^5I_8$); however, the cross-relaxation between Ho^{3+} and Yb^{3+}: Ho^{3+} $^3K_7$ + Yb^{3+} $^2F_{7/2}$→ Ho^{3+} $^5F_5$+ Yb^{3+} $^2F_{5/2}$ (with the energy gap of 10743cm^{-1}), results in enhancement of red emission (655 nm, Ho^{3+} $^5F_5$→$^5I_7$).

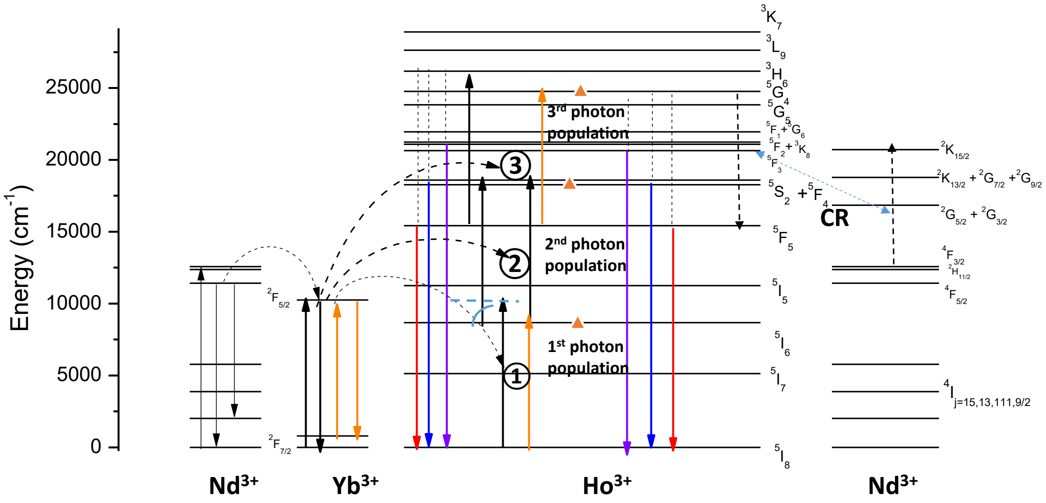

Figure 28. Effect of Nd^{3+}-Ho^{3+} cross-relaxation on red emission of Ho^{3+}.

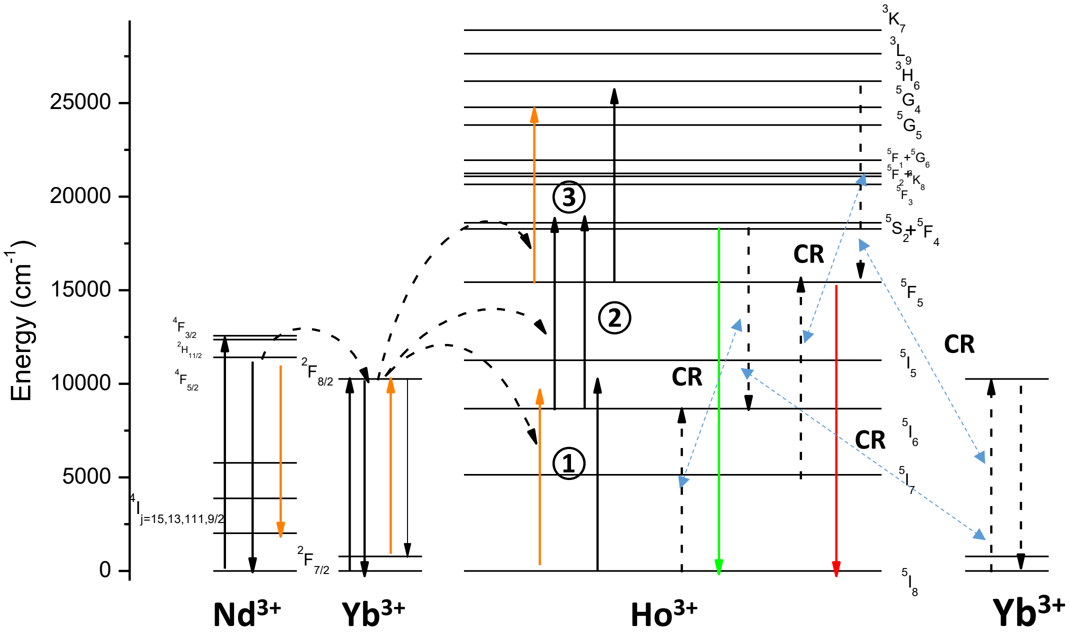

Figure 28. Effect of surface quenching of Yb^{3+} on upconversion process of Ho^{3+}.

2.6. Conclusion

In summary, the UCNPs with the core-multishells structure, Nd^{3+}-Trinity system have gained success in largely enhanced luminescence, high fluorescent quantum yield, prolonged lifetime, larger partition of red emission and deeper penetration. Moreover, it has come to recognized that: the enhanced luminescence and high fluorescent quantum yield result in well-designed UCNPs structures to optimize $Nd^{3+}\rightarrow Yb^{3+}$ energy transfer and avoidance of quenching; and the luminescence is further gained by inducing the Nd^{3+} ions as the sensitizer with higher absorption; the prolonged lifetime is proposed to be result in the 1056 nm selective participation and optimized ETU and PA process; the larger partition of red emission is proposed to be result in surface quenching shielding of Yb^{3+} and Nd^{3+}-Er^{3+} cross-relaxation; the deeper luminescence penetration is contributed by enhanced luminescence and photo-luminescence source attenuation avoiding. Additionally, the UCNPs with Nd^{3+}-Trinity system have shown their potential to be improved as multi-functional bio-imaging probes for their minimized size, superior luminescence properties with excitation of 980 nm and 808 nm laser and high T_1 relaxivity to be utilized as MRI contrast agent. However, there are still limitations that should be overcome, such as the low concentration of the activators, which is considered to be a bottleneck in the ETU process: for high concentration of the activators will result in deleterious cross-relaxation [69] while low concentration of the activators leading to upconversion saturation effects on the luminescent intensity and efficiency [70]. The situation is proposed to be more serious in the Nd^{3+}-sensitized UCNPs with 808 nm excitation, for Nd^{3+} ions acting as the sensitizer with higher photons absorption while the efficiency of ETU remains unchanged for the limited concentration of activators.

References

1. Zhan, Q., J. Qian, H. Liang, G. Somesfalean, D. Wang, S. He, Z. Zhang, and S. Andersson-Engels, *Using 915 nm Laser Excited* $Tm^{3+}/Er^{3+}/Ho^{3+}$*-Doped* $NaYbF_4$ *Upconversion Nanoparticles for in Vitro and Deeper in Vivo Bioimaging without Over-heating Irradiation.* ACS nano, 2011. **5**(5): p. 3744-3757.

2. Xie, X., N. Gao, R. Deng, Q. Sun, Q.-H. Xu, and X. Liu, *Mechanistic investigation of photon upconversion in* Nd^{3+}*-sensitized core–shell nanoparticles.* Journal of the American Chemical Society, 2013. **135**(34): p. 12608-12611.

3. Zhong, Y., G. Tian, Z. Gu, Y. Yang, L. Gu, Y. Zhao, Y. Ma, and J. Yao, *Elimination of Photon Quenching by a Transition Layer to Fabricate a Quenching-Shield Sandwich Structure for 800 nm Excited Upconversion Luminescence of* Nd^{3+}*-Sensitized Nanoparticles.* Advanced Materials, 2014. **26**(18): p. 2831-2837.

4. Xu, B., X. Zhang, W. Huang, Y. Yang, Y. Ma, Z. Gu, T. Zhai, and Y. Zhao, Nd^{3+} *sensitized dumbbell-like upconversion nanoparticles for photodynamic therapy application.* Journal of Materials Chemistry B, 2016. **4**(16): p. 2776-2784.

5. Xi, Y., Z. Chang, X. Ye, H. Huang, Y. Huang, Q. Xiao, and H. Lin, *Ultra-small* Nd^{3+}*-doped nanoparticles as near-infrared luminescent biolabels of hemin in bacteria.* Nanoscale, 2016. **8**(3): p. 1288-1292.

6. Wang, Y.-F., G.-Y. Liu, L.-D. Sun, J.-W. Xiao, J.-C. Zhou, and C.-H. Yan, Nd^{3+}*-sensitized upconversion nanophosphors: Efficient in vivo bioimaging probes with minimized heating effect.* ACS nano, 2013. **7**(8): p. 7200-7206.

7. Wang, L., H. Dong, Y. Li, R. Liu, Y.-F. Wang, H.K. Bisoyi, L.-D. Sun, C.-H. Yan, and Q. Li, *Luminescence-Driven Reversible Handedness Inversion of Self-Organized Helical Superstructures Enabled by a Novel Near-Infrared Light Nanotransducer.* Advanced Materials, 2015. **27**(12): p. 2065-2069.

8. Lu, F., L. Yang, Y. Ding, and J.-J. Zhu, *Highly Emissive Nd^{3+}-Sensitized Multilayered Upconversion Nanoparticles for Efficient 795 nm Operated Photodynamic Therapy.* Advanced Functional Materials, 2016: p. n/a-n/a.

9. Li, X., R. Wang, F. Zhang, L. Zhou, D. Shen, C. Yao, and D. Zhao, *Nd^{3+} Sensitized Up/Down Converting Dual-Mode Nanomaterials for Efficient In-vitro and In-vivo Bioimaging Excited at 800 nm.* Scientific Reports, 2013. **3**: p. 3536.

10. Hou, Z., K. Deng, C. Li, X. Deng, H. Lian, Z. Cheng, D. Jin, and J. Lin, *808 nm Light-triggered and hyaluronic acid-targeted dual-photosensitizers nanoplatform by fully utilizing Nd^{3+}-sensitized upconversion emission with enhanced anti-tumor efficacy.* Biomaterials, 2016. **101**: p. 32-46.

11. He, F., C. Li, X. Zhang, Y. Chen, X. Deng, B. Liu, Z. Hou, S. Huang, D. Jin, and J. Lin, *Optimization of upconversion luminescence of Nd^{3+}-sensitized $BaGdF_5$-based nanostructures and their application in dual-modality imaging and drug delivery.* Dalton Transactions, 2016. **45**(4): p. 1708-1716.

12. Deng, R., F. Qin, R. Chen, W. Huang, M. Hong, and X. Liu, *Temporal full-colour tuning through non-steady-state upconversion.* Nat Nano, 2015. **10**(3): p. 237-242.

13. Chen, Y., B. Liu, X. Deng, S. Huang, Z. Hou, C. Li, and J. Lin, *Multifunctional Nd^{3+}-sensitized upconversion nanomaterials for synchronous tumor diagnosis and treatment.* Nanoscale, 2015. **7**(18): p. 8574-8583.

14. Rivera-La-L4-8583.P. Babu, C. Basavapoornima, C.K. Jayasankar, and V. Lavals *Efficient $Nd^{3+} \rightarrow Yb^{3+}$ energy transfer processes in high phonon energy phosphate glasses for 1.0 μ m Yb^{3+} laser.* Journal of Applied Physics, 2011. **109**(12): p. 123514.

15. Marciniak, L., A. Bednarkiewicz, M. Stefanski, R. Tomala, D. Hreniak, and W. Strek, *Near infrared absorbing near infrared emitting highly-sensitive luminescent nanothermometer*

based on ^{Nd3}*+ to Yb*$^{3+}$ *energy transfer.* Physical Chemistry Chemical Physics, 2015. **17**(37): p. 24315-24321.

16. Cantelar, E. and F. Cussó, *Dynamics of the Yb*$^{3+}$ *to Er*$^{3+}$ *energy transfer in LiNbO3.* Applied Physics B, 1999. **69**(1): p. 29-33.

17. De-Long, Z., W. Dun-Chun, and E.Y.B. Pun, *Numerical analysis of optical amplificationin Er*$^{3+}$*-Yb*$^{3+}$ *codoped Ti:LiNbO*$_3$ *strip waveguides.* IEEE Journal of Quantum Electronics, 2005. **41**(7): p. 958-969.

18. Lei, L., D. Chen, W. Zhu, J. Xu, and Y. Wang, *Impact of High Ytterbium (III) Concentration in the Shell on Upconversion Luminescence of Core–Shell Nanocrystals.* Chemistry–An Asian Journal, 2014. **9**(10): p. 2765-2770.

19. Wang, F., R. Deng, J. Wang, Q. Wang, Y. Han, H. Zhu, X. Chen, and X. Liu, *Tuning upconversion through energy migration in core–shell nanoparticles.* Nat Mater, 2011. **10**(12): p. 968-973.

20. Ren, W., G. Tian, S. Jian, Z. Gu, L. Zhou, L. Yan, S. Jin, W. Yin, and Y. Zhao, *TWEEN coated NaYF*$_4$*:Yb,Er/NaYF*$_4$ *core/shell upconversion nanoparticles for bioimaging and drug delivery.* RSC Advances, 2012. **2**(18): p. 7037-7041.

21. Vetrone, F., R. Naccache, V. Mahalingam, C.G. Morgan, and J.A. Capobianco, *The Active-Core/Active-Shell Approach: A Strategy to Enhance the Upconversion Luminescence in Lanthanide-Doped Nanoparticles.* Advanced Functional Materials, 2009. **19**(18): p. 2924-2929.

22. Wang, Y., K. Liu, X. Liu, K. Dohnalová, T. Gregorkiewicz, X. Kong, M.C.G. Aalders, W.J. Buma, and H. Zhang, *Critical Shell Thickness of Core/Shell Upconversion Luminescence Nanoplatform for FRET Application.* The Journal of Physical Chemistry Letters, 2011. **2**(17): p. 2083-2088.

23. Li, X., D. Shen, J. Yang, C. Yao, R. Che, F. Zhang, and D. Zhao, *Successive Layer-by-Layer Strategy for Multi-Shell Epitaxial Growth: Shell Thickness and Doping Position*

Dependence in Upconverting Optical Properties. Chemistry of Materials, 2013. **25**(1): p. 106-112.

24. He, X., H. Li, Y. Liu, H. Huang, Z. Kang, and S.-T. Lee, *Water soluble carbon nanoparticles: Hydrothermal synthesis and excellent photoluminescence properties.* Colloids and Surfaces B: Biointerfaces, 2011. **87**(2): p. 326-332.

25. Li, C., Z. Quan, J. Yang, P. Yang, and J. Lin, *Highly Uniform and Monodisperse β-NaYF$_4$:Ln^{3+} (Ln = Eu, Tb, Yb/Er, and Yb/Tm) Hexagonal Microprism Crystals: Hydrothermal Synthesis and Luminescent Properties.* Inorganic Chemistry, 2007. **46**(16): p. 6329-6337.

26. João, C., J. Wemans, and G. Figueira, *Numerical Simulation of High-Energy, Ytterbium-Doped Amplifier Tunability.* Applied Sciences, 2013. **3**(1): p. 288.

27. Azkargorta, J., I. Iparraguirre, R. Balda, and J. Fernández, *On the origin of bichromatic laser emission in Nd^{3+}-doped fluoride glasses.* Optics Express, 2008. **16**(16): p. 11894-11906.

28. Malta, O.L. and L.D. Carlos, *Intensities of 4f-4f transitions in glass materials.* Química Nova, 2003. **26**: p. 889-895.

29. Pukhkaya, V., P. Goldner, A. Ferrier, and N. Ollier, *Impact of rare earth element clusters on the excited state lifetime evolution under irradiation in oxide glasses.* Optics Express, 2015. **23**(3): p. 3270-3281.

30. Holsa, J., E. Sailynoja, R.-J. Lamminmaki, P. Deren, W. Strek, and P. Porcher, *Crystal field energy level scheme of Er^{3+} in GdOCl Parametric analysis.* Journal of the Chemical Society, Faraday Transactions, 1997. **93**(13): p. 2241-2246.

31. Reddy, K.R., N.S. Hussain, and S. Buddhudu, *Absorption spectrum - energy level structure parameters of Ho^{3+}:LiTaO$_3$ crystal.* Ferroelectrics Letters Section, 1999. **26**(3-4): p. 61-64.

32. Kebaïli, I., M. Dammak, E. Cavalli, and M. Bettinelli, *Energy levels and crystal-field analysis of* Tm^{3+} *in* $YAl_3(BO_3)_4$ *crystals.* Journal of Luminescence, 2011. **131**(9): p. 2010-2015.

33. Zhang, F., *Photon upconversion nanomaterials*. Nanostructure science and technology. 2015: Springer.

34. Henke, B., F. Pientka, J.A. Johnson, B. Ahrens, P.T. Miclea, and S. Schweizer, *Saturation effects in the upconversion efficiency of Er-doped fluorozirconate glasses.* Journal of Physics: Condensed Matter, 2010. **22**(15): p. 155107.

35. Dong, H., L.-D. Sun, and C.-H. Yan, *Energy transfer in lanthanide upconversion studies for extended optical applications.* Chemical Society Reviews, 2015. **44**(6): p. 1608-1634.

Chapter 3.

808 nm Excited Energy Migration Upconversion (EMU) System Driven by Nd^{3+}-harvest-transfer-sensitization Trinity (Nd^{3+}-Trinity) System

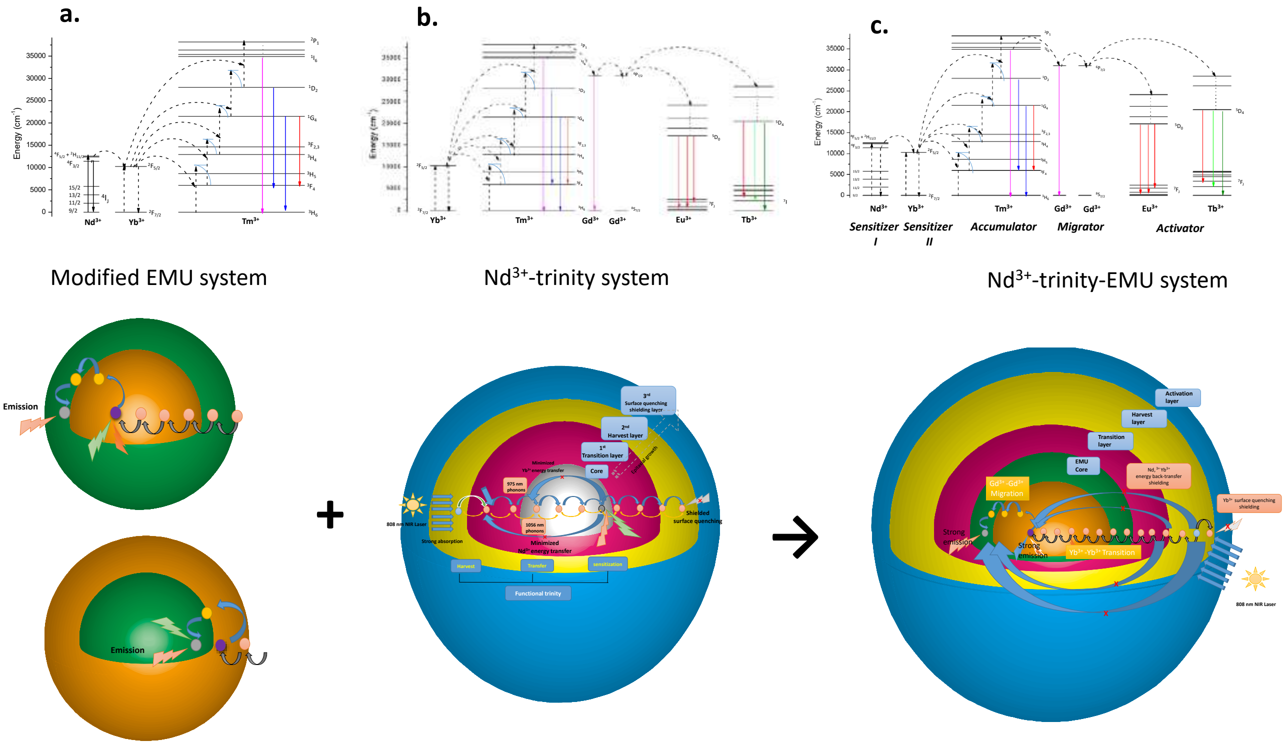

3.1. Background

3.1.1 The energy migration upconversion (EMU) system

The energy migration upconversion (EMU) system is invented by Prof. X.G. Liu's group, which could be considered to be a great process in the area of upconversion nanoparticles (UCNPs). The EMU system are gadolinium-based core-shell UCNPs with sensitizer (Yb^{3+}), accumulator (Tm^{3+}), migrator (Gd^{3+}), and activators (Eu^{3+} and Tb^{3+}). And the cores are composed of NaGdF$_4$:Yb, Tm(49 mmol %/1 mmol %) and shell is composed of NaGdF$_4$:Eu/Tb(15 mmol %). The traditionally developed UCNPs with the Yb^{3+} ions as the sensitizer that absorbs the 980 nm photons and then sensitize the activators, including the Er^{3+}, Tm^{3+} and Ho^{3+}, are strictly depressed the concentration of the activators, which are 1-2 mmol % for Ho^{3+} and Er^{3+} and 0.5-1% mmol for Tm^{3+}. The reason for the depression of the concentration of the activators could be concluded as: a. the saturation effect of the activators [56, 57]; b. the deleterious cross-relaxation between the activators. [7]

However, the invention of the EMU system has increased the concentration of the activators, that are Eu^{3+} with red emission (590 nm and 616 nm) and Tb^{3+} green emission (550 nm), by the 5 phonons accumulation of Tm^{3+} (with blue emission in 450 and 475 nm and red emission in 655 nm), transferring to the $^6P_{7/2}$ (~ 31000 cm^{-1}) excited state of Gd^{3+}, and then exciting the Eu^{3+} and Tb^{3+} The excitation of the activators by Gd^{3+}, that is the migrator, makes the concentration of the activators could be increased to 10 mmol %, which enhanced the upconversion efficiency of the whole system.[29]

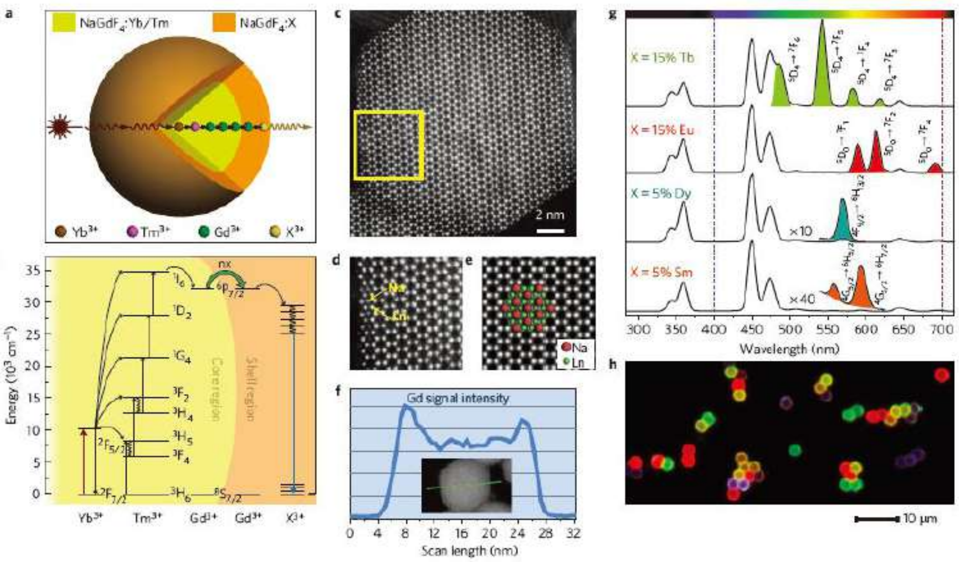

Figure 1. The energy migration upconversion (EMU) system. (a-b). the design of the EMU system; b the basic mechanism of the EMU system; (c-f). Characterization of the morphology, size and the element distribution of the EMU UCNPs; (g-h). Emission spectra and luminescence performance of the UMU UCNPs. [29]

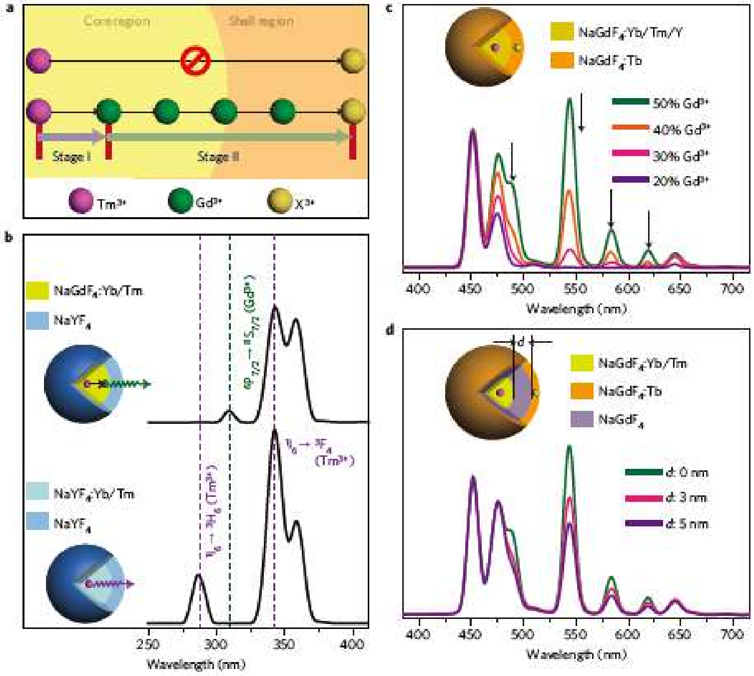

Figure 2. The mechanism investigation of the energy migration upconversion system. (a-b). the investigation of the $Gd^{3+} \rightarrow Gd^{3+}$ migration; (c). the influence of the Gd^{3+} concentration on the $Gd^{3+} \rightarrow Gd^{3+}$ migration; (d) the influence of the distance on the $Gd^{3+} \rightarrow Gd^{3+}$ migration. [29]

3.1.2 The Nd^{3+}-harvest-transfer-sensitization trinity system

As we have stated in the chapter 2 on the design of the Nd^{3+}-harvest-transfer-sensitization trinity (Nd^{3+}-Trinity) system, which has largely enhanced the luminescent intensity, prolonged the lifetime, enlarged the partition of the red emission, elevated the upconversion efficiency (florescent quantum yield), and deepen the penetration, which could be attributed to the well design of the Nd^{3+}-Trinity system for it is designed to shield all the quenching factors in the system as well as absorb the 808 nm photons as possible and transfer to Yb^{3+} as efficient; additionally, besides the function of sensitization that is absorption of the 808 nm photons, the Nd^{3+} ions has acted the roles that enlarge the red emission of the activators by Nd^{3+}-$X(Er/Tm/Ho)^{3+}$cross-relaxation as well as induce the 1056 nm photons selectively participate in ETU(energy transfer upconversion) process, as shown in Figure 3.

And here comes the question that if the Nd^{3+}-Trinity System could be used to sensitize the EMU system that makes the EMU system shows with the superior luminescent properties as mentioned above along with avoidance of the over-heating effect ?

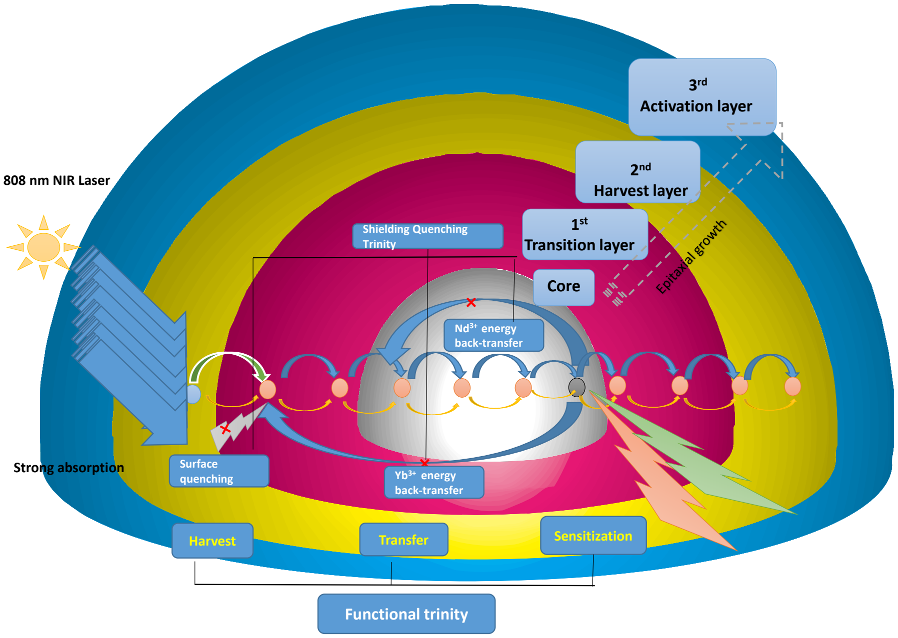

Figure 3. Design and the superiority of the Nd^{3+}-harvest-transfer-sensitization trinity (Nd^{3+}-Trinity) system.

3.1.3. The initial aim of construction of the 808 nm excited, Nd^{3+} sensitized EMU system

Thus, we would like to construct the Nd^{3+}-sensitized EMU system by learning from the EMU system which has largely enhanced the concentration of the activators along with our previous work on the construction of the Nd^{3+}-Trinity system, to realize the EMU system could be excited by 808 nm laser instead of 980 nm laser to avoid the over-heating effect, along with obtaining the superior luminescent properties as mentioned above.

3.2. Design

Our design is the Nd^{3+}-harvest-transfer-sensitization trinity (Nd^{3+}-Trinity) system, which is composed of the **transition layer($NaGdF_4$:Yb)**, **harvest layer($NaGdF_4$:Yb,Nd)** and the **activation layer ($NaGdF_4$)**, coating on the modified the EMU core which are composed of **accumulation layer** that doping with the accumulator that is Tm^{3+} and the **emission layer** that doping with the activators that is Eu^{3+} and Tb^{3+}: a. type I, that is $NaGdF_4$:Yb, Tm(49/1)@$NaGdF_4$:Eu/Tb(15%), Yb (10 %); b. type II, that is $NaGdF_4$:Eu/Tb(15%)@ $NaGdF_4$:Yb, Tm(49/1). For the type I EMU cores the doping of 10 % mmol in the accumulation layer is used to build the Yb^{3+}→Yb^{3+}(~ 10250 cm^{-1}) energy bridge; for the type II EMU cores, the adverse constructing the of the EMU system, is also used to sensitize the activators by the Yb^{3+}→Yb^{3+} (~ 10250 cm^{-1}) energy bridge form the appropriate doping of the Yb^{3+} ions in the harvest layer, transition layer and the accumulation layer ($NaGdF_4$:Yb,Tm). And we would like to call the newly design as the **Nd^{3+}-Trinity EMU** system, as shown in Figure 4.

Herein, we would like to conclude the design is used to obtain the largest extent harvesting by Nd^{3+} absorption of the 808 nm photons and the optimized Nd^{3+}→Yb^{3+} energy transfer by the harvest layer, and then sensitize the accumulator (Tm^{3+}); by 5-phonon ETU process, the accumulator transfer energy to Gd^{3+}; by Gd^{3+}→Gd^{3+} migration, the activators are excited and emitting emissions. And the transition layer is used to minimize the quenching on the accumulator and the activators by Nd^{3+} and Yb^{3+} in the harvest layer; the activation layer is used to shield the surface quenching of the Yb^{3+} in the harvest layer.

And there are two energy bridge: Gd^{3+}→Gd^{3+} migration, which transfer energy on the Gd^{3+} $^6P_{7/2}$, ~31000 cm^{-1}; Yb^{3+}→Yb^{3+} migration, transfers energy on the Yb^{3+} $^2F_{7/2}$ sublevels (as we have discussed in chapter 2), ~102500 cm^{-1} and the ~9469 cm^{-1}.

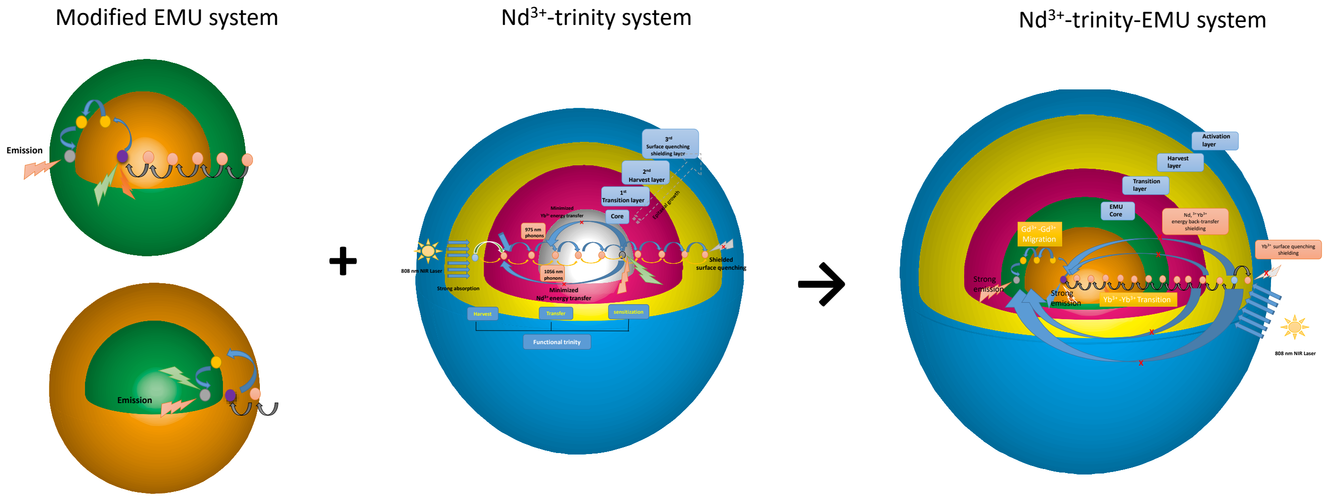
Modified EMU system

Nd^{3+}-trinity system

Nd^{3+}-trinity-EMU system

Figure 4. Construction of the Nd^{3+}-Trinity EMU system, which is coating the Nd^{3+}-trinity system on the modified EMU cores, enables the 808 nm laser could be used to initiate the EMU(energy migration upconversion) system. a. two types of the EMU core; b.Nd^{3+}-trinity system which is composed of the transition layer, harvest layer and activation layer; c the whole EMU system with the structure of core-multishells.

3.3. Investigation of the quenching factors in the Nd^{3+}-sensitized EMU system

By conducting the investigations, the main difficulties that should be resolved in construction of the Nd^{3+}-Trinity EMU system could be concluded as: the conflict between the energy transfer and energy back-transfer, which in specification is that the high concentration of Nd^{3+} ions and Yb^{3+} ions are required to harvest and transfer the photons of 808 nm photo-luminescence source to initiate the Nd^{3+}-Trinity EMU process, however, both of Nd^{3+} ions and Yb^{3+} ions cause manifest quenching at the same time.

Energy transfer and quenching factors in the Nd^{3+}-Trinity EMU system: as shown in Figure 5 (a), in the Nd^{3+}-trinity driven EMU system, all the situation of ET(energy transfer), including energy transfer, energy back-transfer and energy transfer upconversion (ETU), and radiative and non-radiative transition has been generalized. The main quenching factors in the Nd^{3+}-Trinity EMU system, could be concluded as conspicuous cross-relaxation of Nd^{3+}-X^{3+}(Tm^{3+}/Eu^{3+}/Tb^{3+}) and Yb^{3+}-X^{3+}(Tm^{3+}/Eu^{3+}/Tb^{3+}), which in specifically are Nd^{3+} energy back-transfer, Yb^{3+} energy back-transfer and Yb^{3+} surface quenching. For further development of the Nd^{3+}-Trinity driven EMU system, we have done some investigations on the factors of quenching, effect of the transition layer, harvest layer and activation layer in the Nd^{3+}-Trinity system and optimization on the composition of the harvest layer and precursors ratio of the core-multishells structures, which shielding all the quenching factors to the maximum extent by the Nd^{3+}-trinity system, along with sufficient 808 nm photons harvesting, transferring to Yb^{3+}→Yb^{3+} transition and sensitization Tm^{3+} to achieve the 5-phonon accumulation.

Nd^{3+} absorption of photons and energy back-transfer:

Similarity with the previous work that in the Nd^{3+}-Trinity system, the harvest layer that is composed with high concentration of Nd^{3+} ions with certain amount of Yb^{3+} doping (that is $NaNdF_4$:$Yb_{20\,\%}$ or $NaGdF_4$:$Yb_{10\,\%}$, $Nd_{50\,\%}$) is dispensable to harvest the 808 nm photons, as shown in Figure 6, the in the Nd^{3+}-sensitized EMU system, the emission spectra reveals that the Nd^{3+}-sensitized EMU system with harvest layer (that is $NaGdF_4$:$Yb_{49\,\%}$,$Tm_{1\,\%}$@$NaGdF_4$:$Yb_{10\,\%}$,$Tb_{15\,\%}$@$NaGdF_4$:$Yb_{10\,\%}$@$NaGdF_4$:$Yb_{10\,\%}$,$Nd_{50\,\%}$ @$NaGdF_4$) compares with the Nd^{3+}-sensitized EMU system without harvest layer (that is $NaGdF_4$:$Yb_{49\,\%}$,$Tm_{1\,\%}$@$NaGdF_4$:$Yb_{10\,\%}$,$Tb_{15\,\%}$@$NaGdF_4$:$Yb_{10\,\%}$,$Nd_{20\,\%}$@$NaGdF_4$), shows large enhancement.

However, the effect of Nd^{3+} energy back-transfer in the Nd^{3+}-Trinity EMU system influences the accumulator (Tm^{3+}) as well as the activators (Eu^{3+}/Tb^{3+}). On one hand, Nd^{3+} ions invalid the 3/4/5-phonons ETU process of the Tm^{3+} (accumulator) the by Nd^{3+}-Tm^{3+}

cross relaxation. As shown in Figure 5(b), only 1 mmol % Nd^{3+} doping in the $NaGdF_4$:Yb,Tm, which is $NaGdF_4$:$Yb_{49\,\%}$,$Tm_{1\,\%}$,$Nd_{1\,\%}$, or the high concentration of Nd^{3+} in the nearby layer of Tm^{3+}, which is $NaGdF_4$:Yb,Tm@$NaNdF_4$, result in large quenching of the 3/4/5-phonons emission and further invalid the $Gd^{3+}\rightarrow Gd^{3+}$ migration (5-phonons) by the strong cross-relaxation between Yb^{3+} and Tm^{3+}. On the other hand, Nd^{3+} ions are proposed to quench the Tb^{3+} (green emission) and Eu^{3+} (red emission) , that are Nd^{3+} $^2G_{5/2}$ + $^2G_{3/2}$: 16852 cm^{-1} are is proposed to quench the Eu^{3+} $^5D_0$ 17081 cm^{-1} and the Nd^{3+} $^2K_{15/2}$: 20718 cm^{-1} is proposed to quench the Tb^{3+} $^5D_4$: 20504 cm^{-1}. A very high concentration of Nd^{3+} ions in the nearby layer of EMU system is proved to quench the emission of Eu^{3+} and Tb^{3+}**.** It reminds us to isolate Nd^{3+} ions with the EMU cores. And we utilized the method that sandwiching a transition layer with harvest layer and EMU cores. Compared with the UCNPs that are: $NaGdF_4$:Yb,Tm and EMU-Eu^{3+}/Tb^{3+} system driven by Nd^{3+}-sensitized systems, with the differences that are existence and lacking of the transition layer, the emission spectra reveals that: the transition layer avoiding the harvest layer (namely high concentration of Nd^{3+}), quenches the ETU process of Tm^{3+} and further avoiding quenching the emission of Eu^{3+}/Tb^{3+}, which also proves the importance of the transition layer.

Yb^{3+} energy transfer and energy back-transfer: the Yb^{3+} ions are dispensable in $Nd^{3+}\rightarrow Yb^{3+}$ energy transfer as well as the construction of the $Yb^{3+}\rightarrow Yb^{3+}$ energy bridge, as shown in Figure 5 (c), compares with the EMU-Tb cores ($NaGdF_4$:$Yb_{49\,\%}$,$Tm_{1\,\%}$@$NaGdF_4$:$Tb_{15\,\%}$) that driven by Nd^{3+}-Trinity system, with the difference that doping or do not doping 10 mmol % Yb^{3+} ions, we found that properly doping of Yb^{3+} ions in the harvest layer makes the Nd^{3+}-Trinity EMU system more efficient.

Moreover, the 10 mmol % doping of Yb^{3+} in the system forms the $Yb^{3+} \rightarrow Yb^{3+}$ energy bridge, that used to drive the EMU core.

However, when the Yb^{3+} ions are in high concentration, it still invalidates the EMU process of Tm3+ as well as quenching the Eu^{3+}/Tb^{3+} by Yb^{3+} CET process, which remind us to pay more attention to the Yb^{3+} concentration in the transition layer and harvest layer.

Surface quenching of Yb^{3+}: invalid the Tm^{3+} accumulation by Tm^{3+}-Yb^{3+} cross-relaxation, likewise strongly quenches the Eu^{3+}/Tb^{3+} emission. As shown in Figure 5(d), compares the emission spectra of the UCNPs of Nd^{3+}-Trinity EMU system that with and without activation layer ($NaGdF_4$), we found by remedy the surface defect of the harvest layer, which is mainly on Yb^{3+} ions to shield the surface quenching, not only active the 3-phonons emission but also the 4- and 5-phonons ETU process emission.

Conclusively, the main paradoxically issues in our design of the Nd^{3+}-trinity system could be generalized as: on one hand, the harvest layer which could be treated as with the composition of high concentration of Nd^{3+} to guarantee the 808 nm photons harvesting, with certain amount of Yb^{3+} doping to guarantee the $Nd^{3+} \rightarrow Yb^{3+}$ energy transfer and the $Yb^{3+} \rightarrow Yb^{3+}$ transition, which is essentail in the Nd^{3+}-Trinity EMU system; on the other hand, both of them threating the upconversion efficiency by quenching the accumulation and the emission of the activators by Tm^{3+}-Yb^{3+} and Tm^{3+}-Nd^{3+} cross-relaxation. Whereas, the Nd^{3+}-trinity system, solves the problem with the strategies which could be concluded as: a. the accumulator and the activator should be segregated with high concentration of Nd^{3+} ions, which means sandwiching the transition layer between the harvest layer and the $NaGdF_4$: X(Eu/Tb) layer (in type I) or the $NaGdF_4$:Yb,Tm layer(in type II) ; b. high concentration of Yb^{3+} should be avoided in the Nd^{3+}-Trinity EMU system; c. the $NaGdF_4$ layer is needed to activate the emission.

a-1.

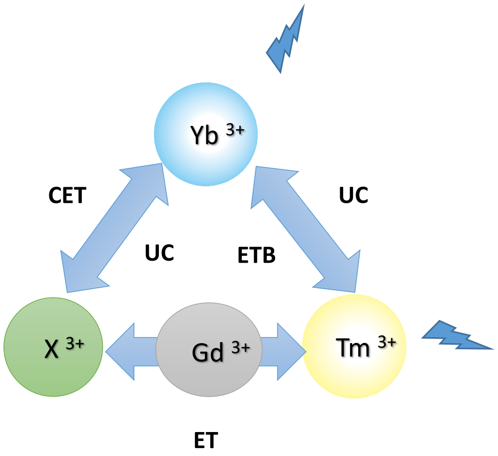

a-2.

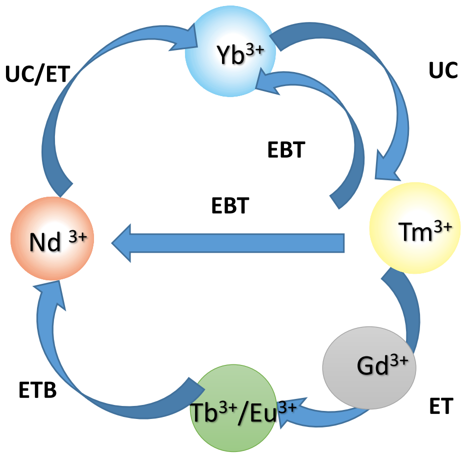

b.

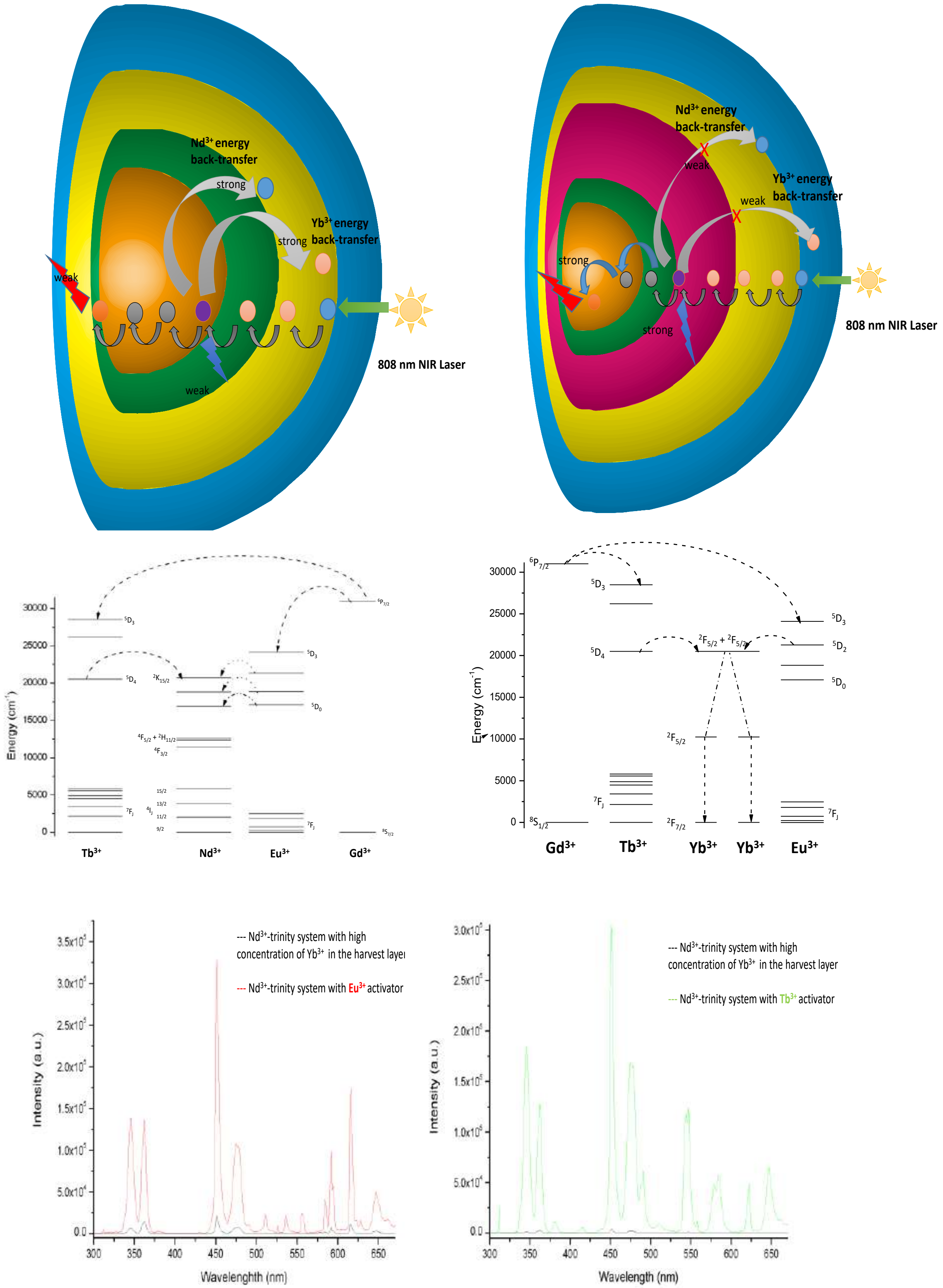
Nd³⁺ energy back-transfer
strong
Yb³⁺ energy back-transfer
strong
weak
weak
808 nm NIR Laser
Nd³⁺ energy back-transfer
weak
Yb³⁺ energy back-transfer
weak
strong
strong
808 nm NIR Laser
Energy (cm⁻¹)
30000
25000
20000
15000
10000
5000
0
⁵D₃
⁵D₄
⁷F_J
²K₁₅/₂
⁴F₅/₂ + ²H₁₁/₂
⁴F₃/₂
15/2
13/2
⁴I_J
11/2
9/2
⁵D₃
⁵D₀
⁷F_J
⁶P₇/₂
⁸S₇/₂
Tb³⁺
Nd³⁺
Eu³⁺
Gd³⁺
⁶P₇/₂
⁵D₃
⁵D₄
⁷F_J
⁸S₁/₂
²F₅/₂ + ²F₅/₂
²F₅/₂
²F₇/₂
⁵D₃
⁵D₂
⁵D₀
⁷F_J
Gd³⁺
Tb³⁺
Yb³⁺
Yb³⁺
Eu³⁺
Intensity (a.u.)
3.5x10⁵
3.0x10⁵
2.5x10⁵
2.0x10⁵
1.5x10⁵
1.0x10⁵
5.0x10⁴
0.0
300
350
400
450
500
550
600
650
Wavelenghth (nm)
--- Nd³⁺-trinity system with high concentration of Yb³⁺ in the harvest layer
--- Nd³⁺-trinity system with Eu³⁺ activator
Intensity (a.u.)
3.0x10⁵
2.5x10⁵
2.0x10⁵
1.5x10⁵
1.0x10⁵
5.0x10⁴
0.0
300
350
400
450
500
550
600
650
Wavelength (nm)
--- Nd³⁺-trinity system with high concentration of Yb³⁺ in the harvest layer
--- Nd³⁺-trinity system with Tb³⁺ activator

c.

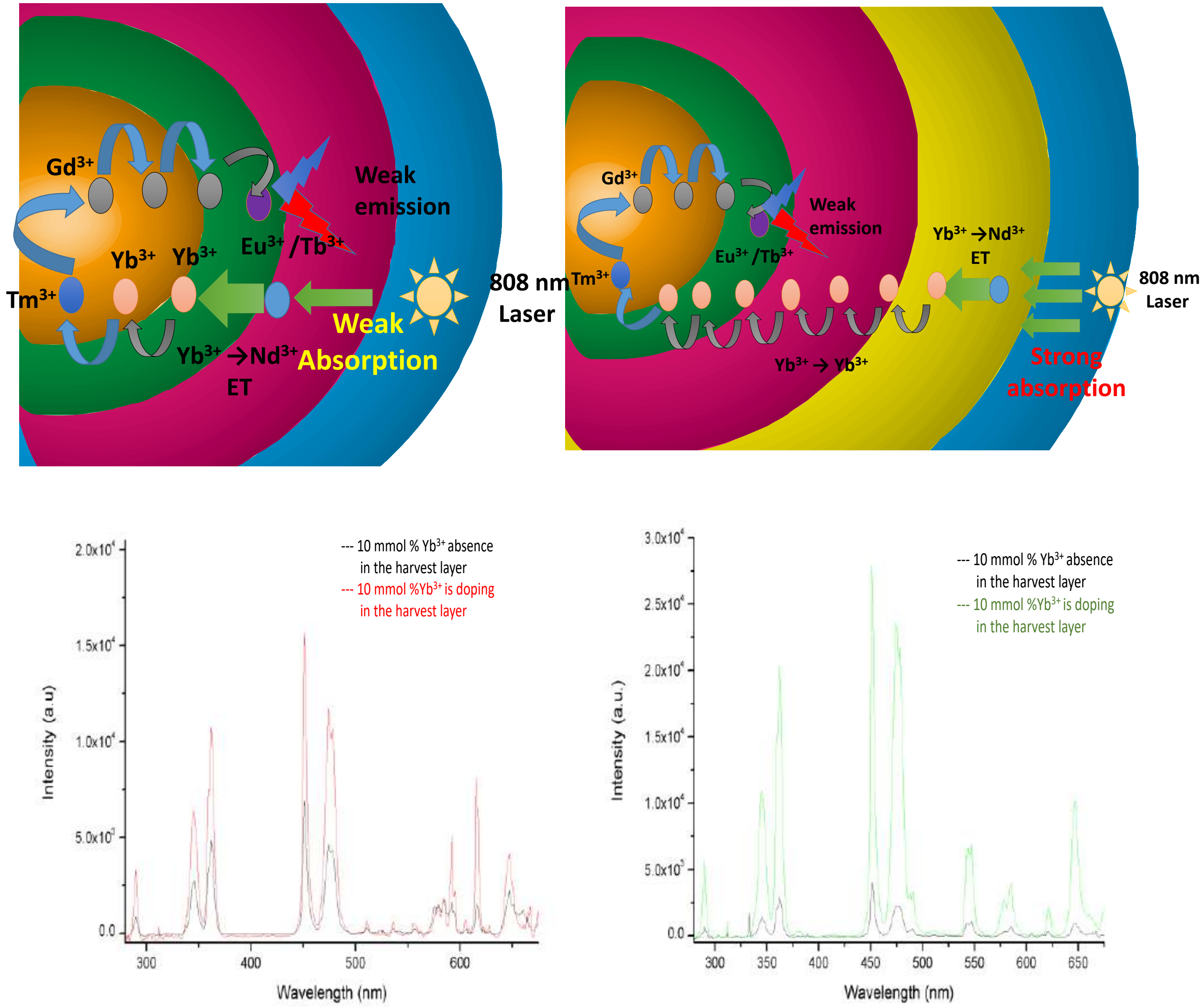
Gd3+
Weak emission
Yb3+
Yb3+
Eu3+ /Tb3+
Tm3+
Weak Absorption
Yb3+ →Nd3+ ET
808 nm Laser
Gd3+
Weak emission
Eu3+ /Tb3+
Tm3+
Yb3+ →Nd3+ ET
808 nm Laser
Yb3+ → Yb3+
Strong absorption
--- 10 mmol % Yb3+ absence in the harvest layer
--- 10 mmol %Yb3+ is doping in the harvest layer
Intensity (a.u)
2.0x10⁴
1.5x10⁴
1.0x10⁴
5.0x10³
0.0
300
400
500
600
Wavelength (nm)
--- 10 mmol % Yb3+ absence in the harvest layer
--- 10 mmol %Yb3+ is doping in the harvest layer
Intensity (a.u.)
3.0x10⁴
2.5x10⁴
2.0x10⁴
1.5x10⁴
1.0x10⁴
5.0x10³
0.0
300
350
400
450
500
550
600
650
Wavelength (nm)

d.

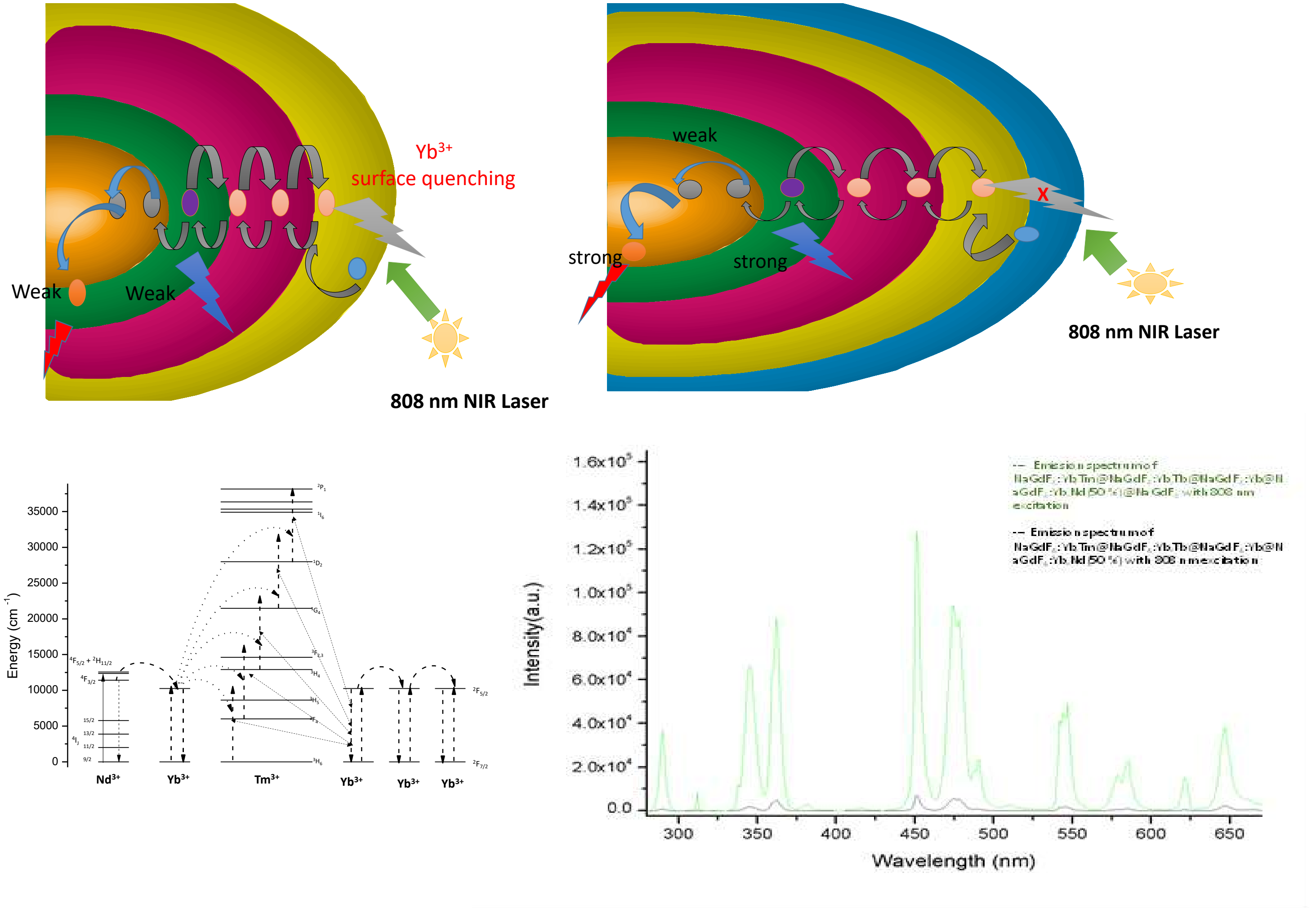
Yb^{3+}
surface quenching
Weak
Weak
808 nm NIR Laser
weak
strong
strong
X
808 nm NIR Laser
Energy (cm^{-1})
35000
30000
25000
20000
15000
10000
5000
0
$^4F_{5/2}+^2H_{11/2}$
$^4F_{3/2}$
^4I
15/2
13/2
11/2
9/2
$^3P_1$
$^1I_6$
$^1D_2$
$^1G_4$
$^3F_{2,3}$
$^3H_4$
$^3H_5$
$^3F_4$
$^3H_6$
$^2F_{5/2}$
$^2F_{7/2}$
Nd^{3+}
Yb^{3+}
Tm^{3+}
Yb^{3+}
Yb^{3+}
Yb^{3+}
Intensity(a.u.)
1.6x10^5
1.4x10^5
1.2x10^5
1.0x10^5
8.0x10^4
6.0x10^4
4.0x10^4
2.0x10^4
0.0
300
350
400
450
500
550
600
650
Wavelength (nm)
— Emission spectrum of NaGdF$_4$:Yb,Tm@NaGdF$_4$:Yb,Tb@NaGdF$_4$:Yb@NaGdF$_4$:Yb,Nd (50 %)@NaGdF$_4$ with 808 nm excitation
— Emission spectrum of NaGdF$_4$:Yb,Tm@NaGdF$_4$:Yb,Tb@NaGdF$_4$:Yb@NaGdF$_4$:Yb,Nd (50 %) with 808 nm excitation

Figure 5. (a). Generalization of all the situation of energy transfer and quenching factors in the Nd^{3+}-trinity system (EBT: energy back-transfer; ET: energy transfer; UC: upconversion); (b). effect of the transition layer and Nd^{3+} energy back-transfer; (c). effect of $Nd^{3+} \rightarrow Yb^{3+}$ energy transfer and Yb^{3+} energy back-transfer; (d).Effect of the Yb^{3+} surface quenching and activation layer. (Measurement conditions: power density: 80 mW/ 1 mm^2 for 808/ 980 nm diode laser; emission bandwidth: 2 nm, concentration: 1.0 wt %.)

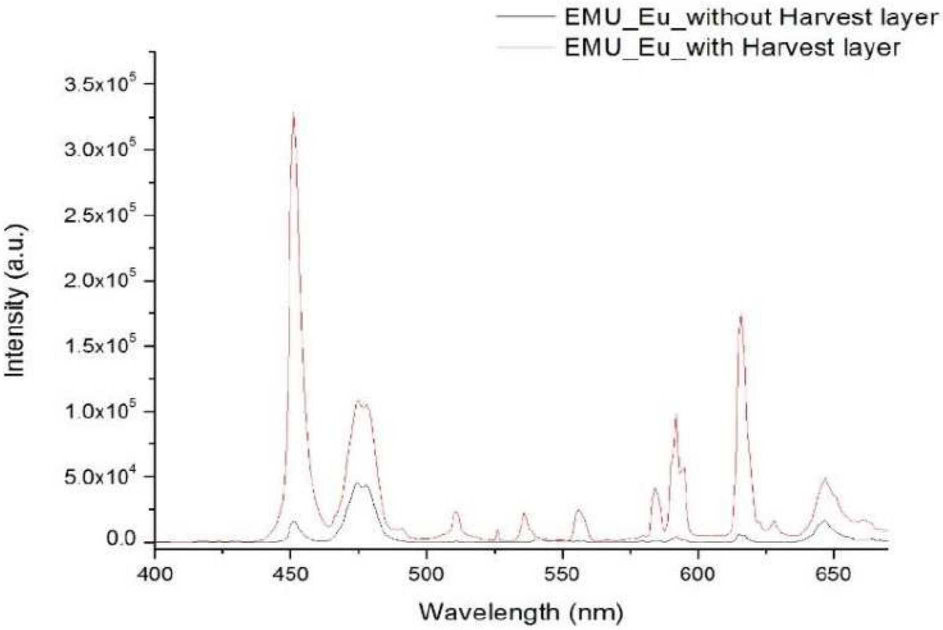

Figure 6. The emission spectra of Nd^{3+}-trinity EMU system with the difference that existence and absence of the harvest layer, which illustrated the importance of the harvest layer. (Measurement conditions: power density: 80 mW/ 1 mm^2 for 808/ 980 nm diode laser; emission bandwidth: 2 nm, concentration: 1.0 wt %.)

3.4. Synthesis and characterization of the Nd^{3+}-Trinity EMU system UCNPs

The UCNPs of the Nd^{3+}-Trinity EMU system UCNPs are synthesized by the method of thermal decomposition by the method of “layer-by-layer” epitaxial growth, as shown in Figure 7, with the accumulation layer coating on the emission layer or the emission layer coating on the accumulation layer that forms the EMU core, and then the transition layer, harvest layer and the activation layer is coating on “layer by layer” [32], result in the core-multishells, gadolinium based UCNPs in minimized size, that is sub-15 nm in very well self-assembly by characterization of TEM.

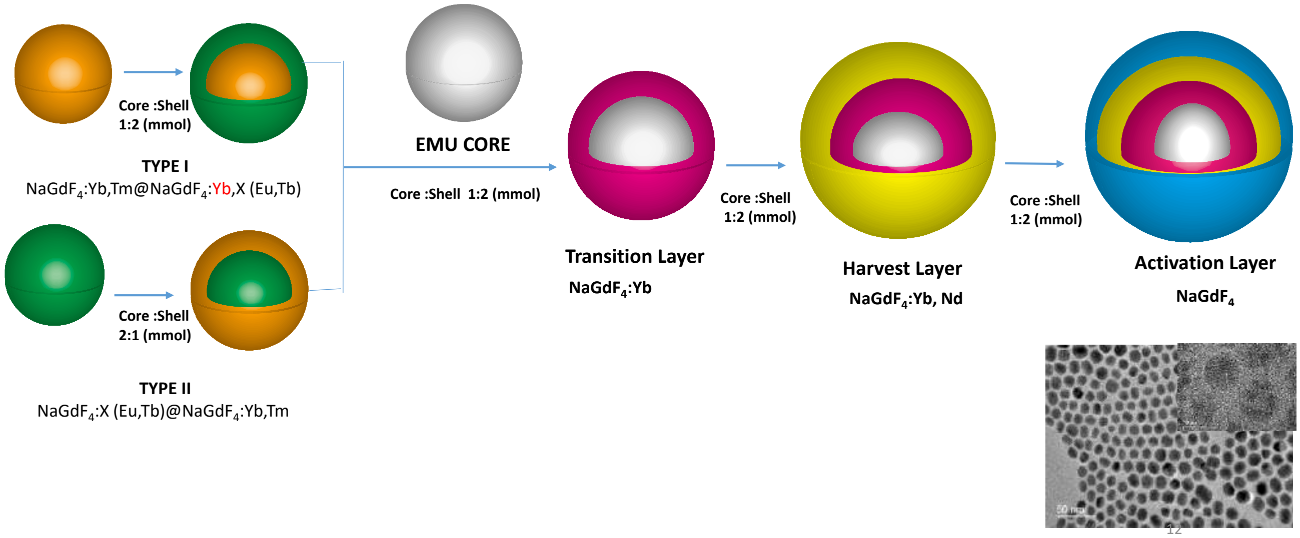

Figure 7. Synthesis of the UCNPs of the core-multishells structures by “layer by layer” epitaxial growth and TEM characterization of the Nd^{3+}-trinity system.

3.5. Optimization of the Nd^{3+}-Trinity EMU system

As we have stated that the luminescence performance of the Nd^{3+}-Trinity EMU system are affected by the quenching factors including the Nd^{3+} and Yb^{3+} quenches Tm^{3+} and Eu^{3+} /Tb^{3+}, and other factors including the concentration of the activator in the emission layer, including the ratio of the precursors in the “layer-by-layer” epitaxial growth [6, 7, 29, 35], the composition of the harvest layer, and the ratio of the sensitizer and accumulators in the accumulation layer.

3.5.1. Optimization of the ratio of the sensitizer and accumulators in the accumulation layer

As the UCNPs with Tm^{3+} activators have been reported on the ratio of the Yb/Tm as 20:0.5 and 49:1(mmol %/mmol %), and the peak area ratio has something different. We have done investigations on which composition is better in the utilization of the EMU system. As shown in Figure 8, the Yb/Tm with the ratio of 49:1(mmol %) [71-73] utilized in the EMU system with activators of Eu^{3+}, shows enhanced intensity (about 10 times that the Yb/Tm with the ratio of 20:0.5) for all the emission bands, especially the 5-phonons emission of Tm^{3+} and the Gd^{3+} $^6P_{7/2}$ emission.

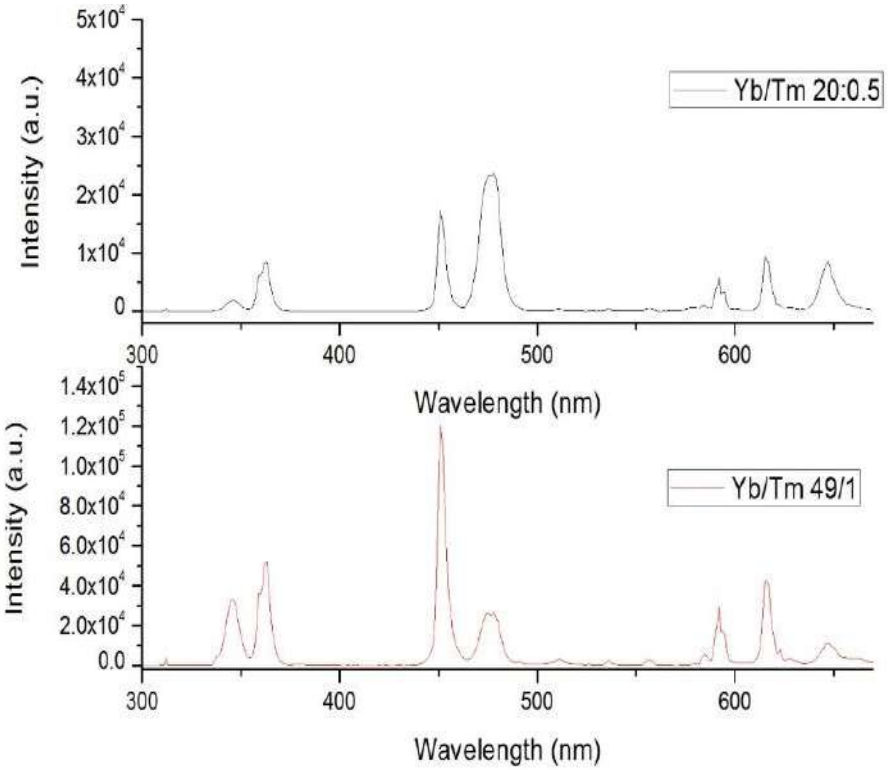

Figure 8. Optimization of the EMU cores in the Nd^{3+}-Trinity EMU system by adjusting the Yb/Tm ratio in the accumulation layer. (Measurement conditions: power density: 80 mW/ 1 mm^2 for 808/ 980 nm diode laser; emission bandwidth: 2 nm, concentration: 1.0 wt %.)

3.5.2. Optimization of the composition of the harvest layer

As we have stated above that the Nd^{3+} and Yb^{3+} have strong quenching on the activators and the accumulator, however, the harvest layer that contains high concentration of the Nd^{3+} and appropriate Yb^{3+} doping is in need, thus the optimization on the harvest layers is imperative. The Nd^{3+}-Trinity EMU system is optimized with the harvest layer by adjusting the composition of the Yb^{3+} and Nd^{3+} in the gadolinium-based layer. As shown in Figure 9, by fixing the Yb^{3+} concentration as 10 mmol %, adjusting the concentration of Nd^{3+}, it could be seen that in the Nd^{3+}-Trinity EMU with Tb^{3+} as activator, when the Nd^{3+} is in 50 mmol %, the system displays the best luminescent performance; as shown in the Figure 10, it could be seen that in the Nd^{3+}-Trinity EMU with Eu^{3+} as activator, when the Nd^{3+} is in 80 mmol % and the Yb^{3+} in 20 mmol % , the system displays the best luminescence performance.

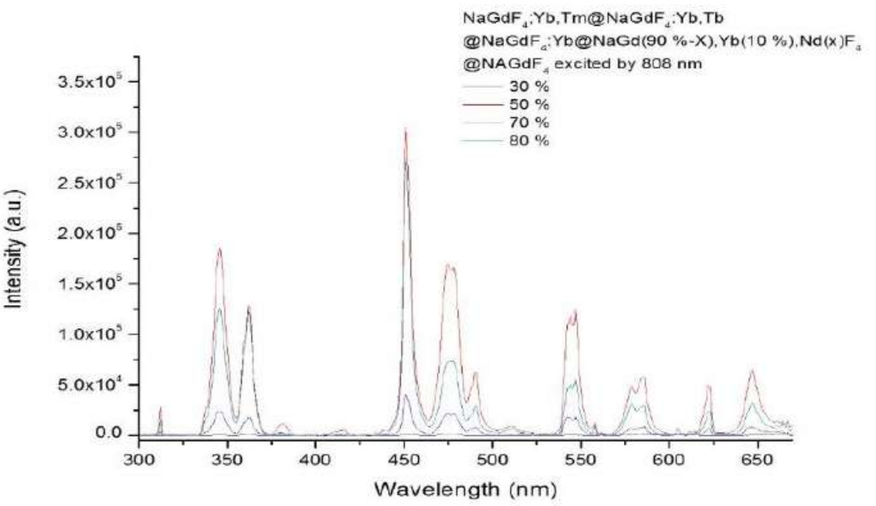

Figure 9. Optimization of the harvest layer of the Nd^{3+}-trinity-EMU system with activator of Tb^{3+}. (Measurement conditions: power density: 80 mW/ 1 mm^2 for 808/ 980 nm diode laser; emission bandwidth: 2 nm, concentration: 1.0 wt %.)

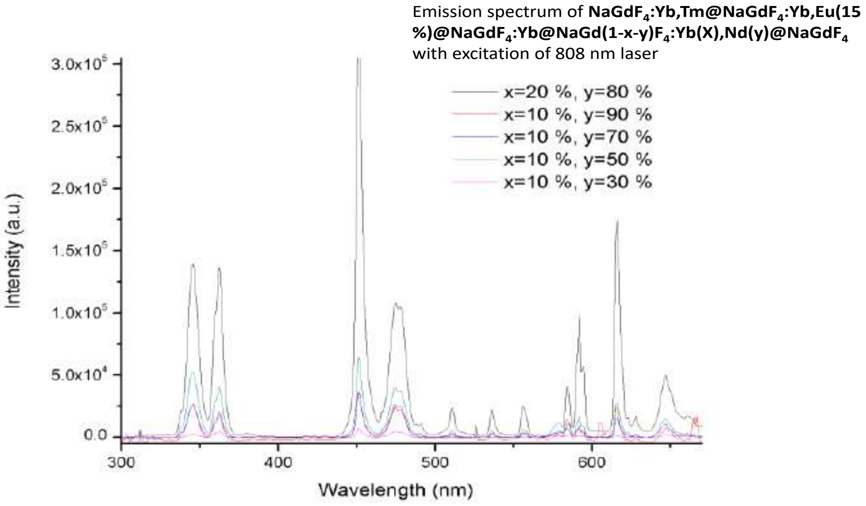

Figure 10. Optimization of the harvest layer of the Nd^{3+}-trinity-EMU system with activator of Eu^{3+}. (Measurement conditions: power density: 80 mW/ 1 mm^2 for 808/ 980 nm diode laser; emission bandwidth: 2 nm, concentration: 1.0 wt %.)

3.5.3. Optimization on the ratio of the precursors

Additionally, we have found that the ratio of the precursors in the synthesis of the core-shell UCNPs depends on the specific situation, for the commonly used ratio of core/shell is 1:1, 2:1 and 2:1. We have done investigation on it to optimize the luminescent performance. As shown in Figure 11, in the Nd^{3+}-trinity EMU system with activator of Eu^{3+}, when coating the harvest layer on the transition layer, we used the ratio as 1:1 and 2:1(other step is 2:1)[15, 16, 18, 30, 32-36, 47, 49, 54], the luminescent performance is shown to be better with the 2:1 ratio, which reflects that although the Nd^{3+} is comparably less in the whole system, the comparably more of the activators has taken effect. Also, the 2:1 ratio result in minimized size of the UCNPs.

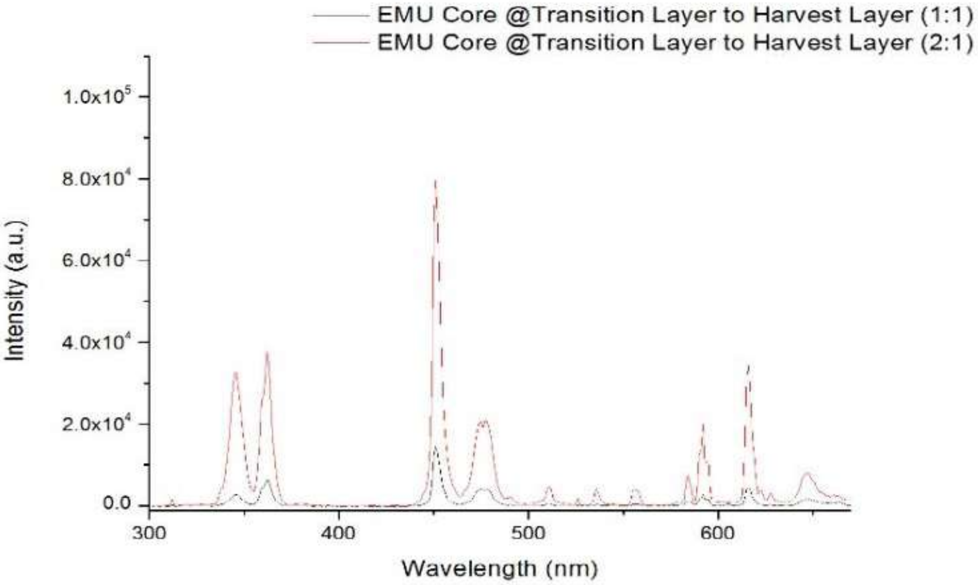

Figure 11. The optimization of the Nd^{3+}-trinity EMU system on the precursors of the core-shell ratio. (Measurement conditions: power density: 80 mW/ 1 mm^2 for 808/ 980 nm diode laser; emission bandwidth: 2 nm, concentration: 1.0 wt %.)

3.6. Study of luminescent properties

As shown in the experimental section, we have established the characterization of the luminescent properties of the UCNPs of the Nd^{3+}-Trinity EMU system by the 808/980 nm pulsed/CW laser: the emission spectra which is used to reflect the situation of the luminescence performance, the UCNPs of the Nd^{3+}-Trinity EMU system are measured with excitation of 808 nm CW laser with comparison of the UCNPs of the EMU system with excitation of the 980 nm CW laser (under the same power density); lifetime decay curves, which is used to reflect the stability of the excited state, is measured with excitation of 808 nm pulsed and 980 nm pulsed laser.

3.6.1. Emission spectra

3.6.1.1. Luminescent intensity

As shown in the Figure 12(a-b) and Table 1 and 2, under the same measurement condition, the UCNPs of the type I Nd^{3+}-Trinity EMU system with activator of Tb^{3+} with 808 nm excitation shows stronger luminescence intensity than the EMU system with activator of Tb^{3+} with 980 nm excitation, that is with 2.58 times enhancement; also the UCNPs of the type I Nd^{3+}-Trinity EMU system with activator of Eu^{3+} with 808 nm excitation shows slight weaker luminescent intensity than the EMU system with activator of Eu^{3+} with 980 nm excitation, that is with 0.79 folds.

For the type II Nd^{3+}-Trinity EMU system with activator of Tb^{3+} and Eu^{3+}, although, the construction is successfully finished, the luminescent intensity is much weaker than the type I Nd^{3+}-Trinity EMU system, which could be attributed to the method in construction of the EMU cores which makes the accumulation layer in the outer layer while the emission layer in the inner layer, thus makes the Tm^{3+}, that is the accumulator with comparatively low concentration while the concentration of the activator is comparatively high in the whole system by contrast with the type II Nd^{3+}-Trinity EMU system which is just on the opposite. And the phenomenon luminescent the importance of the accumulation by Tm^{3+} in the whole process of exciting the activators, as shown in Figure 12 (c-d).

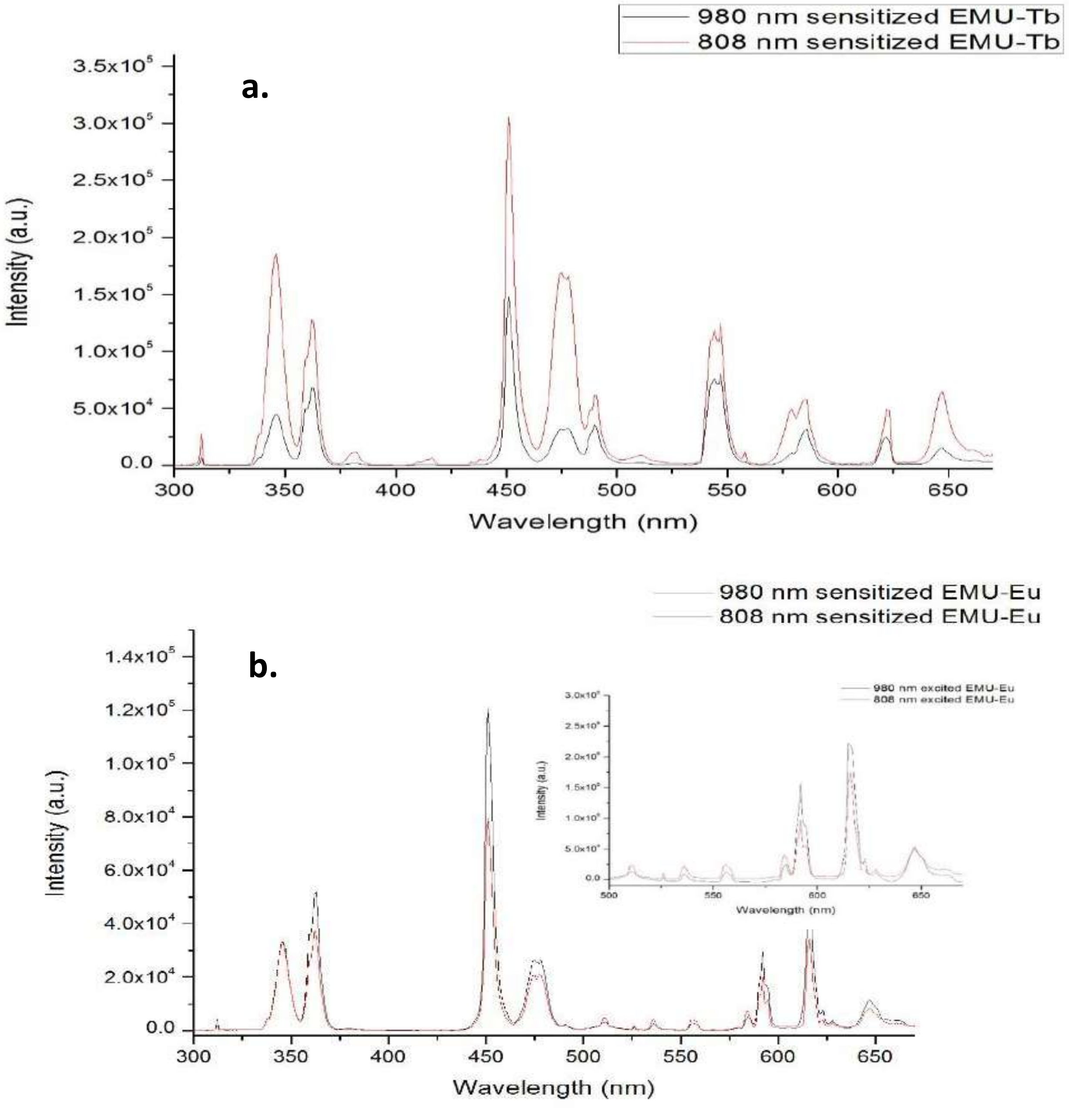

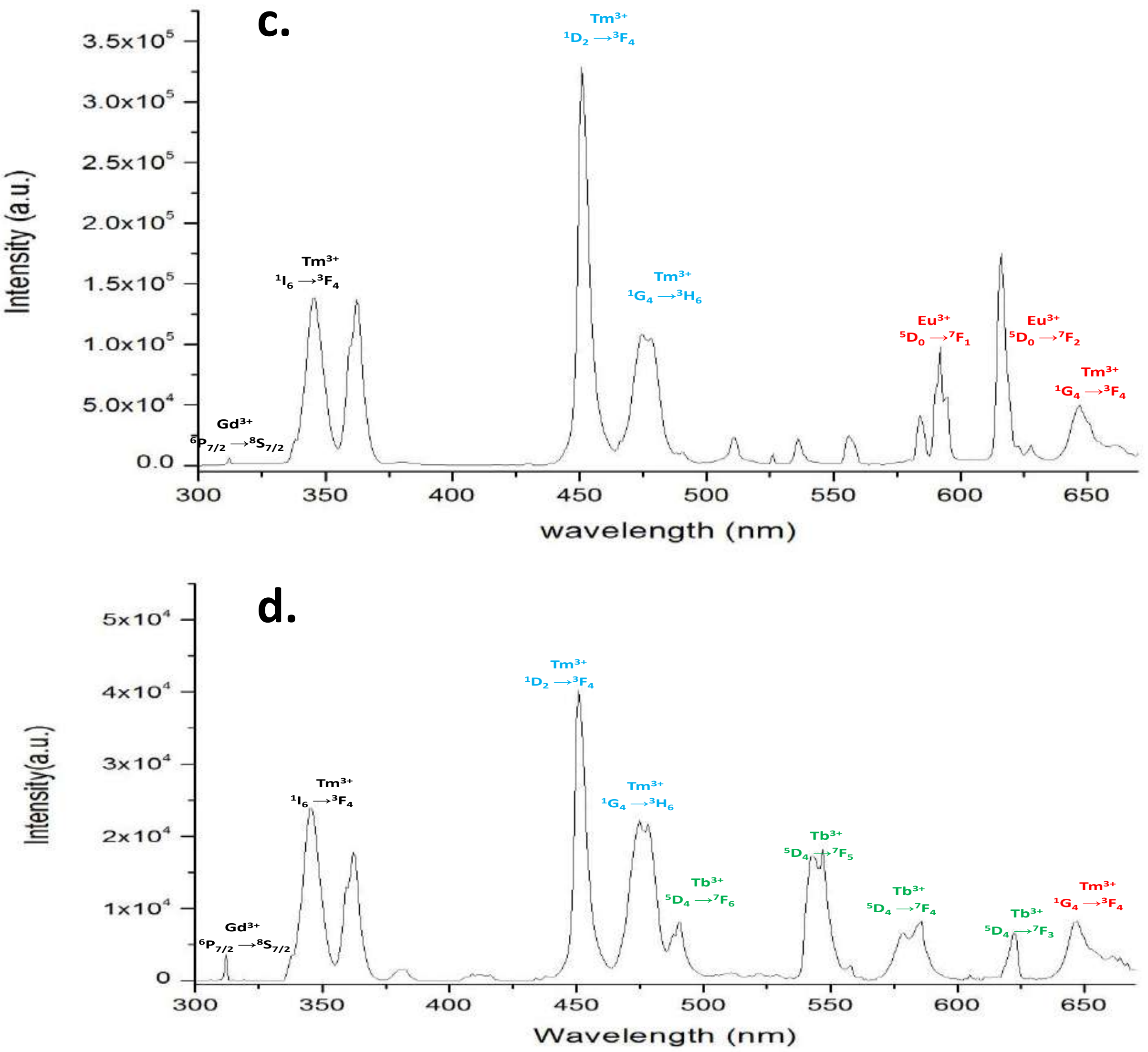

Figure 12. (a) and (b): **emission spectra** of the UCNPs of Type I Nd^{3+}-Trinity EMU system with activators of Eu^{3+} and Tb^{3+} under excitation of 808 nm laser compares with the EMU system under excitation of 980 nm laser. (c) and (d) emission spectra of the Type II Nd^{3+}-Trinity EMU system with activators of Eu^{3+} and Tb^{3+} (Measurement conditions: power density: 80 mW/ 1 mm^2 for 808/ 980 nm diode laser; emission bandwidth: 2 nm, concentration: 1.0 wt %.)

Emission Band	Tm^{3+} Ultraviolet (348, 362 nm)	Tm^{3+} (blue) (450, 478 nm)	Tb^{3+} (483,547,586,622 nm)	Tm^{3+} (red) 647 nm	Visible Emission
Peak area of 808 nm sensitized EMU-Tb (a.u.)	2627492	4505240.28	2181382	780122.4 (10.3 %)	7569609
Peak Area of 980 nm sensitized EMU-Tb	886911.6	1532543.47	1181702	164332.5 (5.6 %)	2931639
808 nm sensitized EMU-Tb Compares with 980 nm sensitized EMU-Tb	**2.96**	**2.94**	**1.85**	**4.75**	**2.58**

Table 1. Peak area ratio of the 808 nm excited Nd^{3+}-trinity EMU system with activator of Tb^{3+} compares with the 980 nm excited EMU system with activator of Tb^{3+}.

Emission Band	Tm^{3+} ultraviolet (348, 362 nm)	Tm^{3+} (blue) (450,475 nm)	Eu^{3+} (584, 592,616 nm)	Tm^{3+} (red) 647 nm	Visible Emission
Peak area of 808 nm sensitized EMU-Tb (a.u.)	547542.2	728769.4	385885.8	116958.2 (9.40 %)	1243063
Peak Area of 980 nm sensitized EMU-Tb	656972.4	1020855	451647.5	139970.1(8.20 %)	1700890
808 nm sensitized EMU-Tb Compares with 980 nm sensitized EMU-Tb	0.83	0.71	0.85	0.84	**0.73**

Table 2. Peak area ratio of the 808 nm excited Nd^{3+}-trinity EMU system with activator of Eu^{3+} compares with the 980 nm excited EMU system with activator of Eu^{3+}.

3.6.1.2 Tm^{3+} red emission partition

As we have stated in previous chapter, which is on the larger partition of red emission of the Er^{3+}, Tm^{3+}, Ho^{3+}- UCNPs with Nd^{3+}-sensitization has been proved to be with larger partition of red emission, that is proposed to be affected by the Nd^{3+}-X(Er/Tm/Ho)$^{3+}$ cross-relaxation for the high concentration of Nd^{3+} in the harvest layer.

Still, in the Nd^{3+}-Trinity EMU system, the emission of the accumulator is found to be with larger partition of red emission: as shown in Table 1 and 2, display that the red emission of Tm^{3+} , which is located at 655 nm, in the Nd^{3+}-Trinity EMU system with Tb^{3+} under the excitation of 808 nm laser as activator occupied 10.3 % in peak area around the visible emission while EMU system with Eu^{3+} under the excitation of 808 nm laser as activator occupied 9.40 % in peak area around the visible emission; EMU system with Eu^{3+} under the excitation of 808 nm laser as activator occupied 8.20 % in peak area around the visible emission.

Still, we would like to explain the situation by the strong cross-relaxation between Nd^{3+} and Tm^{3+}, as shown in Figure 13.

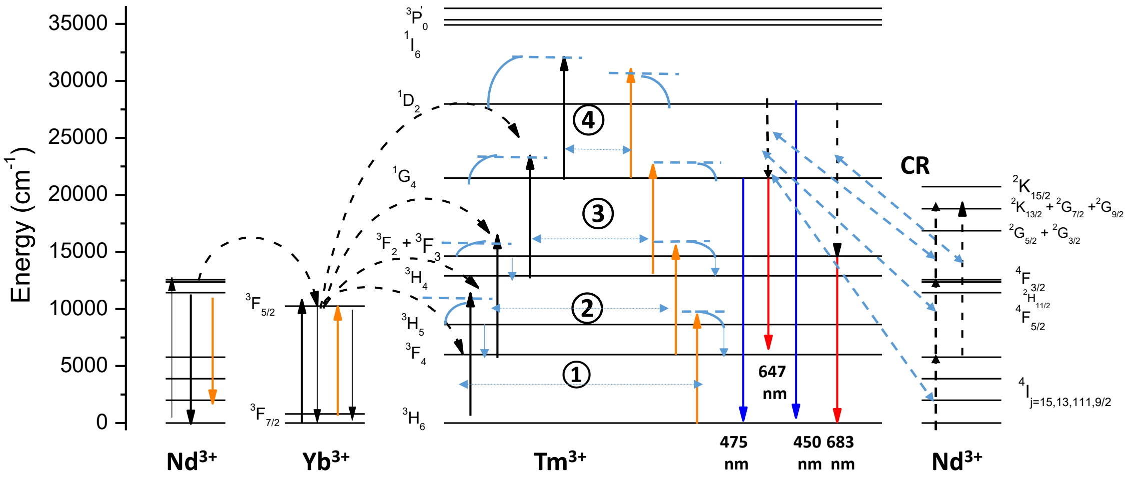

Figure. 13. Effect of Nd^{3+}-Tm^{3+} cross-relaxation on the Nd^{3+}-Trinity EMU system (Measurement conditions: power density: 80 mW/ 1 mm^2 for 808/ 980 nm diode laser; emission bandwidth: 2 nm, concentration: 1.0 wt %.)

3.6.2. Lifetime

By measuring the lifetime under excitation of 808 nm and 980 nm laser, we found that: for the emission band of Eu^{3+} (584, 592, 616 nm) or Tb^{3+} (483, 547, 586, 622 nm), the UCNPs of the Nd^{3+}-Trinity EMU system show prolonged lifetime compares with the EMU system under 980 nm excitation; however, other emission band, including the Tm^{3+} 5/4/3-phonons emission and the Gd^{3+} emission shows shorten lifetime. Additionally, it is clearly that for the Nd^{3+}-Trinity EMU system, the emission bands, except for the Tm^{3+} blue emission that located at 450 nm and 475 nm, shows prolonged lifetime under 808 nm excitation rather than 980 nm excitation; for the Tm^{3+} blue emission that located at 450 nm and 475 nm, just on the opposite, shows shortened lifetime when excited by 808 nm than 980 nm. It is proposed to be a consequence of the Nd^{3+} sensitization of the EMU system as well as the optimization on the Nd^{3+} -Trinity EMU system. Also, for the same Nd^{3+}-Trinity EMU system UCNPs, it shows prolonged lifetime under 808 nm excitation rather than 980 nm excitation.

UCNPs	Photo-luminescence source (nm)	Luminescence (nm)& Photon Numbers								
		290	312	345	362	*450*	*475*	**495**	**550**	*647*
		5	5	5	4	4	3	5	5	3
Nd-EMU-***Tb***-I	808	365.22	470.96	358.08	449.62	*707.05*	*873.14*	**1532.18**	**4227.50**	*1028.14*

	980	321.80	394.87	348.04	417.25	*891.21*	*840.46*	**1166.60**	**4054.40**	*1154.82*
EMU-*Tb*	**980**	**247.43**	**597.45**	**240.54**	**308.76**	**315.64**	**514.68**	**2975.84**	**4058.0**	**524.13**

Table 3. Lifetime of the Nd^{3+}-trinity system with activator of Tb^{3+} with excitation of 808 nm and 980 nm laser compares with EMU system with excitation of 980 nm laser.

Photo-luminescence source (nm) UCNPs		Luminescence (nm) & Photon Numbers								
		290	312	345	362	*450*	*475*	**592**	**616**	*647*
		5	5	5	4	4	3	5	5 3	5
Nd-EMU-Eu-I	808	206.66	338.84	193.34	238.36	216.97	517.39	**-**	**4535.34**	497.31
	980	199.43	292.51	230.04	247.32	282.61	508.93	**3286.23**	**4339.28**	381.55
Nd-EMU-**Eu**-II	808	306.01	318.79	283.34	363.57	*319.49*	*519.49*	**4538.16**	**4421.80**	*519.78*
	980	339.42	488.64	345.71	399.42	*391.36*	*538.89*	**4284.01**	**4117.4**	*546.25*
EMU-Eu	**980**	**410.17**	**597.45**	**425.43**	**463.66**	**572.61**	**806.26**	**3922.5**	**3920.0**	**663.13**

Table 4. Lifetime of the Nd^{3+}-trinity system with activator of Tb^{3+} with excitation of 808 nm and 980 nm laser compares with EMU system with excitation of 980 nm laser.

3.6.3. Luminescence Penetration

As shown in Figure 14, in our specially fabricated cuvette, in which the outer cuvettes has water and the inner cuvettes has sample solution (with a concentration of 10 mg/mL, dissolved in cyclohexane), the emission spectra of the UCNPs of Nd^{3+}-Trinity EMU system with activator of Eu^{3+} under excitation of 808 nm laser and the emission spectra of the EMU system with activator of Eu^{3+} under excitation of 980 nm laser has been collected. It has proven that the UCNPs of Nd^{3+}-Trinity EMU system with 808 nm excitation has deeper penetration than the EMU system with 980 nm excitation, for the peak area is almost 10 times higher, which illustrating that the UCNPs of Nd^{3+}-Trinity EMU system with 808 nm excitation are advantageous in the bio-imaging rather than the UCNPs of EMU system under 980 nm excitation for the reasons that: over-heating effect avoiding; with larger partition of red emission; deeper penetration that contributed by the photo-luminescent source attenuation avoiding and enhanced luminescent intensity.

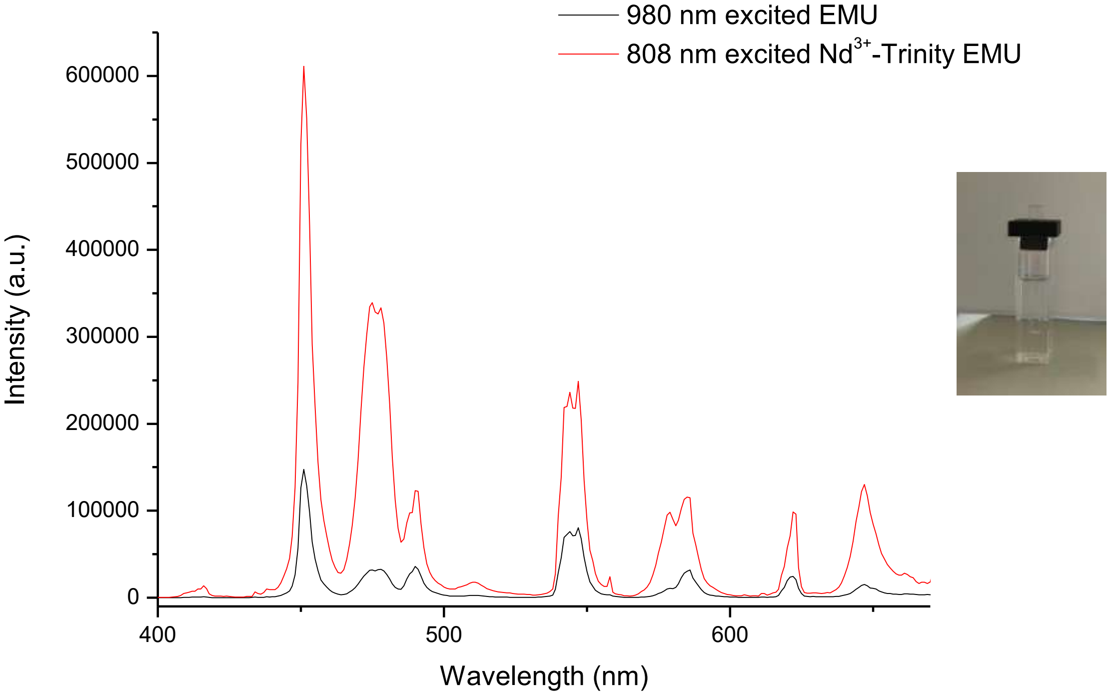

Figure 14. Emission spectra of the 808 nm excited Nd^{3+}-trinity EMU system with activator of Eu^{3+} compares with the 980 nm excited EMU system with activator of Eu^{3+} in the specially fabricated cuvettes, with water in the outer cuvette. (Measurement conditions: power density: 80 mW/ 1 mm^2 for 808/ 980 nm diode laser; emission bandwidth: 2 nm, concentration: 1.0 wt %.)

3.7. Mechanism investigation

In our previous work, by measuring the NIR emission spectra of the Nd^{3+}-Trinity system, we found that the phonons that participate in the ETU process are phonons located at 940-

1030 nm and around 1056 nm, which are proposed to be contributed by the $Nd^{3+}\rightarrow Yb^{3+}$ phonons assistant energy transfer and migrated by the sublevels of Yb^{3+}. Similarity, the participation of the 1056 nm phonons in the ETU process optimized the accumulation of Tm^{3+}, for the energy gaps of the transition in the ETU process, are smaller than the phonons (including 940-1050 nm photons and 1056 nm photons) that Yb^{3+} transfer to Tm^{3+}, which means that the by non-radiative transition, the phonons are transferred form Yb^{3+} to Tm^{3+}; and the participation of the 1056 nm photons makes less energy loss in the non-radiative transition, thus makes the excited state in Tm^{3+} more stable, which is proved by the lifetime of the Nd^{3+}-Trinity EMU system with activators of Tb^{3+}, as shown in Figure 15 (a). Similarly with the 980 nm excited EMU system that invented by Wang F. *et al.* [29], in the Nd^{3+}-Trinity EMU system, 475 nm and 647 nm emission are resulted in 3-phonons ETU process; 348 nm, 362 nm and 450 nm emission are resulted in 4-phonons ETU process; 290 nm Tm^{3+} along with Eu^{3+} emission and Tb^{3+} emission are resulted in 5-phonons ETU process. And the 5-phonons accumulation of Tm^{3+} induced $Gd^{3+}\rightarrow Gd^{3+}$migration as well as Gd^{3+}-Eu^{3+}/Tb^{3+} excitation, for the similarity of the effect of the Yb^{3+} in the two EMU system when the phonons has been transferred from Nd^{3+} to Yb^{3+}.

By measuring the emission spectra and lifetime with 808 nm excitation, with comparison of the Gd^{3+} hosted and Y^{3+} hosted UCNPs, the energy transfer 5-phonons ETU process of Tm^{3+} to Gd^{3+} could be confirmed. As shown in Figure 5(b), compared with $NaYF_4$:Yb,Tm@$NaYF_4$:Yb,Nd@$NaGdF_4$, only displays 5-phonons emission of Tm^{3+}, which is located at 290 nm, the $NaGdF_4$:Yb,Tm@$NaGdF_4$:Yb,Nd@$NaGdF_4$ presents not only Tm^{3+} 5-phonons emission but also Gd^{3+} emission, which is located at 310 nm (32000 cm^{-1}). Furthermore, the measurement of lifetime of Tm^{3+} 5-phonons emission provides corroborative evidences, as shown in Figure 15 (b), under excitation 808 nm pulse laser, the $NaGdF_4$:Yb,Tm@$NaGdF_4$:Yb,Nd@$NaGdF_4$ displays shorter lifetime of Tm^{3+} 5-phonons emission for the existence of Tm^{3+}-Gd^{3+} energy transfer, while the $NaYF_4$:Yb,Tm@$NaYF_4$:Yb,Nd@$NaGdF_4$ shows longer lifetime for the absence of the Tm^{3+}-Gd^{3+} energy transfer.

By measuring the emission spectra and lifetime of Gd^{3+} emission, the excitation of activators (Eu^{3+}/Tb^{3+}) by Gd^{3+} $^6P_{7/2}$ could be confirmed. As shown in Figure 15(d), compares the emission spectra of 808 nm excited UCNPs, with the difference that the existence or absence of Tb^{3+}, which are $NaGdF_4$:Yb,Tm@ $NaGdF_4$:Yb,Tb@$NaGdF_4$:Yb@ $NaGdF_4$:Yb,Nd@$NaGdF_4$ and $NaGdF_4$:Yb,Tm@$NaGdF_4$:Yb @$NaGdF_4$:Yb,Nd@$NaGdF_4$, the emission of Tm^{3+} 5-phonons ETU process shows shorter lifetime in the former UCNP which could be depicted as Nd^{3+}-trinity system sensitized system with activator of Tb^{3+}, for the energy transfer form Gd^{3+} to Tb^{3+}. Additionally, the existence of $Gd^{3+}\rightarrow Gd^{3+}$ migration in the Nd^{3+}-trinity-EMU system with 808 nm excitation could be proved by the design that by sandwiching another transition layer ($NaGdF_4$:Yb or $NaYF_4$:Yb) in the Nd^{3+}-trinity-EMU system (type I), just in the sandwich of the $NaGdF_4$:Yb,Tm and NaGdF4:Yb,Eu, which allowed the transition of $Yb^{3+}\rightarrow Yb^{3+}$ that guarantee ETU process by 808 nm excitation, as shown in Figure 5 (c). And the display of the Eu^{3+} emission confirms the migration of $Gd^{3+}\rightarrow Gd^{3+}$ in varied EMU core ($NaGdF_4$: Yb,Tm), the additional transition layer and the varied EMU shell ($NaGdF_4$:Yb,Eu).

Conclusively, by utilization of the Nd^{3+}-Trinity system to initiate the EMU system with 808 nm excitation, we gained a novel nanoparticle structure to gain energy migration upconversion system with optimized luminescent properties including over-heating effect avoiding, attenuation of luminescent source shielding, enhanced luminescence, prolonged lifetime, larger partition of red emission and deeper penetration in water, which are treated as potential bio-imaging probes. Still, we would like to stress that there still exist limitation in the development of the UCNPs is still the concentration of the activator; specifically in the EMU system, is the accumulator of Tm^{3+}, which limited the 5-phonons ETU process.

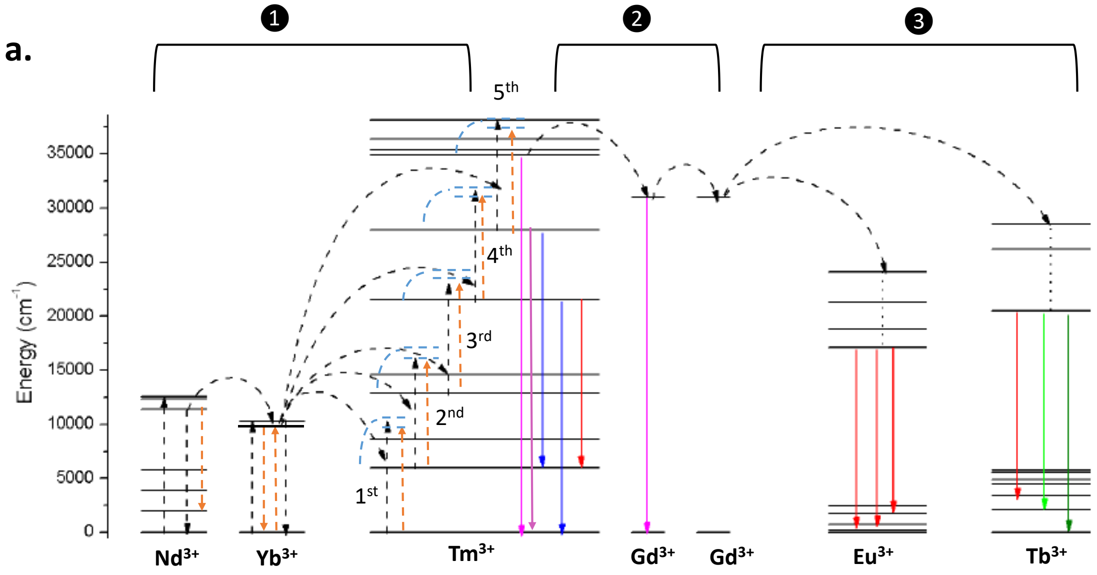

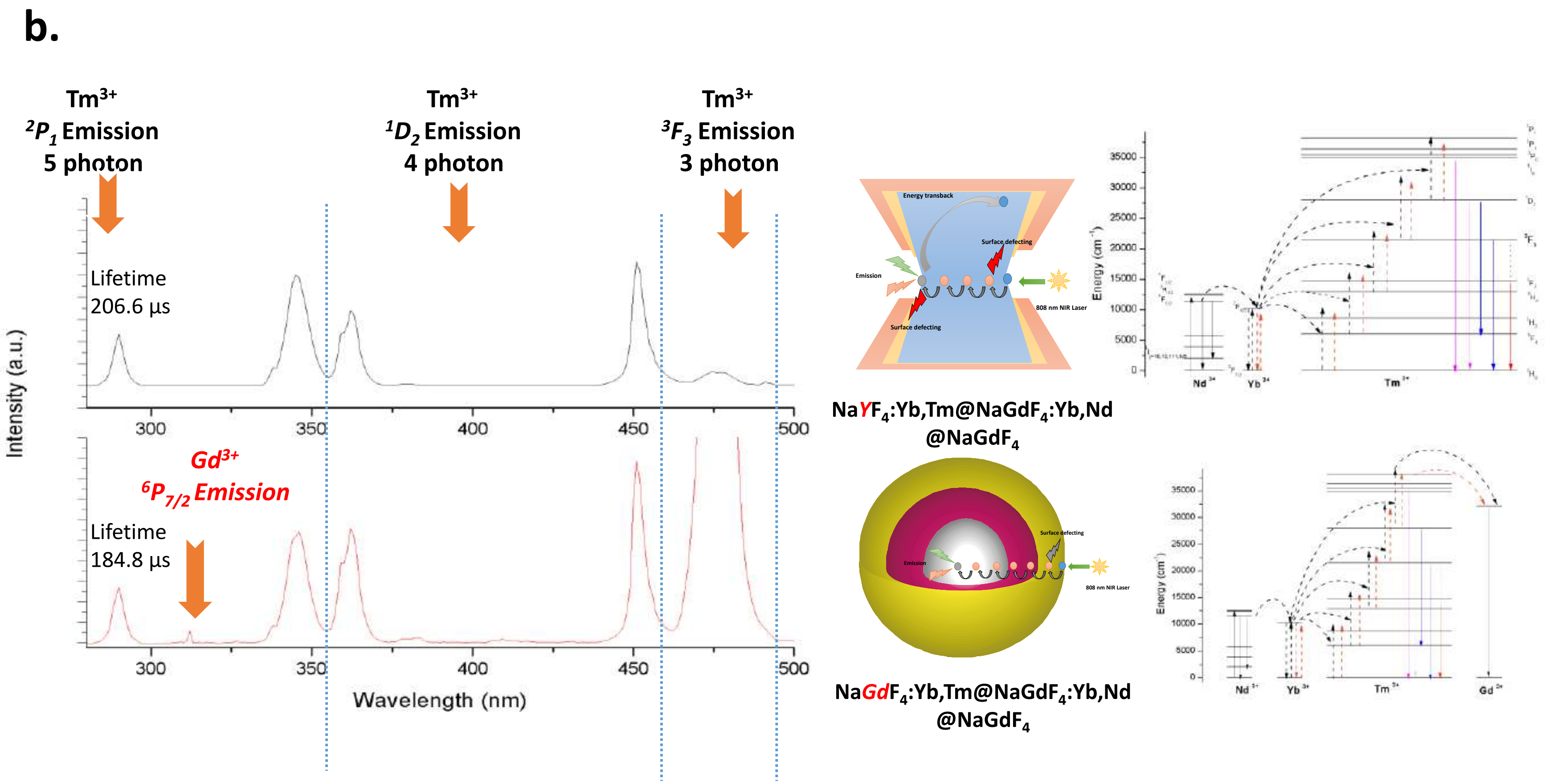
b.
Tm^{3+}
$^{2}P_{1}$ Emission
5 photon
Tm^{3+}
$^{1}D_{2}$ Emission
4 photon
Tm^{3+}
$^{3}F_{3}$ Emission
3 photon
Lifetime
206.6 μs
Intensity (a.u.)
300
350
400
450
500
Gd^{3+}
$^{6}P_{7/2}$ Emission
Lifetime
184.8 μs
300
350
400
450
500
Wavelength (nm)
Energy transback
Surface defecting
Emission
808 nm NIR Laser
Surface defecting
NaYF$_4$:Yb,Tm@NaGdF$_4$:Yb,Nd
@NaGdF$_4$
Surface defecting
Emission
808 nm NIR Laser
NaGdF$_4$:Yb,Tm@NaGdF$_4$:Yb,Nd
@NaGdF$_4$
Energy (cm^{-1})
35000
30000
25000
20000
15000
10000
5000
0
Nd^{3+}
Yb^{3+}
Tm^{3+}
Energy (cm^{-1})
35000
30000
25000
20000
15000
10000
5000
0
Nd^{3+}
Yb^{3+}
Tm^{3+}
Gd^{3+}

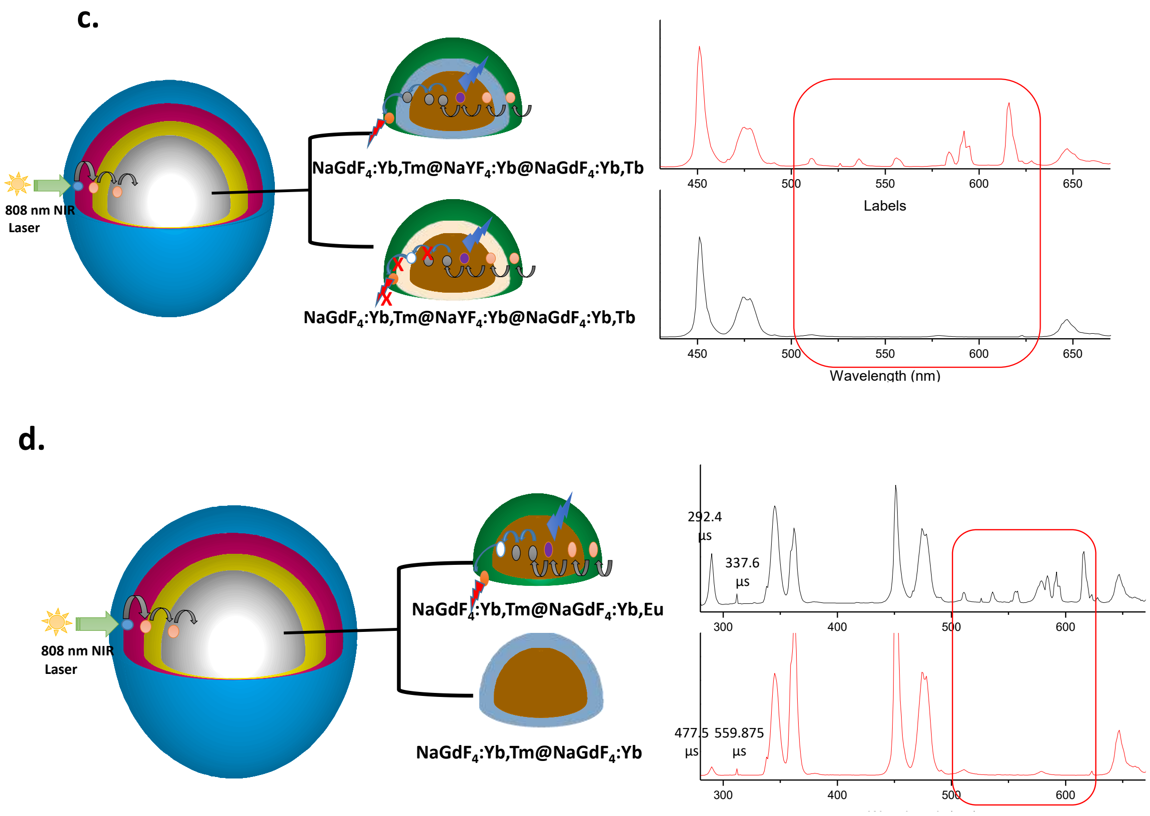

Figure 15. Mechanism investigation of the Nd^{3+}-Trinity EMU system: a. 1056 nm phonons selectively participation in the ETU process; b. Tm^{3+}→Gd^{3+} energy transfer with 808 nm excitation ; c. Gd^{3+}→Gd^{3+} migration with 808 nm excitation ; d. Gd^{3+}→X^{3+}(Eu^{3+}/Tb^{3+}) energy transfer. (Measurement conditions: power density: 80 mW/ 1 mm^2 for 808/ 980 nm diode laser; emission bandwidth: 2 nm, concentration: 1.0 wt %.)

3.8. Conclusion

We have successfully fabricated the 808 nm excited, Nd^{3+}-sensitized EMU system, by coating the Nd^{3+}-Trinity system on the modified EMU system, and proved to be with better luminescent properties including the enhanced luminescent intensity, prolonged lifetime, larger partition of red emission and deeper luminescent penetration under 808 nm excitation. Furthermore, it should be treated as a potential nanoprobe that could be utilized in bio-imaging for its avoiding of the over-heating effect by the utilization of the 808 nm laser.

Moreover, we have done investigations to study the mechanism of the EMU system with Nd^{3+}-sensitization, and found the difference between the 980 nm excited EMU system.

References

1. Wang, F., F. Song, G. Zhang, Y. Han, Q. Li, C. Ming, and J. Tian, *Upconversion and pump saturation mechanisms in* Er^{3+}/Yb^{3+} *co-doped* $Y_2Ti_2O_7$ *nanocrystals.* Journal of Applied Physics, 2014. **115**(13): p. 134310.

2. Lei, Y., H. Song, L. Yang, L. Yu, Z. Liu, G. Pan, X. Bai, and L. Fan, *Upconversion luminescence, intensity saturation effect, and thermal effect in* $Gd_2O_3{:}Er^{3+},Yb^{3+}$ *nanowires.* The Journal of Chemical Physics, 2005. **123**(17): p. 174710.

3. Wang, F., D. Banerjee, Y. Liu, X. Chen, and X. Liu, *Upconversion nanoparticles in biological labeling, imaging, and therapy.* Analyst, 2010. **135**(8): p. 1839-1854.

4. Wang, F., R. Deng, J. Wang, Q. Wang, Y. Han, H. Zhu, X. Chen, and X. Liu, *Tuning upconversion through energy migration in core–shell nanoparticles.* Nat Mater, 2011. **10**(12): p. 968-973.

5. Li, X., D. Shen, J. Yang, C. Yao, R. Che, F. Zhang, and D. Zhao, *Successive Layer-by-Layer Strategy for Multi-Shell Epitaxial Growth: Shell Thickness and Doping Position Dependence in Upconverting Optical Properties.* Chemistry of Materials, 2013. **25**(1): p. 106-112.

6. Wang, C., L. Cheng, and Z. Liu, *Drug delivery with upconversion nanoparticles for multi-functional targeted cancer cell imaging and therapy.* Biomaterials, 2011. **32**(4): p. 1110-1120.

7. Vetrone, F., R. Naccache, V. Mahalingam, C.G. Morgan, and J.A. Capobianco, *The Active-Core/Active-Shell Approach: A Strategy to Enhance the Upconversion Luminescence in Lanthanide-Doped Nanoparticles.* Advanced Functional Materials, 2009. **19**(18): p. 2924-2929.

8. Boyer, J.-C., F. Vetrone, L.A. Cuccia, and J.A. Capobianco, *Synthesis of Colloidal Upconverting NaYF4 Nanocrystals Doped with* Er^{3+}, Yb^{3+} *and* Tm^{3+}, Yb^{3+} *via Thermal*

Decomposition of Lanthanide Trifluoroacetate Precursors. Journal of the American Chemical Society, 2006. **128**(23): p. 7444-7445.

9. Chen, G., T.Y. Ohulchanskyy, R. Kumar, H. Ågren, and P.N. Prasad, *Ultrasmall Monodisperse* $NaYF_4:Yb^{3+}/Tm^{3+}$ *Nanocrystals with Enhanced Near-Infrared to Near-Infrared Upconversion Photoluminescence.* ACS nano, 2010. **4**(6): p. 3163-3168.

10. Nyk, M., R. Kumar, T.Y. Ohulchanskyy, E.J. Bergey, and P.N. Prasad, *High Contrast in Vitro and in Vivo Photoluminescence Bioimaging Using Near Infrared to Near Infrared Up-Conversion in* Tm^{3+} *and* Yb^{3+} *Doped Fluoride Nanophosphors.* Nano Letters, 2008. **8**(11): p. 3834-3838.

11. Shen, J., G. Chen, T.Y. Ohulchanskyy, S.J. Kesseli, S. Buchholz, Z. Li, P.N. Prasad, and G. Han, *Tunable Near Infrared to Ultraviolet Upconversion Luminescence Enhancement in* (α-$NaYF_4:Yb,Tm)/CaF_2$ *Core/Shell Nanoparticles for In situ Real-time Recorded Biocompatible Photoactivation.* Small, 2013. **9**(19): p. 3213-3217.

12. Hu, H., L. Xiong, J. Zhou, F. Li, T. Cao, and C. Huang, *Multimodal-Luminescence Core–Shell Nanocomposites for Targeted Imaging of Tumor Cells.* Chemistry – A European Journal, 2009. **15**(14): p. 3577-3584.

13. Ren, W., G. Tian, S. Jian, Z. Gu, L. Zhou, L. Yan, S. Jin, W. Yin, and Y. Zhao, *TWEEN coated* $NaYF_4:Yb,Er/NaYF_4$ *core/shell upconversion nanoparticles for bioimaging and drug delivery.* RSC Advances, 2012. **2**(18): p. 7037-7041.

14. Wang, Y., K. Liu, X. Liu, K. Dohnalová, T. Gregorkiewicz, X. Kong, M.C.G. Aalders, W.J. Buma, and H. Zhang, *Critical Shell Thickness of Core/Shell Upconversion Luminescence Nanoplatform for FRET Application.* The Journal of Physical Chemistry Letters, 2011. **2**(17): p. 2083-2088.

15. Zhong, Y., G. Tian, Z. Gu, Y. Yang, L. Gu, Y. Zhao, Y. Ma, and J. Yao, *Elimination of Photon Quenching by a Transition Layer to Fabricate a Quenching-Shield Sandwich*

Structure for 800 nm Excited Upconversion Luminescence of Nd3+-Sensitized Nanoparticles. Advanced Materials, 2014. **26**(18): p. 2831-2837.

16. Zhong, Y., I. Rostami, Z. Wang, H. Dai, and Z. Hu, *Energy Migration Engineering of Bright Rare-Earth Upconversion Nanoparticles for Excitation by Light-Emitting Diodes.* Advanced Materials, 2015. **27**(41): p. 6418-6422.
17. Xu, B., X. Zhang, W. Huang, Y. Yang, Y. Ma, Z. Gu, T. Zhai, and Y. Zhao, *Nd^{3+} sensitized dumbbell-like upconversion nanoparticles for photodynamic therapy application.* Journal of Materials Chemistry B, 2016. **4**(16): p. 2776-2784.
18. Li, X., R. Wang, F. Zhang, L. Zhou, D. Shen, C. Yao, and D. Zhao, *Nd^{3+} Sensitized Up/Down Converting Dual-Mode Nanomaterials for Efficient In-vitro and In-vivo Bioimaging Excited at 800 nm.* Scientific Reports, 2013. **3**: p. 3536.
19. Hou, Z., K. Deng, C. Li, X. Deng, H. Lian, Z. Cheng, D. Jin, and J. Lin, *808 nm Light-triggered and hyaluronic acid-targeted dual-photosensitizers nanoplatform by fully utilizing Nd3+-sensitized upconversion emission with enhanced anti-tumor efficacy.* Biomaterials, 2016. **101**: p. 32-46.
20. Chen, Y., B. Liu, X. Deng, S. Huang, Z. Hou, C. Li, and J. Lin, *Multifunctional Nd3+-sensitized upconversion nanomaterials for synchronous tumor diagnosis and treatment.* Nanoscale, 2015. **7**(18): p. 8574-8583.

Chapter 4.

Layer-by-Layer Anisotropic Growth of the Nd^{3+}-harvest-transfer-sensitization Trinity System and Influence on Luminescent Properties

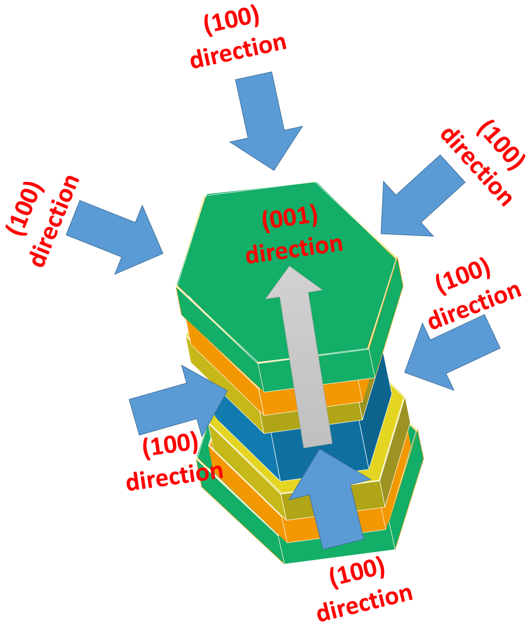

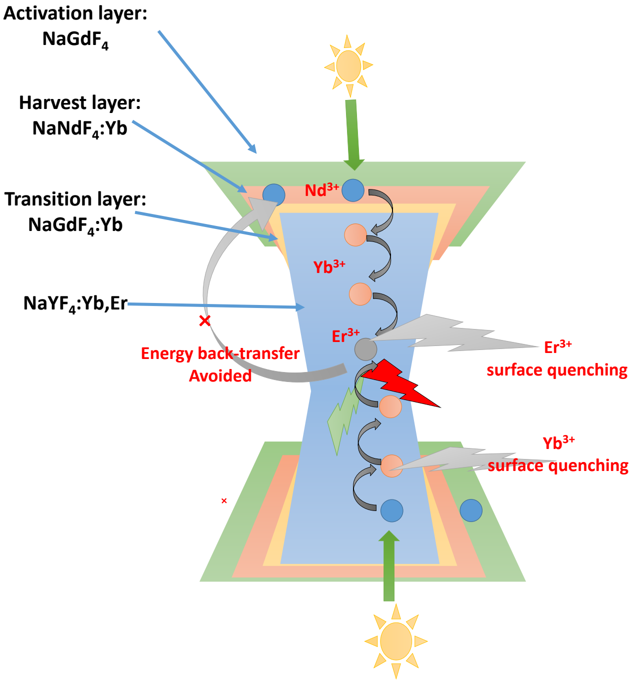

4.1 Background

As discussed in the previous work in chapter 2, the constructed Nd^{3+}-harvest-transfer-sensitization trinity system has largely enhanced luminescent intensity of the $NaGdF_4$:Yb,X(Er/Tm/Ho), as well as prolonged lifetime, enlarged the partition of red emission and improved the luminescence penetration with excitation of 808 nm laser.

However, when the Nd^{3+}-trinity system are coated on the $NaYF_4$:Yb,X(Er/Tm/Ho) cores, the situation has shown something difference for the anisotropic epitaxial growth of the UCNPs, that is the $NaGd/Yb/NdF_4$ epitaxial growth outward $NaYF_4$. And further shows influence on the luminescent properties of the UCNPs.

In this chapter, we would like discuss the situation of the anisotropic growth in UCNPs and the influence on the luminescent properties.

4.2. Generalization of the anisotropic growth

4.2.1. Anisotropic growth in nanoparticles

There have been numerous reports on the anisotropic growth of UCNPs, including gold-silver nanoparticles, NiO, ZnO, and metal alloy. The anisotropic growth of the UCNPs makes the variety of the morphology, properties and function.[1-4]

4.2.2. Anisotropy in UCNPs

However, anisotropic growth in upconversion nanoparticle has very few investigation to be reported, especially on the relationship between the luminescent properties. And the previous work has been summarized below:

As reported by D.M., Liu *et al.*, for the $NaYF_4$ nanoparticles that with the size of sub-50 nm, the coating of the $NaNdF_4$ and $NaGdF_4$ result in anisotropic growth leading to the investigation of controlling a family of rare-earth-doped nanomaterials. And all the controlling anisotropic growth are prompted by the co-existence and different roles of oleate anions (OA) and molecules (OAH) in the crystal formation, which directionally inhibit, promote or etch the crystallographic facets of the nanoparticles by adjusting the ratio of OA to OAH. [5] As shown in Figure 1, the researchers utilized the sub-50 nm $NaYF_4$ nanoparticles to coat $NaGdF_4$ and $NaNdF_4$ to investigate the variable, dynamic roles of the oleate anions (OA) and the dissociated form of oleic acid molecules (OAH) in mediating the growth of $NaREF_4$ nanocrystals.

For the β-$NaYF_4$ nanocrystals, the binging energy of (001) facets is different with the (100) facets, as shown in Figure 1, according to D.M. Liu *et al.*, OA^- preferentially binds to RE^{3+} ions exposed on the (100) facet of the hexagonal fluoride nanocrystal, with a much higher binding energy (35.4 eV) than on the (001) facet (21.8 eV), which means that OAH molecule binds with a higher probability to the (001) facet than the (100) facet and has relatively small binding energies of 9.4 eV and 4.6 eV. [5]

Ref:

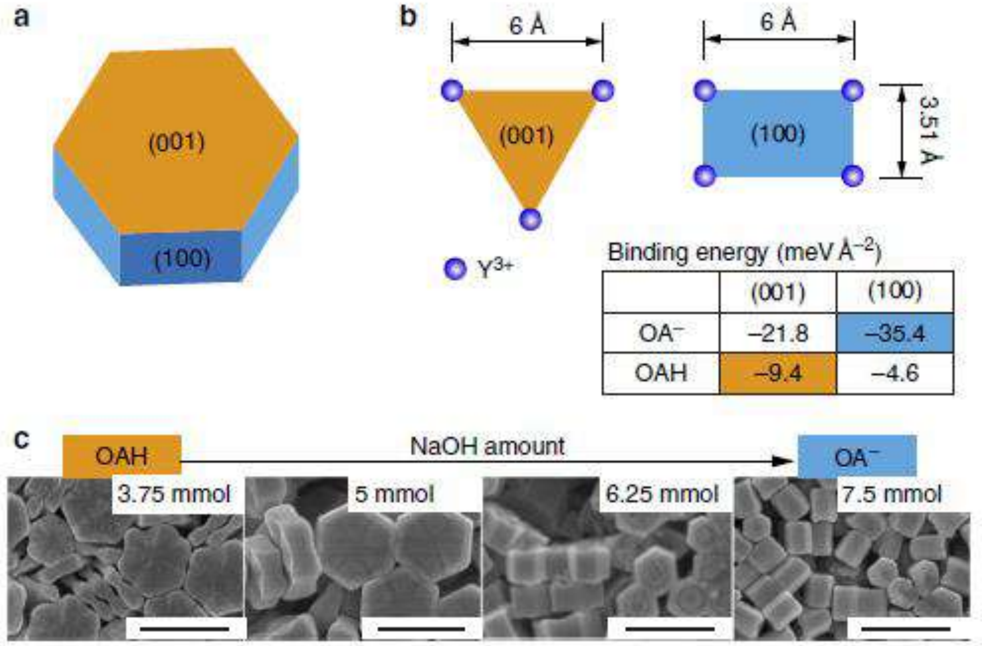

Figure 1. Facets of the β-$NaYF_4$ nanocrystals (a) and the binding energy of oleate (b); the effect of the ratio of NaOH on the surface coating. [5]

Furthermore, the preference of binging of OA^- to the facet of the nanoparticles, result in anisotropic epitaxial growth, for the epitaxial growth actually is the replacement of the F^- ions to OA^-; by the competition of the OA^- and F^- ions, new surface of the nanoparticles are formed. When the OA^- binding are preferred to occur on the (001) facets, which means that the epitaxial growth on the (001) facet is in priority, which happened to coincide with our results in the epitaxial growth of Nd^{3+}-Trinity system. As show in Figure 1, the ratio of OA^- to OAH has been the key of controlling the anisotropic growth, for the high ratio of the OA^- to OAH promote the longitude growth of the $NaYF_4$ nanoparticles, and the low ratio of the OA^- to OAH results in etching of the (100) facets.

The time for the reaction of thermal decomposition is another key factor of anisotropic growth. As shown in Figure 2, with reaction times of 15, 30, 45, 60 min, it could be observed that the $NaYF_4$ core is etched by the OAH. This could be interpreted by the size of the $NaYF_4$ core, dissolved and reformed on the (001) facets, which is called as the migration growth. Furthermore, the 3D-archetecture of the nanoparticles has been realized by the anisotropic growth, by controlling the ratio of OA$^-$/OAH, reaction time, and the composition of the shells, resulting in the formation of the hourglass shaped nanoparticles, flower shaped nanoparticles and nano-cylinders, nanoscale spins with double rings, or nano-dumbbells with smooth or sharp end .[5]

Ref:

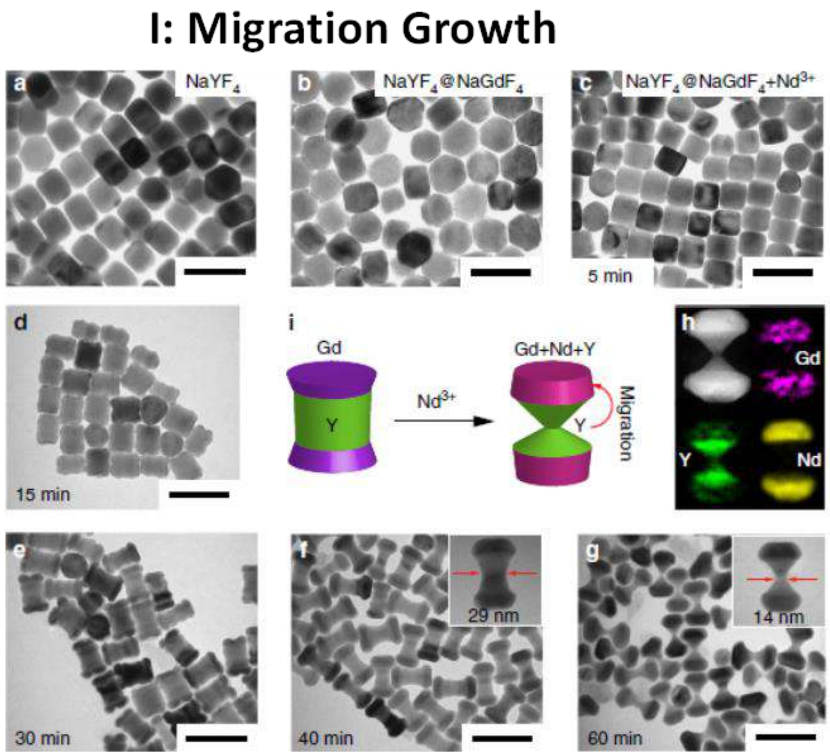

II: 3D-archetectrue

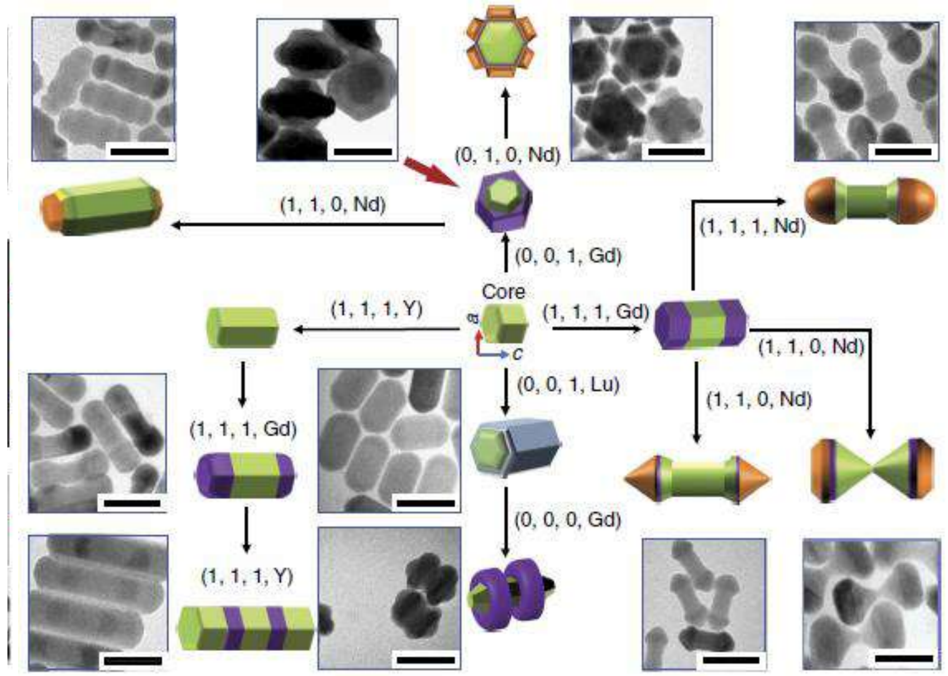

Figure 2. (I) Migration of the β-NaYF$_4$ nanocrystals; (II). 3D-construction of the UCNPs. [5]

The previous work on the anisotropic growth do illuminate us in the study of the Nd^{3+}-Trinity system construction with epitaxial growth [6-8] outward the NaYF$_4$ nanocrystals, which further affect the luminescent properties.

4.2.3. Epitaxial growth

"Epitaxial growth" refers to the deposition of a crystalline over layer on a crystalline substrate [9], which specifically in the area of NaRdF$_4$ nanocrystals, could be defined as: the replacement of the oleate by the F$^-$ ions with further growth of the nanocrystals. [6-8, 10]

The formation of the surface of UCNPs that synthesized by the method of thermal decomposition, are considered to be the competition between the F$^-$ ions and OA$^-$, which is driven by the Ostwald-ripening principles, as shown in Scheme. 1. [11] The oleate, acts as the surfactant that binds on the RE^{3+} ion, could be treated as the excipient for the competition between the OA^- and F^- .[11] And the specific situation of epitaxial growth in UCNPs, could be illustrated as the replacement of the F^- ions of the oleate, which occurs on the surface of the nanocrystals. The epitaxial growth has been considered to be with great importance in the synthesis of the core-shell UCNPs. For the UCNPs with multiple shells, the synthesis method is generalized as the "layer-by-layer" epitaxial growth. [6-8, 12]

Ref:

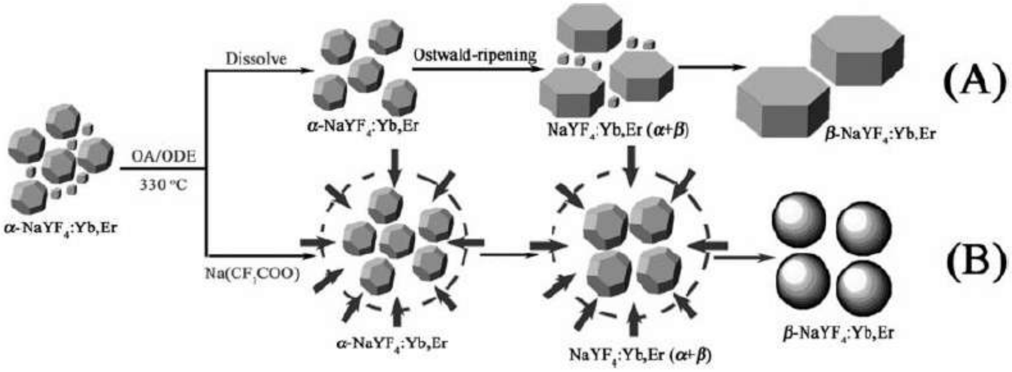

Scheme 1. Schematic Illustration of the Growth Stages of $NaYF_4$:Yb,Er Nanocrystals by the method of thermal decomposition.[11]

4.3. Anisotropic growth in the Nd^{3+}-harvest-transfer-sensitization (Nd^{3+}-Trinity) system

When the situation comes to the Nd^{3+}-Trinity system that composed of the transition layer ($NaGdF_4$:Yb), harvest layer ($NaNdF_4$:Yb) and activation layer ($NaGdF_4$) coating on the $NaYF_4$ cores, which is coated on the $NaYF_4$ cores with the strategy that "layer-by-layer"[8], the anisotropic growth of the Nd^{3+}-Trinity system has been observed, further resulting in the incomplete coating , and extrusion of the $NaYF_4$ cores, and further result in the limitation of the luminescence enhancement as well as the invalidation of the ETU efficiency by the study of the luminescence properties.

4.3.1. Layer-by-layer anisotropic growth outward the $NaYF_4$ cores

As shown in Scheme 2, the β-$NaYF_4$ nanocrystals and the β-$NaGdF_4$ nanocrystals must have difference which result in the difference in the coating of shells. For the β-$NaGdF_4$ nanocrystals, it is in sphere shaped and the binding energy of the oleate to every facets is the same; for the β-$NaYF_4$ nanocrystals, it is in octahedron shape and the binding energy of the oleate has been reported to be various on the (001) facet that is the (001) facets of the $NaYF_4$ nanocrystals, which is lower, and the (100) facets that is the (100) facets of the $NaYF_4$ nanocrystals, which is higher. Thus, the difference leading to the binding preference of oleate and further influence the epitaxial growth: for the OA^- surfactants are prone to binding on the (001) faces with lower binding energy, the replacement of F^- ions to the OA^- is faster and easier on the (001) facets, the longitudes growth is easier to happened; by contrast with the replacement of F^- ions to the OA- is slower and harder on the (100) facets result in the incomplete coating of the (100) facets. Furthermore, it could be observed that the $NaYF_4$ has dissolve or decomposed in the process of the reaction of thermal decomposition, which could be concluded as the OAH binding make the $NaYF_4$ cores are easier to be dissolved for the anions make the nanocrystal unstable or the etching of the oleate on the (001) facets result in extrusion on the $NaYF_4$ cores.

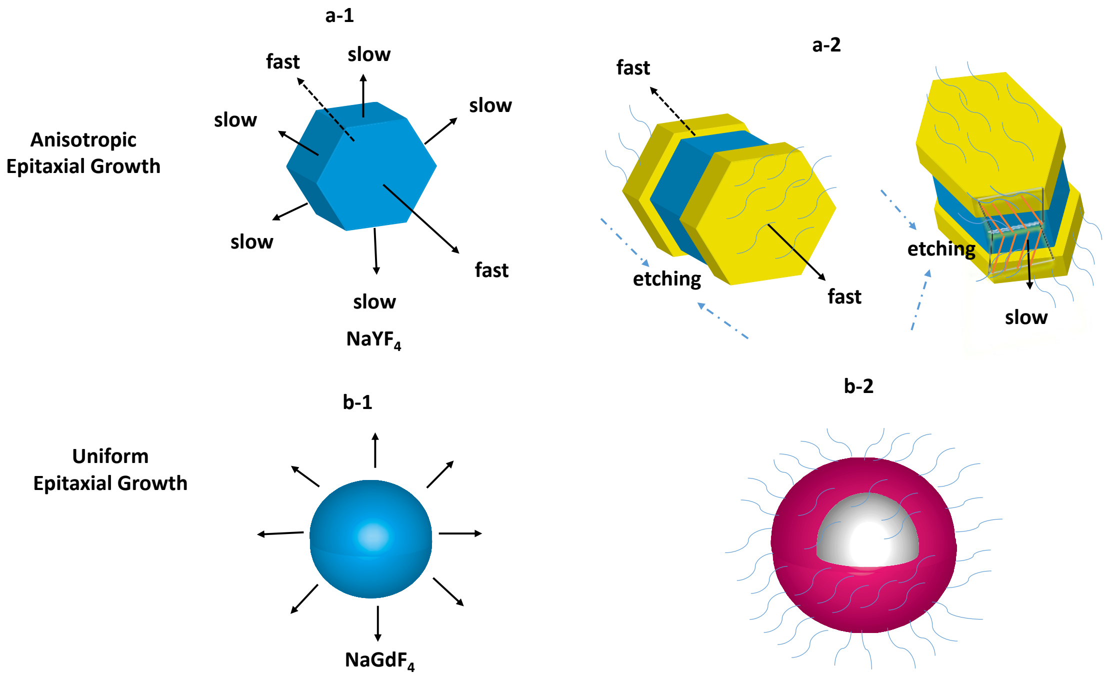

Scheme 2. Anisotropic and Uniform epitaxial growth of the Nd^{3+}-sensitized multiple shells on the surface of $NaYF_4$ and $NaGdF_4$.

4.3.2. Anisotropic coating of $NaGdF_4$:Yb 10%, $NaYbF_4$ and $NaNdF_4$:Yb20% layers

The coating of the Nd^{3+}-Trinity system on the $NaYF_4$ could be treated as the $NaYF_4$ coating with $NaGdF_4$, $NaYbF_4$ and $NaNdF_4$, which has been proven to be anisotropic growth.

As reported by B. Xu *et al.*, the $NaYF_4$ cores coating with $NaNdF_4$ layer has been observed to be dumbbell-like nanoparticles, which is very similar with the Migration growth that discussed above, as shown in Figure 3. [13]

Ref:

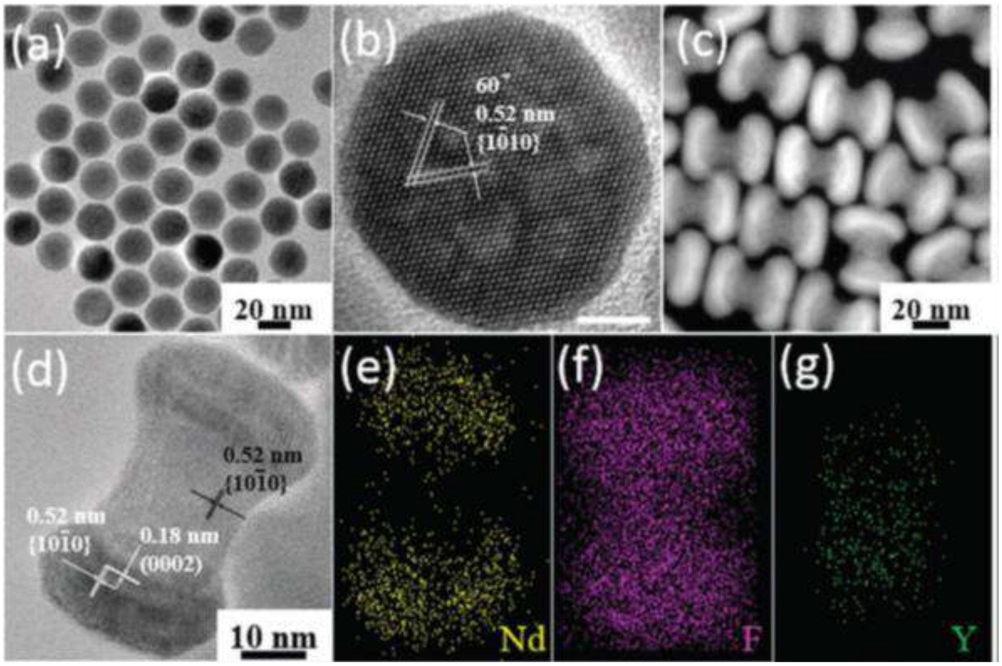

Figure 3. NaYF$_4$@NaNdF$_4$: (a). TEM, (b). HRTEM of the NaYF$_4$:Yb/Er nanoparticles and (c). STEM images of the dumbbell-like NaYF$_4$:Yb/Er@NaNdF$_4$:Y$_{0.1}$ nanoparticles. (d). HR-TEM image of a single dumbbell-like NaYF$_4$:Yb/Er@NaNdF$_4$:Yb nanoparticles. (e–g). Elemental mapping of the distribution of Nd^{3+}, Y^{3+}, F$^-$ ions within a single dumbbell-like nanocrystals. [13]

And in our investigation, which we have on purpose synthesized the sub-30 nm NaYF$_4$:Yb ,Er cores coating with NaNdF$_4$:Yb$_{20\,\%}$ layer, the dumbbell-liked nanoparticles has also been observed, as show in Figure 4, which means that the NaYF$_4$@NaNdF$_4$:Yb$_{20\,\%}$ nanoparticles also shows Y^{3+} migration.

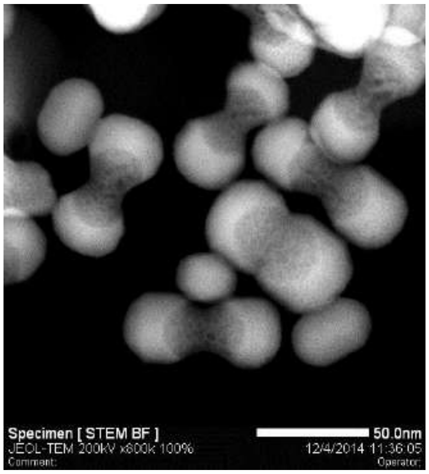

Figure 4. HAADF-STEM image of the **$NaYF_4$@$NaNdF_4$:$Yb_{20\%}$.**

However, when the situation comes to the coating of $NaYbF_4$ and the $NaGdF_4$:Yb, the situation shows some difference for it is easier for the $NaGdF_4$ and $NaYbF_4$ to be coated on the (100) facets rather than the (001) facets, that is on the opposite of the situation of $NaNdF_4$ anisotropic growth on the β-$NaYF_4$:Yb,Er cores, the as shown in Figure 5 and 6, which displays that: from the (001) direction, the contrast of brightness and darkness could been seen that is the darkness field in the inner layer and the very thin brightness field in the outer layer, which mean that the $NaYbF_4$ has grown epitaxial on the (100) facets of the β-$NaYF_4$:Yb,Er cores; form the (100) direction, the contrast cannot be observed which means that there is not epitaxial growth outward the (100) facets.

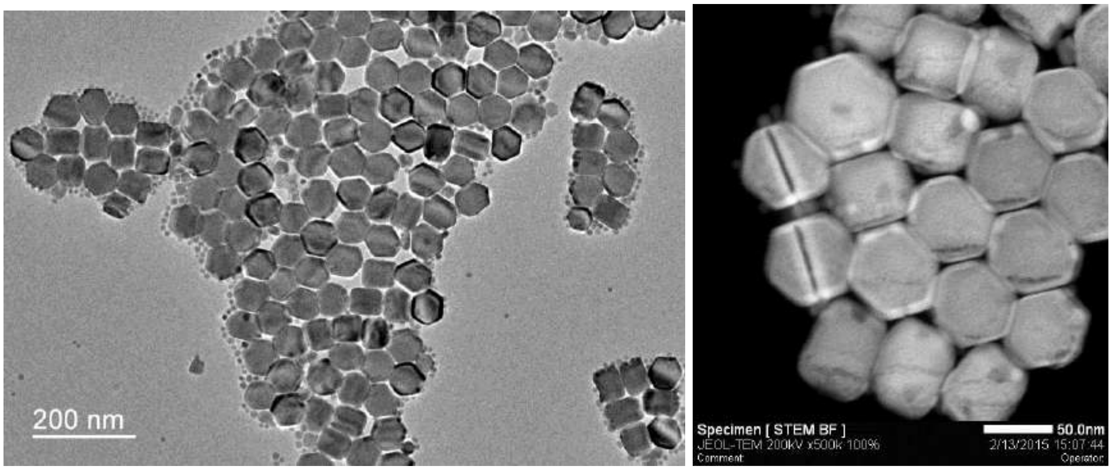

Figure 5. NaYF$_4$@NaGdF$_4$ UCNPs are characterized by TEM and HAADF-STEM.

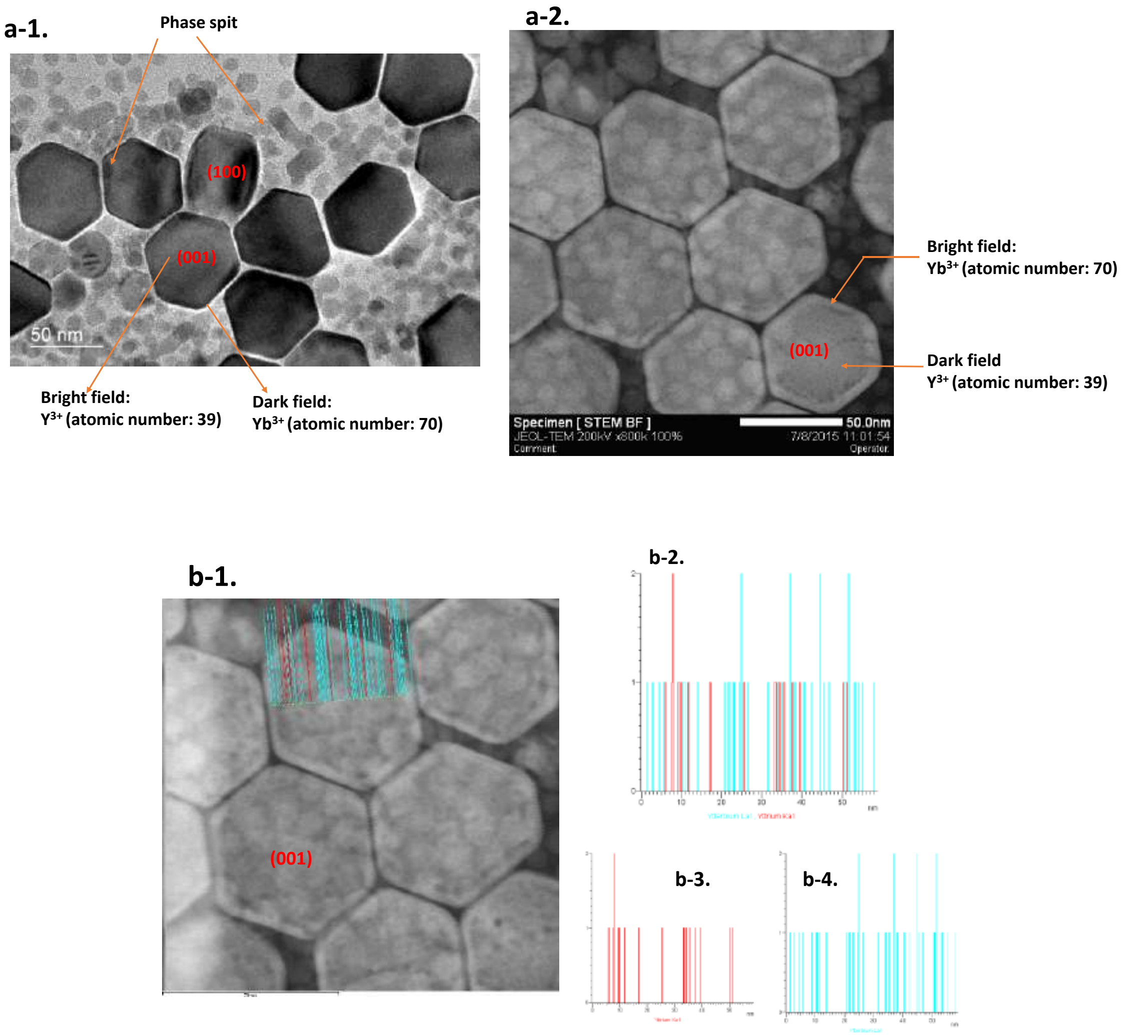

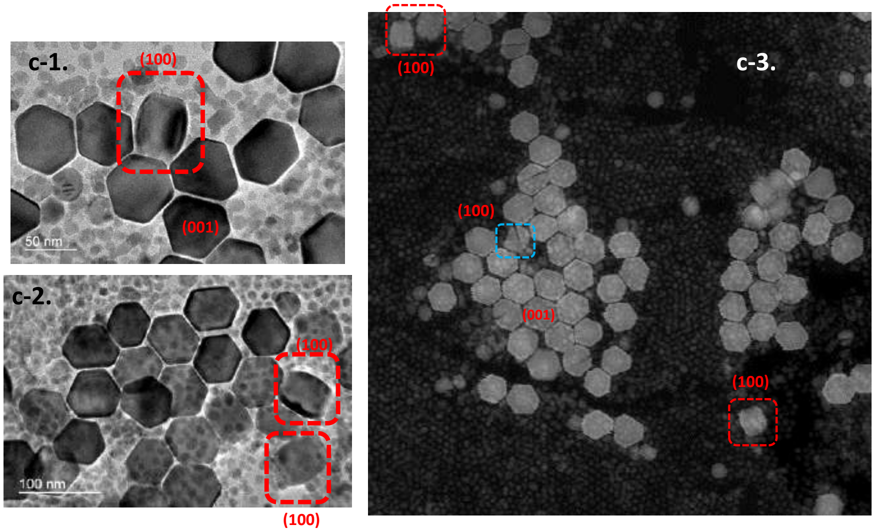

Figure 6. NaYF$_4$@NaYbF$_4$ UCNPs are characterized by TEM, HAADF-STEM and EDX lines on (001) facets of β-NaYF$_4$ nanocrystals (a-b); on (100) facets of β-NaYF$_4$ nanocrystals (c).

It is in consistence with the previous report that is the epitaxial growth of NaGdF$_4$ and NaYbF$_4$ is faster on the (100) facets rather than (001) facets, as shown in Figure 7 (a), which has summarized the principle by characterization of the nanoparticles that are NaYF$_4$@NaGdF$_4$ and NaYF$_4$@NaYbF$_4$. As shown in Figure 7 (c-d), the epitaxial growth of the NaYbF$_4$ and NaGdF$_4$ only coating on the (100) facets, which has been reported as incomplete coating. [15]

Ref:

a.

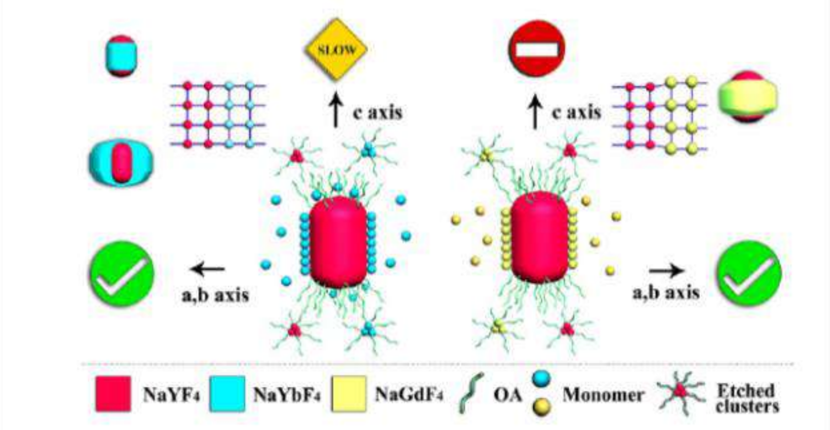

Figure 6. Schematic of anisotropic shell growth in UC CS NSs.

b.

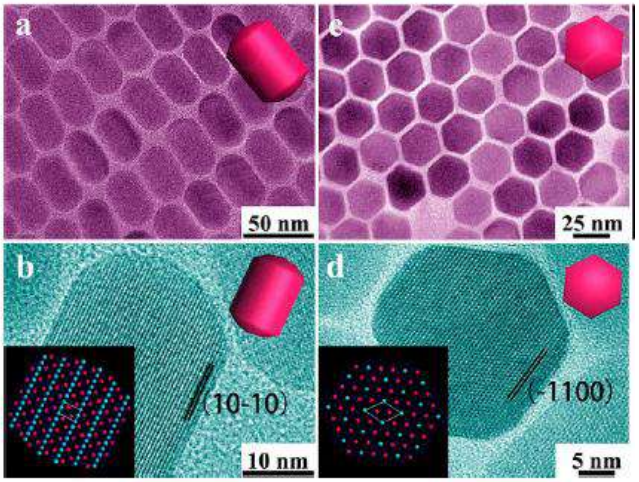

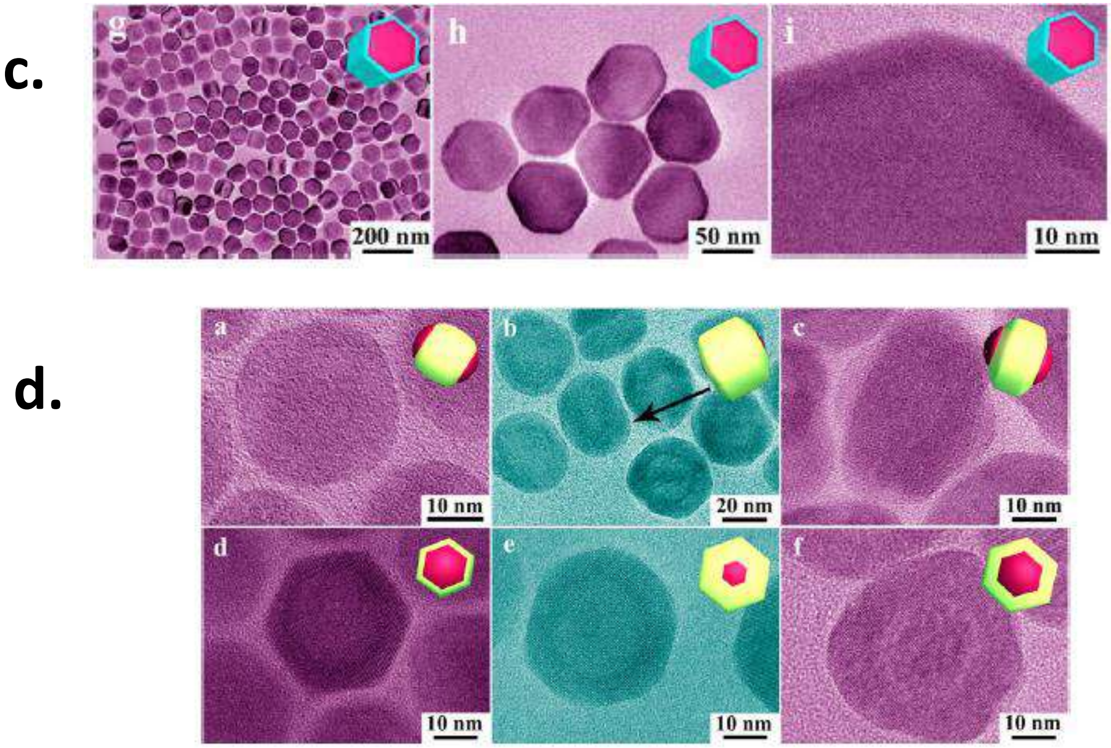

Figure 7. (a) Schemes of the epitaxial growth of $NaGdF_4$ and $NaYbF_4$. (b) Characterization of the $NaYF_4$ nanocrystals; (c). Characterization of the $NaYF_4$@$NaYbF_4$ nanocrystals; (d). Characterization of the $NaYF_4$@$NaGdF_4$ nanocrystals. [15]

Also, the further coating of the $NaGdF_4$ layer on the $NaGdF_4$:Yb layer also shows the similar incomplete coating that is with faster epitaxial growth on the (100) facets and slower growth on the (001) facets, as shown in Figure 8, which is the $NaYF_4$:Yb,Er@$NaGdF_4$Yb@$NaGdF_4$ characterized by TEM and HAADF-STEM images as: on the (001) facets, displays brightness-darkness-brightness in the TEM images and darkness-darkness-brightness; on the (100) facets, most of them shows darkness-brightness in the TEM images and brightness-darkness in the HAADF-STEM images, compares with the situation of $NaYF_4$:Yb,Er@$NaGdF_4$Yb, it clearly indicates that the coating of the $NaGdF_4$ still result in incomplete coating that is caused by the faster growth on the (100) facets and slower growth on the (001) facets. Also, the very few existed completed coating is highlighted in Figure 8 (c).

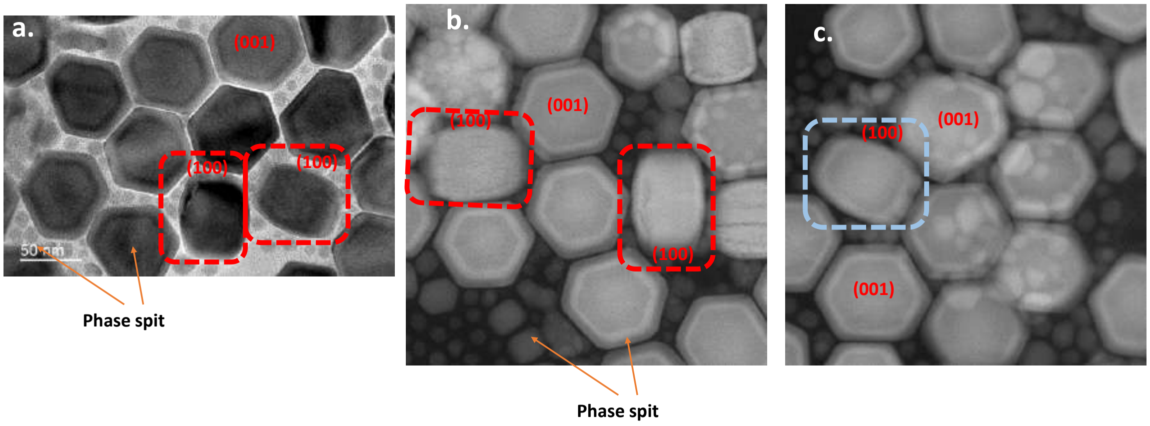

Figure 8. TEM and HAADF-STEM of NaYF$_4$:Yb,Er@NaGdF$_4$Yb@NaGdF$_4$ nanoparticles.

And what will be happened if the when the Nd^{3+}-Trinity system are coating on the β-NaYF$_4$ nanocrystals that is NaYF$_4$:Yb,Er@NaGdF$_4$:Yb,Nd@NaNdF$_4$:Yb@NaGdF$_4$ or NaYF$_4$:Yb,Tm/Ho@NaGdF$_4$:Yb@NaGdF$_4$:Nd,Yb@NaGdF$_4$, which in specifically is that the mixing of the Na(Gd,Yb,Nd)F$_4$ with competition in the epitaxial growth? To answer the question, we have make the Nd^{3+} ions doping in the epitaxial growth of NaGdF$_4$:Yb to observed the effect of Nd^{3+} in the surface coating of NaYF$_4$:Yb,Er(that are NaYF$_4$:Yb,Er@NaGdF$_4$:Yb,Nd) or on the surface coating of NaYF$_4$:Yb,Ho@NaGdF$_4$:Yb which is proved to be incomplete coating (that is NaYF$_4$:Yb,Ho@NaGdF$_4$:Yb@NaGdF$_4$:Yb,Nd. As reported by D.M. Liu *et al.*, the morphology of the core-shell nanoparticle that with β-NaYF$_4$ as core and NaGd/NdF$_4$ as shell has been various with the time of the process of thermal decomposition for the Y^{3+} dissolving and migration [5], here comes to the question that what will happen in the process of layer-by-layer epitaxial growth? As shown in Figure 8(a-b), the when the NaGdF$_4$:Yb,Nd layer are coated on the NaYF$_4$:Yb,Er nanocrystals, it shows complete coating on the (001) faces while "depression" on the (100) facets, which is case by the Y^{3+} migration. As shown in Figure 8(c-d), when the NaGdF$_4$:Yb,Nd layer are coated on the NaYF$_4$:Yb,Ho@NaGdF$_4$:Yb nanocrystals, similarly, complete coating on the (001) faces while "depression" on the (100) facets.

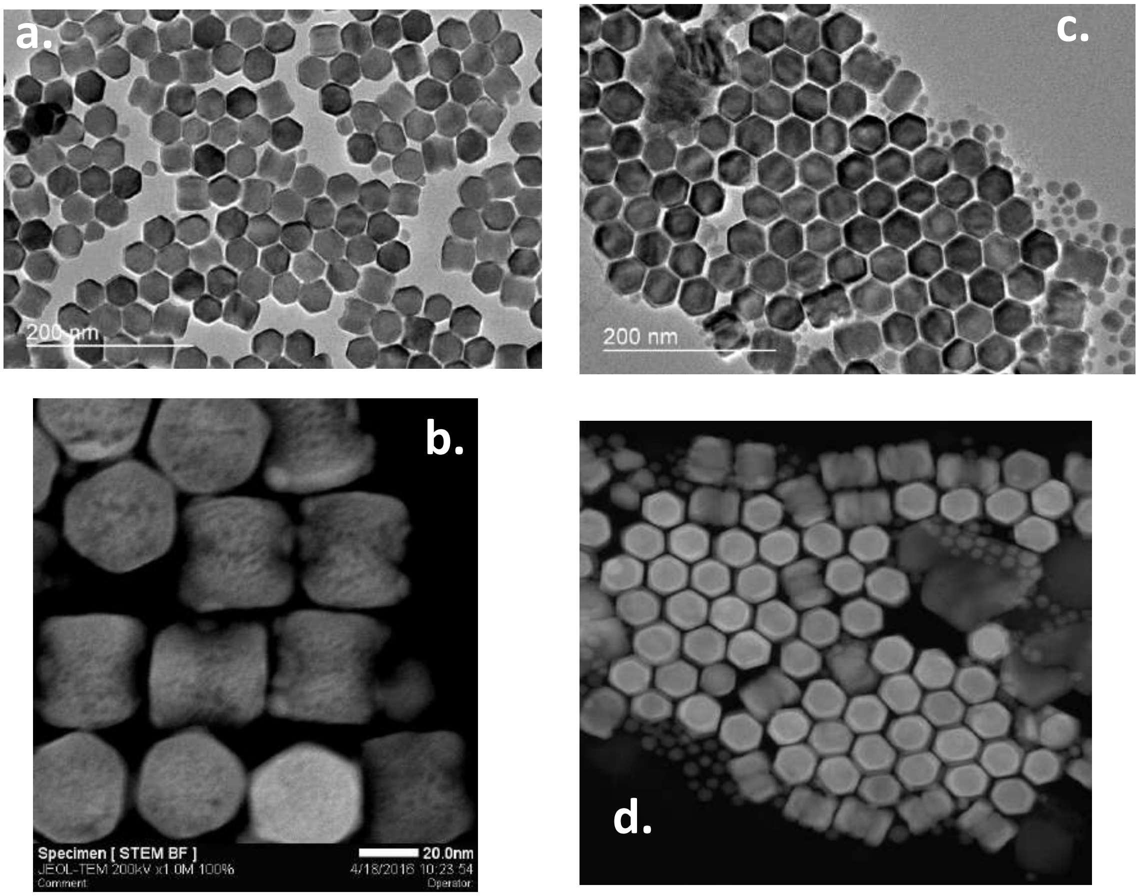

Figure 9. TEM and HAADF-STEM images of NaYF$_4$:Yb,Er@NaYF$_4$:Yb,Nd (a-b) and NaYF$_4$:Yb,Ho@NaYF$_4$:Yb@NaNdF$_4$:Yb (c-d).

Here, we would like to conclude the principles of the Nd^{3+} ions participated epitaxial growth, as shown in Scheme 3, when the NaGdF$_4$:Yb,X(Er/Tm/Ho) nanocrystals are coated with $NaGdF_4$:Yb, it shows faster epitaxial growth on the (001) facets and slow epitaxial growth on the (100) facets, so do the second $NaGdF_4$:Yb epitaxial growth on the $NaGdF_4$:Yb,X(Er/Tm/Ho)@$NaGdF_4$:Yb nanocrystals. When the Nd^{3+} ions participate in the epitaxial growth, migration growth appears which is the $NaGdF_4$:Yb, Nd shows epitaxial growth on the (001) facets and Y^{3+} migration on the (100) facets on the $NaGdF_4$:Yb,X(Er/Tm/Ho) nanocrystals; and even on the $NaGdF_4$:Yb,X(Er/Tm/Ho)@$NaGdF_4$:Yb, the $NaGdF_4$:Yb, Nd shows epitaxial growth on the (001) facets and Y^{3+}/Gd^{3+}/Yb^{3+} migration on the (100) facets. Also, we would like to conclude the migration growth caused by Nd^{3+} ions and the incomplete coating that caused by the Gd^{3+}/Yb^{3+} ions as “anisotropic epitaxial growth”, that could be defined as the epitaxial growth are not equal in all directions that in specifically are the (001) facets and (100) facets of the $NaYF_4$ nanocrystals.

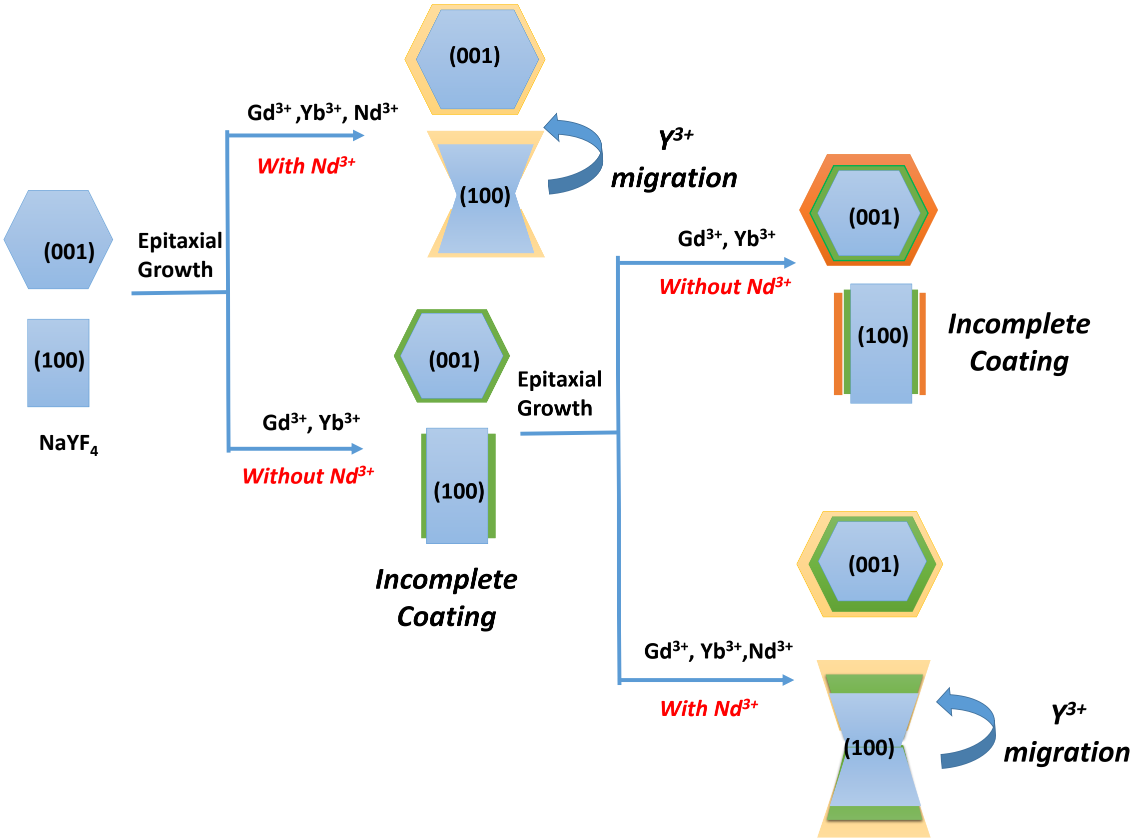

Scheme 3. Anisotropic epitaxial growth of the NaYF$_4$@NaGd/Yb/NdF$_4$ core-shell nanoparticles.

4.3.3. Monitoring of the layer-by-layer anisotropic epitaxial growth of the Nd^{3+}-Trinity system

We have utilized the sub-30 nm NaYF$_4$ as the cores, coating the multiple shells of Nd^{3+}-Trinity system to observe the morphology of the nanoparticles, and further measure the emission spectra, lifetime and florescent quantum yield to study the impact of the anisotropic growth on the luminescent properties.

For better understanding the coating of the Nd^{3+}-Trinity system on the NaYF$_4$ cores, we have prepare the sample that to be characterized by TEM and HAADF-STEM by the solvent of cyclohexane to observe the (001) facets and the cyclohexane-ethanol to observe the (100) facets, for as reported by in the cyclohexane, the UCNP are prone to stand on the (001) facets in the solvent of cyclohexane for the OA^- binding well the UCNP are prone to stand on the (100) facets for the OAH binding in the solvent of cyclohexane-ethanol.

As discussed in Chapter 2, the structure of Nd^{3+}-Trinity system coated on the UCNPs with activators of Er^{3+}(2 mmol%) should be: transition layer ($NaGdF_4$:$Yb_{10\,\%}$), harvest layer ($NaNdF_4$:$Yb_{20\,\%}$) and activator layer ($NaGdF_4$)

As shown in Figure 10, the β-$NaYF_4$:$Yb_{20\,\%}$,$Er_{2\,\%}$ nanoparticles are characterized by TEM, EDX and XRD patterns.

a.

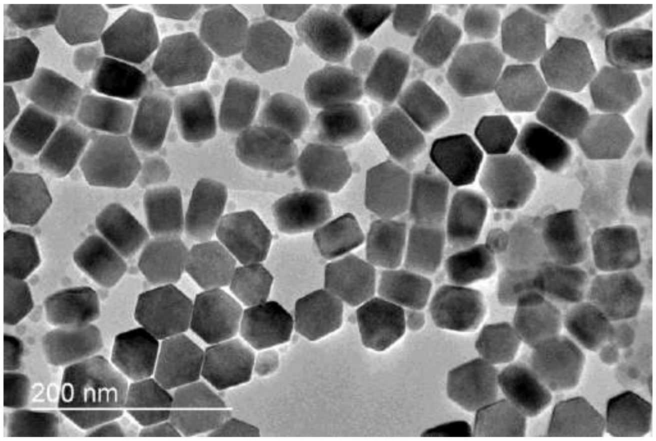

b.

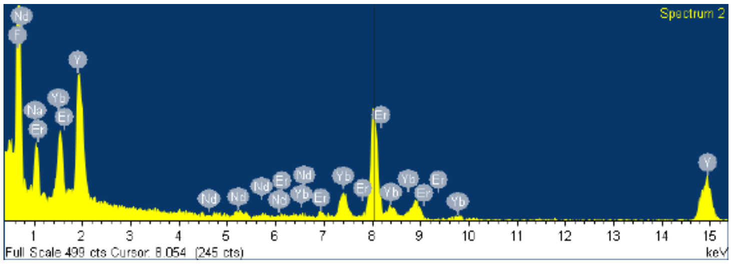

Element	Weight%	Atomic%
F K	32.83	67.35
Na K	6.59	11.18
Y L	36.15	15.85
Nd L	2.56	0.69
Er M	1.82	0.42
Yb L	20.04	4.51
Totals	100.00	

c.

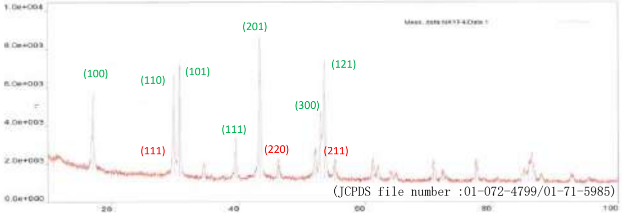

(JCPDS file number :01-072-4799/01-71-5985)

Figure 10. TEM image of the $NaYF_4$ cores and the XRD pattern of the β-$NaYF_4$ nanocrystals and XRD patterns

When the transition layer that is $NaGdF_4:Yb_{10\ \%}$ is coating on the sub-30 nm β-$NaYF_4:Yb_{20\ \%},Er_{2\ \%}$, result in the **"toast like" nanoparticles**, which is the obtained $NaYF_4:Yb_{20\ \%},Er_{2\ \%}@NaGdF_4:Yb_{10\ \%}$. As shown in Figure 11 (a-1~4), most of them stand on the (001) facets, it could be observe that the very thin layer is completed coated on the $NaYF_4:Yb_{20\ \%},Er_{2\ \%}$ cores, with the thickness about 2 nm. Also, it could be further interpreted by the HAADF-STEM Figures, for clearly the brightness field core are coated with a darkness field layer. And the contrast result in the atom numbers for it is 39 for the Y^{3+} element and 64 for the Gd^{3+} element. However, when the UCNPs is characterized in the cyclohexane-ethanol, which makes the UCNPs stand one the (100) facets, it could be clearly observed that not only there is no coating on the (100) facets but also the $NaYF_4$ cores has been "cut-off" for the (100) facets has a curve which is proposed to be result in the OAH binding caused the dissolution of the $NaYF_4$ nanocrystal in the thermal decomposition for the OAH binding make the (100) facets unstable.

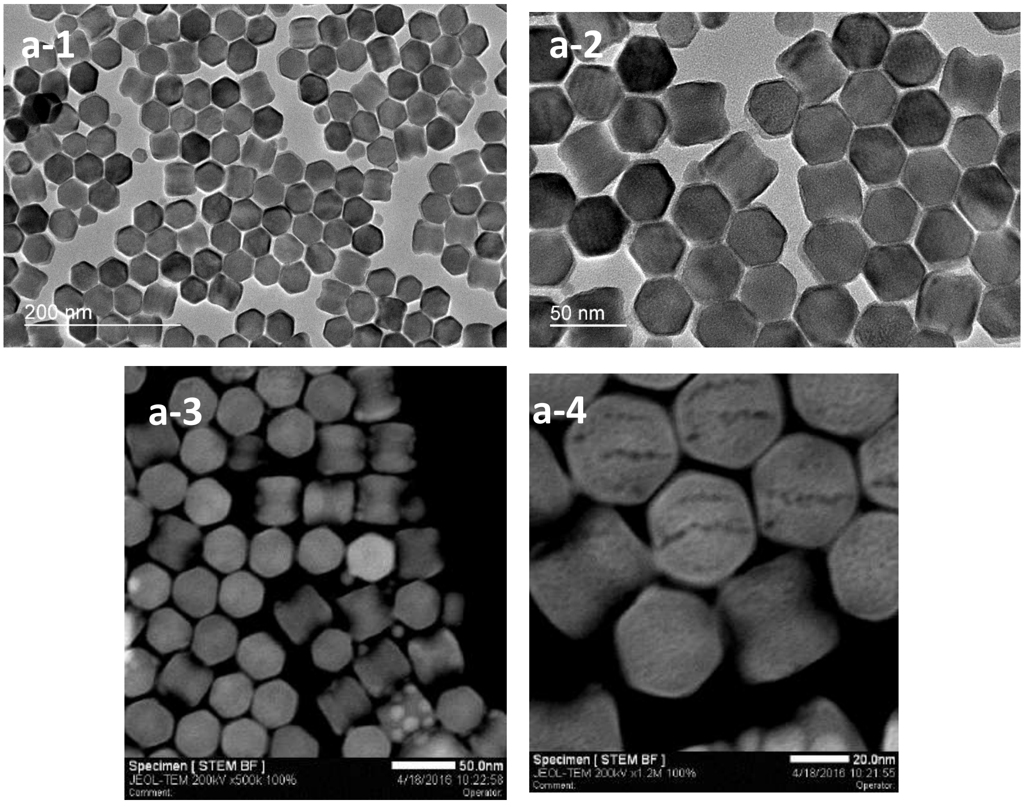
a-1
200 nm
a-2
50 nm
a-3
Specimen [STEM BF]
50.0nm
JEOL-TEM 200kV x500k 100%
4/18/2016 10:22:58
Comment:
Operator:
a-4
Specimen [STEM BF]
20.0nm
JEOL-TEM 200kV x1.2M 100%
4/18/2016 10:21:55
Comment:
Operator:

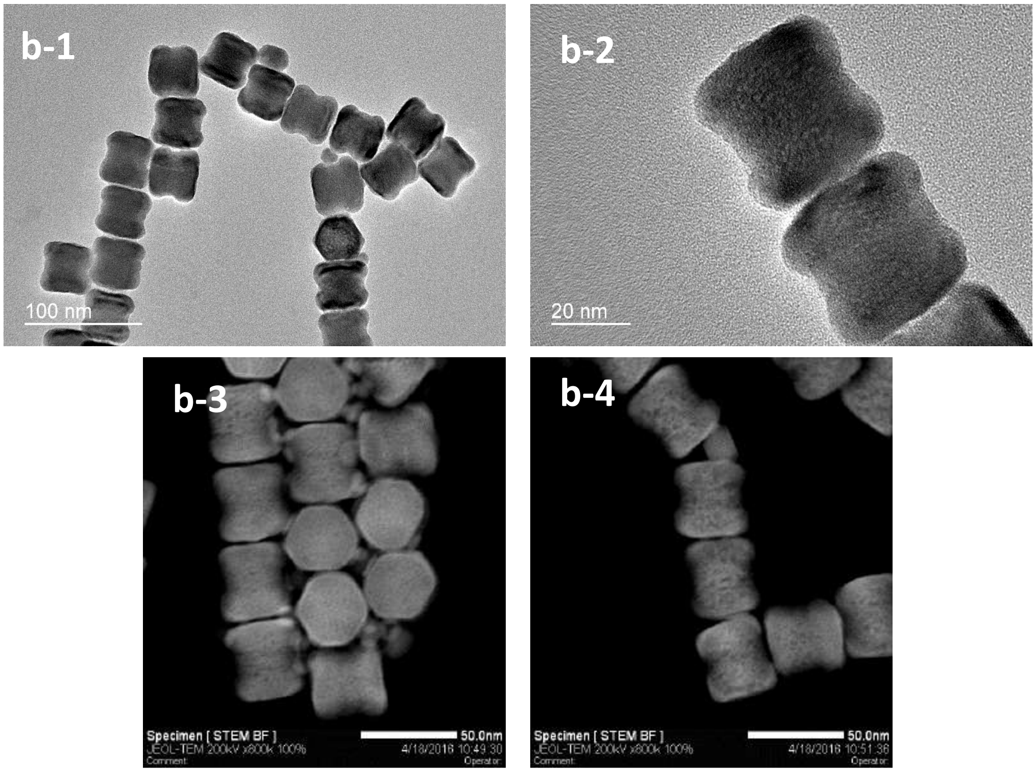
b-1
100 nm
b-2
20 nm
b-3
Specimen [STEM BF]
50.0nm
JEOL-TEM 200kV x800k 100%
4/18/2016 10:49:30
Comment:
Operator:
b-4
Specimen [STEM BF]
50.0nm
JEOL-TEM 200kV x800k 100%
4/18/2016 10:51:36
Comment:
Operator:

Figure 11. Toast nanoparticles: TEM (in cyclohexane: a-1, a-2; in cyclohexane-ethanol: a-3, a-4) and HAADF-STEM (in cyclohexane: b-1, b-2; in cyclohexane-ethanol: b-3, b-4) images of $NaYF_4$: Yb, Er coating with transition layer ($NaGdF_4$:Yb, Nd).

Furthermore, when the harvest layer is coated on, that is the $NaNdF_4$:Yb $_{20\ \%}$, the whole nanoparticle has more variation on the morphology, which would be called as **"twin lotuses" nanoparticles**. As shown in Figure 12, by dissolving the UCNPs that is $NaYF_4$:$Yb_{20\ \%}$,$Er_{2\ \%}$@$NaGdF_4$:$Yb_{10\ \%}$@ $NaNdF_4$:$Yb_{20\ \%}$ in cyclohexane, it could be observed that the (001) facets are further completely coated, which shows a thicker layer (about 3-4 nm), which is in brightness field. However, there appears some interlacement of the two (100) facets in the HAADF-STEM images, illustrating that the whole nanoparticle has some inclination standing on the bottom/end surface which is proposed that in the epitaxial growth, the whole nanoparticles has been entrusted and further result in the distortional deformation of the whole nanoparticles. While the nanoparticles are dissolved in the solvent of cyclohexane-ethanol, the nanoparticles stand on the (100) facets, displays a deep bleaching on the nanoparticle that almost separate the nanoparticle into two part. And it could also be explained as the $NaYF_4$:$Yb_{20\ \%}$,$Er_{2\ \%}$ nanocrystals further dissolved or extracted by the (001) facets.

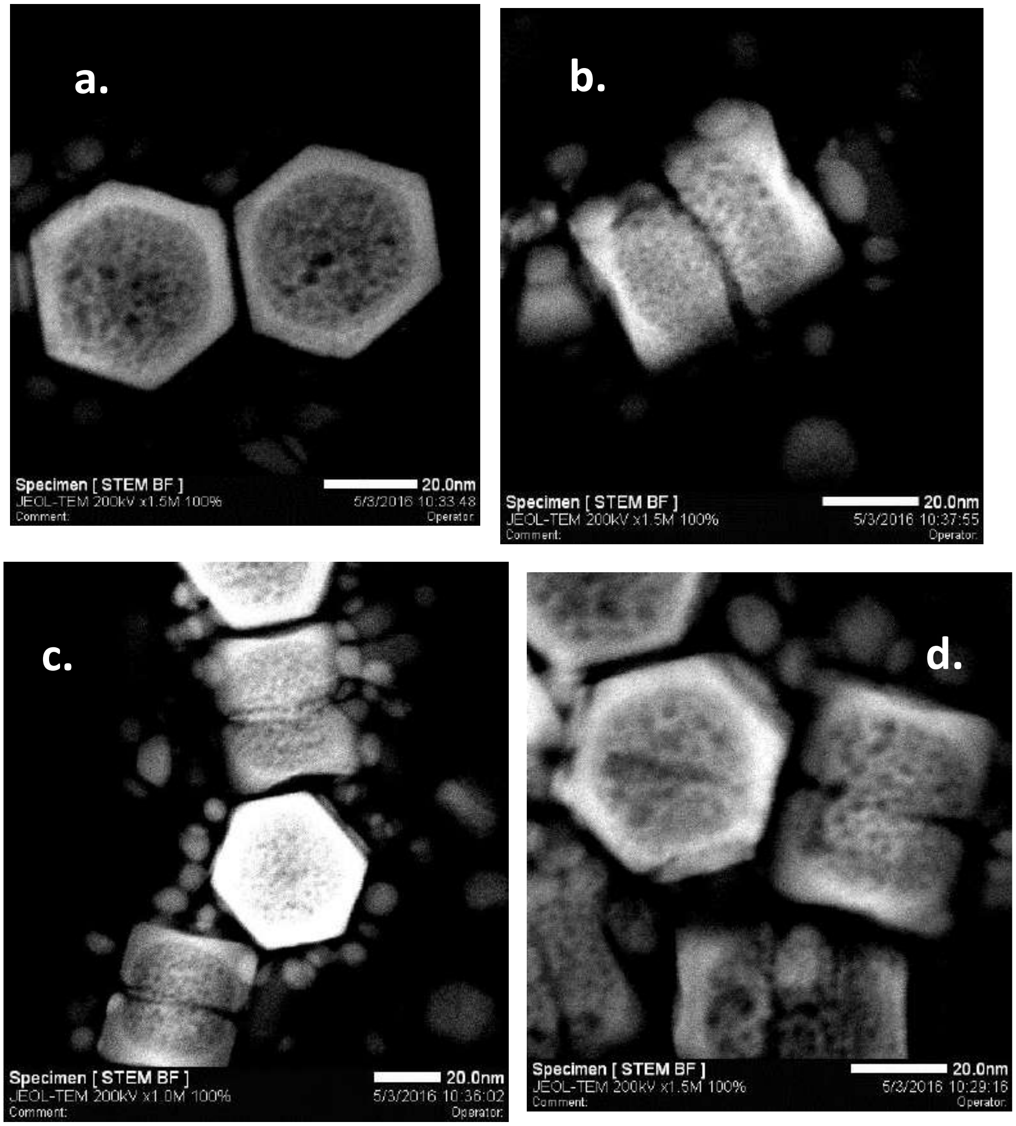

Figure 12. Twin lotuses nanoparticles: HAADF-STEM (in cyclohexane: b-1, b-2; in cyclohexane-ethanol: b-3, b-4) images of $NaYF_4$: Yb, Er coating with transition layer ($NaGdF_4$:Yb, Nd) and harvest layer ($NaGdF_4$:Yb,Nd).

Lastly, when the activation layer $NaGdF_4$ is coated on, which is $NaYF_4$:$Yb_{20\ \%}$,$Er_{2\ \%}$@$NaGdF_4$:$Yb_{10\ \%}$@ $NaNdF_4$:$Yb_{20\ \%}$@$NaGdF_4$, the complete coating on the (001) facet and anisotropic growth on the (100) facet intensified in a further step. It could be observed that the longitude growth make the nanoparticle stand higher in cyclohexane and the anisotropic growth make the nanoparticle in dumbbell-like shape. It is obvious that the regularly epitaxial growth of the (001) facets make a wider hexgon of the (001) facets; and the interlacement of the (001) facets becomes more violent which illustrates that the whole particle has been extracted further in the activation layer coating. By observation of the (100) facets of the nanoparticles, the orderly epitaxial of the (001) facets formed the two ends of the "dumbbell" , and the dissolved or extracted $NaYF_4$ cores become thicker, which looks like the holder of the "dumbbell".

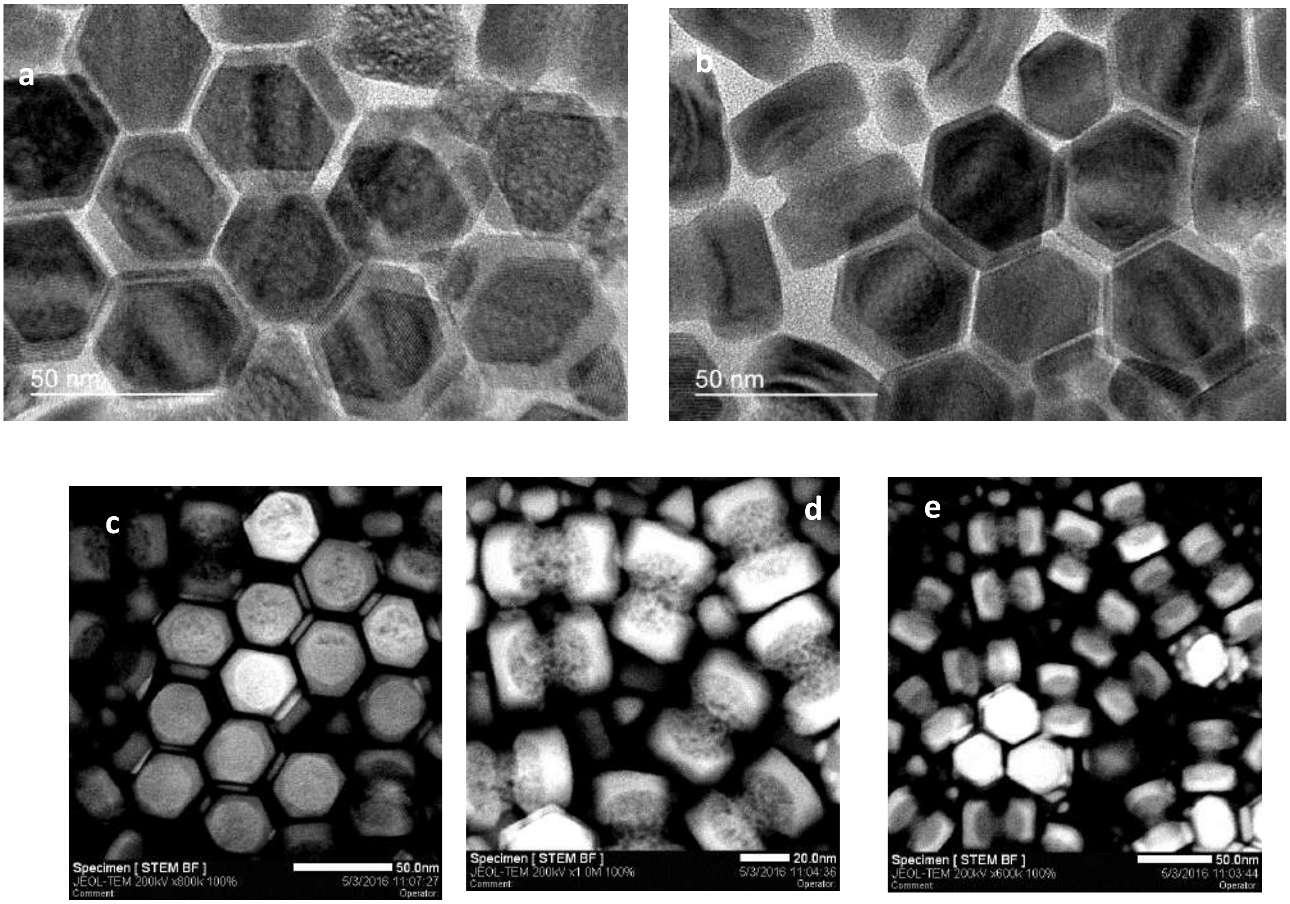

Figure 13. Dumbbell-like nanoparticles: images of $NaYF_4$: Yb, Er coating with transition layer ($NaGdF_4$:Yb, Nd) and harvest layer($NaGdF_4$:Yb,Nd) and activation layer ($NaGdF_4$):

TEM images in cyclohexane (a) and in cyclohexane-ethanol (b); HAADF-STEM in cyclohexane (c) and in cyclohexane-ethanol (d-e).

For the Nd^{3+}-trinity system that coating on the $NaYF_4$:Yb,Tm/Ho, that composed of the transition layer ($NaGdF_4$:$Yb_{10\ \%}$), harvest layer($NaGdF_4$:$Yb_{10\ \%}$,$Nd_{70\ \%}$) and activation layer ($NaGdF_4$), the monitoring of the anisotropic growth are shown in Figure 14:

For the coating of the transition layer ($NaGdF_4$:$Yb_{10\ \%}$), the situation has been discussed above as the incomplete coating with faster epitaxial on the (100) facets rather than the (001) facets, that show incomplete coating.

For the coating of the harvest layer ($NaGdF_4$:$Yb_{10\ \%}$, $Nd_{70\ \%}$), the epitaxial growth is just on the opposite of the transition layer, shows faster epitaxial on the (001) facets rather than the (100) facets. Furthermore, the coated $NaGdF_4$:Yb layer that is on the surface of (001) facets, could be observed to have disappeared, as shown in Scheme 4: from the images of HAADF-STEM, the bright field on the (100) facet disappear, which is proposed to be dissolved and migrated growth. And the (100) facets are “naked”.

For the coating of the activation layer that is $NaGdF_4$, they finally become the dumbbell-like nanoparticles, with complete coating on the (001) facets and dissolving and migration of the “naked” $NaYF_4$ (100) facets.

Also, some small nanoparticle could always been seen for the reason that they are caused by the phase splitting grow up by the layer-by-layer epitaxial growth or the (001) facets dissolving and recrystallization.

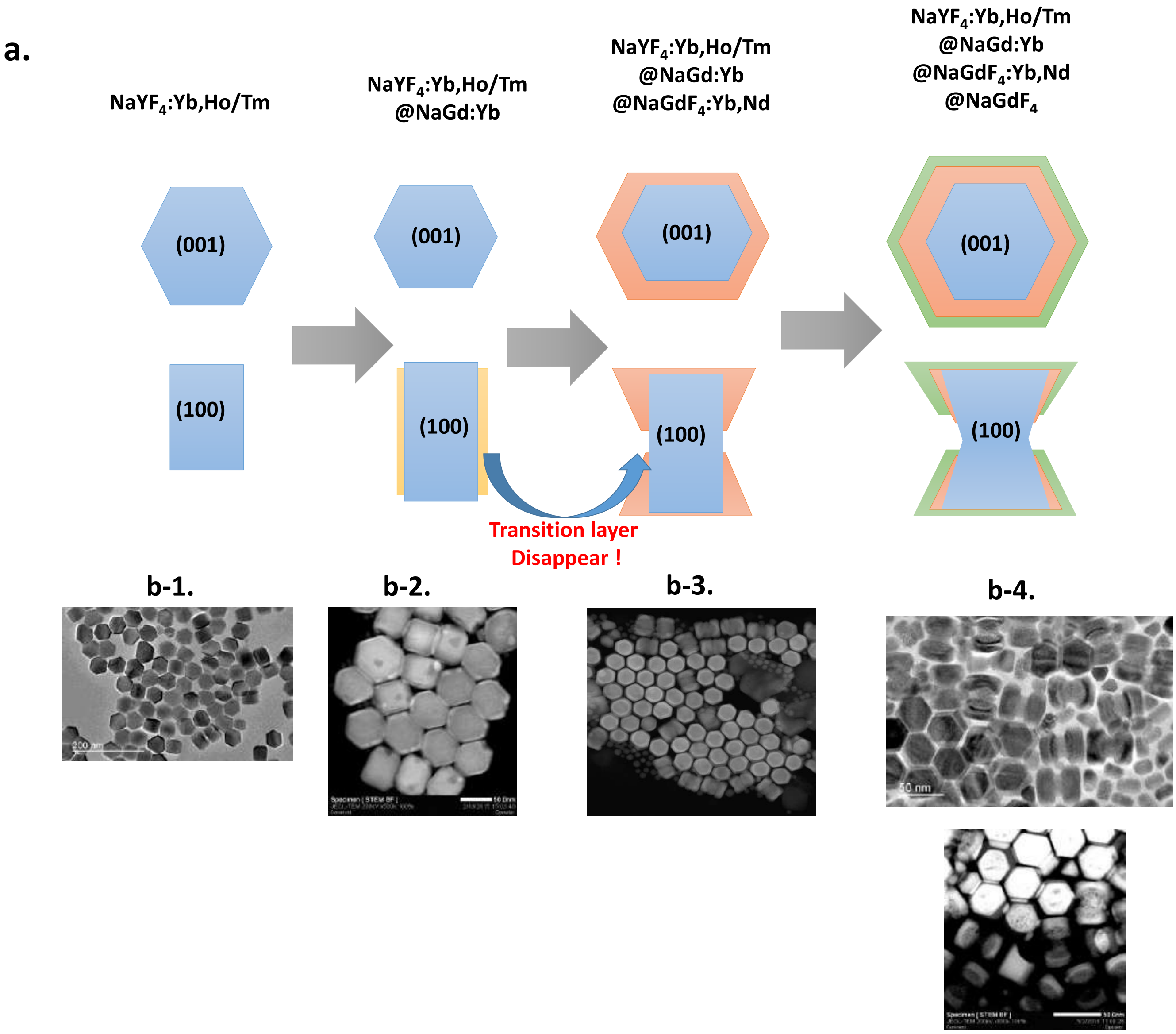

Figure 14. Anisotropic growth of the Nd^{3+}-trinity system coating on NaYF$_4$:Yb,Tm/Ho. (a). Scheme of the characterization of anisotropic growth on the (001) facets and (100) facets; (b). TEM and HAADF-STEM images of NaYF$_4$:Yb,Ho (b-1), NaYF$_4$:Yb$_{20\,\%}$, Ho$_{2\,\%}$@NaGdF$_4$:Yb$_{10\,\%}$ (b-2), NaYF$_4$:Yb$_{20\,\%}$,Ho$_{2\,\%}$@NaGdF$_4$:Yb$_{10\,\%}$@NaGdF$_4$:Yb$_{10\,\%}$, Nd$_{70\,\%}$ (b-3), NaYF$_4$:Yb$_{20\,\%}$,Ho$_{2\,\%}$ @NaGdF$_4$:Yb$_{10\,\%}$ @NaGdF$_4$:Yb$_{10\,\%}$,Nd$_{70\,\%}$@NaGdF$_4$ (b-4).

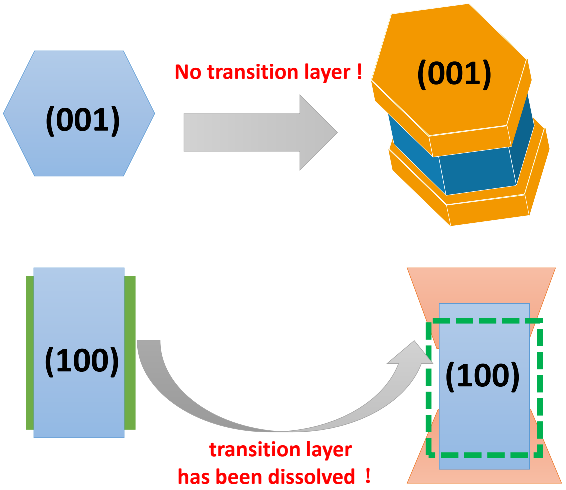

Scheme 4. Disappearance of the transition layer in $NaYF_4$:Yb,Tm/Ho@$NaGdF_4$:$Yb_{10\ \%}$@$NaGdF_4$:$Nd_{70\ \%}$,$Yb_{10\ \%}$ @$NaGdF_4$.

4.4. The influence on the luminescent properties by the layer-by-layer anisotropic epitaxial growth of the Nd^{3+}-Trinity system

Here comes the question: what is influence of the anisotropic layer-by-layer epitaxial growth on the luminescence properties of the obtained UCNPs? As shown in scheme. 5, the UCNPs with Nd^{3+}-Trinity system that coating on $NaYF_4$:$Yb_{20\ \%}$,$Er_{2\ \%}$ that is $NaYF_4$:$Yb_{20\ \%}$,$Er_{2\ \%}$@$NaGdF_4$:$Nd_{20\ \%}$,$Yb_{10\ \%}$@ $NaNdF_4$:$Yb_{20\ \%}$@$NaGdF_4$, display as dumbbell-like nanoparticles, with completed epitaxial growth on the (001) facets and Y^{3+} migration on the (100) facets, which could be considered as the completed formation of the Nd+-Trinity system on the (001) facets but the “naked” and “etched” (100) facets that with surface quenching of the sensitizers (Yb^{3+}) and activators (Er^{3+}); the UCNPs with Nd^{3+}-Trinity system that coating on $NaYF_4$:Yb,Ho/Tm that is $NaYF_4$:Yb,Ho/Tm @$NaGdF_4$:$Yb_{10\ \%}$@ $NaGdF_4$: $Nd_{70\ \%}$,$Yb_{10\ \%}$@$NaGdF_4$, also display as dumbbell-like nanoparticles with incomplete Nd^{3+}-Trinity system coating on the (001) facets for the missing of the transition layer that caused by the $NaGdF_4$:$Yb_{10\,\%}$ uncompleted coating on the (001) facets and completed coating of the harvest layer ($NaGdF_4$: $Nd_{70\,\%}$,$Yb_{10\,\%}$) and activation layer ($NaGdF_4$), which makes the $NaGdF_4$:Yb,Tm/Ho cores be in directly "contacted" with harvest layer that is the high concentration of Nd^{3+} ions, which is proposed to cause the violent Nd^{3+} energy back-transfer as discussed in Chapter 2. The further dissolving and etching in the process of coating of the harvest layer ($NaGdF_4$: $Nd_{70\,\%}$,$Yb_{10\,\%}$) that makes the (100) facets of the $NaGdF_4$:Yb,Tm/Ho cores "naked" and further "etched" in the process of coating of the activation layers ($NaGdF_4$).

In other words, the anisotropic growth of the Nd^{3+}-Trinity system coating $NaYF_4$:Yb,X(Er/Tm/Ho), on one hand enables the 808 nm photon absorption, transfer, and sensitization the activators with minimized quenching caused by the Nd^{3+}-Er^{3+}/Tm^{3+}/Ho^{3+} cross-relaxation and the Yb^{3+}-Er^{3+}/Tm^{3+}/Ho^{3+} cross-relaxation; on the other hand, the exposure and dissolving of the $NaYF_4$:Yb,X(Er/Tm/Ho) cores result in the surface quenching of Yb^{3+} or the activators(Er^{3+}/Tm^{3+}/Ho^{3+}), which caused the energy loss and luminescence quenching and attenuating. As shown in Scheme 5, the proposed process of photons absorption, energy transfer and surface quenching in the anisotropic growth of the Nd^{3+}-Trinity system.

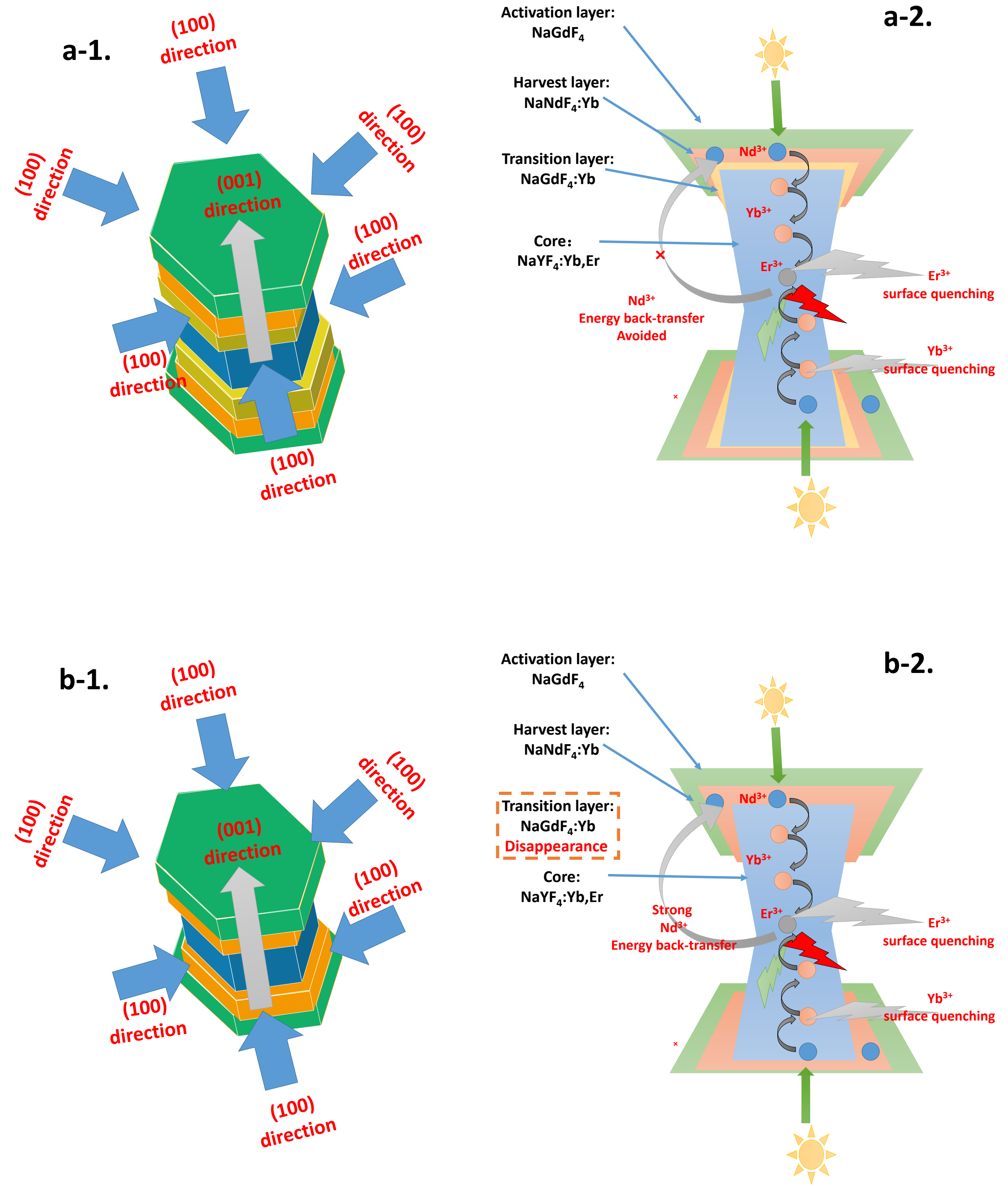

Scheme 5. Layer-by-layer epitaxial growth of the Nd^{3+}-Trinity system coating on the NaYF$_4$:Yb,Er (a-1) and NaYF$_4$:Yb,Tm/Ho (b-1) and the influence on the function of the

Nd^{3+}-Trinity system that is the failure on avoidance of the quenching factors, including the surface quenching of Yb^{3+} and activators (a-2, b-2) and Nd^{3+}-energy back-transfer.

Furthermore, we have done investigations on the luminescence properties, including the measurement of the luminescence spectra to observe the enhancement of the luminescence intensity and by excitation of 808 nm laser, the lifetime of the UCNPs and florescent quantum yield.

To illustrate the invalidation of the harvest layer, we have developed two types of the Nd^{3+}-Trinity system that coated on the sub-30 nm $NaYF_4$ nanocrystals, the same as the work we have stated in Chapter 2: type I is composed of transition layer ($NaGdF_4$:Yb,Nd)and activation layer($NaGdF_4$) while type II is composed of the transition layer, harvest layer and activation layer. What the type I Nd^{3+}-Trinity system differ the type II system is the Nd^{3+} amount and distribution, for in the type I Nd^{3+}-Trinity system only with 20 mmol% Nd^{3+} doping in the transition layer while the in the type I Nd^{3+}-Trinity system there is a harvest layer which is the $NaNdF_4$:Yb that used to harvest 808 nm photons and transfer energy from Nd^{3+} to Yb^{3+}.

The morphology of the Type I Nd^{3+}-Trinity system coated UCNPs could be characterized as shown in Figure 15.

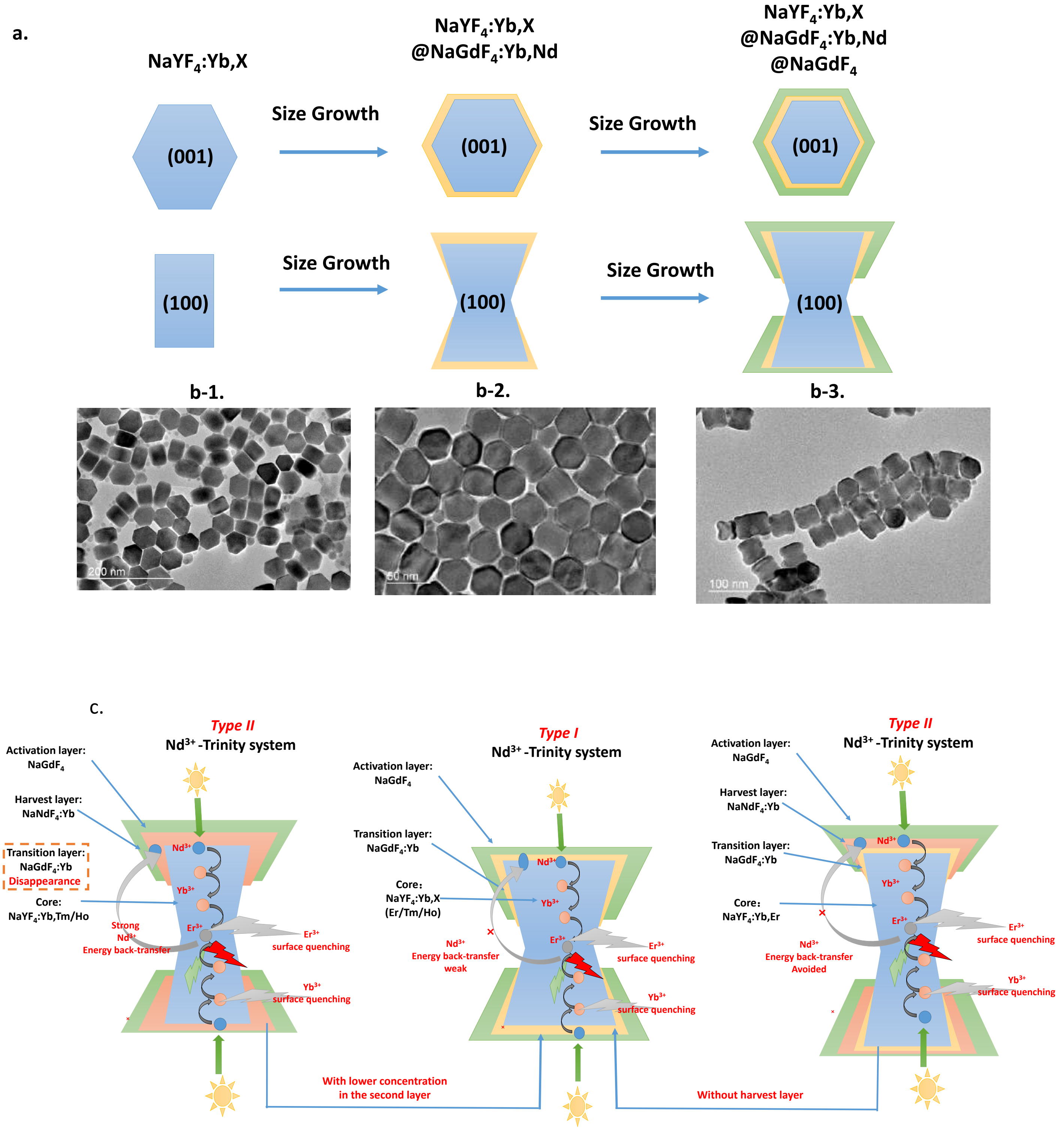
a.
NaYF$_4$:Yb,X
NaYF$_4$:Yb,X
@NaGdF$_4$:Yb,Nd
NaYF$_4$:Yb,X
@NaGdF$_4$:Yb,Nd
@NaGdF$_4$
Size Growth
Size Growth
(001)
(001)
(001)
Size Growth
Size Growth
(100)
(100)
(100)
b-1.
b-2.
b-3.
200 nm
50 nm
100 nm
c.
Type II
Nd^{3+} -Trinity system
Activation layer:
NaGdF$_4$
Harvest layer:
NaNdF$_4$:Yb
Transition layer:
NaGdF$_4$:Yb
Disappearance
Core:
NaYF$_4$:Yb,Tm/Ho
Nd^{3+}
Yb^{3+}
Er^{3+}
Strong
Nd^{3+}
Energy back-transfer
Er^{3+}
surface quenching
Yb^{3+}
surface quenching
Type I
Nd^{3+} -Trinity system
Activation layer:
NaGdF$_4$
Transition layer:
NaGdF$_4$:Yb
Core:
NaYF$_4$:Yb,X
(Er/Tm/Ho)
Nd^{3+}
Yb^{3+}
Er^{3+}
Nd^{3+}
Energy back-transfer
weak
Er^{3+}
surface quenching
Yb^{3+}
surface quenching
Type II
Nd^{3+} -Trinity system
Activation layer:
NaGdF$_4$
Harvest layer:
NaNdF$_4$:Yb
Transition layer:
NaGdF$_4$:Yb
Core:
NaYF$_4$:Yb,Er
Nd^{3+}
Yb^{3+}
Er^{3+}
Nd^{3+}
Energy back-transfer
Avoided
Er^{3+}
surface quenching
Yb^{3+}
surface quenching
With lower concentration
in the second layer
Without harvest layer

Figure 15. Scheme of epitaxial growth (a) and characterization on the type I Nd^{3+}-Trinity system. (c). Scheme of the difference between the UCNPs coated with type I Nd^{3+}-Trinity system and Type II Nd^{3+}-Trinity system.

Emission spectra & Enhancement of the luminescence intensity

As seen in the experimental section, we have established the characterization of the luminescent properties of the UCNPs by the 808/980 nm pulsed/CW laser: the emission spectra which is used to reflect the situation of the luminescence performance, are measured with excitation of 808 nm CW laser and 980 nm CW laser (under the same power density), with comparison of the peak are and the Ig/r value; lifetime decay curves, which is used to reflect the stability of the excited state, is measured with excitation of 808 nm pulsed and 980 nm pulsed laser; the florescent quantum yield of the UCNPs that is $NaYF_4$:Yb,Er coating with the type II Nd^{3+}-Trinity system (that is $NaYF_4:Yb_{20\,\%},Er_{2\,\%}@NaGdF_4:Yb_{10\,\%},Nd_{20\,\%}@NaNdF_4:Yb_{20\,\%}@NaGdF_4$), which reflects the upconversion efficiency, is measured with 808 nm excitation with certain modification on the Edinburgh spectrometer with 808 nm excitation.

As we have discussed in Chapter 2, the type II Nd^{3+}-Trinity system that coating on the $NaGdF_4$:Yb,X(Er/Tm/Ho) core, has largely enhanced the luminescence intensity for 232 (Er^{3+})/449.78 (Tm^{3+})/195.18 (Ho^{3+}) folds. However, when it comes to the situation of the Nd^{3+}-Trinity system coated $NaYF_4$:Yb,X(Er/Tm/Ho) cores, the situation has great difference, for the enhancement of the luminescence intensity has been inhabited by the layer-by-layer anisotropic epitaxial growth of the Nd^{3+}-Trinity system, which has leaded to the incomplete construction of the Nd^{3+}-Trinity system, as discussed in Scheme 5. Actually, the design of the Nd^{3+}-Trinity system, is used to harvest 808 nm photons as much as possible, to guarantee the Nd^{3+}-Yb^{3+} along while avoiding all the possible quenching factors including the surface quenching as possible and shielding the deleterious Nd^{3+}-$X(Er/Tm/Ho)^{3+}$ and the Yb^{3+}-$X(Er/Tm/Ho)^{3+}$, which contributes to the luminescence performance and upconversion efficiency. However, for the Nd^{3+}-Trinity system that coated on the $NaYF_4$:Yb,Er cores, the design has only be realized on the (001) facets to realized the harvest-transfer-sensitization function as well as shielding all the quenching factors and be invalid on the (100) facets for the migration growth induced surface quenching of Yb^{3+} and Er^{3+}, that is why the luminescence enhancement has been limited; for the Nd^{3+}-Trinity system that coated on the $NaYF_4$:Yb,Tm or $NaYF_4$:Yb,Ho cores, the design has been invalid on the (001) facets for the absence of the transition layer and be invalid on the (100) facets for the migration growth leading to the surface quenching of Yb^{3+} and activators (Tm^{3+}/Ho^{3+}), that is why the luminescence enhancement has been limited.

The emission spectra are shown in Figure 16-19, which is the comparison of the emission spectra of the $NaYF_4$:Yb,X(Er/Tm/Ho) with 980 nm excitation and the $NaYF_4$:Yb,X(Er/Tm/Ho) coated Type I and Type II Nd^{3+}-Trinity system with excitation of 808 nm. The peak area ratio comparison for the UCNPs with activator of Er^{3+}/Tm^{3+}/Ho^{3+} are shown in Table 1-3.

For the comparison of the UCNPs with activator of Er^{3+}, the type II Nd^{3+}-Trinity system coated $NaYF_4$:Yb, Er under 808 nm excitation, only shows the enhancement of 13.06 folds, with comparison of the $NaYF_4$:Yb, Er under 980 nm excitation; the type I Nd^{3+}-Trinity system coated $NaYF_4$:Yb, Er under 808 nm excitation even shows only 9.19 folds enhancement, which in contrast with the $NaYF_4$:Yb,Er with the $NaGdF_4$ coating (that is

$NaYF_4$:Yb,Er@$NaGdF_4$, which also results in incomplete coating) with the 1.70 folds of enhancement, which reveals severity of consequence of the surface quenching of the Yb^{3+} and Er^{3+} in the Nd^{3+}-Trinity system; for the type I Nd^{3+}-Trinity system, the luminescence peak area, which on the contrary, even shows the weaken luminescent intensity than the $NaYF_4$:Yb,Er.

When the type I and II Nd^{3+}-Trinity system are excited by 980 nm, compares with the $NaYF_4$:Yb, Er with excitation of 980 nm, the enhancement are only 1.04 times for the type II Nd^{3+}-Trinity system and even shows weaken on the type I Nd^{3+}-Trinity system (0.94 folds). In contrast with the $NaYF_4$:Yb,Er@$NaGdF_4$, shows surface quenching on the (001) facets that is an invalid activation shell coated UCNPs, still shows 1.70 folds enhancement, which illustrates the deleterious effect of the layer-by-layer anisotropic growth.

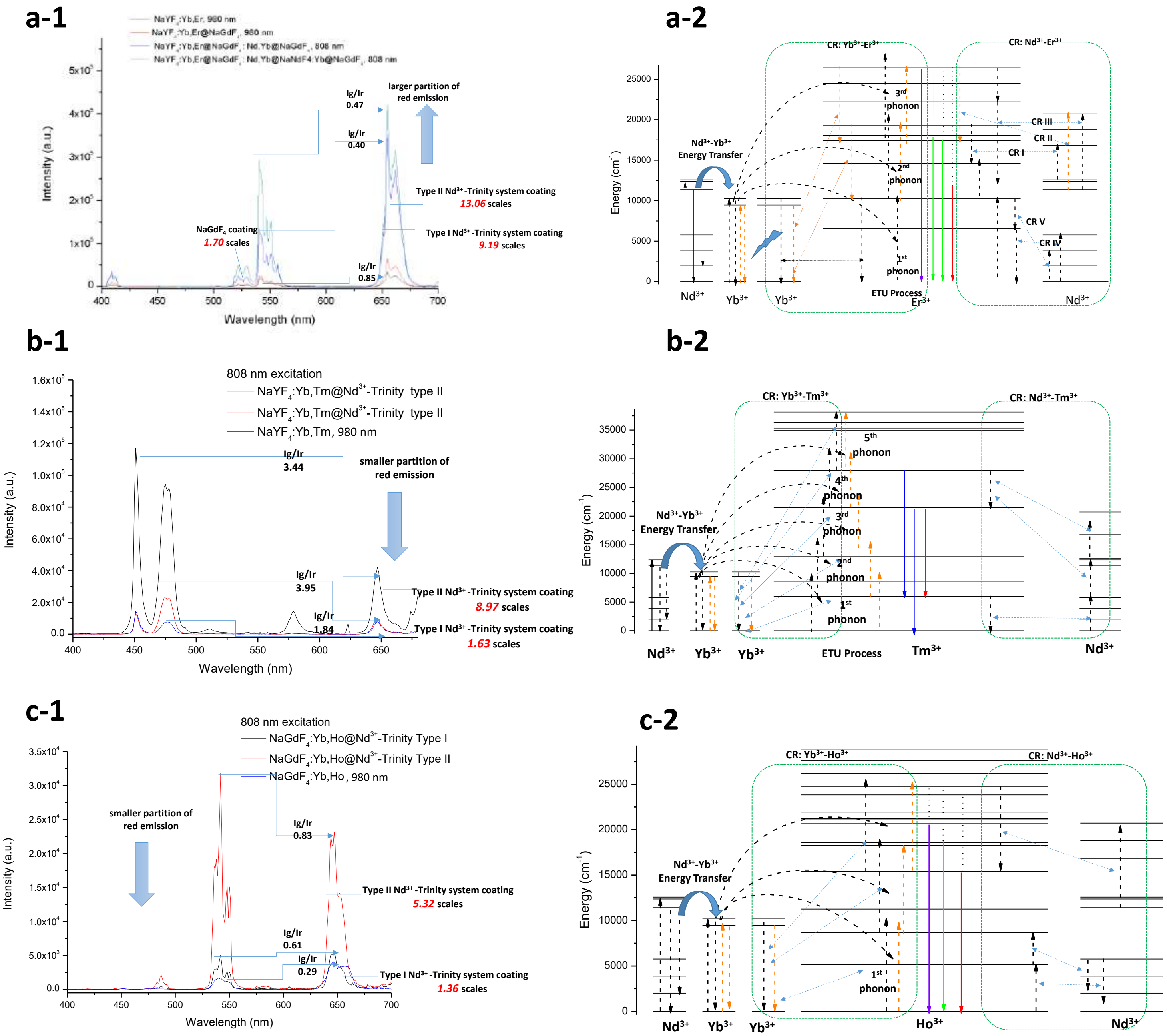

Figure 16. Emission spectra of the UCNPs that NaYF$_4$:Yb, X(Er/Tm/Ho) coating with Nd^{3+}-Trinity system with excitation of 808 nm and NaYF$_4$:Yb, X(Er/Tm/Ho) with 980 nm excitation.

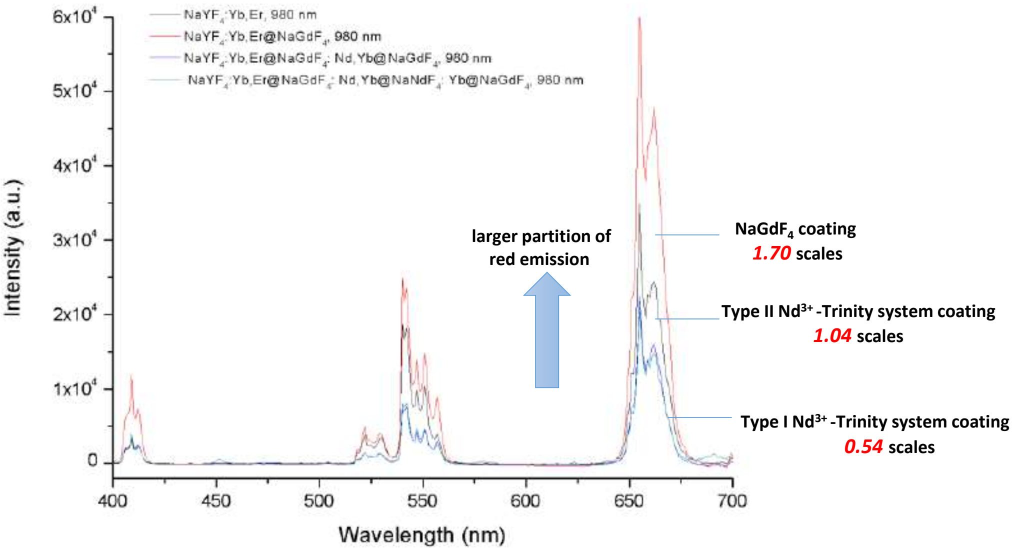

Figure 17. Emission spectra of the anisotropic growth Nd^{3+}-Trinity system coated NaYF$_4$:Yb, Er with excitation of 980 nm laser.

Ratio of Peak Area (a.u.) compares with NaYF$_4$:Yb, Er excited by 808 nm	Photo-luminescent source (nm)	Wavelength (nm)				In total	
		410	521	541	655		Ig/Ir
NaYF$_4$:Yb, Er @Nd^{3+}-trinity system type I	808	5.04	1.43	7.54	10.18	9.19	0.37
	980	0.49	0.07	0.42	0.61	0.54	0.35
NaYF$_4$:Yb, Er @ Nd^{3+}-trinity system type II	808	4.52	3.21	14.58	12.28	13.06	0.61
	980	1.06	1.19	1.11	0.97	1.04	0.40
NaYF$_4$:Yb,Er@NaGdF$_4$	980	1.62	0.26	1.41	1.84	1.7	0.39
NaYF$_4$:Yb,Er	980	-	-	-	-	-	0.85

Table 1. Luminescence enhancement effect of the Nd^{3+}-trinity system on NaYF$_4$:Yb, Er and the Ig/Ir value of the UCNPs.

The situation are similar to the UCNPs with activators of Tm^{3+} and Ho^{3+}, as shown in Figure 16 and Table 2 and 3, for the limitation on the enhancement of the UCNPs with

Nd^{3+}-Trinity system, which are measured to be 8.97 folds (type II, Tm^{3+}), 1.63 scale (type I, Tm^{3+}), 5.32 folds (type I, Ho^{3+}) and 1.36 folds (type I, Ho^{3+}) under 808 nm excitation, which should be attributed to layer-by-layer epitaxial growth of the Nd^{3+}-Trinity system that makes the transition layer disappeared that cause the conspicuous Nd^{3+} energy back-transfer along with the surface quenching on the (100) facets caused by the migration growth. For the 980 nm exited UCNPs that is Nd^{3+}-Trinity system coated NaYF$_4$:Yb,Tm or NaYF$_4$:Yb,Ho, the luminescent intensity enhancement is also inhibited or even shows weakened luminescent intensity, which could be attribute to the surface quenching on the (100) facets.

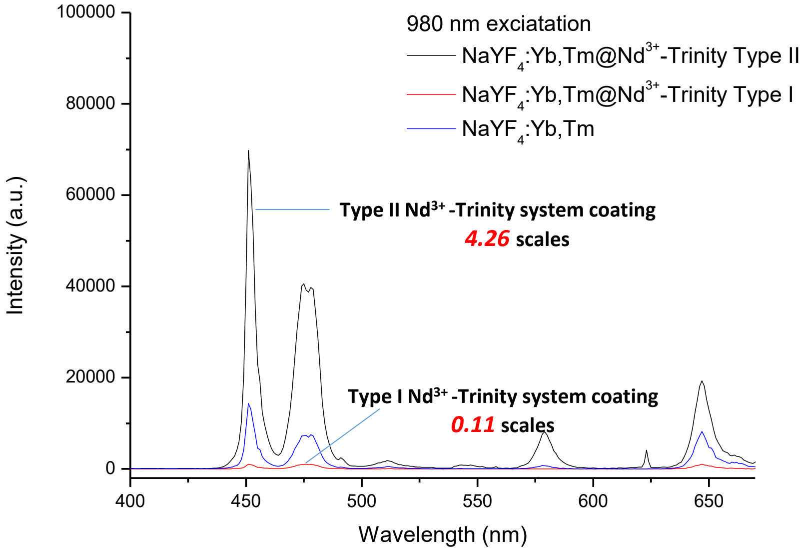

Figure 18. Emission spectra of the anisotropic growth Nd^{3+}-Trinity system coated NaYF$_4$:Yb, Tm with excitation of 980 nm laser.

Ratio of Peak Area (a.u.) compares with NaYF$_4$:Yb, Tm excited by 808 nm	Wavelength (nm)			In total	Ib/Ir
	450	475	655		
NaYF$_4$:Yb, Tm@ Type IIexcited by 808 nm	8.67	12.84	5	8.97	3.44

NaYF$_4$:Yb, Tm@ tpye II excited by 980 nm	4.78	5.87	2.16	4.26	1.66
NaYF$_4$:Yb, Tm@ tpye I excited by 808 nm	0.86	3.1	1.08	1.63	3.95
NaYF$_4$:Yb, Tm@ tpye I excited by 980 nm	0.08	0.14	0.12	0.11	4.51
NaYF$_4$:Yb,Tm excited by 980 nm	-	-	-	-	1.84

Table 2. Luminescence enhancement effect of the Nd^{3+}-trinity system on NaYF$_4$:Yb, Tm and the Ig/Ir value of the UCNPs.

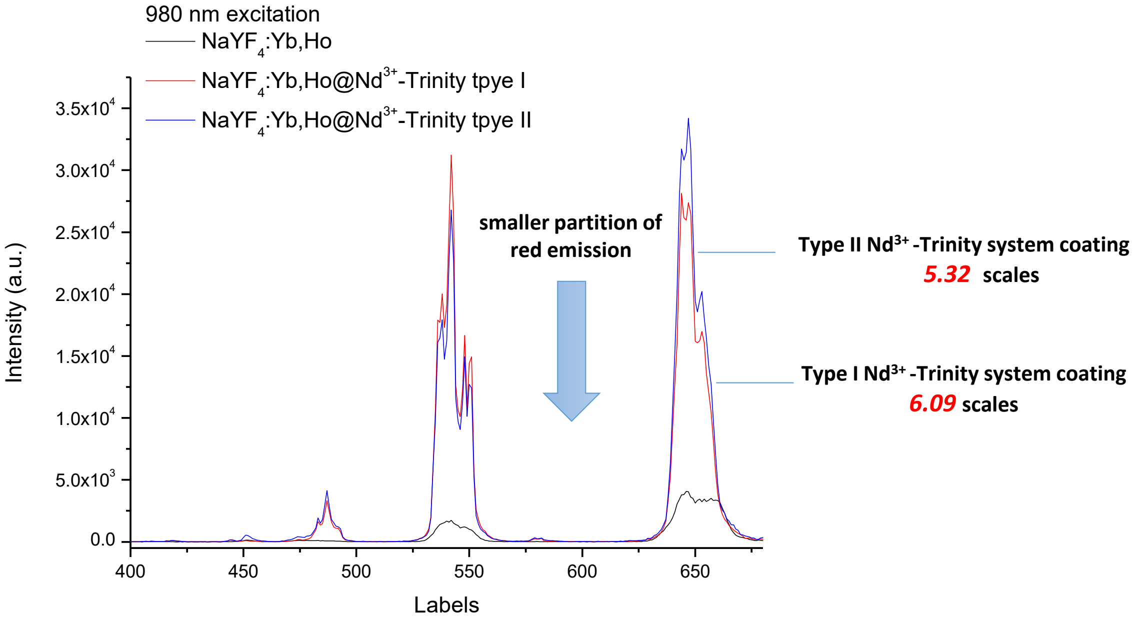

Figure 19. Emission spectra of the anisotropic growth Nd^{3+}-Trinity system coated NaYF$_4$:Yb, Ho with excitation of 980 nm laser.

Ratio of Peak Area (a.u.) compares with NaYF$_4$:Yb, Ho excited by 808 nm	Photo-luminescent source (nm)	Wavelength (nm)		In total	Ig/Ir
		550	655		
NaYF$_4$:Yb, Ho@ tpye I Nd^{3+}-trinity	808	2.02	0.97	1.36	0.59
	980	10.4	4.87	6.09	0.61
	808	11.64	3.44	5.32	0.97

NaYF$_4$:Yb, Ho @ tpye II Nd^{3+}-trinity system	980	11.66	4.05	5.73	0.83
NaYF$_4$:Yb,Ho	980	-	-	-	0.29

Table 3. Luminescence enhancement effect of the Nd^{3+}-trinity system on NaYF$_4$:Yb, Ho and the Ig/Ir value of the UCNPs.-

Florescent quantum yield

As shown in Figure 20, we have measured the florescent quantum yield of the UCNPs that is the NaYF$_4$:Yb, Er coating with type II Nd^{3+}-Trinity system, that is the NaYF$_4$:Yb$_{20\ \%}$,Er$_{2\ \%}$ @NaGdF$_4$:Yb$_{10\ \%}$,Nd$_{20\ \%}$@NaNdF$_4$:Yb $_{20\ \%}$@NaGdF$_4$, the florescent quantum yield is measured with only 0.01 %, which could be considered to be a very low value that reflect the situation of upconversion efficiency with our previous work : as discussed in Chapter 2, we have reported that that the NaGdF$_4$:Yb, Er coating with type II Nd^{3+}-Trinity system, that is the NaGdF$_4$: Yb$_{20\ \%}$,Er$_{2\ \%}$ @NaGdF$_4$:Yb$_{10\ \%}$,Nd$_{20\ \%}$@NaNdF$_4$:Yb $_{20\ \%}$@NaGdF$_4$ is measured with the florescent quantum yield of 0.42 % with 808 nm excitation and 0.84 % with 980 nm excitation. Also, as reported by J.C. Boyer *et al.*, the absolute florescent quantum yield of NaYF$_4$:Yb, Er (0.005 %)is much higher than that of the NaGdF$_4$:Yb, Er (0.0005 %) with excitation of 980 nm laser [14]. It reveals that the anisotropic growth of the Nd^{3+}-Trinity system inhibits the upconversion efficiency along with luminescent intensity for the surface quenching of Yb^{3+} and Er^{3+}.

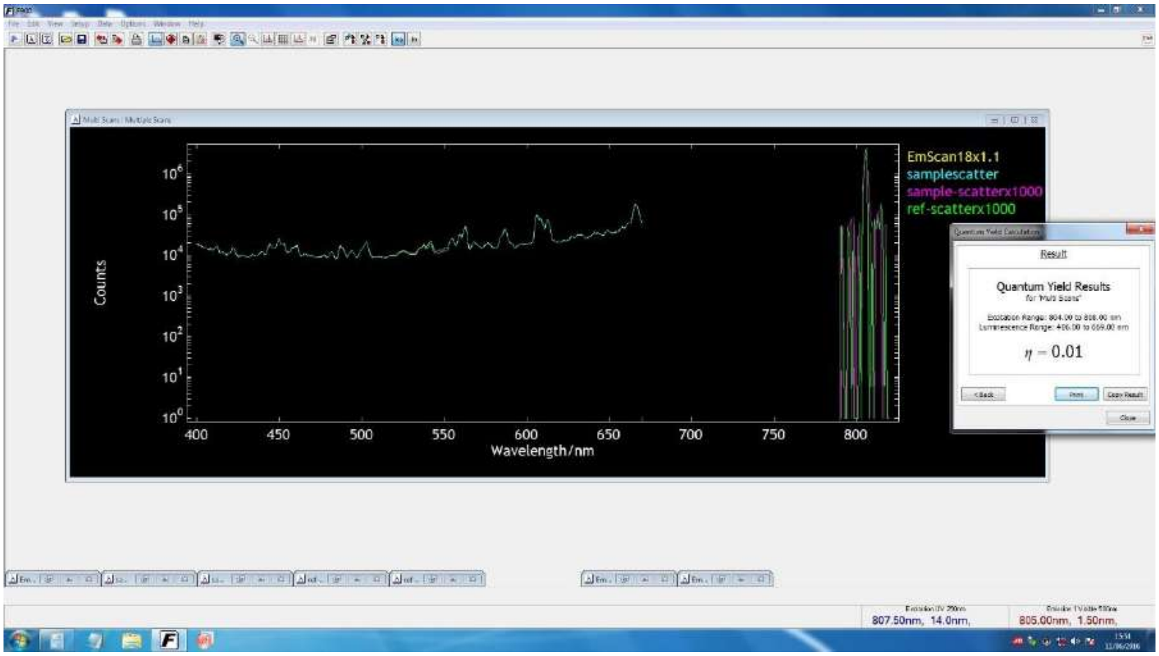

Quantum Yield Results
for "Multi Scans"

Excitation Range: 804.00 to 808.00 nm
Luminescence Range: 406.00 to 669.00 nm

$\eta = 0.01$

807.50nm, 14.0nm,
805.00nm, 1.50nm,

Figure 20. Florescent quantum yield of the $NaYF_4$:Yb, Er@$NaGdF_4$:Yb@$NaNdF_4$:Yb@$NaGdF_4$ with excitation of 808 nm laser.

Peak area ratio

For the partition of red emission, that is the smaller value of Ig/r (as shown in Table 1-3), as we have discussed in Chapter 2, the Nd^{3+}-Trinity system has made the activators prone to emit red emission affected by the Nd^{3+}-X(Er/Tm/Ho)$^{3+}$ cross-relaxation and Yb^{3+} surface quenching. Similarly, in the Nd^{3+}-Trinity system with layer-by-layer anisotropic growth, which exists the strong Nd^{3+}-X(Er/Tm/Ho)$^{3+}$ cross-relaxation. However, the Yb^{3+} surface quenching has always exits for the layer-by-layer epitaxial growth that could be neglected.

Lifetime

As shown in Table 4-6, the UCNPs coated with Nd^{3+}-Trinity system shows prolonged lifetime with excitation of 808 nm and 980 nm pulsed laser rather than the $NaYF_4$:Yb, X(Er/Tm/Ho) cores; furthermore, for the same UCNPs that with Nd^{3+}-Trinity system coating, the lifetime is prolonged under 808 nm excitation rather than the 980 nm excitation. Additionally, the UCNPs coating with type II Nd^{3+}-Trinity system shows prolonged lifetime rather than that coating with type I Nd^{3+}-Trinity system. The prolonged lifetime is proposed to be contributed by the coating of the Nd^{3+}-Trinity system layers for the partially avoided surface quenching of the Yb^{3+} and activators (Er^{3+}/Tm^{3+}/Ho^{3+}).

Furthermore, for the same UCNPs coating with Nd^{3+}-Trinity system, it shows prolonged lifetime under 808 nm excitation rather than the 980 nm excitation, which could be attribute to the Nd^{3+}-sensitization that we have proposed, that is under 808 nm excitation the activators have utilized two parts of the photons that transfer form Nd^{3+} to Yb^{3+}($Nd^{3+}\rightarrow Yb^{3+}$ assisted energy transfer), including the phonons around 950-10340 nm (with maximum at 975 nm) and 1056 nm phonons, which results in the less non-radiative transition further result in the more stable excited states of the emissions that is the prolonged lifetime. And still in this case, by Nd^{3+} absorption of 808 nm excitation, and $Nd^{3+}\rightarrow Yb^{3+}$ energy transfer and then sensitization of the activators, although there exist Yb^{3+} and activator surface quenching, the 1056 nm selectively participation of the ETU (energy transfer upconversion) process, still with the function of the less non-raditive transition and further result in prolonged lifetime, as shown in Figure 21. And the hypothesis could also illustrate why type II Nd^{3+}-Trinity system coated $NaYF_4$:Yb,X(Er/Tm/Ho) shows prolonged lifetime than the type I Nd^{3+}-Trinity system for the higher concentration of Nd^{3+} ions that make more 1056 nm photons participated in the ETU process.

lifetime	Wavelength (nm)

(μs)	Photo-luminescent source (nm)	410	521	541	655
NaYF$_4$:Yb, Er	980	69.88	96.58	96.85	207.4
NaYF$_4$:Yb, Er @NaGdF$_4$	980	204.21	280.40	286.91	346.87
NaYF$_4$:Yb, Er @Nd^{3+}-trinity system type I	808	265.53	321.84	334.60	490.76
	980	213.00	275.38	272.24	442.42
NaYF$_4$:Yb, Er @ Nd^{3+}-trinity system type II	808	199.87	191.69	342.76	189.14

Table 4. Lifetime of the UCNPs of NaYF$_4$:Yb, Er and NaYF$_4$:Yb, Er coating with Nd^{3+}-trinity system.

lifetime (μs)	Photo-luminescent source (nm)	Wavelength (nm)		
		450	475	655
NaYF$_4$:Yb, Tm	980	248.96	550.38	511.91
NaYF$_4$:Yb, Tm@ Nd^{3+}-Tri-Type I	808	448.54	788.22	774.115
	980	458.35	785.58	786.27
NaYF$_4$:Yb, Tm@ Nd^{3+}-Tri-Type II	808	465.18	842.49	813.99
	980	519.12	851.06	783.12

Table 5. Lifetime of the UCNPs of NaYF$_4$:Yb, Tm and NaYF$_4$:Yb, Tm coating with Nd^{3+}-trinity system.

lifetime (μs)	Photo-luminescent source (nm)	Wavelength (nm)	
		550	655
NaYF$_4$:Yb,Ho	980	44.53	44.73
NaYF$_4$:Yb,Ho@ Nd^{3+} -Tri- Type I	808	391.01	530.86
	980	355.24	480.41
NaYF$_4$:Yb,Ho@ Nd^{3+} -Tri- Type II	808	375.14	532.7
	980	302.57	492.97

Table 6. Lifetime of the UCNPs of NaYF$_4$:Yb, Ho and NaYF$_4$:Yb, Ho coating with Nd^{3+}-trinity system.

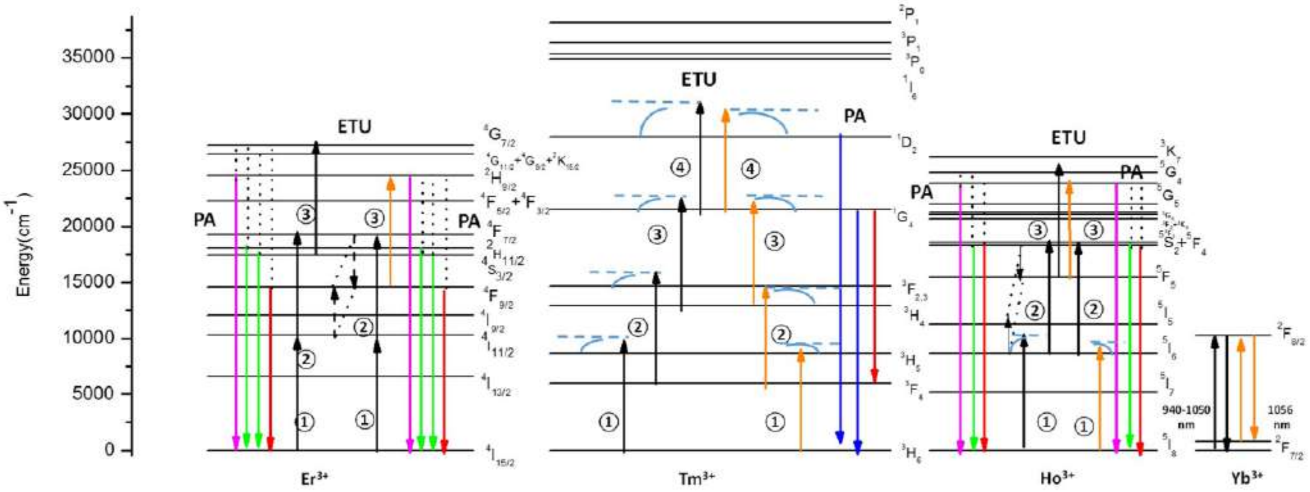

Figure 21. Selective participation of 1056 nm in the ETU (energy transfer upconversion) process in Er^{3+}, Tm^{3+} and Ho^{3+}. (i) 940-1030 nm (with maximum at 975 nm) photons; (ii) 1056 nm photons .

4.5. Discussion

In this chapter, we have generalized the anisotropic growth in the epitaxial growth of UCNPs, which has been influenced by the bonding energy oleate in the (001) and (100) facets of the β-$NaYF_4$ nanocrystals, that is the NaGd/YbF_4 has a faster growth rate on the (100) facets rather than the (001) facets of the β-$NaYF_4$ nanocrystals while $NaNdF_4$ only coating on the (001) facets and makes the (100) facets with migration growth. And further the anisotropic growth influence on the layer-by-layer epitaxial growth of the Nd^{3+}-Trinity system by the characterization on the morphologic properties and the energy harvest, transfer and sensitization of the activators by characterization on the luminescent properties.

It could be treated as another aspect in Nd^{3+}-Trinity system that is on the influence of nanoparticle growth and morphology on luminescent properties.

References

1. Crespo, P., R. Litrán, T.C. Rojas, M. Multigner, J.M. de la Fuente, J.C. Sánchez-López, M.A. García, A. Hernando, S. Penadés, and A. Fernández, *Permanent Magnetism, Magnetic Anisotropy, and Hysteresis of Thiol-Capped Gold Nanoparticles.* Physical Review Letters, 2004. **93**(8): p. 087204.
2. Garanin, D.A. and H. Kachkachi, *Surface Contribution to the Anisotropy of Magnetic Nanoparticles.* Physical Review Letters, 2003. **90**(6): p. 065504.
3. Johnson, C.L., E. Snoeck, M. Ezcurdia, B. Rodriguez-Gonzalez, I. Pastoriza-Santos, L.M. Liz-Marzan, and M.J. Hytch, *Effects of elastic anisotropy on strain distributions in decahedral gold nanoparticles.* Nat Mater, 2008. **7**(2): p. 120-124.
4. Winkler, E., R.D. Zysler, M.V. Mansilla, and D. Fiorani, *Surface anisotropy effects in NiO nanoparticles.* Physical Review B, 2005. **72**(13): p. 132409.
5. Liu, D., X. Xu, Y. Du, X. Qin, Y. Zhang, C. Ma, S. Wen, W. Ren, E.M. Goldys, J.A. Piper, S. Dou, X. Liu, and D. Jin, *Three-dimensional controlled growth of monodisperse sub-50 nm heterogeneous nanocrystals.* Nature Communications, 2016. **7**: p. 10254.
6. Wang, F., R. Deng, J. Wang, Q. Wang, Y. Han, H. Zhu, X. Chen, and X. Liu, *Tuning upconversion through energy migration in core–shell nanoparticles.* Nat Mater, 2011. **10**(12): p. 968-973.
7. Vetrone, F., R. Naccache, V. Mahalingam, C.G. Morgan, and J.A. Capobianco, *The Active-Core/Active-Shell Approach: A Strategy to Enhance the Upconversion Luminescence in Lanthanide-Doped Nanoparticles.* Advanced Functional Materials, 2009. **19**(18): p. 2924-2929.
8. Li, X., D. Shen, J. Yang, C. Yao, R. Che, F. Zhang, and D. Zhao, *Successive Layer-by-Layer Strategy for Multi-Shell Epitaxial Growth: Shell Thickness and Doping Position Dependence in Upconverting Optical Properties.* Chemistry of Materials, 2013. **25**(1): p. 106-112.

9. Matthews, J., *Epitaxial growth*. 2012: Elsevier.

10. Wang, Y., K. Liu, X. Liu, K. Dohnalová, T. Gregorkiewicz, X. Kong, M.C.G. Aalders, W.J. Buma, and H. Zhang, *Critical Shell Thickness of Core/Shell Upconversion Luminescence Nanoplatform for FRET Application.* The Journal of Physical Chemistry Letters, 2011. **2**(17): p. 2083-2088.

11. Mai, H.-X., Y.-W. Zhang, L.-D. Sun, and C.-H. Yan, *Size- and Phase-Controlled Synthesis of Monodisperse NaYF4:Yb,Er Nanocrystals from a Unique Delayed Nucleation Pathway Monitored with Upconversion Spectroscopy.* The Journal of Physical Chemistry C, 2007. **111**(37): p. 13730-13739.

12. Lei, L., D. Chen, W. Zhu, J. Xu, and Y. Wang, *Impact of High Ytterbium (III) Concentration in the Shell on Upconversion Luminescence of Core–Shell Nanocrystals.* Chemistry–An Asian Journal, 2014. **9**(10): p. 2765-2770.

13. Xu, B., X. Zhang, W. Huang, Y. Yang, Y. Ma, Z. Gu, T. Zhai, and Y. Zhao, *Nd3+ sensitized dumbbell-like upconversion nanoparticles for photodynamic therapy application.* Journal of Materials Chemistry B, 2016. **4**(16): p. 2776-2784.

14. Boyer, J.-C. and F.C.J.M. van Veggel, *Absolute quantum yield measurements of colloidal* $NaYF_4$*:* Er^{3+}*,* Yb^{3+} *upconverting nanoparticles.* Nanoscale, 2010. **2**(8): p. 1417-1419.

15. Zhang, C. and J.Y. Lee, *Prevalence of anisotropic shell growth in rare earth core–shell upconversion nanocrystals.* ACS nano, 2013. **7**(5): p. 4393-4402.

Chapter 5.

Theory Advance and Mechanism Investigation on 808 nm and 980 nm Steady/Non-steady Laser induce RGD Full-color Luminescent Janus UCNPs

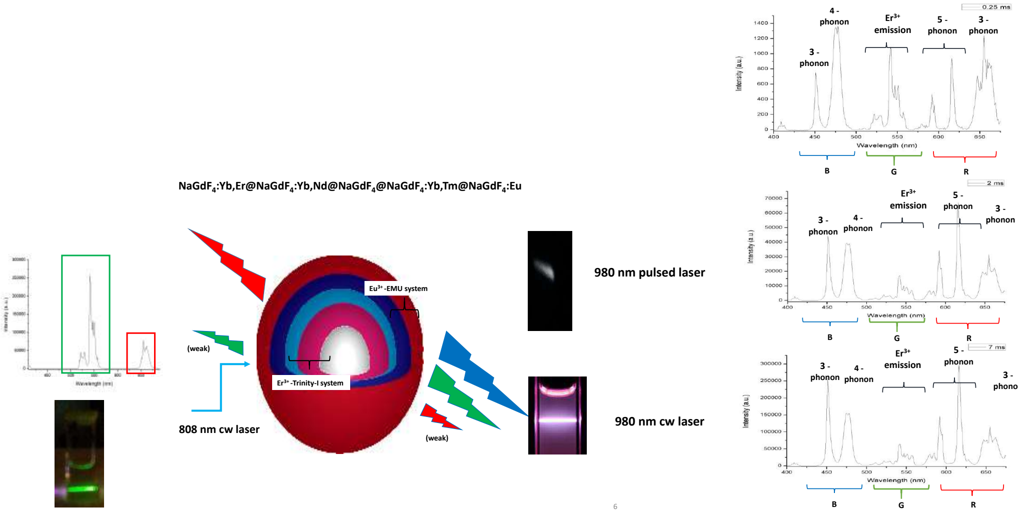

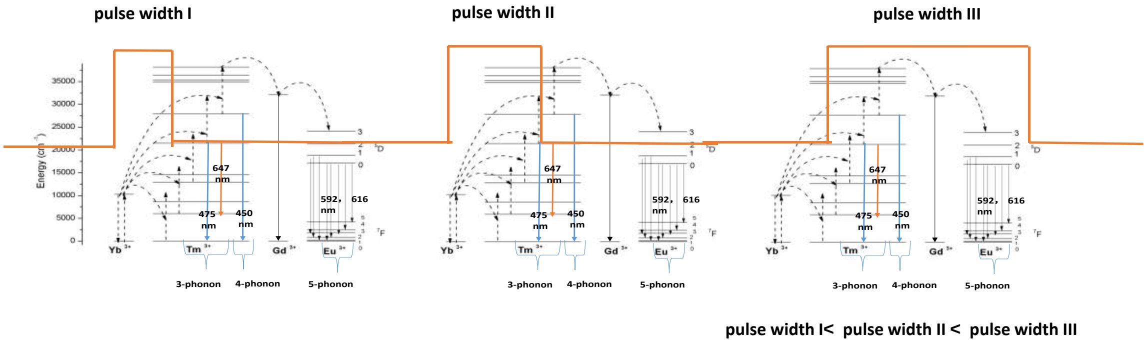

5.1. Introduction on the newly proposed concept: Luminescent Janus UCNPs

5.1.1 Janus Particles

For the Janus Particles, that are defined as are special types of nanoparticles whose surfaces have two or more distinct physical properties, which has been widely studies in the area of nanoparticles, for the synthesis of alloy/core-shell structure of the heterogeneous particles. As shown below in Scheme 1, the Janus nanoparticles are name as Janus is for the reason that the Janus God in the legends are always represented with two heads placed back to back, and the Janus Particles/Micelle/Dendrimers are just in coincide in the characteristics for the view of morphology. And all the presentation of the Janus particles are shown in Scheme.2, including the nanoparticle with distinct properties on the surface, bicompartmental particles, dumbbell-like particles, half-raspberry-like particle, acorn-like particle and snowman-like particles. [1, 2]

Ref:

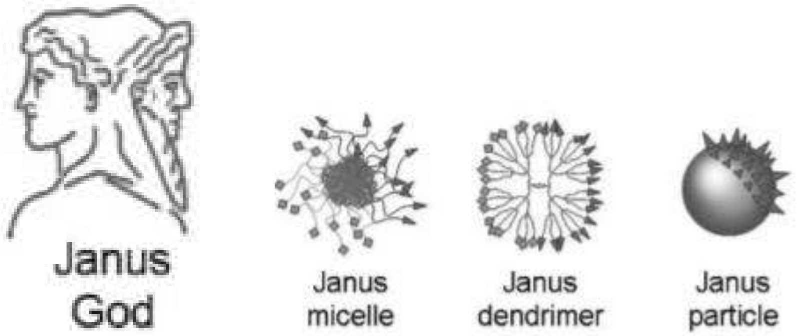

Sheme 1. The characristic of "Janus" and the destription of the Janus Particles/Micelle and dendrimer.[2]

Ref:

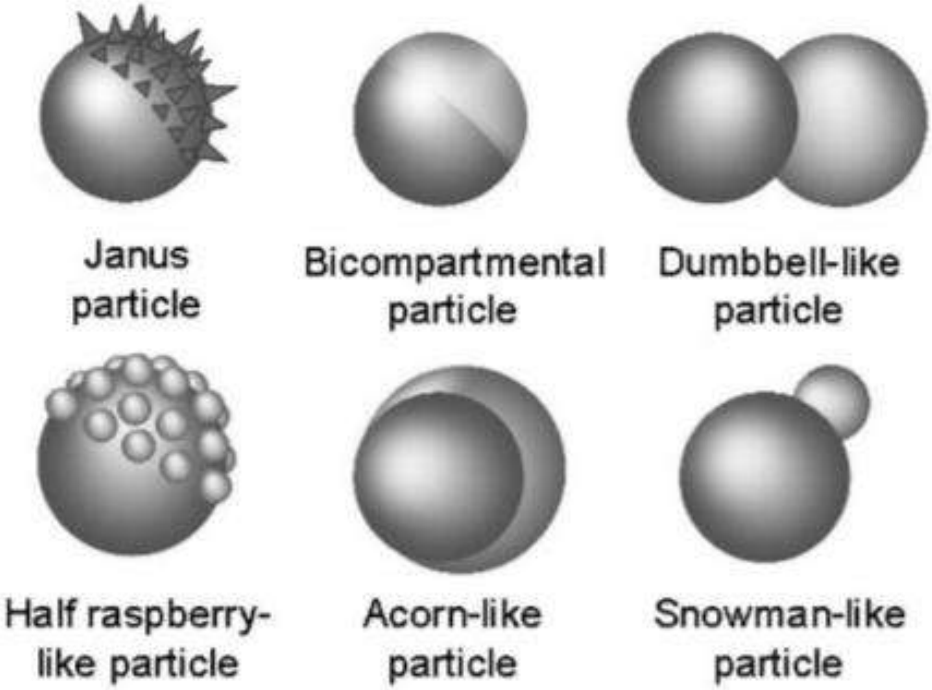

Scheme 2. Schematic representation of Janus and comparable particles. [2]

According to Marco Lattuada, a range of the Janus Particles has been presented below :

Ref:

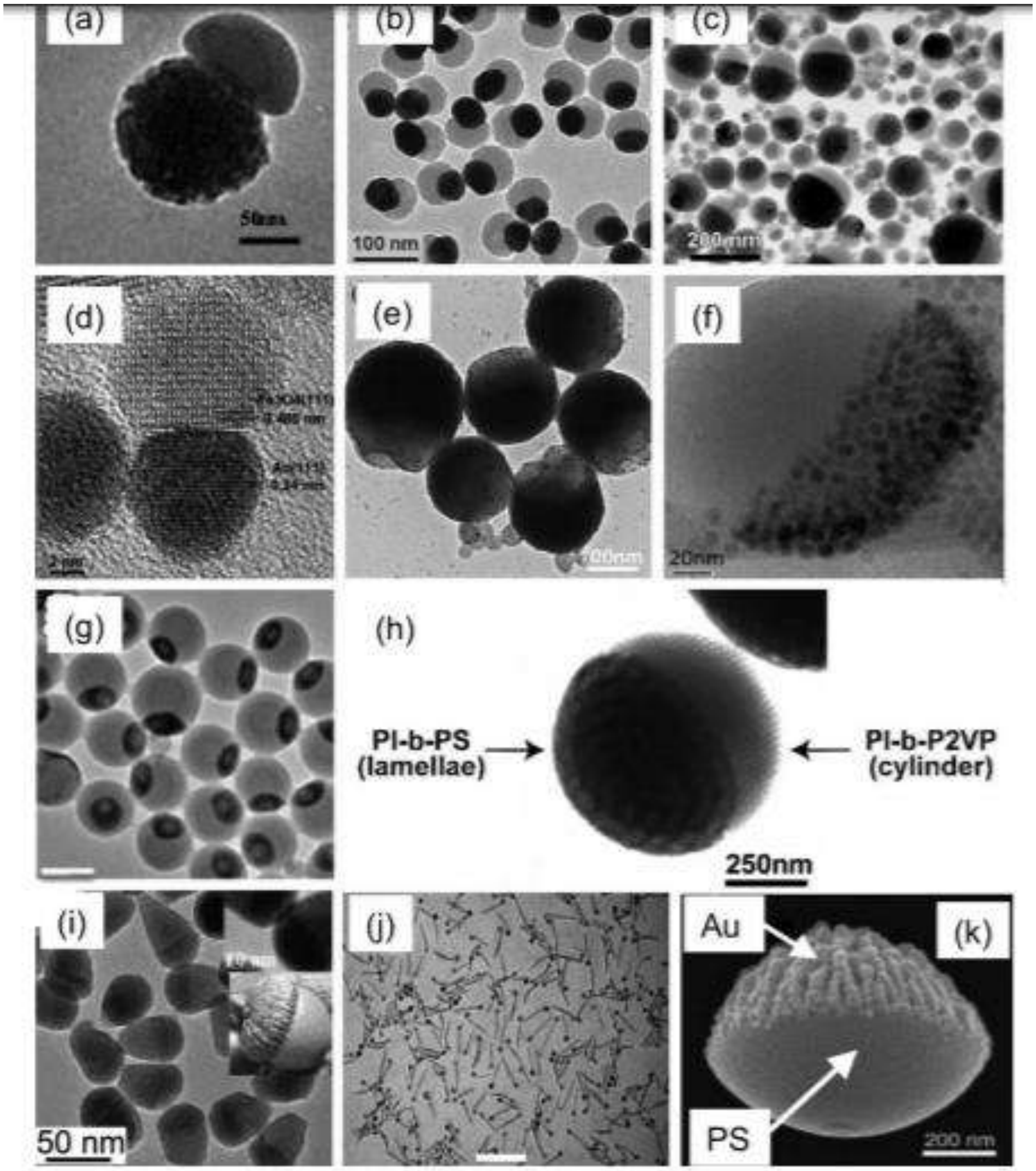

Figure 1. TEM micrographs showing a range of Janus nanoparticle morphologies: (a) silica-PS heterodimer, from reference; (b). gold-silica heterodimers; (c). SiO_2-Fe_2O_3 nanoparticles; (d). Au-Fe_3O_4; (e). PI/PS/AuNP@PS-b-P2VP nanoparticles; (f). PS-magnetite nanoparticles; (g). PS-b-PAAl-magnetite nanoparticles; (h). PI-b-PS and PI-b-P2VP Janus nanoparticles; (i). Acorn-shaped Copper-Indium Sulphides [2]

5.1.2. Luminescent Janus UCNPs

The traditionally used methods in encoding, manipulating and controlling color in the research of material science, could be concluded as: a. the white-color emission such as the phosphor powder emitted LED; b. the full-color or multi-color emitting materials with modulation of the photo-luminescence sources on the laser pulse width or power density. Furthermore, based on the reported on the Ce^{3+} doped $NaYF_4$:Yb, Ho UCNPs with the tunable emission color by varying the doping concentration of Ce^{3+} or the modulation on the laser width.

Since then, we would like to put forward the new concept that is **Luminescent Janus**, which indicated that the luminescent properties of the specially designed UCNPs ar different under excitation of a plurality of different pulse width NIR (808 nm or 980 nm) lasers NIR (808 nm or 980 nm) wave laser, with emitting various ratio of red-green-blue emissions. It is proposed to be employable in the developing of the sensors, bio-imaging probes and RGB color models that developed by the UCNPs.

The **Luminescent Janus UCNPs** are developed as:

Type I: the UCNPs with 808 nm pulsed laser excited, Nd^{3+}-trinity system with activator of Ho^{3+}-Ce^{3+}, driven by Ho^{3+}-Ce^{3+} cross relaxation;

Type II: 808 nm pulsed laser excited, Nd^{3+}-trinity system coated EMU (energy migration upconversion) system with activator of Tb^{3+} or 980 nm pulsed laser excited EMU (energy migration upconversion) system with activator of Tb^{3+}, driven by Tm^{3+}-Yb^{3+} cross relaxation;

Type III: the UCNPs with Er^{3+} (green and red emission) under 808 nm C.W. (continuous wave) laser excited while with Tm^{3+} (ultraviolet, blue, red) and Eu^{3+}

(red) emission by 980 nm C.W. laser; under 980 nm pulsed laser excitation, displays Red-Green-Blue color model with tenability.

Type IV: the UCNPs that is utilized the EMU system to sensitize the activator of Eu^{3+} and Tb^{3+}, the RGB tenability is realized by the Tm^{3+}-Yb^{3+} cross-relaxation and the slight quenching effect on the accumulation of Tm^{3+} by Eu^{3+} under 980 nm pulsed laser excitation.

We have estimated the potential utilization of the Luminescent Janus UCNPs could be used in:

a. Bio-imaging and therapy: the Type III shows potential to develop system to combine the bio-imaging probe and therapy, which is on one hand, detecting the tumor by targeting proteins with green emission under 808 nm excitation, on the other hand, delivery the drug by the photo-sensitive molecule under excitation of 980 nm with the signal of red emission. The key of the design is that: the photo-sensitive is driven by the ultraviolet emission under excitation of 980 nm laser.

b. Sensors: Type III is also potential to be developed to be bio-sensors for the photo-sensitive molecule.

c. RGB color models: Type I-IV could be used as RGB color models with tenability as discussed below.

5.2. Background

5.2.1. Background of the RGB color model

The basic principle of RGB could be illustrated as: "an additive color model in which red, green and blue light are added together in various ways to reproduce a broad array of colors." RGB is the device dependent color model for the utilization of sensing, representation and images displaying in electronic systems, such as televisions and computers. The RGB color model are composed of the red, green and blue light. And when the three kinds of emission has been added together, it will give white emission.

Ref:

Scheme 3. The basic principle of RGB color model

The research of RGB model could be concluded as

a. full-color emitting materials with tenability on the red-green-blue emission ratio;

b. White emitting material with broad emission bands that covers the emission rang of blue, green and red, such as the phosphor powder for LED. [3-7]

5.2.2 Previous work

To construct the Full-color emission system by Ho^{3+}-Ce^{3+} system:

Prof. X.G. Liu’s group has reported on the 3D-printer with temporal full color tuning induced by the 808 nm and 980 nm steady and non-steady laser. It could be concluded as a method in emitting color controlled by a pulse-width modulated approach based on the Ho^{3+}-Ce^{3+} cross relation. In the specially constructed UCNPs that is $NaNdF_4$:Yb@$NaYF_4$:Yb,Tm@$NaYF_4$@$NaYF_4$:Yb,Ho,Ce@$NaYF_4$, which could be treated as the combination of two system that are $NaNdF_4$:Yb@$NaYF_4$:Yb,Tm@$NaYF_4$ that could be excited by 808 nm laser with blue emission (Tm^{3+}, 450 nm 475 nm) while the $NaYF_4$:Yb,Ho,Ce@$NaYF_4$ could be controlled by the 980 nm pulsed laser with green and red emission with adjusting ratio [8].

The basic principle in the research work could be conclude as: the blue (450 nm, 475 nm) emission under 808 nm excitation is ascribed to Nd^{3+}-sensitization system that is, Nd^{3+} ions absorb the 808 nm photons and transfer to Yb^{3+} by $Nd^{3+}\rightarrow Yb^{3+}$ energy transfer, further sensitizes on Tm^{3+} with emission of $^1G_4$ state; the key mechanism in the system that modulate the red/green emissions could be concluded as: Ho^{3+} emissions could be interpreted to be affected by the Ho^{3+}-Ce^{3+} cross-relaxation under excitation of 980 nm pulsed laser, as the authors have stated that: “non-steady-state upconversion process, in which deactivation of the excitation energy and the energy transfer process occur at different rates. The modulation on the emission color, as shown in Figure 3(a-d). As the population of excited states at a particular energy level requires sequential pumping of its lower-lying energy levels, activator emission from distinct energy levels may take place at different time intervals. It is important to note that, because of the complex radiative and non-radiative transitions of the 4f electrons in excited lanthanide ions, it may take several milliseconds for the population of different energy levels to reach their steady states." [8] As shown in Figure 3, the green emission is emitted by the Ho^{3+} $^5F_4$, $^5S_4$ energy level by two-phonon upconversion process and the red emission is emitted by the Ho^{3+} $^5F_5$ energy level two-phonon upconversion process. The difference in the two upconversion processes could be concluded as the non-radiative transition in the upconversion process that is $^5I_6 \rightarrow {}^5I_7$, that exist in the upconversion process of red emission, which further make the difference of emitting rate between the green emission and red emission, although it is still a very low process. And the Ce^{3+} is used to facilitate the "quenching factor" on Ho^{3+}, for the Ho^{3+}-Ce^{3+} cross relaxation. And the result is shown in Figure 3(d), longer width modulation of the 980 nm laser, the larger partition of red emission, for the longer width pulsed 980 nm laser allows the non-radiative transition that cased by Ho^{3+}-Ce^{3+} cross-relaxation with the proof of the lifetime dependence emission spectra.

Ref:

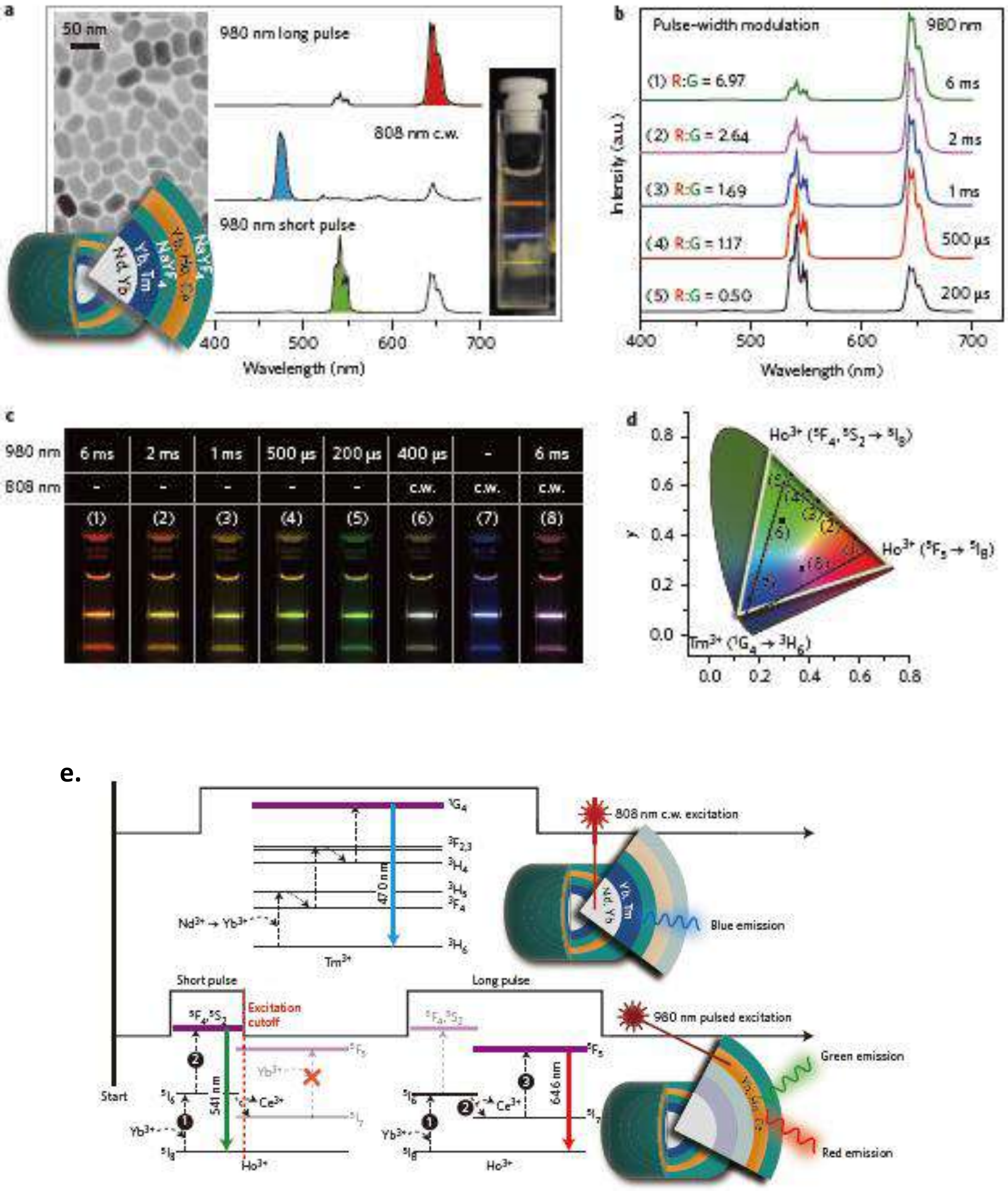

Figure 3. Design and mechanism of the core-multishells UCNs with color-tenability under excitation of 808 nm C.W. laser and 980 nm pulsed laser [8]

As shown in Figure 4 (a), in the measurement range of 10 ms, the decay curve of the green emission shows a sharper decay than the red emission which illustrating the non-steady state upconversion process that enhances the red emission by quenching the green emission which is in coincidence with the variation of Ig/r to the pulse width, as shown in Figure 4 (b) [8] Furthermore, the two-phonons process of the upconversion process is illustrated by Figure 4 (b), which is the calibration curve of the log(intensity)-log(power density) and the slope is about 2; as displayed in Figure 4 (d), the ratio of green emission to red emission do not change with various of powder density, which means that the intensity of the laser source has no influence on the peak area ratio.

Ref:

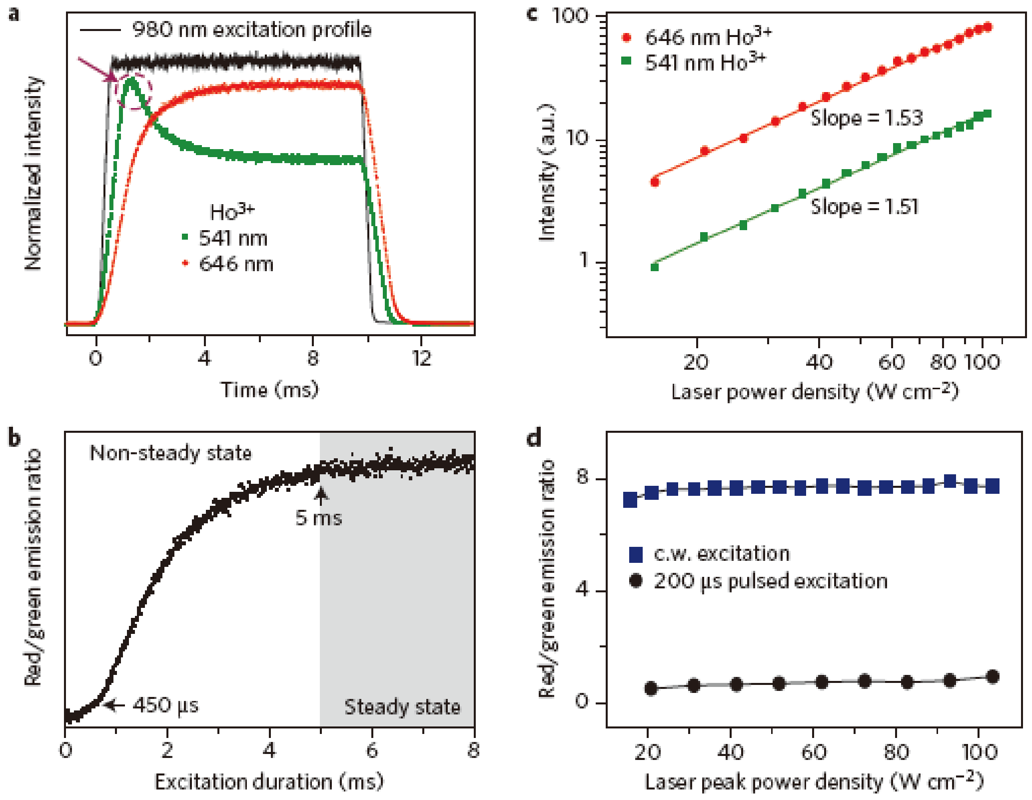

Figure 4. Mechanism investigation on the non-steady controlled UCNPs on by the time-dependent spectrum (a), plotting of the lg (power density)-lg (luminescent intensity)(b), the relationship between Ig/Ir and pulse width (c) and power density (d).

For the applications of the RGB modulation system, as shown in Figure 5, by the excitation of 808 nm c.w. laser along with the 980 nm pulsed laser, with the principle of RGB, the full coloring displays has been realized by the 3D-printer, that is every additive color model in which red, green and blue light are added together in various ways to reproduce a broad array of colors.[8]

Ref:

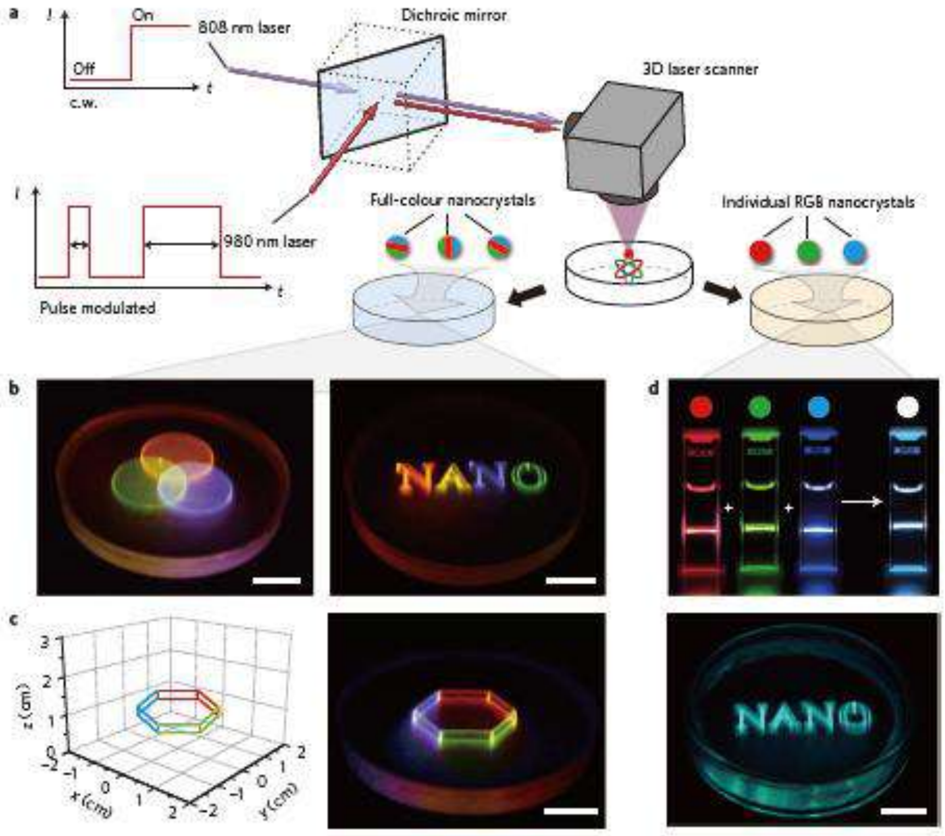

Figure 5. Utilization of the steady and non-steady modulation upconversion in 3D-scanner. [8]

To construct the UV/visible tunable system by isolated 808 nm/980 nm sensitized dual-system model:

As reported by Prof. C.H. Yan's group, in their work on "luminescence-driven reversible handedness inversion of self-organized helical superstructures enabled by a novel near-infrared light nanotransducer", a novel structure has been proposed that is $NaNdF_4$@$NaYF_4$:Yb,Tm@$NaYF_4$@$NaGdF_4$:Yb,Er@$NaYF_4$, with ultraviolet (290 nm,310 nm , 345 nm and 364 nm) and blue emission under excitation of 808 nm C.W. laser and green/red emission under 980 nm laser. The nanostructure could be treated as being composed with two parts: $NaNdF_4$@$NaYF_4$:Yb,Tm@$NaYF_4$ which is mainly used to generate ultraviolet emission; and $NaGdF_4$:Yb,Er@$NaYF_4$ which is mainly used to generate visible emission. And it is designed to drive the chiral photoisomerizable molecular, that is the photo-responsive cholesteric LCs (CLCs), with the closed form under ultraviolet and open form und visible light. Furthermore, the UCNPs directs self-organized supramolecular architectures of LCs as shown in Figure 6 c. The advantages for developing the UCNPs to directs the supramolecular architectures is that it utilized the NIR lasers to generate the UV and visible light instead of the high-energy of UV avoiding material damage. As shown in Figure 7, under the 808 nm and 980 nm excitation, the effect of the obtained UCNPs is shown. Conclusively, a convenient and versatile pathway has been invented for the spatially and temporally regulating the self-organized helical photonic superstructures.[9]

Ref:

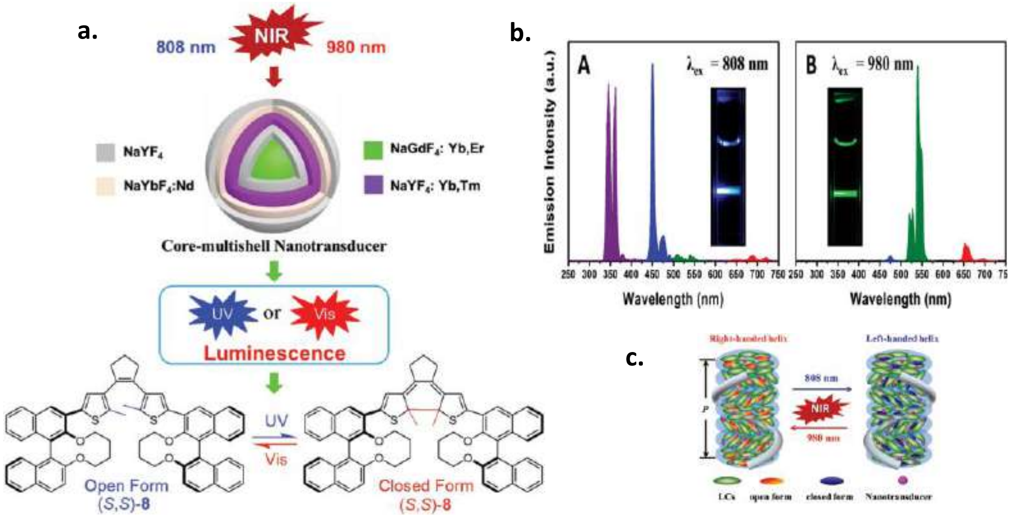

Figure 6. (a). Design of the core-multishells UCNPs with light driven on the photo-responsive cholesteric LCs (CLCs) and (c) the structure and the stimuli-directing self-organized supramolecular architectures of the LCs. (b) emission spectra of the UCNPs under 980 nm C.W. laser and the 808 nm C.W. laser. [9]

Ref:

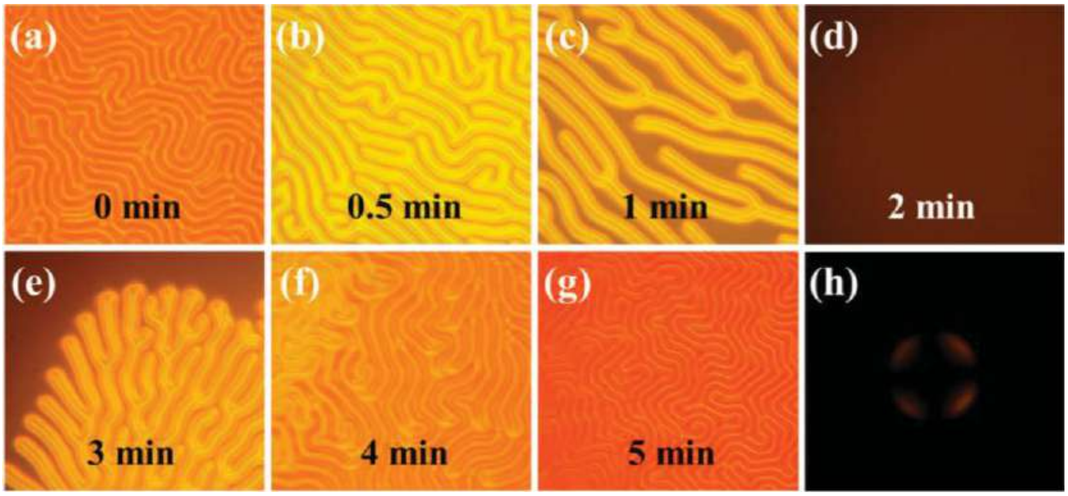

Figure 7. Effect of the UCNPs on handedness inversion. 2 wt% (S ,S) -8 and 1.5 wt% nanotransducers in E7 was observed in a homeotropic cell upon 808 nm NIR laser irradiation (2 W) from right-handed (a-c) to left-handed CLC (e-g) through a transient nematic phase (d), observed using a crossed polarized transmissive mode optical microscopy. (h). Conoscopic observation of the transient nematic state (d). [9]

Here, we would like to put forward the concept of **Luminescent Janus** UCNPs, which is defined as: the same nanoparticles (UCNPs) showing various luminescent properties, mainly on the luminescence performance depending on the various photo-luminescence source with different on the photons energy/wavelength and pulse width.

Also, we would like to summarize the method to construct the Luminescent Janus UCNPs as: a. by the cross-relaxation that quenches the activators; b. by the segregated UCNPs system with different photo-luminescence source; c. to tune the emission color by certain energy transfer such as Tb^{3+}→Eu^{3+} energy transfer.

Additionally, we have just proposed to doping the UCNPs with different emission performance with certain ratios, however, it is not appropriate in the application for the activators of the UCNPs seldom emits single bandwidths, for Er^{3+} and Ho^{3+} emitting red/green emission, Tm^{3+} emitting blue/red emission, for Eu^{3+} and Tb^{3+} although displaying the individual emission colors (red or green), the EMU system (as we discussed in Chapter 3) that sensitize them always shows Tm^{3+} blue emission for the acting as the activator.

5.3. Type I Luminescent Janus UCNPs: New invention on Green-Red emission tunable color model by 808 nm pulsed laser

As illuminated by the steady and un-steady upconversion process with excitation of 980 nm laser which is result in the Ho^{3+}-Ce^{3+} cross-relaxation enhanced deactivated upconversion process.

We have developed Nd^{3+}-trinity system coated $NaGdF_4$:Yb,Ho,Ce, that is $NaGdF_4$:Yb,Ho,Ce@$NaGdF_4$:Yb,$Nd_{20\,\%}$@$NaGdF_4$, with excitation of 808 nm pulsed laser. The Nd^{3+}-trinity system that is the Nd^{3+}-harvest-transfer-sensitization system, which we have fully illustrated on the design in Chapter 1. As shown in Figure 8, that is the design of the Nd^{3+}-Trinity system coated Ho^{3+}-Ce^{3+} R-G model with modulation on green and red emission which is with the prolong of the laser width, the red emission has a larger partition, which is in consistence with the mechanism that we propose.

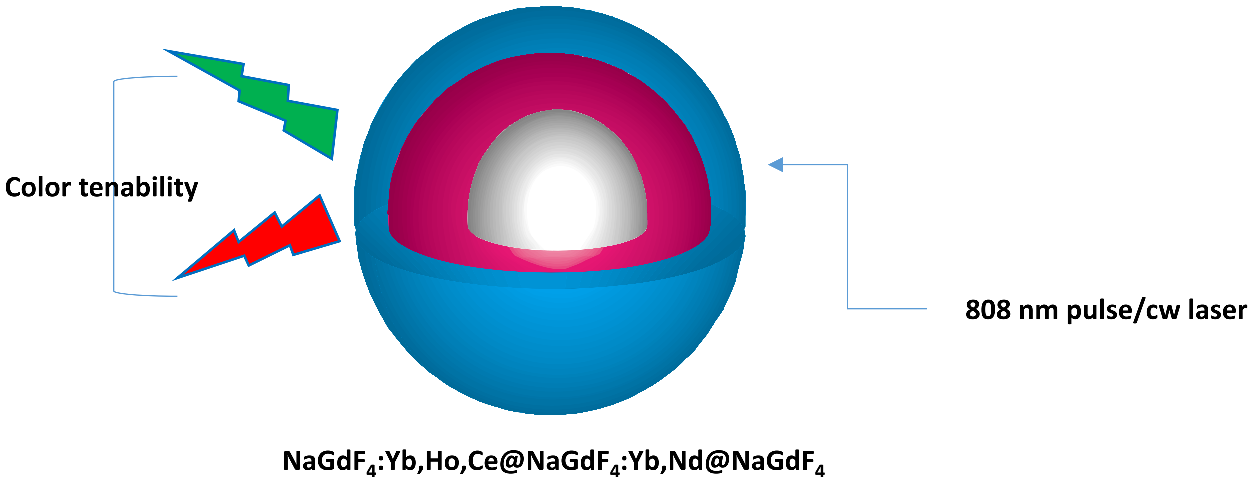

Figure 8. Design of the Nd^{3+}-Trinity system coated Ho^{3+}-Ce^{3+} modulated by 808 nm pulsed laser.

There have been numerous reports on the Ho^{3+}-Ce^{3+} cross-relaxation, which could be concluded as Ce^{3+}-Ho^{3+}: Ho^{3+} $^5I_6$ +Ce^{3+} $^2F_{5/2}$→Ho^{3+} $^5I_8$ +Ce^{3+} $^2F_{7/2}$, and Ce^{3+}-Ho^{3+}: Ho^{3+} $^5F_4$, $^5S_2$ +Ce^{3+} $^2F_{5/2}$→Ho^{3+} $^5I_8$ +Ce^{3+} $^2F_{7/2}$ [10]. In the upconversion process of the certain amount Ce^{3+} doped $NaYF_4$:Yb, Ho core, the Ho^{3+}-Ce^{3+} cross-relaxation makes the whole process are prone to emit red emission (655 nm, Ho^{3+} $^5F_5$→$^5I_8$), thus make the R-G ratio of Ho^{3+} could the altered by adjusting the concentration of the Ce^{3+} doping. As shown in Figure 10, by adjusting the Ce^{3+} doping concentration in the rang that is 0, 4, 6, 8, 12 %, the red emission shows apparent enhancement thus the emission color has been changesfrom green to red. In our view mind, the research work that on the Ce^{3+} doping $NaYF_4$:Yb, Ho^{3+} should be treated as the foundation of the un-steady laser modulation on the emission colors.

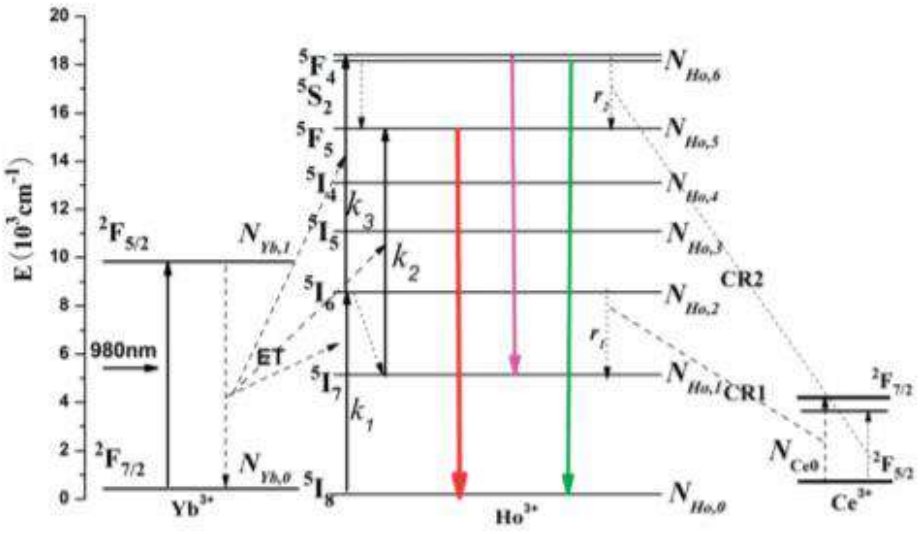

Figure 9. Ho^{3+}-Ce^{3+} cross-relaxation [10]

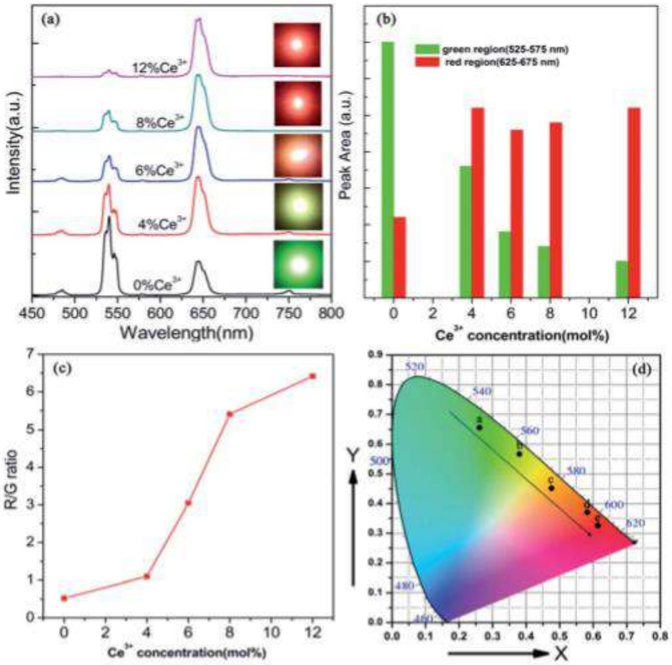

Figure 10. Emission spectra (a), peak area ratio (b), relationship between Ce^{3+} concentration and R/G ratio (c) and CIE chromatography (d) of the Ce^{3+} doped $NaYF_4$: Yb,Ho UCNPs with variation form 0, 4, 6, 8, 12 mmol %. [10]

$$\mathrm{Ho}^{3+}(^{5}\mathrm{I}_{8}): \quad \frac{dn_0}{dt} = w_4 n_4 + w_3 n_3 - u_1 n_{Yb1} n_0 \qquad \text{Eq. S1}$$

$$\mathrm{Ho}^{3+}(^{5}\mathrm{I}_{7}): \quad \frac{dn_1}{dt} = s_1 n_{Ce0} n_2 - w_1 n_1 - u_3 n_{Yb1} n_1 \qquad \text{Eq. S2}$$

$$\mathrm{Ho}^{3+}(^{5}\mathrm{I}_{6}): \quad \frac{dn_2}{dt} = u_1 n_{Yb1} n_0 - w_2 n_2 - u_2 n_{Yb1} n_2 - s_1 n_{Ce0} n_2 \qquad \text{Eq. S3}$$

$$\mathrm{Ho}^{3+}(^{5}\mathrm{F}_{5}): \quad \frac{dn_3}{dt} = u_3 n_{Yb1} n_1 + s_2 n_{Ce0} n_4 - w_3 n_3 \qquad \text{Eq. S4}$$

$$\mathrm{Ho}^{3+}(^{5}\mathrm{F}_{4}, {}^{5}\mathrm{S}_{2}): \quad \frac{dn_4}{dt} = u_2 n_{Yb1} n_2 - w_4 n_4 - s_2 n_{Ce0} n_4 \qquad \text{Eq. S5}$$

$$\mathrm{Y}b^{3+}(^{2}\mathrm{F}_{5/2}): \quad \frac{dn_{Yb1}}{dt} = \sigma_{Yb} I n_{Yb0} - w_{Yb1} n_{Yb1} - u_1 n_{Yb1} n_0 - u_2 n_{Yb1} n_2 - u_3 n_{Yb1} n_1 \qquad \text{Eq. S6}$$

$$\mathrm{Y}b^{3+}(^{2}\mathrm{F}_{7/2}): \quad \frac{dn_{Yb0}}{dt} = -\frac{dn_{Yb1}}{dt} \qquad \text{Eq. S7}$$

$$n_{Ho} = n_0 + n_1 + n_2 + n_3 + n_4 \qquad \text{Eq. S8}$$

$$n_{Yb} = n_{Yb0} + n_{Yb1} \qquad \text{Eq. S9}$$

Figure 11. The proposed mechanism on the Ce^{3+} tenability on the Ho^{3+} emission.

And we would like to propose the mechanism of the Nd^{3+}-Trinity system sensitized Ho^{3+}-Ce^{3+} UCNPs with 808 nm pulsed laser modulation as : with Nd^{3+} ions absorbs the 808 nm photons, and transferring to Yb^{3+} ions by Nd^{3+}→Yb^{3+} energy transfer, [11, 12], the Yb^{3+} ions transfer phonons to Ho^{3+}. By absorbing 2 photons, the ETU process occurs along with the Ho^{3+}-Ce^{3+} cross-relaxation. Similarly with the research on the 980 nm pulsed laser modulated NaYF$_4$:Yb, Ho, Ce, the 808 nm pulsed laser modulated Nd^{3+}-Trinity system sensitized Ho^{3+}-Ce^{3+} UCNPs are sensitive to the 808 nm pulsed laser on the width, which determines if the cross-relaxation will happen and further induce a larger partition of red emission. As shown in Figure 11, the proposed mechanism could be illustrated as the cutting off effect on the Ho^{3+}-Ce^{3+} cross-relaxation by the pulsed laser: for the deactivation of the excitation energy of the green emission and red emission; at the same time, the energy transfer process occurs at difference rate, including the radiative and non-radiative transition. The inducing of the Ho^{3+}-Ce^{3+} cross-relaxation benefits the difference in PA (phonon avalanche) process, and further forms the cut-off effect of the pulsed laser.

And the energy transfer process of $Nd^{3+} \rightarrow Yb^{3+} \rightarrow Ho^{3+}$ has never been affected by the cut-off effect for the reason that compares with process of the cross-relaxation that is in the range of ~ milliseconds, the process of energy transfer is a fast process which is in the range of ~ femtosecond, including the $Nd^{3+} \rightarrow Yb^{3+}$ energy transfer and the $Yb^{3+} \rightarrow Ho^{3+}$ energy transfer that result in the ETU process.

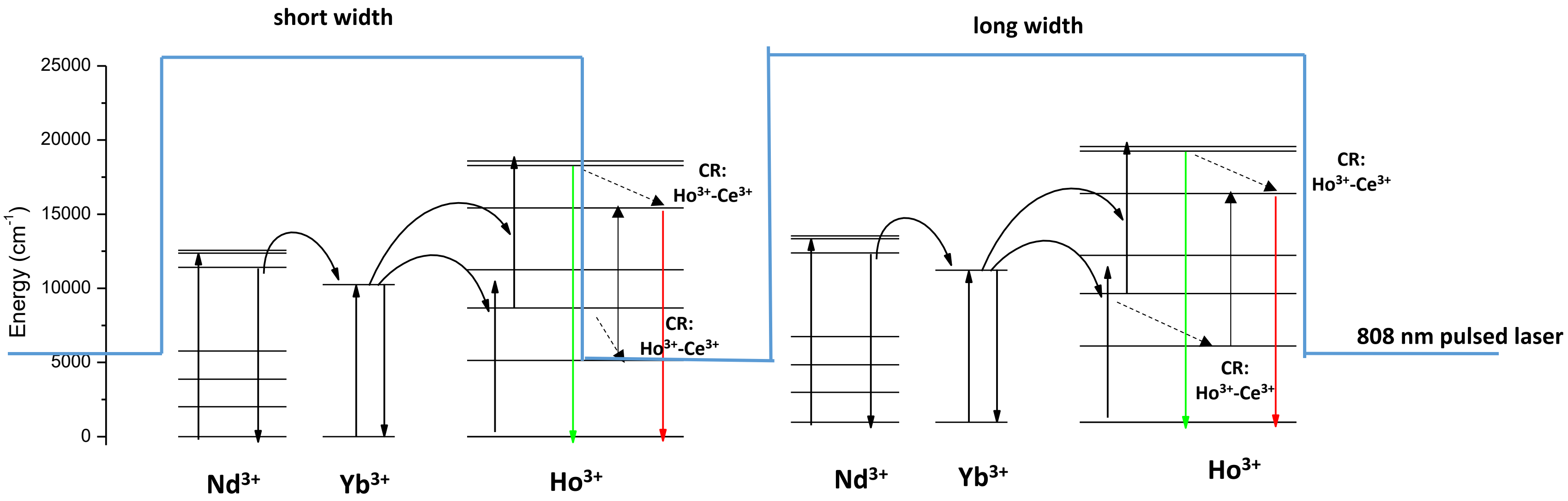

Figure 11. Proposed mechanism of the 808 nm pulsed laser induced modulation

The characterization on morphology could be seen in Figure 12, that are TEM images to characterize the size growth: 6.43±0.99 nm for the NaGdF$_4$:Yb,Ho core, 9.11±1.05 nm for the NaGdF$_4$:Yb$_{20\,\%}$,Ho$_{2\,\%}$ @NaGdF$_4$:Yb$_{10\,\%}$,Nd$_{20\,\%}$ core/shell (CS) structure, 12.44 ±1.03 nm for the NaGdF$_4$:Yb$_{20\,\%}$,Ho$_{2\,\%}$@NaGdF$_4$:Yb$_{10\,\%}$,Nd$_{20\,\%}$@NaGdF$_4$ core/shell/shell (CSS) structure.

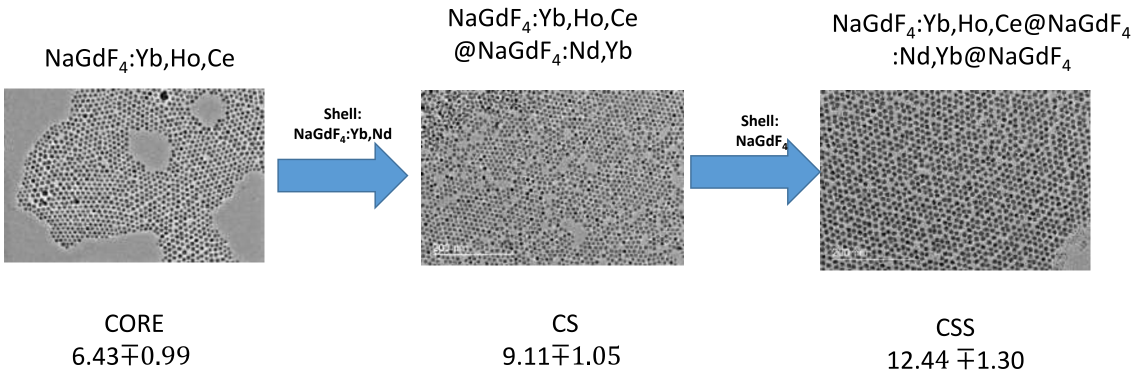

Figure 12. TEM images of the Nd^{3+}-Trinity system coated NaGdF$_4$:Yb, Ho, Ce UCNPs .

The 808 nm modulation of R-G model has been realized by the 808 nm pulsed laser, with the tenability on the pulse width: 0.25, 0.50. 0.75, 1, 2 ms and c.w.. with the vibration of the ratio green emission to red emission (f $_{g/r}$), that is 0.42, 0.37, 0.33, 0.31, 0.26, 0.22, illustrating the longer pulse width makes the red emission prone to emit while the shorter pulse width make the green emission prone to emit that is in coincidence with the mechanism that we have proposed above, with the change of the emission color form yellow to red.

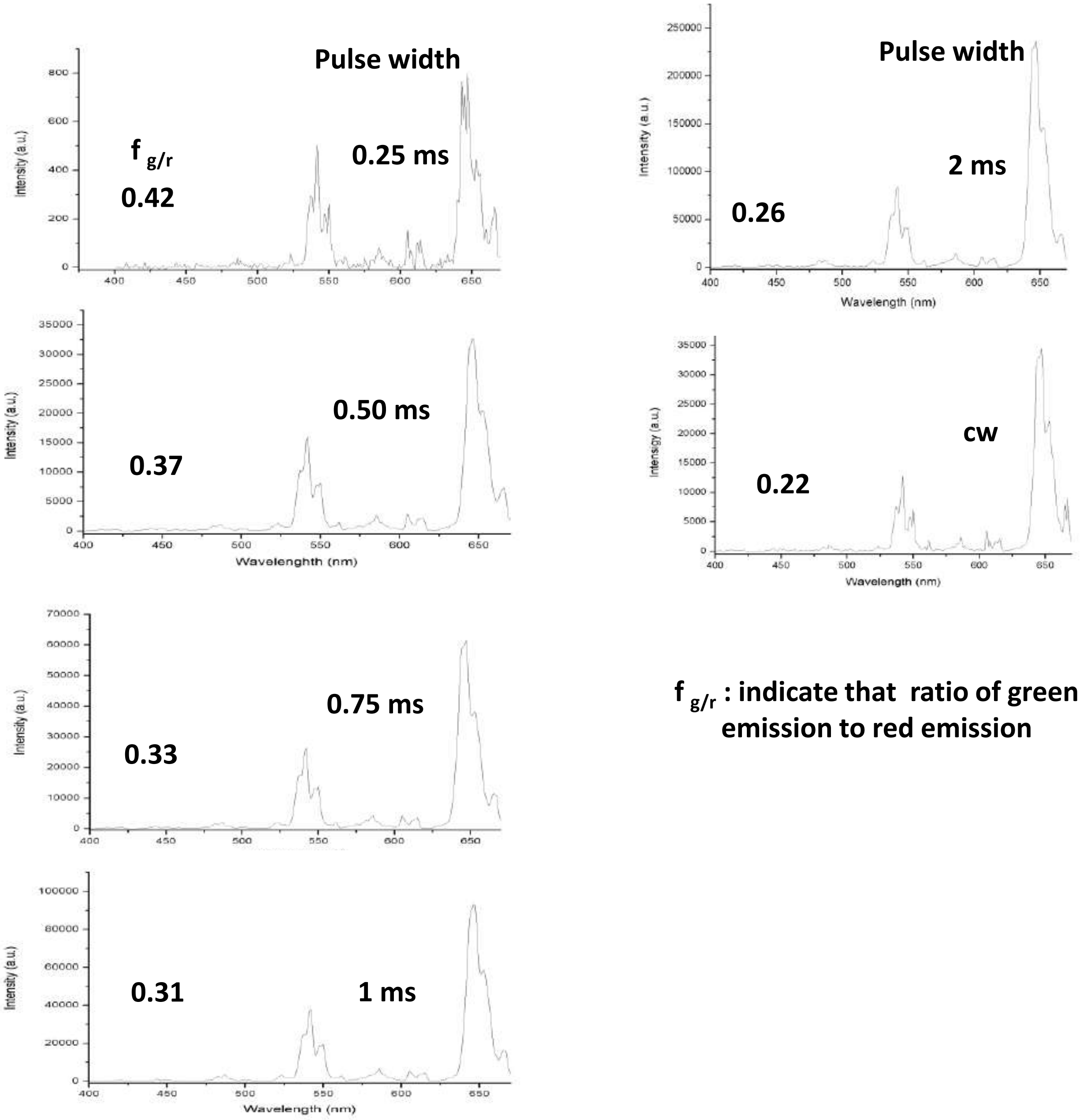

Figure 13. Emission spectra of the Nd^{3+}-Trinity system sensitized Ho^{3+}-Ce^{3+} system with excitation of the pulsed/c.w. 808 nm laser.

5.4. Type II Luminescent Janus UCNPs: UV-VIS tunable model/ RGB tunable color model initiate by EMU system under 980 nm pulsed laser

As shown in Figure 14, the design of the Type I Luminescent Janus Nanoparticles, is the conjugation of the Type II Nd^{3+}-Trinity system (as discussed Chapter 2) coating on the $NaGdF_4$:Yb, Er, and the EMU system with the activator of Eu^{3+} [13], with the nanostructure as $NaGdF_4$:Yb,Er@$NaGdF_4$:Yb,Nd@$NaGdF_4$@$NaGdF_4$:Yb,Tm@$NaGdF_4$:Eu, sub-15 nm as shown in Figure 15. It complies with the concept of Luminescent Janus: when excited by 808 nm c.w. laser, it displays the emission of green (Er^{3+}: 525 and 545 nm) and red (Er^{3+}:645 nm) emission by the layers of $NaGdF_4$:Yb,Er@$NaGdF_4$:Yb,Nd@$NaGdF_4$; when excited by 980 nm pulsed/c.w. laser, it shows multiple emission color that is red (Eu^{3+} 592 nm, Eu^{3+} 615, Er^{3+} 645 and Tm^{3+} 655 nm), green (525 nm 545 nm) and blue (Tm^{3+} 450 nm and 475 nm) along with the ultraviolet emission (290, 310, 345 and 364 nm) by the layers of $NaGdF_4$:Yb,Tm@$NaGdF_4$:Eu. Additionally, the third layer that is the $NaGdF_4$ is the displays as the “segregation layer” that makes the Nd^{3+}-Trinity system with activator of Er^{3+} and EMU system with activator of Eu^{3+} [13] independently, which means the energy transfer between the two systems has been completely cut off. The full-color emission also shows tenability on RGB by the excitation of 980 nm pulsed laser, with the changing of emission colors.

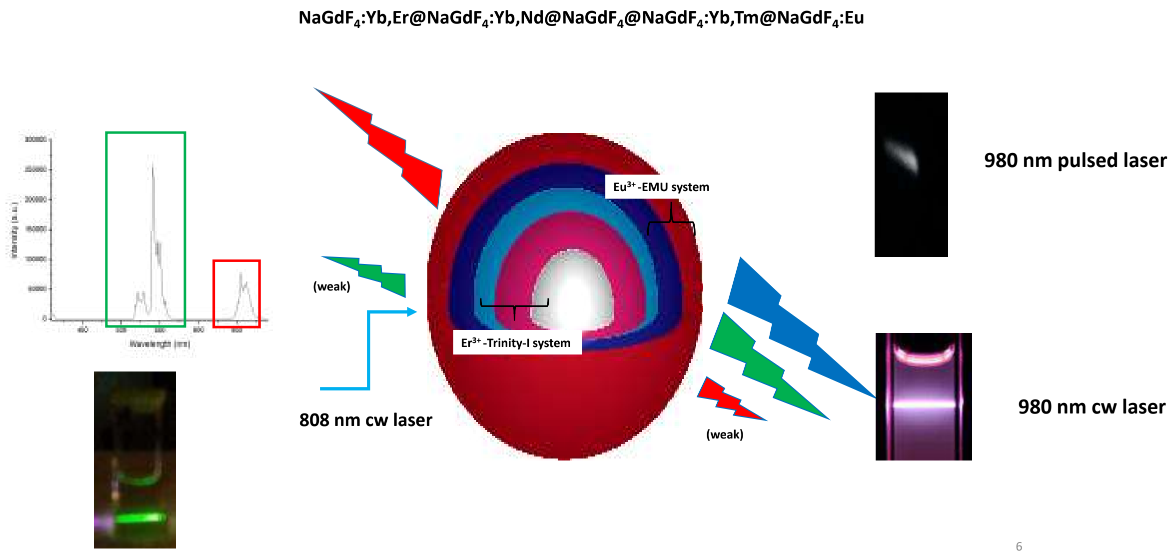

Figure 14. Design of the Type II Luminescent Janus UCNPs and the luminescence performance.

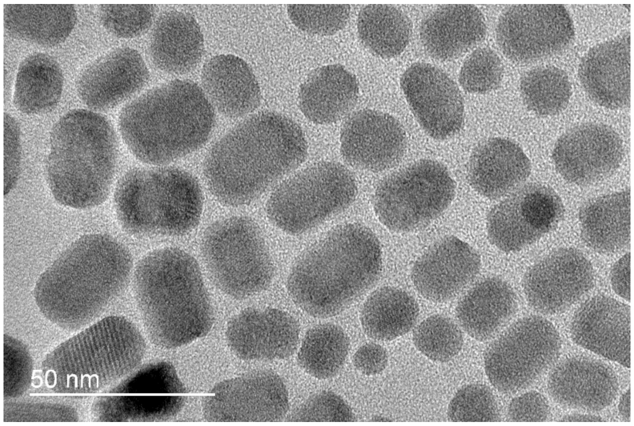

Figure 15. TEM images of the Luminescent Janus UCNPs that is $NaGdF_4$:Yb, Er@$NaGdF_4$:Yb, Nd@$NaGdF_4$@$NaGdF_4$:Yb, Tm@$NaGdF_4$:Eu.

As shown in Figure 16, when under excitation of the pulsed laser of 980 nm with the variation of the pulse width for 0.25 ms to 7 ms, the emission color shows tenability form white to violet, which could be illustrated by the tenability of the emission peaks of RGB: when excited by the short pulse width 980 nm laser, the EMU system shows weak emission, which is the same as the Er^{3+} emission; besides, the EMU system shows higher intensity of the 4-phonons ETU process induced blue emission rather than the 3-photons blue emission and red emission, with the white emission color; however, when the system is excited by the 980 nm pulsed laser that is 7 ms, the system shows violet emission, which is composed by the weak Er^{3+} green emission and the strong red and blue emission by the EMU system, for under the longer puled width excitation, the EMU system shows stronger emission, along with the stronger 4-phonons ETU process induced blue/red emission and the 5-phonons ETU process induced Eu^{3+} red emission.

What we would conclude from the emission spectra is that: in the EMU system, with longer width of the pulsed laser, with easier happening of the 5-phonon ETU process, which is result in the larger partition of Eu^{3+} emission; with shorter width of the pulsed laser, with less chance to happen the 5-phonon ETU process, which result in the Tm^{3+} 3-phonon and 4-phonon blue emission in lager partition.

Here, we would like to summarize that for the variation of the of the 3/4/5-photon ETU process emission, the ratio of the red and blue emission could be adjusted by the width of the pulsed laser, as well as the addition of the Er^{3+} emission intensity shows enhancement with longer width pulsed laser, the UCNPs under 980 nm excitation is a full-color emitting with tenability that is from white to red/violet and the green emission of Er^{3+} under 808 nm excitation.

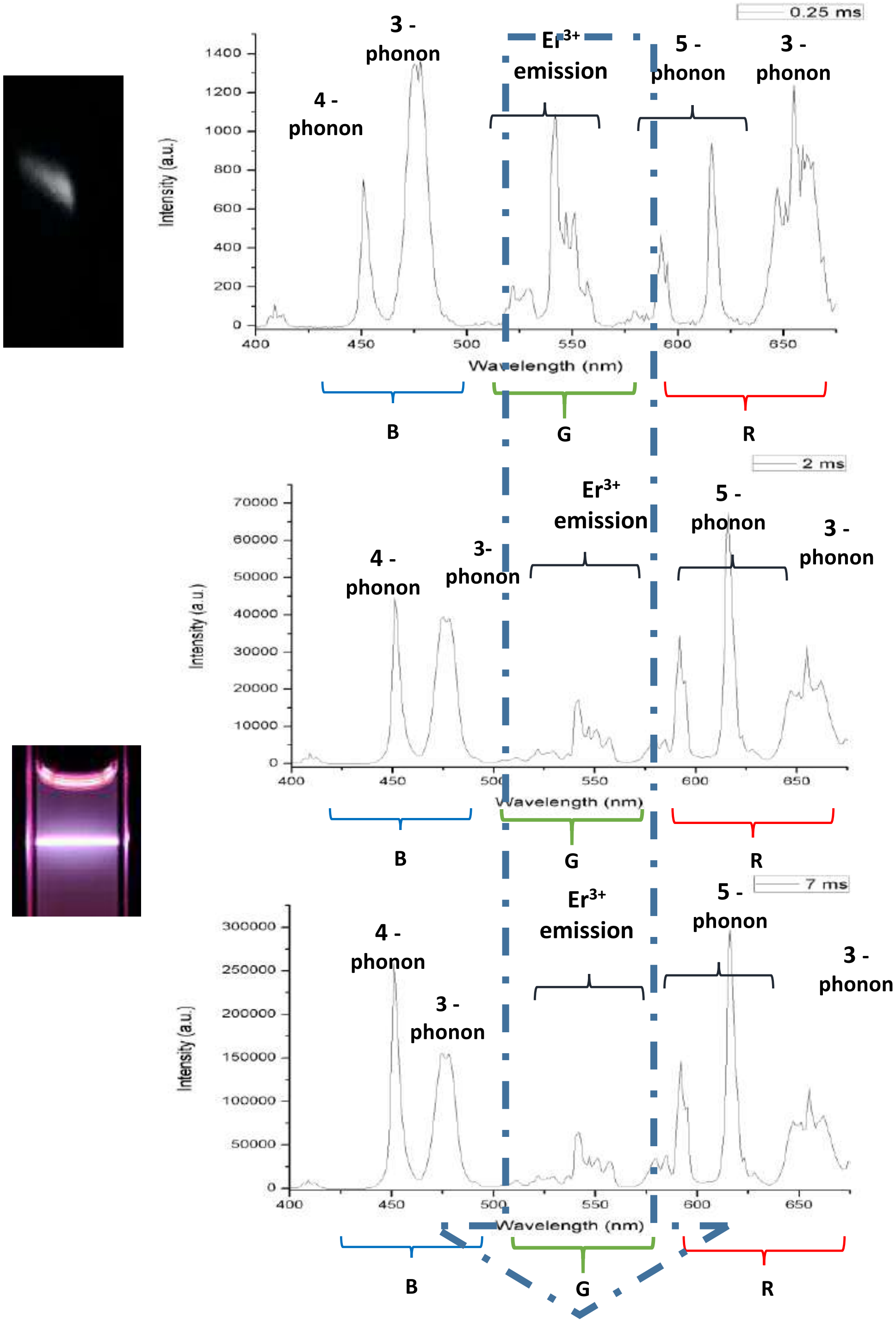

Dramatically decreased green emission ratio!

Figure 16. Emission spectra of the Type II Luminescent Janus UCNPs with 980 nm pulsed laser excitation

Mechanism investigation

And here comes the question: why the non-steady state 980 nm laser could modulate the EMU system? By fully understanding of the mechanism of the EMU system, we would like propose that the in the ladder-like Tm^{3+} energy levels, the ETU process that caused by the ETU process that induced by Yb^{3+} energy transfer, at the same time, affected by the Yb^{3+}-Tm^{3+} energy back-transfer, that is the Yb^{3+}-Tm^{3+} cross-relaxation. And it is very similar with the Ho^{3+}-Ce^{3+} system, for the Ho^{3+}-Ce^{3+} cross-relaxation has caused the ETU process sensitive to the pulsed laser on the pulse width of the 980 nm laser. Furthermore, we would like to conclude that the reason that 980 nm laser could modulate the ETU process of Tm^{3+} and further modulate the emission of the EMU system, is that: the difference in rate between the Yb^{3+}-Tm^{3+} with is in the scale of femtoseconds(10^{-15} s) and the Tm^{3+}-Yb^{3+} cross-relaxation in the folds of milliseconds(10^{-3} s), that could be illustrated as the difference of "very fast" which cannot be affected by the pulse width and "comparably slow" which shows conspicuous effect when the pulse width is shorter than the lifetime of the excited state of activators that induced by the ETU process.

Additionally, the difference between the Ho^{3+}-Ce^{3+} system and the ETU system is that: in the upconversion process of Ho^{3+}, the Ho^{3+}-Ce^{3+} cross-relaxation should be induced by doping Ce^{3+} ions, in contrast with EMU system that is the with existence of the Tm^{3+}-Yb^{3+} cross-relaxation itself, for the difference of ETU process: the red/green emission of Ho^{3+} activators are emitted by the same excited cross-relaxation with the difference of the non-radiative transition; while in the EMU system, the emissions are emitted by 3-phonon, 4-phonon and 5-phonon ETU process, namely the red /blue emission and Eu^{3+} red emission are emitted by different excited state. And the different is induced by the numbers of phonons that participated in the ETU process of Tm^{3+}. That is why the EMU system are "born" to be sensitive with the 980 nm pulsed laser.

Furthermore, to support our proposed mechanism, we have established the EMU-Yb^{3+} surface quenching system with activator of Eu^{3+} that is doping certain amount of 5 % Yb^{3+} ions in the shell layer of the EMU system, which is $NaGdF_4$:Yb, Tm @$NaGdF_4$:Yb (10 %), Eu (15 %); and the EMU and the EMU-Yb^{3+} surface quenching shielding system, that with a $NaGdF_4$ layer coating to shield the induced Yb^{3+} surface quenching, which is $NaGdF_4$:Yb, Tm@$NaGdF_4$:Yb (10 %), Eu (15 %)@$NaGdF_4$. The emission spectra under 980 nm pulsed laser with 0.25 ms, 2 ms and 7 ms are shown in Figure 17 and Figure 18. For the EMU system that inducing the Yb^{3+} surface quenching, not only the emission of the Eu^{3+} and Tm^{3+} under 980 nm c.w. excitation are quenched, but also the variation of the emission peak ratio of the EMU system under the 980 nm pulsed laser has been deactivated; however, when the Yb^{3+} surface quenching has been shielded by the $NaGdF_4$ coating, the variation of the emission peak ratio of the EMU system under the 980 nm pulsed laser has been activated again.

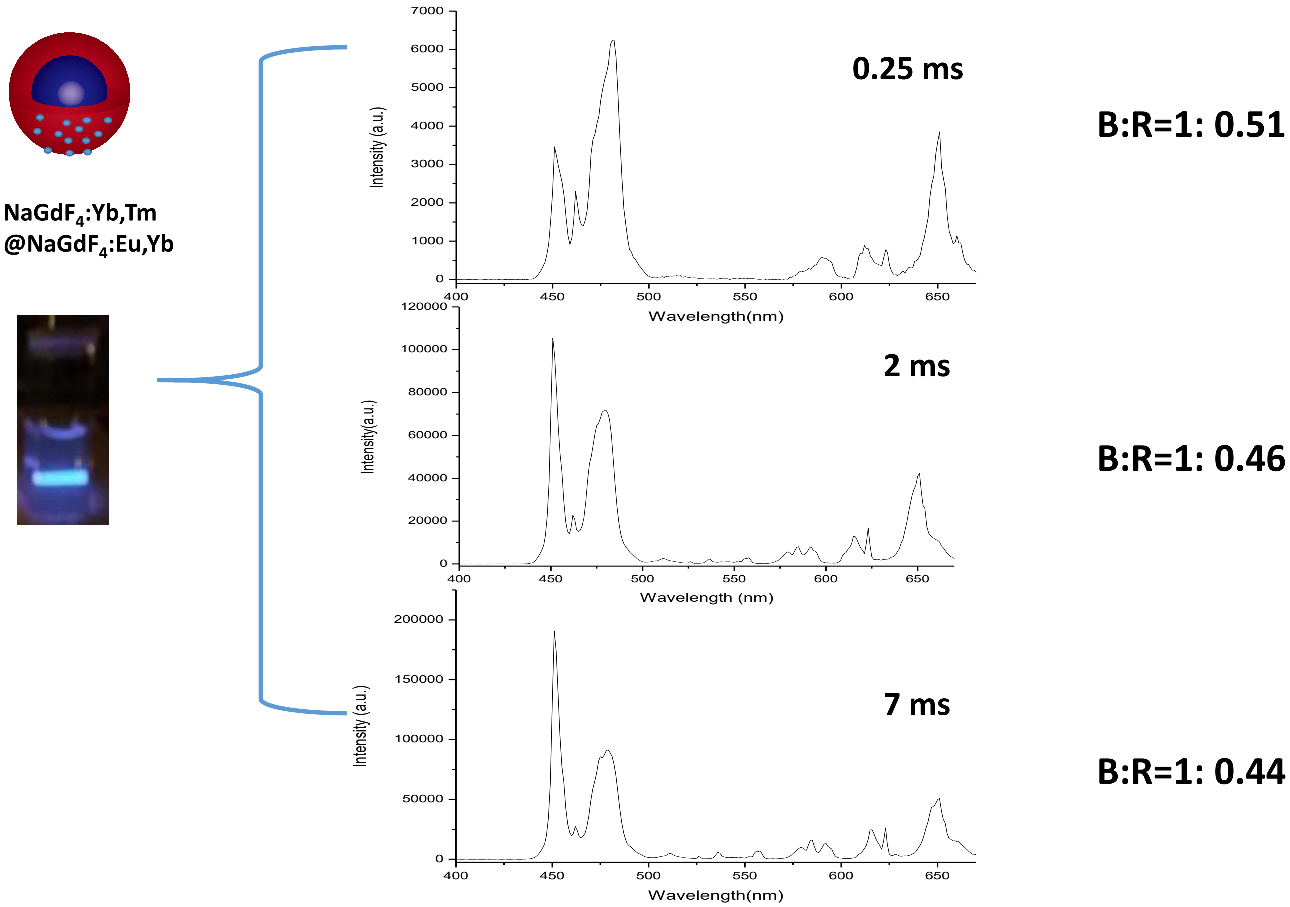

Figure 17. Emission spectra of the EMU-Yb^{3+} surface quenching system under excitation of 980 nm pulsed laser with the pulse width of 0.25 ms, 2 ms, and 7 ms.

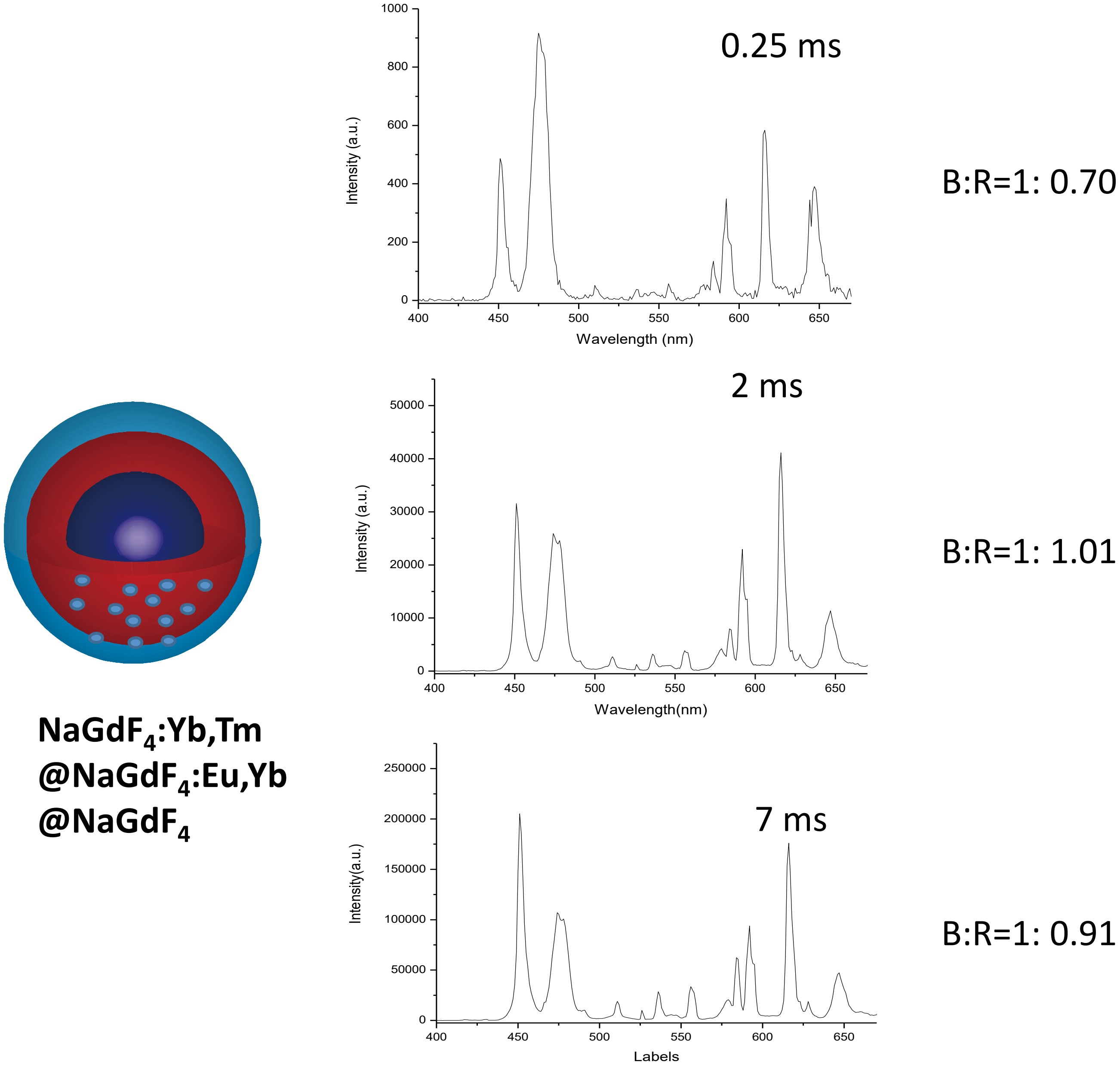

Figure 18. Emission spectra of the EMU-Yb^{3+} surface quenching shielding system under excitation of 980 nm pulsed laser with the pulse width of 0.25 ms, 2 ms, and 7 ms.

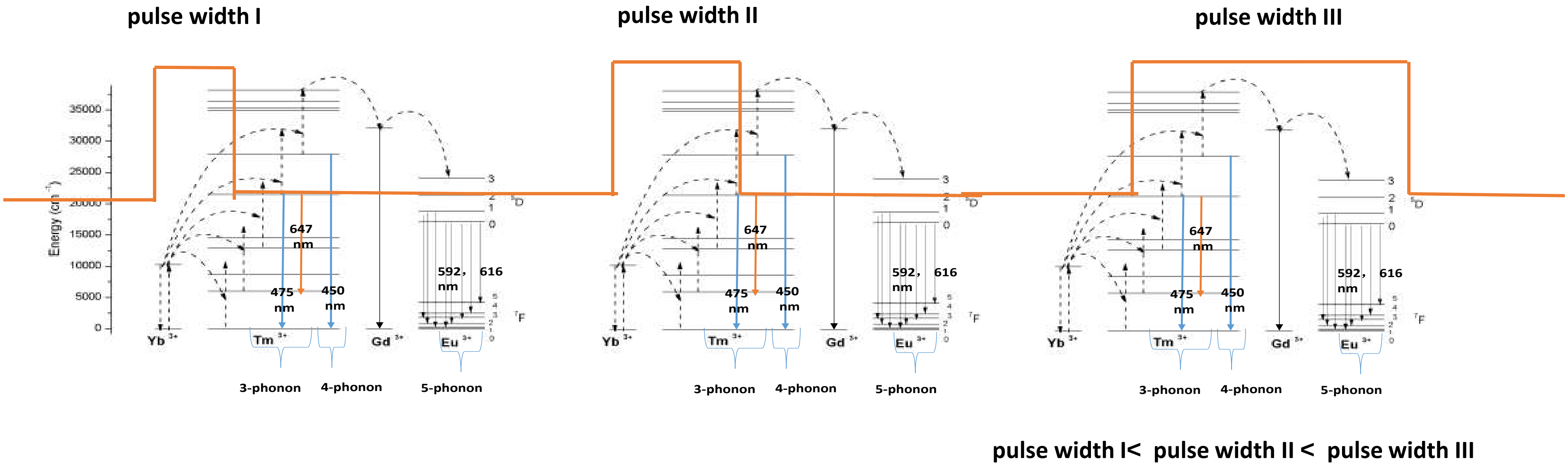

Figure 19. Mechanism of the EMU system sensitization with the 980 nm pulsed laser.

5.5. Type III Luminescent Janus UCNPs: RGB tunable color model initiate by EMU system under 980 nm and 808 nm pulsed laser

Another finding is that the EMU system with activator of Tb^{3+} is "born" to be a RGB nanoprobe for the reason that it displays blue (Tm^{3+}, 3-phonons and 4- phonon ETU process), green (Tb^{3+} emission) and red (Tm^{3+}, 3-phonon emission) emission; also, it is in coincidence with 980 nm pulsed laser modulation on the EMU system by the accumulation of Tm^{3+} by the 3-phonon, 4-phonon and 5 phonon ETU process.

The UCNPs that is EMU system with activator of Tb^{3+} with the nanostructure that is $NaGdF_4$:Yb,Tm@$NaGdF_4$:Yb, when excited by the 980 nm pulsed laser, shows the emission peak in variation, which is mainly on the ratio of green emission of Tb^{3+} (550 nm, $^5D_4 \rightarrow {}^7F_5$), that is with the larger emission ratio when the pulse width is prolonged.

Also, the phenomenon is found when UCNPs that is the Nd^{3+} -Trinity EMU system with activator of Tb^{3+} is excited by 808 nm pulsed laser.

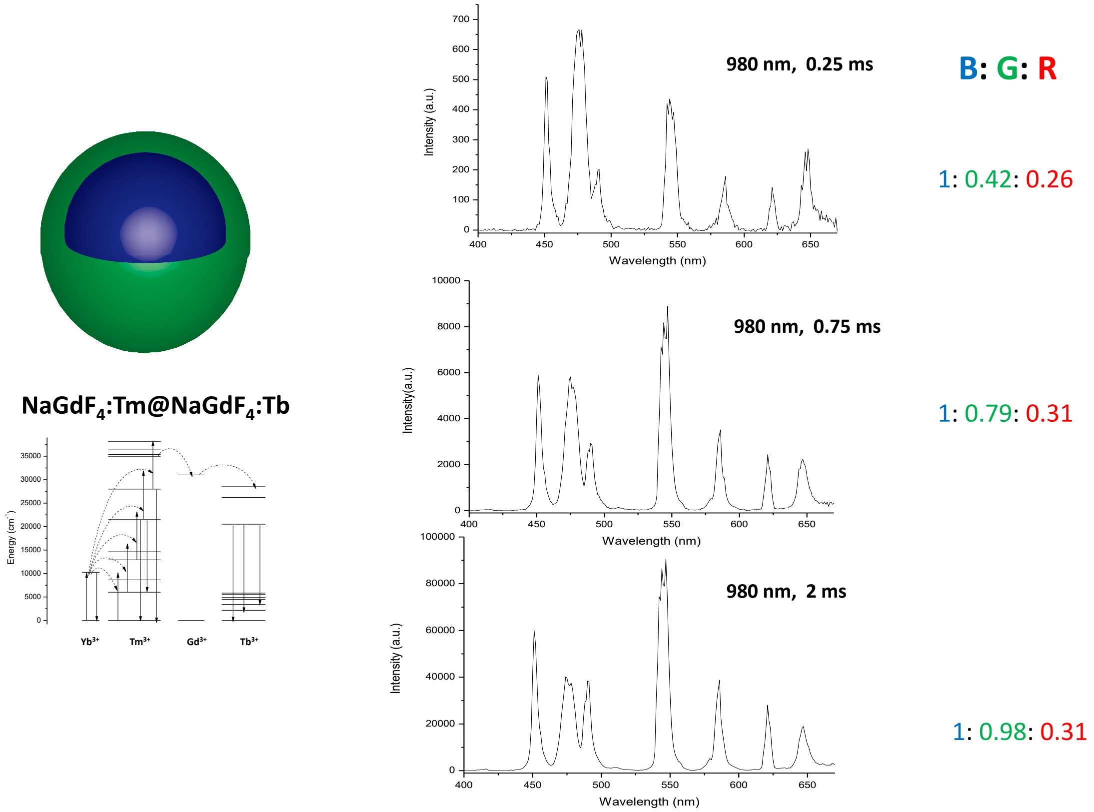

Figure 20. Emission spectra of the EMU system with activator of Tb^{3+} under excitation of 980 nm pulsed laser with the pulse width of 0.25 ms, 2 ms, and 7 ms.

5.6. Type IV Luminescent Janus UCNPs: RGB tunable color model initiate by EMU system under 980 nm and 808 nm pulsed laser and Tb^{3+}→Eu^{3+} interfacial energy transfer

The interfacial Tb^{3+}→Eu^{3+} energy transfer has been reported [14], which has illustrated that the Tb^{3+}→Eu^{3+} energy transfer could only occurs on the surface of the layers in the core-multishells layer of UCNPs. Also there have been numerous reports on the Tb^{3+}→Eu^{3+} energy transfer. In our view, the Tb^{3+}→Eu^{3+} energy transfer only occurs between the nearby Tb^{3+} and Eu^{3+} ions whanever they are stabled in the nanocrystals or act as Re^{3+} ions in the liquid solutions.

Moreover, we have conceived that utilizing the $Tb^{3+}\rightarrow Eu^{3+}$ energy transfer or the $Tb^{3+}\rightarrow Sm^{3+}$ energy transfer with the sensitization of EMU system to construct the RGB system for the blue emission of Tm^{3+}(450 nm and 475 nm) and Tb^{3+}(480 nm), green emission of Tb^{3+}(550 nm) and the red emission of Eu^{3+}(592 nm and 616 nm) and Tm^{3+}(655 nm).

The design of our investigation is that: a. 980 nm exited EMU system with activator of Tb^{3+}($NaGdF_4$:Yb $_{49\ \%}$,Tm $_{1\ \%}$@$NaGdF_4$:Tb $_{15\ \%}$) is used to sensitize the Eu^{3+} or Sm^{3+} by doping certain amount of Eu^{3+} or Sm^{3+} ions in the shell layer or warping a shell layer that is $NaGdF_4$:X(Eu/Sm)$^{3+}$ (15 %) that is $NaGdF_4$:Yb $_{49\ \%}$,Tm $_{1\ \%}$@$NaGdF_4$:Tb $_{15\ \%}$@ $NaGdF_4$:X(Eu/Sm)$^{3+}$ (15 %); b. 808 nm exited EMU system with activator of Tb^{3+}($NaGdF_4$:Yb $_{49\ \%}$,Tm $_{1\ \%}$@$NaGdF_4$:Tb $_{15\ \%}$) is used to sensitize the Eu^{3+} or Sm^{3+} by the same methods. As shown in Figure 21 and 22.

However, in our further investigation, we found that: a. for Sm^{3+} ions, it act as the EMU system killer for it quenches the ETU process for by its cross-relaxation between the multi-levels of ^4G_J and ^6H_J; b. for the Eu^{3+} ions, it shows strong luminescence when sensitized by the EMU system, while act as the EMU quencher when sensitized by Tb^{3+}. It has been investigated by the emission spectra:

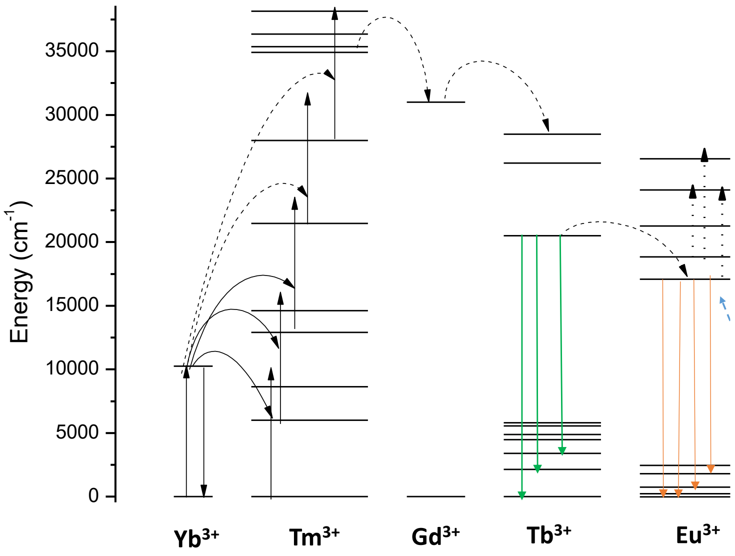

Figure 20. Interfacial Tb^{3+}→Eu^{3+} energy transfer with sensitization of EMU system with excitation of 980 nm laser

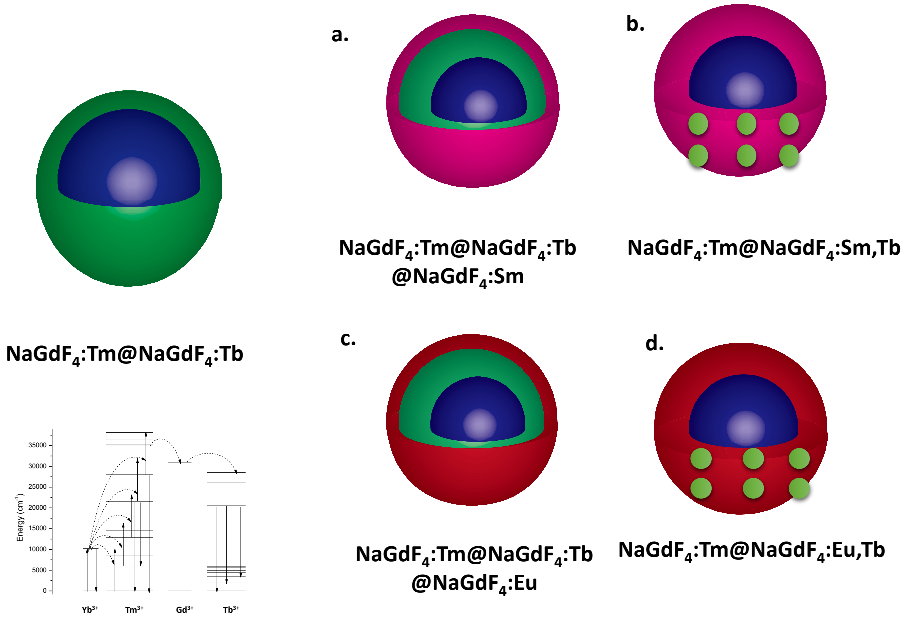

Figure 21. 980 nm excited EMU system with activator of Tb^{3+} utilized in the research of Tb^{3+}-Eu^{3+} and Tb^{3+}-Sm^{3+} energy transfer.

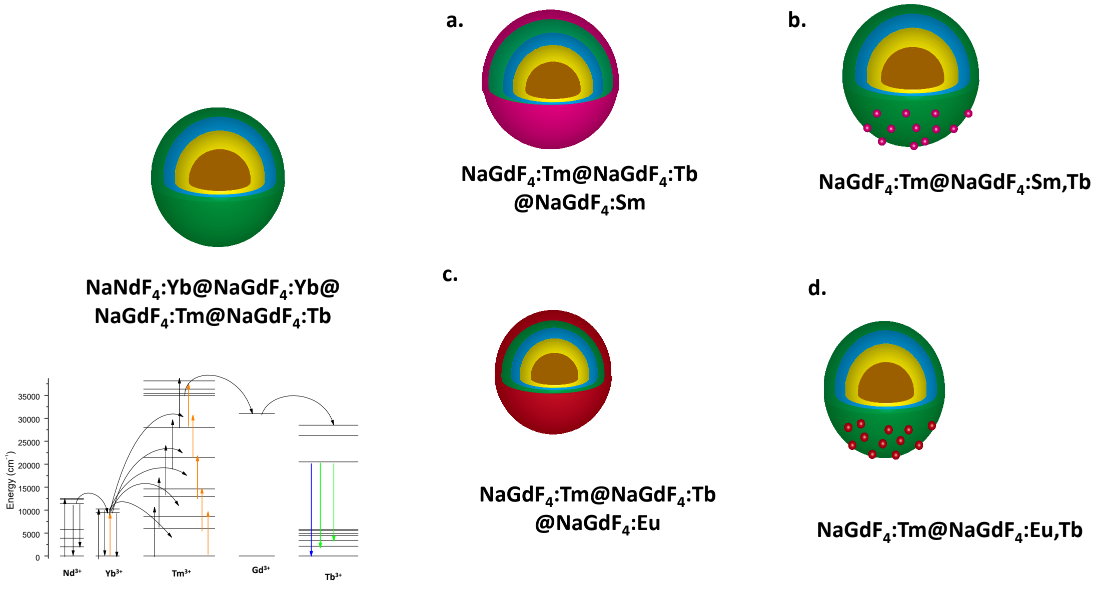

Figure 22. 808 nm excited EMU system with activator of Tb^{3+} utilized in the research of Tb^{3+}-Eu^{3+} and Tb^{3+}-Sm^{3+} energy transfer.

For the investigation on the Tb^{3+}→Sm^{3+} energy transfer, as shown in Figure 23, that is the specific effect of the Sm^{3+} ions to EMU system: when warpping a $NaGdF_4$: Sm layer outward the EMU-Tb^{3+}, not only no Sm^{3+} emission has been observed but also the Tb^{3+} emission have been attenuated; when the Sm^{3+} ions are doping in the shell layer of the EMU-Tb^{3+}, the Tb^{3+} emission has disappeared as well as the Tm^{3+} emission has been largely attenuated, which reveals the hazards of the Sm^{3+} to the EMU system, which has quenched the phonons that participate in the 3-/4-/5-phonons ETU process as shown in Figure 24.

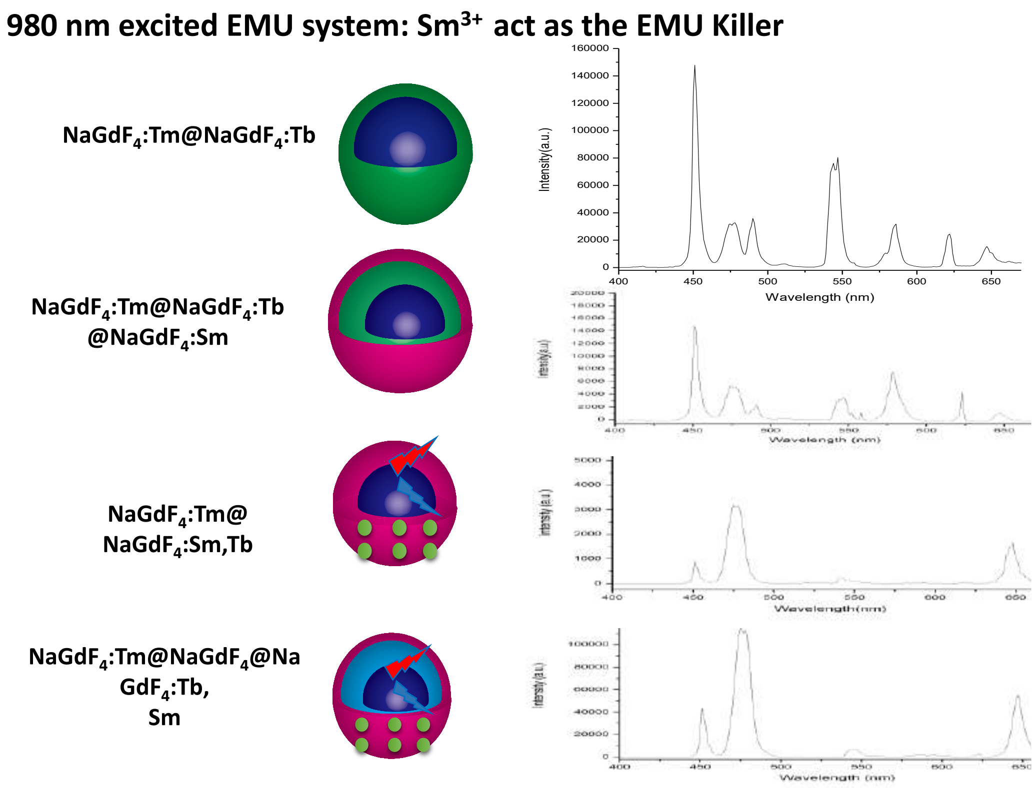

Figure 23. Emission spectra of the 980 nm excited EMU-Tb^{3+} sensitization of Sm^{3+}.

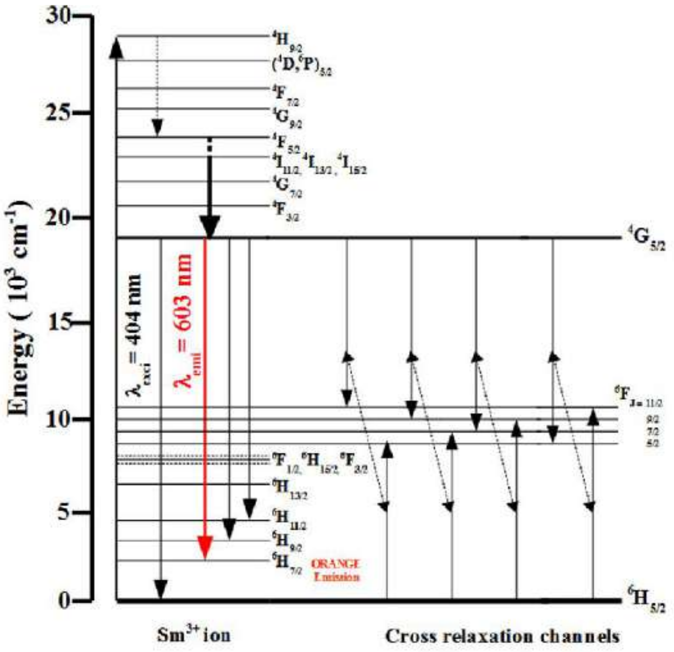

Figure 24. The energy levels and situations of cross-relaxation of the Sm^{3+} ions

For the investigation on the effect of Eu^{3+} on the 808 nm excited EMU-Tb^{3+} system that is $NaNdF_4$:Yb@$NaGdF_4$:Yb@$NaGdF_4$:Yb,Tm@$NaGdF_4$:Tb: when the $NaYF_4$:Eu layer is coating outwards, or doping certain amount of Eu^{3+} in the $NaGdF_4$:Tb layer, the emission of the whole system has been attenuated; also, when the Eu^{3+} is sensitized by $NaNdF_4$:Yb@$NaGdF_4$:Yb@$NaGdF_4$:Yb,Tm, that is the 808 nm excited EMU-Eu^{3+} system, compares with the satisfied luminescent performance of the 808 nm excited EMU-Tb^{3+}, is still shows “killed” 808 nm excited EMU emission, as shown in Figure 25. However, in our previous work, that is the Nd^{3+}-Trinity EMU system, the type I has shown preferred luminescence performance while type II system has shown weaken luminescence performance for the anti-EMU system. also, in this design, the Nd^{3+}-trinity system is reversed, which is probably the reason that why the 808 nm excited EMU system are easier to be quenched, as shown in Figure 26.

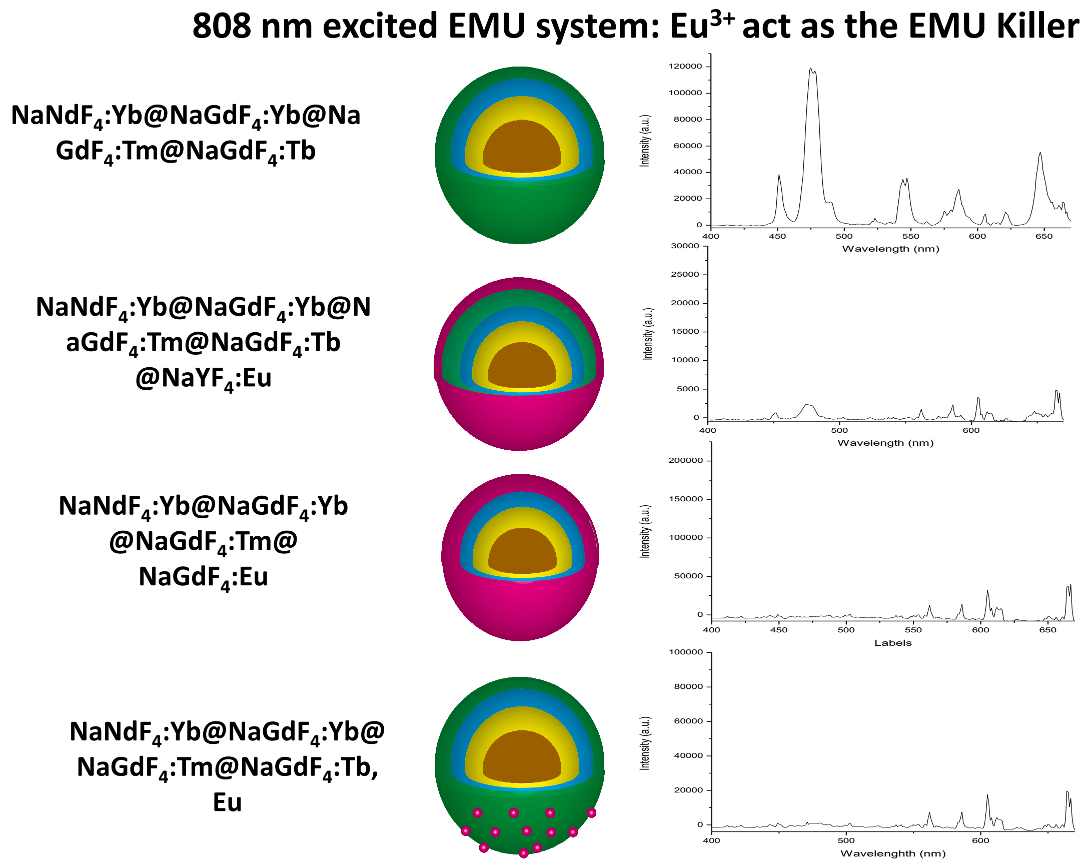

Figure 25. Emission spectra of the 808 nm excited EMU-Tb^{3+} sensitization of Eu^{3+}.

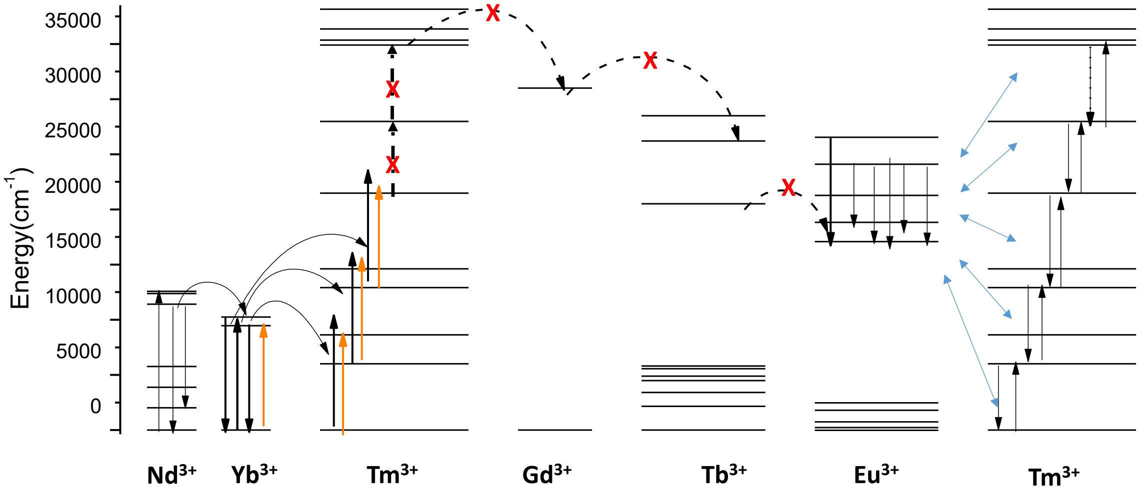

Figure 26. Eu^{3+} act as the EMU quencher with the excitation of 808 nm laser excited EMU-Tb^{3+} system. .

For the investigation on the effect of Eu^{3+} on the 980 nm excited EMU-Tb^{3+} system, as show in Figure 27, when the $NaYF_4$:Eu is coated outward, the Eu^{3+} emission appears while the Tb^{3+} emission shows depression which demonstrates that energy transfer of $Tb^{3+}\rightarrow Eu^{3+}$, with further supporting by the shortened lifetime; when the Eu^{3+} ions is doping in the shell layer of the EMU-Tb^{3+} system, the Eu^{3+} emission is further enhanced compares with the Tb^{3+} emission is further depressed.

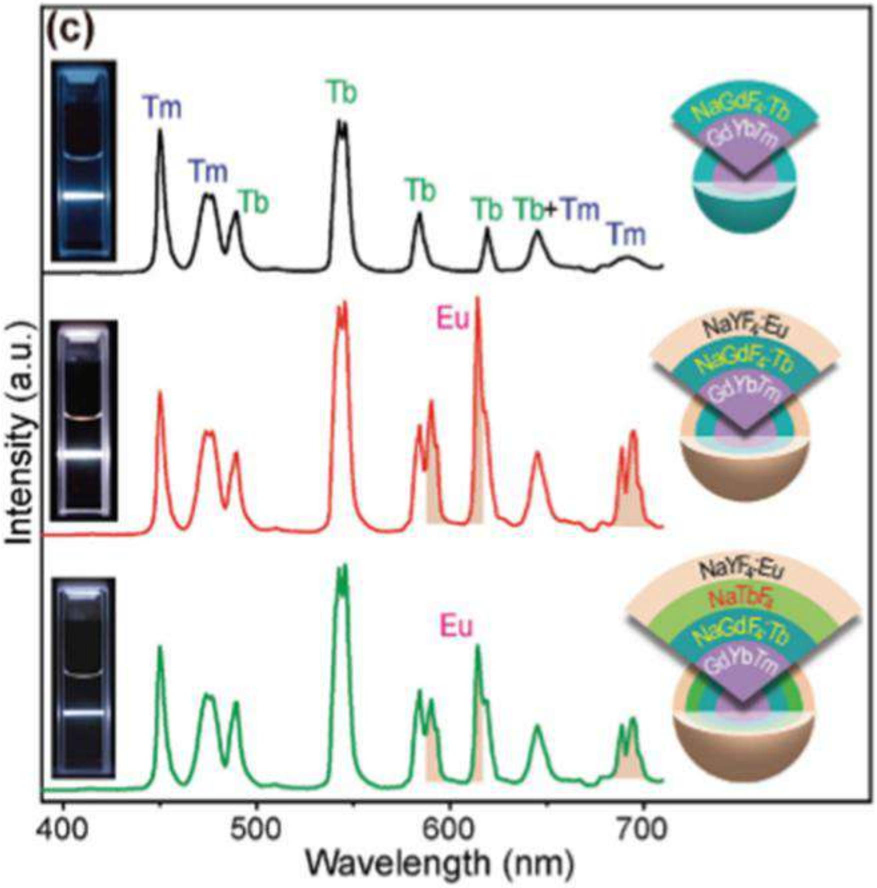

Figure 27. EMU-Tb-Eu system for RGB design

And the reason that we used the yttrium-based Eu^{3+} doping shells, is to prevent the distance $Gd^{3+}\rightarrow Gd^{3+}$ migration that will exciting the Eu^{3+} ions. However, the doped Eu^{3+} ions are proved with excitation by Tb^{3+}, and the excitation of Gd^{3+} cannot not be excluded.

And the EMU-Tb^{3+}-Eu^{3+} system could be developed to be a RGB system that fixed with the ratio of red to green ratio, but with variation of blue emission by the pulsed 980 nm excitation, which is also modulation of the EMU system by the pulse width, as shown in Figure 28.

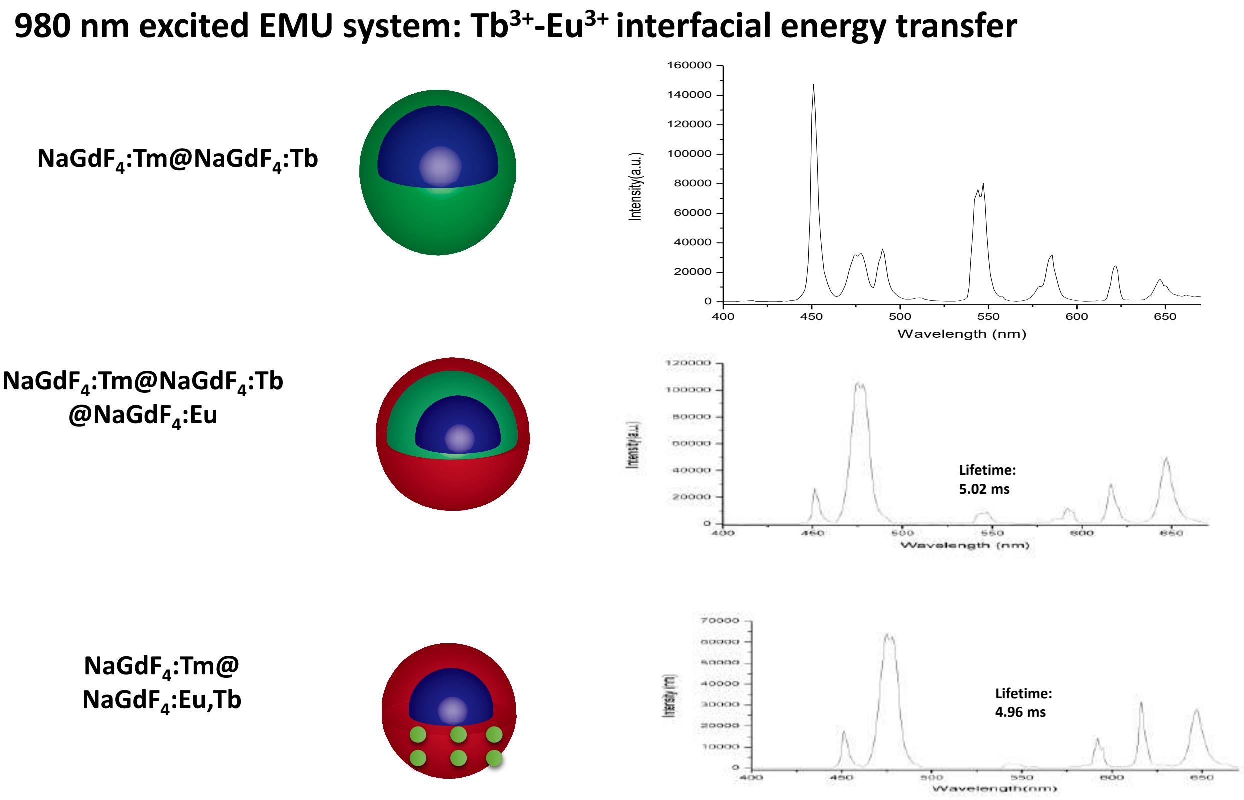

Figure 28. Emission spectra of the 980nm excited EMU-Tb^{3+} sensitization of Eu^{3+}.

5.7. Conclusion

Conclusively, we have construct the Lumiance Janus UNCNPs with specific charaterizaion that:

For the Type I, is the green-red sysetm with modulation of Ho^{3+} -Ce^{3+} modulation under excitation of 808 nm laser.

For the RGB system, with moduliation of EMU system that is the type II, III and IV: the Type II and III is red/green/blue triple modulation system which is the ratio of the three basic emission color has changed. The difference is that: for the type II, it is also a UV-visilbe, green-red/white/violet swich-on/off system; for the type III, it is a “born” to be RGB system that is the 980 nm excited EMU-Tb^{3+} and the 808 nm exited Nd^{3+}-Trinity EMU-Tb^{3+} system; the Type IV system is the red to green fixed only with the viration of blue system.

All the Luminescent Janus UCNPs will extend the utilization of the UCNPs, in the aspects including bio-imaing, bio-sensor and full-color printing, etc.

References

1. Perro, A., S. Reculusa, S. Ravaine, E. Bourgeat-Lami, and E. Duguet, *Design and synthesis of Janus micro- and nanoparticles.* Journal of Materials Chemistry, 2005. **15**(35-36): p. 3745-3760.
2. Lattuada, M. and T.A. Hatton, *Synthesis, properties and applications of Janus nanoparticles.* Nano Today, 2011. **6**(3): p. 286-308.
3. Thejokalyani, N. and S.J. Dhoble, *Novel approaches for energy efficient solid state lighting by RGB organic light emitting diodes – A review.* Renewable and Sustainable Energy Reviews, 2014. **32**: p. 448-467.
4. Thejo Kalyani, N. and S.J. Dhoble, *Organic light emitting diodes: Energy saving lighting technology—A review.* Renewable and Sustainable Energy Reviews, 2012. **16**(5): p. 2696-2723.
5. Chen, D., W. Xiang, X. Liang, J. Zhong, H. Yu, M. Ding, H. Lu, and Z. Ji, *Advances in transparent glass–ceramic phosphors for white light-emitting diodes—A review.* Journal of the European Ceramic Society, 2015. **35**(3): p. 859-869.
6. Chang, M.-H., D. Das, P.V. Varde, and M. Pecht, *Light emitting diodes reliability review.* Microelectronics Reliability, 2012. **52**(5): p. 762-782.
7. Ajovalasit, A., G. Petrucci, and M. Scafidi, *RGB Photoelasticity: Review and Improvements.* Strain, 2010. **46**(2): p. 137-147.
8. Deng, R., F. Qin, R. Chen, W. Huang, M. Hong, and X. Liu, *Temporal full-colour tuning through non-steady-state upconversion.* Nat Nano, 2015. **10**(3): p. 237-242.
9. Wang, L., H. Dong, Y. Li, R. Liu, Y.-F. Wang, H.K. Bisoyi, L.-D. Sun, C.-H. Yan, and Q. Li, *Luminescence-Driven Reversible Handedness Inversion of Self-Organized Helical Superstructures Enabled by a Novel Near-Infrared Light Nanotransducer.* Advanced Materials, 2015. **27**(12): p. 2065-2069.

10. Gao, W., H. Zheng, Q. Han, E. He, F. Gao, and R. Wang, *Enhanced red upconversion luminescence by codoping Ce*$^{3+}$ *in -NaY(Gd*$_{0.4}$*)F*$_4$*:Yb*$^{3+}$*/Ho*$^{3+}$ *nanocrystals.* Journal of Materials Chemistry C, 2014. **2**(27): p. 5327-5334.

11. Lupei, V., A. Lupei, C. Gheorghe, S. Hau, and A. Ikesue, *Efficient sensitization of Yb*$^{3+}$ *emission by Nd*$^{3+}$ *in Y*$_2$*O*$_3$ *transparent ceramics and the prospect for high-energy Yb lasers.* Optics Letters, 2009. **34**(14): p. 2141-2143.

12. Rivera-López, F., P. Babu, C. Basavapoornima, C.K. Jayasankar, and V. Lavín, *Efficient Nd*$^{3+}$*→Yb*$^{3+}$ *energy transfer processes in high phonon energy phosphate glasses for 1.0 μm Yb*$^{3+}$ *laser*. Journal of Applied Physics, 2011. **109**(12): p. 123514.

13. Wang, F., R. Deng, J. Wang, Q. Wang, Y. Han, H. Zhu, X. Chen, and X. Liu, *Tuning upconversion through energy migration in core–shell nanoparticles.* Nat Mater, 2011. **10**(12): p. 968-973.

14. Dong, H., L.-D. Sun, Y.-F. Wang, J.-W. Xiao, D. Tu, X. Chen, and C.-H. Yan, *Photon upconversion in Yb*$^{3+}$*-Tb*$^{3+}$ *and Yb*$^{3+}$*-Eu*$^{3+}$ *activated core/shell nanoparticles with dual-band excitation.* Journal of Materials Chemistry C, 2016. **4**(19): p. 4186-4192.

Experimental

Synthesis: all the nanoparticles were synthesized by thermal decomposition.

Cores

a) $NaGdF_4$:$Yb_{20\ \%}$, $Er_{2\ \%}$ / $Yb_{49\ \%}$, $Tm_{1\ \%}$ / $Yb_{20\ \%}$, $Ho_{2\ \%}$: 8 mL oleic acid and $Ln(CH_3CO_2)_3$•xH_2O DI water solution (0.8 mmol Ln^{3+} in total) were placed in a 100 ml three-neck flask, and degassed by nitrogen for 15 min. The mixture was heated to 150 °C and the temperature was kept for 0.5 h to remove water. 12 mL 1-ODE was then added and the mixture was kept at 150°C for 0.5 h to form a uniform solution. Cooling down the solution to 50°C, 5 mL MeOH that containing 80 mg NaOH and 240 mg NH_4F was added drop wise. Then solution was stirred for 0.5 h at 50°C. The solution was then heated to 120°C to remove water and methanol, and keeping under vacuum for 10 min to prevent bumping at high temperature. And then heated to 290°C and kept for 1.5 h. The product was achieved by precipitation by adding exceeded ethanol and collection by centrifuging at 12, 000 rpm for 10 min and washed by ethanol for 3 times.

b) $NaYF_4$:$Yb_{20\ \%}$, $Er_{2\ \%}$ / $Yb_{20\ \%}$, $Tm_{0.5\ \%}$ / $Yb_{20\ \%}$, $Ho_{2\ \%}$: 6 mL oleic acid, 14 ml 1-ODE and $Ln(CH_3CO_2)_3$•xH_2O DI water solution (0.8 mmol Ln^{3+} in total) were placed in a 100 ml three-neck flask, and degassed by nitrogen for 15 min. The mixture was heated to 150 °C and the temperature was kept for 1.0 h to remove water and form a uniform solution. Cooling down the solution to 50°C, 5 mL MeOH that containing 80 mg NaOH and 240 mg NH_4F was added drop wise. Then solution was stirred for 0.5 h at 50°C. The solution was then heated to 120°C to remove water and methanol, and keeping under vacuum for 10 min to prevent bumping at high temperature. And then heated to 290°C and kept for 1.5 h. The product was achieved by precipitation by adding exceeded ethanol and collection by centrifuging at 12, 000 rpm for 10 min and washed by ethanol for 3 times.

Core-multishells structures by “seeded growth”: 4 mL oleic acid and $Ln(CH_3CO_2)_3$•xH_2O DI water solution (0.4 mmol Ln^{3+} in total) were placed in a 100 ml three-neck flask, and degassed by nitrogen for 15 min. The mixture was heated to 150°C and the temperature was kept for 0.5 h to remove water. 6 mL 1-ODE was then added and the mixture was kept at 150 °C for 0.5 h to form a uniform solution. Cooling down the solution to 50 °C, the “seed” UCNPs (0.8 mmol) that dispersed in cyclohexane were added, along with 5 mL MeOH that containing 80 mg NaOH and 240 mg NH_4F was added drop wise. Then solution was stirred for 0.5 h at 50 °C. The solution was then heated to 120 °C to remove water and methanol, and keeping under vacuum for 10 min to prevent bumping at high temperature. And then heated to 290 °C and kept for 1.5 h. The product was achieved by precipitation by adding exceeded ethanol and collection by centrifuging at 12, 000 rpm for 10 min and washed by ethanol for 3 times.

Characterization:

Morphology: TEM, STEM, and EDX Spectroscopy (JEOL operating at 200 kV), SEAD and XRD patterns were used to characterize the upconversion nanoparticles. Samples were dispersed in cyclohexane and dropped on the amorphous carbon-coated copper grids.

Emission spectra: all the emission spectra were measured by Edinburgh FLS 920 conjugated with 808/980 nm laser (CW, tunable, 0-2 W, Changchun New Industries Optoelectronics Technology Co., Ltd.). A condenser lens was fixed in the most appropriate location between the photo-luminescence source and sample chamber to make sure the emission spectra were comparable under the same measurement conditions. Measurement conditions include power density, sample concentration, instrument settings (especially the emission band width) as well as the conjugation of the lasers to the EI spectrometer (distance of the laser to the sample chamber, position of the focus lens should be adjusted to the maximum focusing position).

Pulse laser generation: by the DG-535 Digital Delay/Pulse Generator conjugation with 980 nm/808 nm with the mode of "modulation".

Lifetime measurement: all the decay curves were measured by Edinburgh FLS 920 conjugated with DG-535 Digital Delay/Pulse Generator and 808/980 nm laser (modulation, Changchun New Industries Optoelectronics Technology Co., Ltd.). A condenser lens was placed in the most appropriate location between the photo-luminescence source and sample chamber.

Absolute florescent quantum yield: by Edinburgh FLS 980 conjugated with 808/980 nm laser (CW, tunable, 0 - 2 W, Changchun New Industries Optoelectronics Technology Co., Ltd.) by the optical entrance. A reflector was used to vertically reflect the laser and a condenser lens was used to focus the laser beam before it entering the integrating sphere. For the 980 nm absolute quantum yield, NIR PMT (500 nm – 1700 nm) was used to measure the scattering of samples and reference (attenuator was used to prevent the saturation of PMT) and Visible PMT (200 nm – 900 nm) was used to measure the visible emission of samples and reference (400 - 700 nm). NIR and visible PMT were corrected; for 808 nm excited absolute quantum yield, visible PMT was used to measure the scattering of samples and reference (attenuator was used to prevent the saturation of PMT) and the visible emission of samples and reference. The absolute quantum yield was calculated by the equation:

Absolute florescent quantum yield (%)

$$= \frac{\textbf{photons emitted}}{\textbf{photons absorbed}} \times \mathbf{100}\ \%$$

$$= \frac{(\mathbf{E\ sam-E\ ref})}{(\mathbf{L\ ref-L\ sam})} \times \mathbf{100}\ \%$$

Cyclohexane is used as references.

E sam: luminescence of sample

E ref: luminescence of reference

L ref: scattering of reference

L sam: scattering of sample

Cell culture

Human cervical carcinoma HeLa cells were cultured in Dulbecco’s Modified Eagle Medium (DMEM) supplemented with 10% fetal bovine serum (FBS) and 1% penicillin/streptomycin at 37 ˚C and 5% CO2.

In vitro fluorescence imaging

HeLa cells were seeded onto coverslip in 35-mm culture dishes overnight. The cells were then incubated with UCNP for 20h at 37 ˚C and 5% CO_2, and were subsequently washed with PBS for three times before imaging. The emitted fluorescent signals of UCNP were examined with Leica TCS SP8 multi-photon Confocal Microscope (Libra II, coherent) equipped with a pulsed Titanium: Sapphire laser. Incubation with 200 ug/ml UCNP for 20 h.

Future Work

As we have established the Nd^{3+}-Trinity system that coating on the $NaGdF_4$:Yb, X(Er/Tm/Ho) and the EMU cores, with study on their luminescent, magnetic and morphologic properties; furthermore, we have summarized the principle of the anisotropic growth by studying the layer-by-layer epitaxial growth on the Nd^{3+}-Trinity system; also, we have put forward the new concept that is “Luminescent Janus” UCNPs to characterize the UCNPs with various luminescent performance under different photo-luminescence source. And our newly invented “Luminescent Janus” UCNPs is the 808 nm/980 nm pulsed/c.w. excited Full-color RGB model with tenability, which is the influence of the pulse width on the EMU system.

In my own view mind, the future work in UCNPs focus on:

a. To conquer the bottleneck of the concentration of the activators (Er^{3+}, Tm^{3+}, Ho^{3+}) and accumulator (Tm^{3+}) in the EMU system, which limited the upconversion efficiency, some modification of the nanocrystal on the host matrices should be made; furthermore, it will benefit the 808 nm excited, Nd^{3+}-sensitized UCNPs
b. More research is still in need to illustrate the saturation effect in the upconversion process, especially in the Nd^{3+}-sensitized upconversion process.
c. The full-color RGB model should be utilized in the 3D-imaging.
d. The Nd^{3+}-Trinity system coated UCNPs should be utilized in bio-imaging, drug delivery and therapy, etc, by surface modification, conjugation of peptides.
e. $NaCeF_4$ nanoparticles could be developed to be a new type of phosphor powder for we found it is also a full-colour emitting model under excitation of 330 nm.